

**EXTRACELLULAR MATRIX FOR REPAIR OF GASTROINTESTINAL MUCOSA**

by

Timothy Joseph Keane Jr.

Bachelor of Science in Chemical Engineering, University of Pittsburgh, 2011

Submitted to the Graduate Faculty of  
Swanson School of Engineering in partial fulfillment  
of the requirements for the degree of  
Doctor of Philosophy

University of Pittsburgh

2016

**UNIVERSITY OF PITTSBURGH**  
**SWANSON SCHOOL OF ENGINEERING**

This dissertation was presented

by

Timothy Joseph Keane Jr.

It was defended on

June 3, 2016

and approved by

Stephen F. Badylak, M.D., PhD, Professor, Departments of Surgery and Bioengineering

Bryan Brown, PhD, Professor, Department of Bioengineering

David J. Hackam, M.D., PhD, Professor, Department of Surgery

Donna Beer Stolz, PhD, Professor, Department of Cell Biology

Yadong Wang, PhD, Professor, Department of Bioengineering

**Copyright © by Timothy Joseph Keane Jr.**

2016

# EXTRACELLULAR MATRIX FOR REPAIR OF GASTROINTESTINAL MUCOSA

Timothy Joseph Keane Jr., Ph.D.

University of Pittsburgh, 2016

Extracellular matrix (ECM) bioscaffolds have been shown to promote site-appropriate functional tissue remodeling in multiple anatomic sites, including the gastrointestinal (GI) tract. Discovery work over the past 2 decades has identified contributing mechanistic factors of ECM-induced tissue remodeling to be the modulation of the innate immune response by the action of embedded signaling molecules while naturally occurring cryptic peptide motifs released or exposed during ECM degradation and remodeling simultaneously promote stem/progenitor cell chemotaxis, proliferation, and differentiation. This immune stimulatory approach, paired with rapid restoration of the GI mucosal tissue, represents a novel therapeutic strategy for treating disease of the GI tract such as inflammatory bowel disease (IBD). The objective of the present thesis was to determine the efficacy of ECM for the repair of GI mucosal tissue. First, ECM was isolated from the proximal (esophagus) and distal (colon) of the GI tract to characterize spatial differences in the biochemical and mechanical properties of GI ECM. Next, we measured the effect of GI-ECM on epithelial cell remodeling and the inflammatory response. Finally, the efficacy of ECM for treating colonic mucosal tissue was tested in a rat model of IBD. Results show expected spatial changes in ECM along the GI tract with esophageal and colonic ECM having unique properties. Exposure of intestinal epithelial cells to GI ECM in-vitro led to enhanced epithelial cell remodeling and an increased barrier function. Macrophages exposed to degradation products of GI-ECM in-vitro were shown to exhibit an immunoregulatory and anti-inflammatory phenotype. Finally, an enema hydrogel composed of GI ECM was shown effectively treat a rodent model of IBD. We defined effective therapy according to two essential physiologic processes that were positively directed by ECMH treatment. First, the colonic

epithelial barrier function, which protects the host from the relentless barrage of pro-inflammatory luminal contents, was restored. Second, the pro-inflammatory state of tissue macrophages, which propagate inflammation by releasing inflammatory cytokines, was resolved. Together, this strategy represents a proactive therapeutic approach and is a distinct departure from the immunosuppressive (defensive) and surgical (salvage) methods currently used to treat IBD.

## TABLE OF CONTENTS

<b>PREFACE</b> .....	<b>xxiii</b>
<b>1.0 THE ROLE OF ECM IN GASTROINTESTINAL (GI) TRACT DEVELOPMENT &amp; DISEASE</b>	<b>1</b>
1.1 ABSTRACT .....	1
1.2 INTRODUCTION.....	2
1.3 ROLE OF ECM IN GI TRACT DEVELOPMENT .....	3
1.3.1 <i>Germ Layer Contributions to the Histologic Structures of the GI Tract</i> .....	3
1.3.2 <i>ECM Components in the GI Tract</i> .....	5
1.3.3 <i>The Role of ECM During Gut Development</i> .....	6
1.4 ROLE OF ECM REMODELING IN GASTROINTESTINAL TRACT DISORDERS.....	9
1.4.1 <i>Inflammatory Bowel Disease (IBD)</i> .....	9
1.4.2 <i>Fibrosis</i> .....	12
1.4.3 <i>Cancer</i> .....	14
1.5 FUTURE PERSPECTIVES.....	15
1.5.1 <i>Role of ECM in Tissue Engineering of the GI Tract</i> .....	15
1.6 CONCLUSIONS .....	17
<b>2.0 THE ECM AS A BIOLOGIC SCAFFOLD FOR TISSUE ENGINEERING APPLICATIONS</b>	<b>18</b>
2.1 ABSTRACT .....	18
2.2 INTRODUCTION.....	19
2.3 BIOMATERIALS FOR TISSUE ENGINEERING .....	20
2.3.1 <i>Improving Synthetic Biomaterials</i> .....	21

2.3.2	<i>Naturally Derived Biomaterials</i> .....	25
2.3.3	<i>The ECM as a Bioscaffold for Tissue Repair</i> .....	26
2.4	TISSUE SPECIFICITY OF ECM.....	28
2.5	MECHANISMS OF ECM MEDIATED CONSTRUCTIVE REMODELING.....	31
2.5.1	<i>ECM-mediated remodeling of the Gastrointestinal Tract</i> .....	32
2.6	INJECTABLE VS. IMPLANTABLE ECM .....	33
<b>3.0</b>	<b>PREPARING BIOMATERIALS FROM DECELLULARIZED TISSUES</b> .....	<b>34</b>
3.1	ABSTRACT .....	34
3.2	INTRODUCTION.....	35
3.3	DECELLULARIZATION AGENTS AND TECHNIQUES .....	37
3.3.1	<i>Physical methods</i> .....	38
3.3.1.1	Freeze-thaw.....	38
3.3.1.2	Agitation and immersion .....	38
3.3.1.3	Use of pressure for decellularization .....	41
3.3.1.4	Supercritical fluids for decellularization .....	42
3.3.2	<i>Chemical and biologic agents for decellularization</i> .....	43
3.3.2.1	Alkalines and Acids for decellularization.....	43
3.3.2.2	Non-ionic detergents.....	44
3.3.2.3	Ionic detergents .....	45
3.3.2.4	Zwitterionic detergents.....	45
3.3.2.5	Alcohols.....	46
3.3.2.6	Enzymatic agents .....	46
3.3.2.7	Chelators and toxins .....	48
3.4	PERFUSION DECELLULARIZATION OF WHOLE ORGAN CONSTRUCTS .....	48
3.5	EFFECTS OF RESIDUAL DETERGENTS FROM DECELLULARIZATION .....	54

3.6	ESTABLISHING METRICS FOR EFFECTIVE DECELLULARIZATION.....	56
3.7	TERMINAL STERILIZATION OF DECELLULARIZED TISSUES .....	58
<b>4.0</b>	<b>THE HOST RESPONSE TO ECM.....</b>	<b>59</b>
4.1	ABSTRACT .....	59
4.2	INTRODUCTION.....	60
4.3	RAW MATERIAL SOURCE OF BIOLOGIC SCAFFOLDS.....	61
4.4	INNATE AND ADAPTIVE RESPONSE TO BIOLOGIC SCAFFOLD MATERIALS .....	62
4.5	MACROPHAGE PARTICIPATION IN ECM MEDITATED TISSUE REMODELING .....	64
4.6	XENOGENIEC VS. ALLOGENEIC TISSUE SOURCE: LOGISTICAL AND REGULATORY CONSIDERATIONS.....	66
<b>5.0</b>	<b>OBJECTIVES .....</b>	<b>68</b>
<b>6.0</b>	<b>CENTRAL HYPOTHESIS AND SPECIFIC AIMS .....</b>	<b>70</b>
<b>7.0</b>	<b>PREPARATION AND CHARACTERIZATION OF A BIOLOGIC SCAFFOLD FROM ESOPHAGEAL MUCOSA .....</b>	<b>73</b>
7.1	ABSTRACT .....	73
7.2	INTRODUCTION.....	74
7.3	MATERIALS AND METHODS .....	75
7.3.1	<i>Harvest and preparation of ECM from porcine esophagus.....</i>	75
7.3.2	<i>Assessment of DNA content .....</i>	76
7.3.4	<i>Sulfated glycosaminoglycan assay.....</i>	78
7.3.5	<i>Growth factor assay.....</i>	79
7.3.6	<i>Scanning electron microscopy.....</i>	79
7.3.7	<i>Perivascular stem cell (PVSC) culture.....</i>	80
7.3.8	<i>In-vivo cytocompatibility.....</i>	81
7.3.9	<i>Biomechanical testing .....</i>	83
7.3.10	<i>Statistical analysis .....</i>	84

7.4	RESULTS .....	85
7.4.1	<i>Decellularization efficacy</i> .....	85
7.4.2	<i>Biochemical and ultrastructural characteristics of esophageal ECM</i> .....	87
7.4.3	<i>Biomechanical properties</i> .....	89
7.4.4	<i>Cytocompatibility</i> .....	91
7.5	DISCUSSION.....	95
7.6	CONCLUSION.....	99
7.7	ACKNOWLEDGMENTS.....	100
<b>8.0</b>	<b>PREPARATION AND CHARACTERIZATION OF A BIOLOGIC SCAFFOLD FROM COLONIC MUCOSA.....</b>	<b>101</b>
8.1	ABSTRACT .....	101
8.2	INTRODUCTION.....	102
8.3	MATERIALS AND METHODS .....	104
8.3.1	<i>Preparation of colonic ECM (coECM)</i> .....	104
8.3.2	<i>Hydrogel preparation</i> .....	105
8.3.3	<i>Determining decellularization efficacy</i> .....	105
8.3.3.1	Histologic analysis .....	105
8.3.3.2	DNA concentration and fragment analysis .....	106
8.3.3.3	Phospholipid measurement.....	106
8.3.4	<i>Glycosaminoglycan and growth factor measurement</i> .....	107
8.3.5	<i>Immunohistochemistry</i> .....	107
8.3.6	<i>Scanning electron microscopy</i> .....	108
8.3.7	<i>Mechanical testing of coECM scaffolds</i> .....	109
8.3.7.1	Planar biaxial testing.....	109
8.3.7.2	Suture retention testing.....	110
8.3.7.3	Rheologic testing of coECM hydrogels .....	110

8.3.7.4	Turbidometric gelation kinetics .....	110
8.3.7.5	In-vitro cytocompatibility: .....	111
8.3.8	<i>In-vitro macrophage response</i> .....	112
8.3.9	<i>In-vivo cytocompatibility</i> .....	113
8.3.9.1	Abdominal wall defect model .....	113
8.3.9.2	Histomorphologic scoring .....	114
8.3.9.3	Host response .....	114
8.3.10	<i>Statistical analysis</i> .....	115
8.4	RESULTS .....	116
8.4.1	<i>Decellularization efficacy</i> .....	116
8.4.2	<i>Biochemical and structural properties of coECM</i> .....	118
8.4.3	<i>Mechanical properties of coECM scaffold</i> .....	121
8.4.4	<i>Rheologic and turbidometric properties of coECM hydrogel</i> .....	123
8.4.5	<i>In-vitro cell response to coECM</i> .....	125
8.4.6	<i>In-vivo host response</i> .....	127
8.5	DISCUSSION.....	129
8.6	CONCLUSION.....	132
8.7	ACKNOWLEDGMENT .....	133
<b>9.0</b>	<b>TISSUE-SPECIFIC EFFECTS OF ESOPHAGEAL EXTRACELLULAR MATRIX .....</b>	<b>134</b>
9.1	ABSTRACT .....	134
9.2	INTRODUCTION.....	135
9.3	MATERIALS AND METHODS .....	136
9.3.1	<i>Overview of experimental design</i> .....	136
9.3.2	<i>Mice and rats</i> .....	137
9.3.3	<i>Harvesting and preparation of ECM and hydrogels</i> .....	137

9.3.4	<i>SDS gel chromatography</i> .....	138
9.3.5	<i>Isolation and culture of esophageal stem cells</i> .....	139
9.3.6	<i>Migration assay</i> .....	139
9.3.7	<i>Generation of 3D organoids</i> .....	140
9.3.8	<i>Proliferation assay</i> .....	140
9.3.9	<i>Surgical procedure and ECM implantation</i> .....	141
9.3.10	<i>Histology and immunolabeling</i> .....	142
9.3.11	<i>Statistical analysis</i> .....	143
9.4	<b>RESULTS</b> .....	143
9.4.1	<i>ECM characteristics</i> .....	143
9.4.2	<i>Esophageal stem cell characteristics</i> .....	144
9.4.3	<i>Organoid forming capacity of ECM hydrogels</i> .....	146
9.4.4	<i>Proliferation of esophageal stem cells</i> .....	149
9.4.5	<i>Esophageal mucosal remodeling</i> .....	150
9.5	<b>DISCUSSION</b> .....	152
9.6	<b>CONCLUSION</b> .....	155
<b>10.0</b>	<b>RESTORING MUCOSAL BARRIER FUNCTION AND MODIFYING MACROPHAGE PHENOTYPE WITH AN EXTRACELLULAR MATRIX HYDROGEL: POTENTIAL THERAPY FOR ULCERATIVE COLITIS</b> .....	<b>156</b>
10.1	<b>ABSTRACT</b> .....	156
10.2	<b>INTRODUCTION</b> .....	157
10.3	<b>MATERIALS AND METHODS</b> .....	158
10.3.1	<i>Experimental design</i> .....	158
10.3.2	<i>ECM hydrogel preparation and formulations</i> .....	159
10.3.3	<i>Characterization of ECM hydrogel</i> .....	160
10.3.4	<i>ECM adhesion testing</i> .....	161

10.3.5	<i>Animals and husbandry</i> .....	161
10.3.6	<i>Disease induction and monitoring</i> .....	162
10.3.7	<i>Enema administration</i> .....	163
10.3.8	<i>ECM retention studies with FITC- and <sup>14</sup>C-ECMH</i> .....	163
10.3.9	<i>Explanting and scoring colonic tissue</i> .....	164
10.3.10	<i>TRITC-Dextran permeability assay</i> .....	166
10.3.11	<i>Organ cultures</i> .....	167
10.3.12	<i>LPMC isolation and culture</i> .....	167
10.3.13	<i>IEC culture</i> .....	167
10.3.14	<i>Trans-epithelial electrical resistance (TEER) measurement</i> .....	168
10.3.15	<i>Immunolabeling</i> .....	168
10.3.16	<i>Statistical analysis</i> .....	170
10.4	<b>RESULTS</b> .....	170
10.4.1	<i>ECMH is adhesive to colon tissue</i> .....	170
10.4.2	<i>ECMH treatment mitigates disease state</i> .....	172
10.4.3	<i>ECMH restores epithelial barrier function</i> .....	176
10.4.4	<i>ECMH mitigates the inflammatory response</i> .....	177
10.5	<b>DISCUSSION</b> .....	179
10.6	<b>CONCLUSION</b> .....	182
<b>11.0</b>	<b>SUMMARY OF MILESTONES AND FUTURE DIRECTIONS</b> .....	<b>183</b>
<b>APPENDIX</b>	.....	<b>187</b>
<b>APPENDIX A CONSEQUENCES OF INEFFECTIVE DECELLULARIZATION OF BIOLOGIC SCAFFOLDS ON THE HOST RESPONSE</b> .....		
A.1	<b>Abstract</b> .....	188
A.2	<b>Introduction</b> .....	189
A.3	<b>Materials and Methods</b> .....	192

A.3.1	Harvest and preparation of ECM from porcine small intestine.....	192
A.3.2	Histologic assessment of decellularization.....	192
A.3.3	Quantification of DNA content.....	193
A.3.4	In-vitro culture of macrophages on SIS-ECM devices.....	193
A.3.5	In-vivo macrophage response to SIS-ECM scaffolds.....	194
A.3.6	Immunolabeling .....	195
A.3.7	Quantification of M1/M2 macrophage staining .....	196
A.3.8	Statistical analysis.....	197
A.4	Results.....	197
A.4.1	DNA concentration and fragmentation in scaffolds.....	197
A.4.2	In-vitro macrophage response.....	199
A.4.3	Macrophage response In-vivo.....	202
A.4.3.1	Macrophage response to PBS-treated scaffolds.....	202
A.4.3.2	Macrophage response to 1hr PAA treated scaffolds.....	203
A.4.3.3	Macrophage response to 2hr PAA treated scaffolds.....	204
A.5	Discussion.....	206
A.6	Conclusion .....	210
A.7	Acknowledgement .....	210
<b>APPENDIX B THE EFFECT OF TERMINAL STERILIZATION ON MATERIAL PROPERTIES AND IN-VIVO REMODELING OF A PORCINE DERMAL BIOLOGIC SCAFFOLD .....</b>		<b>211</b>
B.1	Abstract .....	211
B.2	Introduction.....	212
B.3	Methods.....	213
B.3.1	Experimental Design.....	213
B.3.2	Preparation and Sterilization of Dermal ECM Scaffolds.....	214
B.3.3	Assessment of Cellular Content.....	214

B.3.4	Measuring DNA content .....	215
B.3.5	DNA Fragmentation Analysis .....	215
B.3.6	Sulfated Glycosaminoglycan Assay .....	215
B.3.7	Growth Factor Quantification.....	216
B.3.8	Scanning Electron Microscopy .....	216
B.3.9	Thickness Measurements of Sterilized Samples.....	217
B.3.10	Porosity Index .....	217
B.3.11	Ball-burst Testing .....	217
B.3.12	Suture Retention Strength .....	218
B.3.13	In-vitro Cytocompatibility .....	218
B.3.14	Surgical Procedure and Test Article Collection .....	219
B.3.15	Histologic Analysis of Tissue Explants .....	220
B.3.16	Macrophage Immunolabeling .....	221
B.3.17	Statistical Analysis: .....	222
<b>B.4</b>	<b>Results.....</b>	<b>223</b>
B.4.1	Cellular Content.....	223
B.4.2	Biochemical Properties.....	224
B.4.3	Ultrastructural Properties.....	224
B.4.4	Mechanical Properties and Porosity.....	225
B.4.5	Cytocompatibility .....	226
B.4.6	Host Response: .....	227
<b>B.5</b>	<b>Discussion.....</b>	<b>230</b>
<b>B.6</b>	<b>Conclusion .....</b>	<b>233</b>
<b>B.7</b>	<b>Acknowledgements .....</b>	<b>233</b>
	<b>BIBLIOGRAPHY.....</b>	<b>235</b>

## LIST OF TABLES

<b>Table 1.</b> Clinically Available Biomaterials for Tissue Engineering .....	22
<b>Table 2.</b> Source tissue and species of commercial biologic scaffold materials .....	29
<b>Table 3.</b> Decellularization techniques used for various tissues .....	37
<b>Table 4.</b> Esophageal tissue decellularization protocols .....	39
<b>Table 5.</b> Effects of decellularization on tissue mechanical properties .....	40
<b>Table 6.</b> Results and considerations for varying decellularization methods .....	50
<b>Table 7.</b> Semiquantitative scoring criteria for day 14 and day 35 explants .....	82
<b>Table 8.</b> Native esophagus and emECM suture retention test .....	90
<b>Table 9.</b> Criteria for clinical symptom scoring .....	162
<b>Table 10.</b> Criteria for gross anatomical scoring of colon specimens .....	165
<b>Table 11.</b> Criteria for histologic scoring of colon specimens .....	166

## LIST OF FIGURES

- Figure 1. Diagram depicting the origins, regions, and histology of the major segments of the GI-tract. GI tissues that arise from the foregut include the esophagus, stomach, and the proximal portion of the duodenum. The midgut develops into the posterior portion of the duodenum, the jejunum, ileum, ascending colon and two-thirds of the transverse colon. The distal one-third of the transverse colon, and rectum arise from the hindgut of the embryonic tube. The epithelium of GI tissues, with its tissue-specific structures (e.g. gastric pits, villi, or crypts) is derived solely from the endoderm, whereas the basement membrane arises from both the endodermal and mesodermal germ layer. The remaining histological layers of GI tissues including the lamina propria of the mucosa layer, the submucosa, muscularis externa, adventitia, and serosa are mesodermal in origin. .... 4
- Figure 2. Schematic representation of normal intestinal wound healing, fistula formation, and fibrosis. In response to tissue damage, regulated production and degradation of ECM results in physiologic wound healing but IBD can progress in opposing directions based on the balance of ECM deposition or degradation. Fibrosis is characterized by excess ECM deposition that results from the coupling of increased number of ECM-producing myofibroblasts with increased cell proliferation and decreased apoptosis. In contrast, ECM destruction, mediated largely by MMPs, and decreased myofibroblast involvement leads to fistulae formation..... 10
- Figure 3. Perfusion decellularization of rat liver. The cadaveric rat liver (A) is cannulated through the portal vein. Following the decellularization protocol, the matrix is devoid of cells and has a white/translucent appearance (B). Perfusion decellularization allows for the maintenance of an intact vascular network, visualized by injection of a colored dye (C). Scale bar = 1 cm. .... 54
- Figure 4. Decellularization efficacy. Decellularization of emECM was assessed by the amount and size of remaining DNA and histologically by hematoxylin and eosin (H&E). The amount dsDNA in emECM was less than 50ng/mg, which was significantly less (asterisk;  $p < 0.001$ ) than native tissue (A). DNA fragment length was assessed by gel electrophoresis using a reference 100 bp ladder (B). No intact nuclei were visible after decellularization by H&E staining (C). Data represented as mean  $\pm$  standard error. Scale bar = 100  $\mu\text{m}$ . .... 86

Figure 5. Retention of biologic components. Growth factor protein and glycosaminoglycans (GAGs) remain after decellularization. The amount of (A) GAGs and (B) basic fibroblast growth factor (bFGF) remaining after decellularization was measured. Data represented as mean  $\pm$  standard error. Asterisk signifies  $p < 0.05$ .....87

Figure 6. Immunolabeling of collagen IV, laminin, and fibronectin in emECM samples. Dark brown indicates positive stain. Immunolabeling of native tissue (A,C,E) is shown as a comparison to emECM (B,D,F). L indicates luminal surface. Scale bar = 200  $\mu\text{m}$ . .....88

Figure 7. Scanning electron micrographs (SEM) of emECM surface. The luminal surface of the emECM scaffold was characterized by a smoother surface (A,C) compared to the abluminal surface which was more textured and fibrous (B,D) .....89

Figure 8. Native and decellularized esophagus mechanical characterization. The equibiaxial stress response was characterized along the circumferential and longitudinal axes (A). The maximum strain defined at a stress of 250 kPa for both circumferential (C) and longitudinal (L) axes (B). Significant differences ( $p < 0.05$ ) between the circumferential and longitudinal axes of the same sample are denoted as the following: (\*) as different from circumferential. Significant differences between samples in each axis are denoted as the following: (^) as different from native. Data represented as mean  $\pm$  standard error. ....91

Figure 9. Cytocompatibility of emECM and XL-emECM. The viability of perivascular stem cells (PVSCs) after 48 h culture on emECM (A), XL-emECM (B), and tissue culture plastic (TCP) was assessed. Percentage of live cells was quantified and compared across groups (C). Data represented as mean  $\pm$  standard error. Scale bar = 50  $\mu\text{m}$ . .....92

Figure 10. In-vivo cytocompatibility. Tissue sections were stained with H&E at 14 and 35 days after implantation of emECM (A,B) and XL-emECM (C,D). Histomorphologic sections were evaluated and scored according to previously established criteria (E). Scale bar= 100  $\mu\text{m}$  .....93

Figure 11. In-vivo macrophage response. Macrophage immunolabeling in emECM (A) and XL-emECM (B) in explants 14 d after implantation was quantified and represented as a ratio of M2/M1 phenotype (C). Dashed line indicates the interface of native tissue (marked by a triangle) and the surgical site. Data represented as mean  $\pm$  standard error. Scale bar = 50  $\mu\text{m}$ . .....95

Figure 12. Decellularization efficacy. (A) The presence of nuclei in the decellularized tissue was assessed by hematoxylin and eosin (H&E) staining and 4',6-diamidino-2-phenylindole (DAPI) staining. (B) DNA concentration was quantified using PicoGreen® assay. (C) The fragment length of residual DNA was visualized by gel electrophoresis. (D) Residual cell membrane components were quantified using EnzyChrom™ phospholipid assay. Scale bar = 200  $\mu\text{m}$ . \*\* =  $p < 0.01$  .....117

Figure 13. CoECM composition and ultrastructure. (A) The presence and distribution of laminin and fibronectin was assessed by immunohistochemical staining. (B) The ultrastructure of

the luminal and abluminal surfaces of the scaffold was visualized at low and high (inset) magnification. Scale bar in 2A = 200  $\mu\text{m}$ . Scale bar in 2B = 50  $\mu\text{m}$ . .....119

Figure 14. Biochemical composition. The retention of biochemical constituents in coECM was compared to native colonic tissue. (A) The concentration of sulfated glycosaminoglycans (sGAGs) was measured using Blyscan™ assay. (B) Non-sulfated GAG hyaluronic acid (HA) content was measured using an ELISA. (C) Fibrillar collagen was quantified using Sircol™ assay. The presence of two growth factors, bFGF (D) and VEGF (E), was detected using ELISA kits. \* =  $p < 0.05$ , \*\* =  $p < 0.01$  .....121

Figure 15. Scaffold mechanical properties. (A) The response of the scaffold to equibiaxial stress was assessed using planar biaxial testing. (B) Maximum strain of the scaffold at a stress of 250 kPa was quantified in the longitudinal and circumferential direction. (C) The suture retention strength of multi-laminate scaffolds was compared prior to in-vivo implantation. \* =  $p < 0.05$ , \*\* =  $p < 0.01$  .....122

Figure 16. Hydrogel turbidometric and rheological properties. (A) Two concentrations of coECM hydrogel, 4 and 8 mg/mL, were formed in a ring mold and compared macroscopically. Turbidometric analysis was used to measure the  $t_{lag}$  (B),  $t_{1/2}$  (C), and rate of gelation (D) of the hydrogel at two different concentrations. Parallel plate rheology was used to measure the viscosity of the pre-gel (E) and maximum storage modulus of the hydrogel (F). Scale bar = 1cm, \* =  $p < 0.05$ , \*\* =  $p < 0.01$  .....124

Figure 17. In-vitro cell response. (A) Intestinal epithelial cells cultured on coECM scaffold, coECM hydrogel, XL-coECM, and native submucosa were stained with LIVE/DEAD® cell viability dye and (B) the percentage of live and dead cells were quantified. (C) Bone marrow derived macrophages were cultured in the presence of enzymatically digested coECM and immunolabeled for F4/80 (pan macrophage), iNOS (M1), and Fizz1 (M2). Controls included MCSF (baseline), IFN $\gamma$  +LPS (M1), IL-4 (M2), and pepsin (digestion buffer). (D) The percentage of cells expressing the markers indicative of M1 and M2 phenotypes was quantified and compared. \*\* =  $p < 0.01$  .....126

Figure 18. Host response. The host response to coECM scaffold and hydrogel was compared in-vivo to XL-coECM and native submucosa in a rat abdominal defect model. (A) Representative H&E images show the histologic response at 14 and 35 days. (B) The combined histologic score at each time point was quantified and compared across groups. (C) The macrophage response at 14 days post surgery was analyzed by immunofluorescent staining for M2 indicator CD206 (green), M1 indicator CD86 (orange), and pan-macrophage CD68 (red). (D) The ratio of M2 (CD68+/CD206+) to M1 (CD68+/CD86+) was quantified and compared across groups. Dashed lines indicate interface between scaffold and underlying muscle. \* =  $p < 0.05$ , \*\* =  $p < 0.01$  .....128

Figure 19. Preparation and characteristics of ECM scaffolds. (A) Overview of decellularization process for preparing UBM, SIS, and eECM. (B) Gel chromatography of ECM materials showing features in banding patterns of different ECM materials. ....144

Figure 20. Migration of esophageal stem cells. (A) Representative images of DAPI stained migrating cells towards varying concentrations of ECM. (B) Quantification of migrated cells in response to ECM scaffolds.....	146
Figure 21. Capacity of ECM hydrogels to support organoid formation. (A) Comparison number of organoids formed in different ECM types. Data are normalized to the number of organoids formed in SIS. (B) Comparison of number of organoids formed in ECM at 2 mg/ml and 6 mg/ml. Data are normalized to the number of organoids present at 2mg/mL concentration of ECM .....	147
Figure 22. Cytokeratin immunolabeling. (A) Representative images of organoids formed in eECM. (B) Representative image of normal esophageal mucosa. Cytokeratin 14, a basal epithelial cell marker, is stained red. Cytokeratin 13, a marker of suprabasal epithelial cells, is stained green. Nuclei (DAPI) is shown blue. Scale bars = 50 $\mu$ m. ....	149
Figure 23. Proliferation of organoid cells. (A) Representative images of EdU stained organoids following 2h EdU exposure. EdU+ cells are shown in red. (B) Quantification of number of cells per organoid and number of EdU+ cells per organoid. Scale bar = 50 $\mu$ m. ....	150
Figure 24. Histology and immunolabeling of explants at 14 days post-surgery. The in-vivo host response to no treatment (A, D), UBM scaffold (B, E), and eECM (C, F) was assessed histologically with hematoxylin and eosin (H&E) staining and by immunolabeling for stratified squamous epithelium (cytokeratin 14, green). Blood vessel endothelial cells stain positive for cytokeratin 14. Arrows indicate positive staining and scale bars = 100 $\mu$ m.....	152
Figure 25. Schematic of experimental overview. Rats were administered 5% DSS in drinking water for 7 days to induce ulcerative colitis followed by daily enema treatments with either ECMH or the vehicle buffer (pepsin). Animals were sacrificed at days 7 and 14. ....	159
Figure 26. Material properties of ECMH. (A) ECMH material properties allow injection as a liquid and the subsequent gelation at 37°C ensures that the treatment remains localized. (B) Viscoelastic properties of ECMH, including storage modulus ( $G'$ ) and loss modulus ( $G''$ ), were measured with parallel plate rheology. (C) The biochemical and hydrogel properties were measured in 6 separate batches of ECMH. ....	171
Figure 27. ECMH is Mucoadhesive. Tensile tests show dose-dependent increase in adhesion strength of ECMH to healthy colon (A) and equivalent adhesion in healthy vs. diseased colon (B). The resident time of ECMH following enema delivery was tested with $^{14}$ C (C) and FITC-labeled ECMH (D).....	172
Figure 28. DSS-colitis model effectively induces disease. Weight change (A), the presence of blood in stool (B), and stool consistency (C) were tracked as clinical indicators of disease. Following 7 days of exposure to DSS, colon length (D) was measured as an indicator of disease severity and barrier dysfunction was measured by TRITC-dextran permeability (E). ....	173

Figure 29. ECMH Treatment Reduces Disease Activity. The effect of ECMH treatment on clinical symptoms (A-C), colon length (D), and gross score at explant (E) was tracked and compared to the vehicle (i.e., pepsin buffer) alone. ....174

Figure 30. Histologic Response to ECMH. Histomorphologic scoring of hematoxylin and eosin stained tissue sections was used to assess the effect of ECMH treatment on ulceration and inflammation extent. ....175

Figure 31. ECMH Treatment Lowers Histologic Score. Distal and proximal tissue sections stained with hematoxylin and eosin were scored by blinded investigators and compared with vehicle/pepsin buffer. The extent of inflammation and degree of ulceration were quantified at 7 days (A,B,E,F) and 14 days (C,D,G,H).....175

Figure 32. ECM Restores Barrier Function. TRITC-Dextran permeability assay show that the barrier function of ECMH-treated animals is similar to healthy animals while the colonic epithelial barrier in the vehicle-treated control group remain impaired compared to the healthy control (A). Differentiated and LPS-damaged monolayers of IECs respond to ECMH treatment in-vitro with functional recovery as shown by TEER readings (B). The increased barrier function is associated with an increased presence of E-cadherin compared with negative controls (C-D). ....177

Figure 33. ECMH Mediates Inflammation. Lamina propria cells exposed to ECMH results in lowered levels of TNF $\alpha$  (A) but didn't affect PGE2 production (B). Organ cultures, however showed ECMH had a significant impact on PGE2 levels (C). ECMH treatment led to a decrease in total number of M1, TNF $\alpha$  expressing macrophages (D).....179

Figure 34. Histologic images of SIS-ECM scaffolds. Decellularization of ECM devices was assessed histologically by hematoxylin and eosin (H&E) and 4',6-diamidino-2-phenylindole (DAPI) staining. Scaffolds prepared by the PBS protocol contained intact nuclei visible by H&E and DAPI staining (A,B). No intact nuclei were seen on scaffolds prepared following the 1 hr PAA protocol and 2 hr PAA protocol by H&E staining (C,E). While no DNA fragments were seen by DAPI staining in samples following the 2 hr PAA protocol (F), small fragments were seen in scaffolds following the 1 hr PAA protocol (D).....198

Figure 35. Concentration of remnant DNA in ECM scaffolds. The amount of DNA remaining in the ECM scaffolds prepared by varying methods was quantified as a marker of remaining cellular material. Dagger symbol indicates ECM prepared using the 1 hr PAA protocol contained the highest DNA concentration while, interestingly, ECM prepared using the PBS protocol showed lower levels of DNA. Asterisk indicates both of these levels were significantly higher ( $p < 0.05$ ) than ECM prepared using the 2 hr PAA protocol (B). DNA fragment length was assessed by gel electrophoresis using a reference 100bp ladder (A). ....199

Figure 36. Macrophage response in-vitro. In vitro immunolabeling images of macrophage phenotype. The macrophage response to ECM scaffolds was assessed in vitro using the RAW 264.7 macrophage cell line. Immunolabeling for M1, CCR7+, macrophages (orange)

and M2, CD206+, macrophages (green) showed that macrophages show distinct polarization profiles depending on the method of decellularization. On scaffolds prepared following the PBS and 1hr PAA protocols, macrophages showed high levels of CCR7+ staining (A, C) and lower levels of CD206+ staining (B, D). However, macrophages responded with a predominant M2 phenotype on scaffolds prepared using the 2hr PAA protocol with high levels of CD206+ staining (F) and little CCR7+ staining (E). Arrows indicate positive staining and scale bars= 50  $\mu$ m. ....201

Figure 37. Histologic and immunolabeling images of the tissue surrounding implant site at 14 weeks post-surgery. The in vivo host response to scaffolds prepared using varying methods of decellularization was assessed histologically with Masson’s Trichrome and hematoxylin and eosin (H&E) staining and by the immunolabeling of macrophages. Devices prepared using the PBS protocol (A-C) showed the highest levels of mononuclear cell infiltration with M1 cells (orange) predominating in a layer surrounding the ECM scaffold, while M2 cells were mainly located toward the anastomoses and in areas surrounding the ECM scaffold. Devices prepared using the 1hr PAA protocol (D-F) showed a similar distribution of macrophages, however, some M2 cells were observed surrounding the scaffold and the M2 cell distribution was more even than the PBS treated scaffold. Characterization of the polarized macrophages in the 2hr PAA treated scaffolds (G-I) showed that while M1 macrophages still predominated around the scaffold fibers, M2 macrophages were more evenly distributed throughout the scaffold rather than being limited to the margins of the wound as seen with PBS scaffolds. Immunohistochemical staining showed the presence of macrophages (red) in all scaffolds and used DRAQ5 (blue) as a nuclear stain. Calculation of the M1/M2 ratio (J) for PBS and 2hr PAA showed the macrophage response favored M2 while 1hr PAA favored M1 slightly. However, no treatment resulted in a significantly different macrophage profile. A M1/M2 value of 1 indicates equal amounts of cells expressing CCR7 and CD206. M1/M2 ratios above 1 indicates an M1 majority and below 1 is an M2 majority. Scale bars=50  $\mu$ m, asterisks=scaffold .....205

Figure 38. Overview of animal model and histologic evaluation schema. (A) Schematic of animal model and histologic cross section. The green “x” represents site of suture placement at corners of each device (yellow squares). The material is explanted en bloc and bisected. The histologic cross section depicts the rat abdominal wall defect, where the external and internal oblique is removed and replaced with a dermal ECM scaffold material. (B) Table describing the scoring system used to evaluate the histologic sections. (C) Schematic of histologic evaluation of explanted materials. Colored boxes represent the approximate location of 20X images used for histologic evaluation for each location.....222

Figure 39. Decellularization Quantification. Cellular content of dermis samples was assessed by three previously published criteria: (1) a Quant-iT Pico-Green assay for quantification of double-stranded DNA (A); (2) evaluation of a 2% agarose gel to determine the size of remaining DNA fragments (B); [23] the absence of visible nuclear material on hematoxylin and eosin (H&E) stained (C) and 40,6-diamidino-2-phenylindole (DAPI) stained sections (D).....224

Figure 40. Biochemical Composition. Concentration of basic fibroblast growth factor (bFGF) in urea–heparin extracts of samples were determined with the Quantikine Human FGF basic Immunoassay (A). All results were normalized to dry weight tissue. Assays were performed in duplicate on three independent samples for each treatment group. ....225

Figure 41. Scanning Electron Microscopy. SEM was used to examine the surface topology of each experimental group. SEM images were captured using a JEOL 6335F Field Emission SEM instrument with a backscatter detector. ....226

Figure 42. Mechanical Properties & Hydrostatic Porosity Index. The ball-burst test conducted in compliance with the Standard Test Method for Bursting Strength of Knitted Goods, Constant-Rate-of-Travel (CRT) Ball-burst Test (ASTM D 3787-89) (A). The suture retention test was performed according to ANSI/AAMI VP20–1994 Guidelines for Cardiovascular Implants-Vascular Prostheses (B). The hydrostatic PI was calculated by dividing the volume collected by the area of the porosity testing apparatus’ orifice, and the duration of the test (C). ....227

Figure 43. Cytocompatibility. HMEC were grown on each test article for 7 days and subsequently scored for cellular confluence, infiltration, and phenotype. ....228

Figure 44. In Vivo Remodeling Response. Following euthanasia, the skin was gently dissected, reflected, and photographs were taken of each animal and each test or control article *in situ* (A). The entire body wall that includes the test or control article was explanted *en bloc*. The sample was then cut in half and submitted for histological analysis. Masson’s Trichrome stained slides were mosaic imaged to illustrate the entire cross section of each test article at each time point (B). Additional slides were stained with H&E and imaged for histomorphologic analysis. Representative microscopic images (40x) were captured for each test article (C). ....229

Figure 45. Semi-Quantitative Histomorphologic Scoring. Semi-quantitative scoring of each interface of each device was conducted for cellularity (A), neovascularization (B), multinucleate giant cell formation (C), and material degradation (D). Four blinded individuals scored each image independently and the average score was used to compile the results. ....230

Figure 46. Macrophage Phenotype Assessment. Quantification of M1/M2 polarization was achieved using a custom image analysis pipeline developed using the cell profiler image analysis package. This custom pipeline identified and quantified the number of CD68<sup>+</sup>CD86<sup>+</sup> (M1 phenotype) and CD68<sup>+</sup>CD206<sup>+</sup> (M2 phenotype) cells present within the tissue sections. These numbers were then expressed as a ratio of M2/M1. Any cells that co-express the CD86<sup>+</sup> and CD206<sup>+</sup> markers were counted separately. ....231

## PREFACE

My doctoral studies in the Badylak laboratory have given me a breadth of experiences that were each valuable in my development as a scientist. I was intimately involved in basic science, preclinical studies, translation, and commercialization aspects of regenerative medicine. Dr. Stephen Badylak was an exceptional advisor and mentor throughout the years that I've spent in the lab. His perspective on translational focused research has given me a unique perspective, which has motivated my future plans as a scientist. I've learned and accomplished a great deal during my tenure in the lab and I thank him for fostering an environment that encourages collaboration and productivity.

The Badylak lab as a group has made countless contributions with their time, assistance, and advice that are too numerous to recount. Dr. Neill Turner ushered me into the lab as an undergraduate student and has been a constant source of advice and constructive feedback since. Dr. Chris Dearth, Dr. Peter Slivka, Dr. Lisa White, and Dr. Michelle Scarritt we're always supportive as mentors and friends who I could always count on frank advice and support from them when needed. Fellow graduate students Dr. Christopher Medberry, Dr. Brian Sicari, Dr. Matt Wolf, Dr. Denver Faulk, Dr. Ricardo Londono, Dr. Christopher Carruthers, Lisa Carey, Jenna Dziki, Catalina Pineda Molina, Lindsey Saldin, Mark Murdock, Yoojin Lee together were a friendly and fun group of lab members and I appreciate each of them. I also appreciate the patience, technical support, and guidance from Janet Reing, Li Zhang, Scott Johnson, Dr.

Jeremy Kelly, DLAR staff members, Lynda Guzik, Deanna Rhoads, and Lori Walton. Expertise and support from these individuals, as well as Jocelyn Runyon, Eve Simpson, Ally Lacovey, and Rachel Thomas both expedited and simplified my work.

My accomplishments in the lab were facilitated to a great degree by undergraduate and rotational students. I have had the opportunity to mentor several students who ultimately made invaluable contributions to my work. Arthur Castelon, Adam Smoulder, Eric Sobieski, Ryan Carey, Victoria Messerschmidt, Dan Cognetti, Dominic Pezzone, Jeremy Gale, and Nick Smith are all high potential scientists who I enjoyed working with.

The Swanson School of Engineering (Bevier fellowship), National Science Foundation (Graduate Research Fellowship), Asana Medical, Inc, and McGowan Institute for Regenerative Medicine provided the funding necessary to complete this work and I will always be thankful for this assistance.

Without family and friends, work would be without purpose. To my mother and father: thank you for supporting my development and always being there for me. They instilled the importance of integrity and hard work in life, and these are qualities I try to carry with me. Finally to my wife, Brogan: I am forever grateful for your love, support no matter the hour, dedication, and sacrifice. Your support has been essential to my success and everything that I do, including this body of work, is dedicated to you.

## **1.0 THE ROLE OF ECM IN GASTROINTESTINAL (GI) TRACT DEVELOPMENT & DISEASE**

### **1.1 ABSTRACT**

The extracellular matrix (ECM) represents a dynamic complex of structural and soluble components that play a vital and regulatory role in countless biological processes. ECM is synthesized and secreted by cells beginning at the earliest stages of development and continues throughout life in both health and disease. During embryonic development of the gut, ECM largely acts as a permissive substrate through asymmetries and spatiotemporal patterning of the ECM. Following development, however the role of ECM shifts from permissive to instructive. Dynamic reciprocity between cells and ECM results in a context-dependent composition of ECM. Tissue in a healthy state is composed of healthy ECM but a change to disease state confers changes to both the cellular and ECM components of the tissue. The present review considers the range of cell and tissue functions attributable to the ECM molecules during gastrointestinal tract development and in disease. The importance of ECM during gut development and morphogenesis is highlighted in addition to the often overlooked role of ECM in inflammatory bowel disease. The use of ECM for tissue engineering therapies in the gastrointestinal tract represents an emerging field of study.

## 1.2 INTRODUCTION

The extracellular matrix (ECM) represents the composite accumulation of structural and functional molecules secreted by the cells of every tissue and organ. In addition to the mechanical and structural functions of the ECM, extensive cell signaling activity occurs through a variety of soluble and insoluble molecular components. The resultant phenotypic changes in resident cells are manifestations of the essential role that the ECM plays in development, maintenance of normal tissue and organ function, the response to injury, and in the progression to neoplastic disease<sup>1-4</sup>. Stated differently, the ECM is not only a product of cell activity but a regulator of cell activity, and therefore central to tissue and organ health and disease.

The composition and structure of ECM changes with age and in response to alterations in the macro- and microenvironments<sup>5-8</sup>. The relationship between cells and the surrounding ECM, and the associated cross talk, has been aptly described as one of “dynamic reciprocity”<sup>9</sup>. The dynamic changes in matrix composition and organization that occur with normal tissue/organ development, or with abnormal conditions such as injury, inflammation or neoplasia, provide an opportunity to investigate and understand the drivers of such events and identify potential biomarkers and therapeutic targets. To a limited extent, such investigations have occurred with heart tissue<sup>10</sup>, skeletal muscle<sup>11</sup>, and liver<sup>12,13</sup>, but relatively little has been explored in the gastrointestinal tract. The focus of the present manuscript is to provide an overview of the role of the ECM during gut development and morphogenesis, and during pathology of the gastrointestinal (GI) tract. In addition, a discussion of the potential role of biologic scaffold materials composed of ECM for GI tract engineering and regenerative medicine is presented.

### 1.3 ROLE OF ECM IN GI TRACT DEVELOPMENT

Development of the GI tract is highly conserved across vertebrate species. The GI tract begins as a simple and uniform embryonic tube that differentiates along the anterior-posterior axis to form complex organs from the foregut, midgut, and hindgut regions. The foregut is the precursor of the pharynx, esophagus, stomach, liver, gall bladder, pancreas, and the proximal portion of the duodenum. The midgut gives rise to the posterior portion of the duodenum, the jejunum, ileum, the ascending colon, and two-thirds of the transverse colon. The hindgut is the precursor of the distal one-third of the transverse colon, the descending colon, and rectum<sup>14</sup>.

#### 1.3.1 *Germ Layer Contributions to the Histologic Structures of the GI Tract*

The hollow tubular organs of the GI tract have functions that range from a transit tube (esophagus) to digestion (stomach) to nutrient and water absorption (intestine), functions which require specialized cell types organized within distinct histologic layers. Although the inner layer (mucosa) of each GI segment has unique cellular structures, the histomorphology is similar along the GI tract with a distinct luminal mucosa, underlying submucosa, muscularis externa, and an abluminal adventia or serosa. The majority of the muscularis externa in the GI tract is bound by serosa with the exception of the thoracic esophagus, ascending colon, descending colon and the rectum where the muscularis externa is instead surrounded by adventitia<sup>15</sup>.

The histologic layers of the GI tract derive from all three germ layers and each germ layer contributes to the respective cell population and ECM constituents of the GI tract<sup>16</sup> (Figure 1) The majority of ECM mass in the GI tract arises from the mesoderm, which contributes to almost all layers beneath the mucosal epithelium, including the lamina propria, the submucosa,

vascular elements, muscularis externa, and the adventia and serosa<sup>17</sup>. Intestinal subepithelial myofibroblasts, although their germ layer lineage is uncertain, reside in the mesenchyme at the base of intestinal crypts and contribute largely to the ECM of the basement membrane between mucosal epithelium and subjacent lamina propria and muscularis mucosa<sup>17,18</sup>. The endodermal germ layer contributes to the majority of luminal structures of the GI tract including the mucosal epithelium, mucosal glands, and submucosal glands<sup>19</sup>. Lastly, while contributing to only a small portion of the GI tract, the ectoderm gives rise to the epithelium in the most proximal (mouth) and distal (anus) regions of the GI tract as well as the neural crest-derived submucosal and myenteric plexuses<sup>18</sup>.

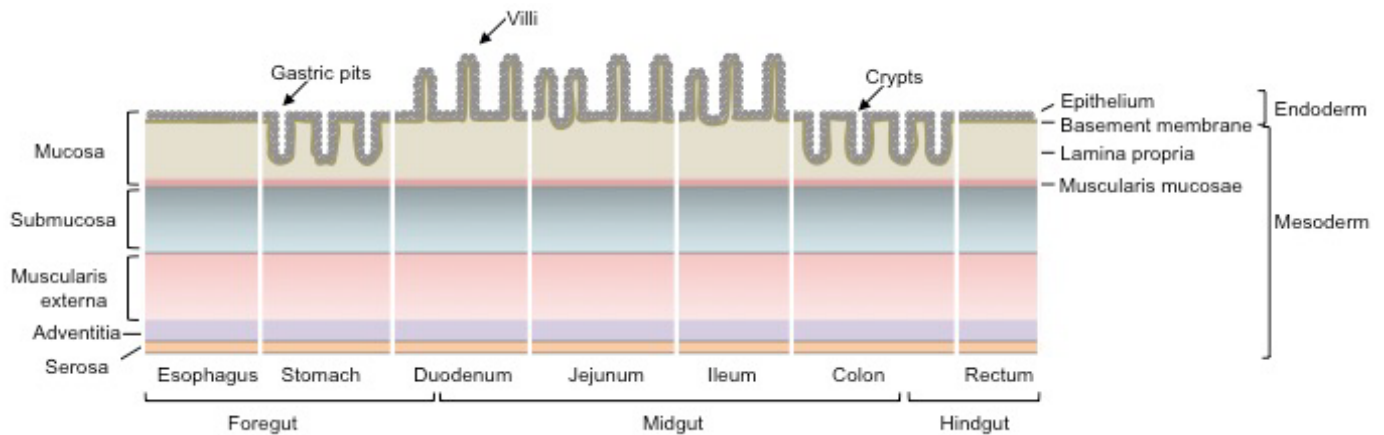


**Figure 1. Diagram depicting the origins, regions, and histology of the major segments of the GI-tract.** GI tissues that arise from the foregut include the esophagus, stomach, and the proximal portion of the duodenum. The midgut develops into the posterior portion of the duodenum, the jejunum, ileum, ascending colon and two-thirds of the transverse colon. The distal one-third of the transverse colon, and rectum arise from the hindgut of the embryonic tube. The epithelium of GI tissues, with its tissue-specific structures (e.g. gastric pits, villi, or crypts) is derived solely from the endoderm, whereas the basement membrane arises from both the endodermal and mesodermal germ layer. The remaining histological layers of GI tissues including the lamina propria of the mucosa layer, the submucosa, muscularis externa, adventitia, and serosa are mesodermal in origin.

### 1.3.2 *ECM Components in the GI Tract*

Although substantial progress has been made in the understanding of cellular and genetic mechanisms that drive morphogenesis of the GI tract<sup>16,18</sup>, the contribution of the ECM is not completely understood. Once simply thought of as a structural component to provide shape and strength, the ECM is now recognized as a dynamic regulator of cell phenotype and function and is in a constant state of remodeling as cells differentiate along their site-specific developmental pathways<sup>20</sup>. As with many tissues and organs, the ECM of the GI tract can be divided into two main functional compartments: basement membrane (BM) and interstitial ECM<sup>21-23</sup>. The BM is a specialized two-dimensional sheet-like ECM that separates the subjacent connective tissue from epithelia, forming an interface between tissues of endodermal and mesodermal origin, and is composed mainly of type IV collagen, laminin, entactin, nidogen and sulfated proteoglycans<sup>21,22</sup>. Although the epithelium is derived from the endodermal germ layer, the subepithelial BM has a dual origin from both the gut epithelia and mesenchymal cells. BM components are present at the epithelial/mesenchymal interface in early developmental stages and variations in the spatial distribution of ECM components contribute to morphogenetic processes such as cell migration and branching morphogenesis<sup>24</sup>. In contrast, the interstitial matrix surrounds cells in the stromal connective tissue and consists of both fibrillar structural components, such as fibronectin, type I collagen and elastin fibers that confer tensile strength and elasticity to the matrix, and non-fibrillar components such as mucopolysaccharides and glycosaminoglycans (GAGs) that confer structural support for mesenchymal cells<sup>21,23,25</sup>. Extensive crosslinking of GAGs and collagen provides for a three-dimensional gel like matrix which aids in compression and expansion and also may play a role in epithelial-mesenchymal cell interactions during stabilization of epithelial layers<sup>26</sup>.

### 1.3.3 *The Role of ECM During Gut Development*

In the fully developed adult GI tract, the molecular constituents of the BM and interstitial matrix are generally restricted to their respective compartments. However, during early development, BM proteins are transiently distributed throughout the mesenchyme. Studies utilizing inter-species tissue recombinations have shown that collagen type IV, a major component of the basement membrane, is produced by mesenchymal cells rather than cells of the epithelia<sup>27</sup>. The transient and widespread distribution of type-IV collagen within the mesenchyme is paralleled by other constituents of the BM including laminin, perlecan, entactin and nidogen<sup>24</sup>. These major BM components are present at the intestinal epithelial/mesenchymal interface during the early stages of intestinal development<sup>24</sup>. However, the mesenchymal origin of BM components is not necessarily a general phenomenon for the full repertoire of BM constituents. Although intestinal BM contains both laminin A and B chains, only laminin B chains are expressed within the mesenchymal interstitial matrix, suggesting an epithelial source for laminin A<sup>28</sup>. Similarly, the use of interspecies associations of rat and chick embryonic tissue shows that intestinal epithelial cells are the source of basement membrane heparan sulfate proteoglycans (HSPG)<sup>29</sup>. The distribution of HSPG at the epithelial-mesenchymal interface varies with the stages of intestinal development, suggesting that remodeling of this proteoglycan is essential for regulating cell behavior during morphogenesis<sup>29</sup>. These findings show the parallel, and likely dependent, development of epithelial differentiation and mesenchymal cell BM production<sup>24,30,31</sup>.

Although the expression of known ECM components in the ontogeny of the small intestine is similar for other segments of the digestive tract, the spatiotemporal distribution of these ECM components is not necessarily mirrored in all tissues of the gut. In the developing small intestine, for example, fibronectin expression occurs as early as 10 weeks of gestation and is followed by the expression of tenascin only after formation of differentiated epithelial cells lining the villi<sup>32,33</sup>.

Tenascin is a fibronectin antagonist contributing to the process of epithelial cell shedding<sup>34</sup>. In contrast, in the gastric mucosa, tenascin is co-expressed with fibronectin before gastric gland formation when the epithelium is composed mainly of undifferentiated cells<sup>35,36</sup>. The simultaneous expression of tenascin and fibronectin at this early developmental stage is unique to the gastric mucosa raising the possibility that these ECM components may play a differential role in the morphogenesis of the gastric mucosa compared to other tissues of the GI tract. This differential pattern of ECM expression and distribution throughout the gastric mesenchyme suggests that since GI layers have different origins, functions and fate, each may require a unique ECM composition and pattern of expression during morphogenesis of the individual organs of the gut.

Although a comprehensive analysis of the major ECM components of the entire alimentary canal, i.e. the esophagus through the anal canal, has not been reported for the developing fetal GI tract, a similar study has been reported for the adult GI tract<sup>37</sup>. Immunohistochemical analysis of type IV collagen  $\alpha$ -chains revealed a differential distribution of select  $\alpha$ -chains throughout the subepithelial BM. Type IV collagen is comprised of six genetically distinct  $\alpha$ -chains designated  $\alpha 1(IV)$  to  $\alpha 6(IV)$  which interact and assemble to form three heterotrimers of  $\alpha 1\alpha 1\alpha 2$ ,  $\alpha 3\alpha 4\alpha 5$ , and  $\alpha 5\alpha 5\alpha 6$ <sup>38</sup>. Whereas the  $\alpha 1$ ,  $\alpha 2$ ,  $\alpha 5$  and  $\alpha 6$  chains were shown to be expressed throughout the entire GI tract, the  $\alpha 3$  and  $\alpha 4$  chains are only expressed at restricted regions of the gastric and intestinal epithelium<sup>37</sup>. Compared to the other type IV heterotrimeric molecules, the  $\alpha 3\alpha 4\alpha 5$  heterotrimer forms a stronger network due to extensive disulfide bonds between cysteine residues in  $\alpha 3$  and  $\alpha 4$ <sup>39</sup>. Given the differential expression of  $\alpha 3$  and  $\alpha 4$  in the stomach and large intestine, the  $\alpha 3\alpha 4\alpha 5$  heterotrimer may confer site specific effects, possibly by acting as a selective permeability barrier in these regions<sup>37</sup>. Similarly, in the developing fetal GI tract, the spatial and temporal distribution of ECM components may also confer tissue-specific effects during morphogenesis of the different segments of the digestive tract.

Evidence shows that the BM is required to promote maximal gene transcription in epithelial cells. Cell culture studies using laminin-1 as a substratum showed that intestinal epithelial cells cultured on a laminin substrate resulted in increased expression of the enterocyte differentiation markers lactase and sucrase<sup>40</sup>. Similarly, lactase expression is inhibited using laminin-1 blocking antibodies in co-cultures of embryonic gut epithelial cells and mesenchyme-derived cells<sup>41</sup>. In addition to the physiologic role of ECM as a substrate for cell adhesion, *in silico* analysis suggests that during morphogenesis of the primitive gut tube, the counterclockwise coiling of the intestine is at least partially directed by asymmetries in the composition of the ECM<sup>42</sup>. Despite these findings, evidence to support a direct and instructive role of ECM in promoting terminal differentiation is lacking in developmental models. In short summary, although it is clear that the ECM is essential and required for normal gut development, it appears that the ECM plays more of a permissive rather than proactive role in morphogenesis allowing for critical epithelial-mesenchymal cell interactions and the establishment of cytokine and growth factor paracrine signaling<sup>16,43-35</sup>. This hypothesis is reflected in studies using Null mice harboring deletions of major ECM components and integrin receptors. Although not critically examined for intestinal effects, these studies failed to provide any obvious indication of a significant proactive influence of individual ECM components on GI morphogenesis<sup>16,46</sup>. In addition, studies have shown that single matrix molecules do not allow survival or elicit terminal differentiation of intestinal epithelial cells, a process which is only triggered by viable mesenchymal or fibroblastic cells<sup>43</sup>. However, before a conclusive opinion can be drawn on the permissive role of ECM in development, additional studies are required to determine if the intricate temporal and spatial changes of the ECM observed during gut morphogenesis are a result of developmental reorganization, or if they directly confer instructive signals to mediate enterocyte differentiation during GI morphogenesis.

## 1.4 ROLE OF ECM REMODELING IN GASTROINTESTINAL TRACT DISORDERS

Given the vital role of ECM during development and tissue homeostasis, it follows that disease can arise when ECM components are dysregulated. Abnormal ECM is present in diseased conditions and reflects the important role of ECM in controlling cell behavior. While it is speculated that ECM is largely a permissive factor in development, the role of the ECM is more instructive thereafter. Since healthy ECM instructs healthy cell phenotypes, it is logical and plausible that ECM dysregulation can promote or initiate disease progression and maintain a disease state<sup>47,48</sup>.

### 1.4.1 *Inflammatory Bowel Disease (IBD)*

IBD, which includes ulcerative colitis and Crohn's disease (CD), is a worldwide health problem. The debilitating, chronic relapsing disease consists of acute flares followed by periods of healing<sup>49</sup>. The specific etiology of IBD is unknown but genetic predisposition and immunologic factors are known contributors. Generally, IBD is characterized by an aberrant immune response and defects in intestinal epithelial cell barrier function<sup>50</sup>. Tissue damage associated with IBD has long been considered a downstream effect of disease and not a contributing factor. This interpretation has led to development of numerous treatments that solely target inflammation, but all treatments to date far have shown limited efficacy. While its role is often overlooked, the ECM is a critical component of intestinal inflammation and progression of IBD.

Macroscopic tissue damage and clinical signs of IBD are preceded by changes in the ECM. Changes in collagen microarchitecture and thickening of ECM at crypts are evident in the colonic mucosa of patients with IBD<sup>51</sup>. IBD can progress in diametrically opposing directions based on the balance of ECM deposition or degradation. For example, CD can advance towards

stricturing or penetrating disease. Stricturing disease, or fibrostenosis, is the result of excess ECM deposition<sup>52-54</sup>. In contrast, penetrating disease is characterized by ECM destruction and fistulae formation<sup>54</sup>, thereby underscoring the central role of ECM in IBD (Figure 2).

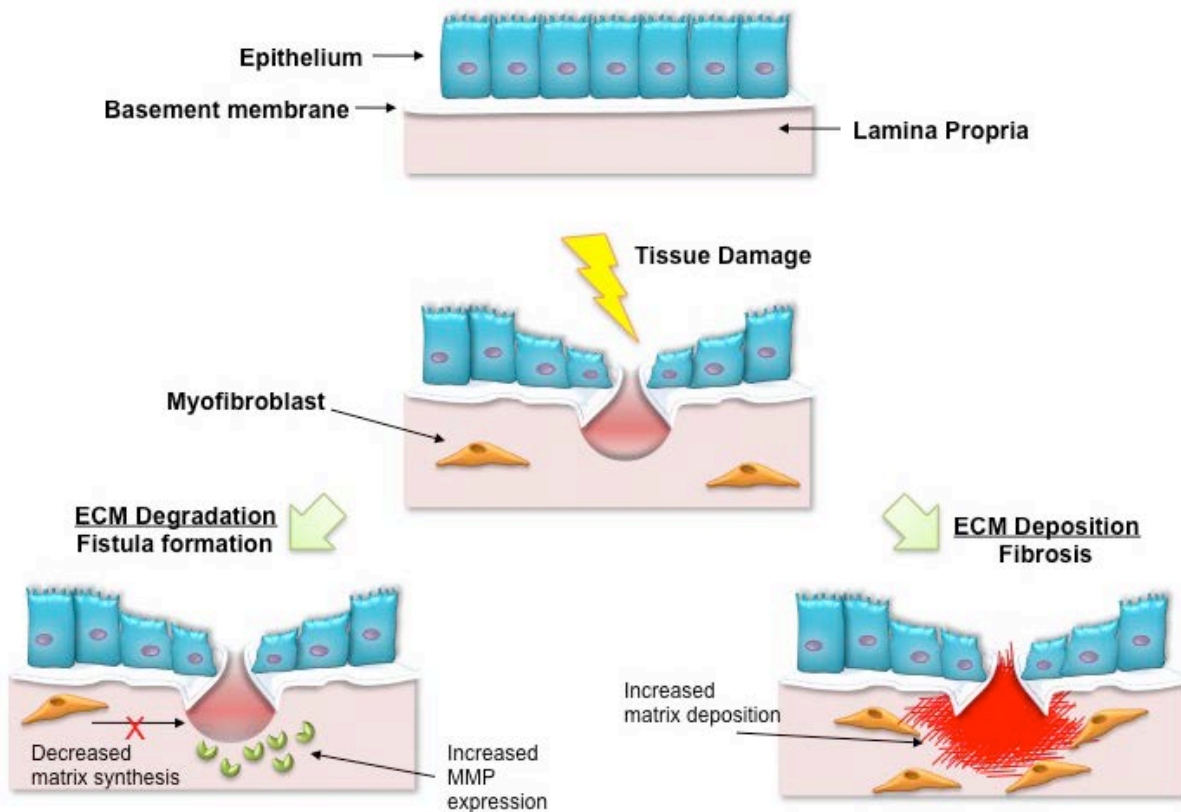


**Figure 2. Schematic representation of normal intestinal wound healing, fistula formation, and fibrosis.** In response to tissue damage, regulated production and degradation of ECM results in physiologic wound healing but IBD can progress in opposing directions based on the balance of ECM deposition or degradation. Fibrosis is characterized by excess ECM deposition that results from the coupling of increased number of ECM-producing myfibroblasts with increased cell proliferation and decreased apoptosis. In contrast, ECM destruction, mediated largely by MMPs, and decreased myfibroblast involvement leads to fistulae formation.

ECM remodeling enzymes, such as matrix metalloproteinases (MMPs), have long been studied in the context of IBD. Most MMPs are stimulated in response to pro-inflammatory cytokines, cell-cell, or cell-ECM interactions<sup>55</sup>. Collagenases (MMP-1, -8), gelatinases (MMP-2 and -9), stromelysins (MMP-3), matrilysin (MMP-7), and macrophage elastase (MMP-12) are all upregulated in IBD and are among the most studied in the context of CD and UC<sup>56-59</sup>. Notable examples of the effect of these matrix remodeling enzymes can be seen with the gelatinase MMP-2 and MMP-9. Although MMP-2 is commonly associated with tissue homeostasis, MMP-9 is highly expressed in pathologic scenarios and has been implicated as a disease biomarker<sup>60-63</sup>. The gelatinases act on ECM by digesting denatured collagens as well as collagen type IV thus contributing to loss of BM integrity, increased permeability and cell invasion<sup>64</sup>. High levels of MMP-9 also inhibit wound healing, in part due to modulating ECM-cell interactions and preventing epithelial cell adhesion<sup>65</sup>. MMP-3, another proteinase considered pivotal for tissue damage in IBD, acts on a wide range of ECM substrates (e.g., proteoglycans, types IV, V, IX, and X collagens, laminin, and fibronectin)<sup>66-68</sup>. Not surprisingly, based on its ability to degrade ECM, expression of MMP-3 has been associated with fistulae formation in patients with CD<sup>69</sup>. Both MMP-9 and MMP-3 contribute to tissue damage and mediate inflammation in patients with IBD. Together, these data suggest a vital role for ECM remodeling in IBD pathogenesis rather than simply a consequence of inflammation.

The individual components of ECM, in addition to their role in structural support and tissue maintenance, are active participants in intestinal inflammation. For example, hyaluronic acid (HA) is an abundant GAG in the ECM and its degree of polymerization is indicative of ECM integrity. Small fragment HA is deposited throughout the inflamed colon in IBD and leads to innate immune cell activation<sup>70,71</sup>, while high-molecular weight HA has been shown to have therapeutic effects on experimental colitis<sup>72</sup>. In addition to HA, other ECM components have been shown to contribute to innate immunity, such the interaction of the proteoglycan Lumican with toll-like receptor 4. As

shown in mouse models, when Lumican is absent, animals react to colitis with a dampened immune response, increased morbidity, and tissue damage<sup>73,74</sup>. Given the pivotal role of ECM in progression of IBD, development of novel targeted therapeutic approaches may benefit by focusing on restoration of ECM integrity and homeostasis in addition to the more typical approaches of immunomodulation.

#### **1.4.2 Fibrosis**

Intestinal injury is a common occurrence, even in healthy individuals, and one that is invariably followed by acute inflammation. Acute inflammation triggers a highly regulated wound healing process that resolves with two possible endpoints: reconstitution of normal tissue morphology or fibrosis. In most cases, rapid restoration of intestinal structure and function occurs and the inflammatory response abates. However, if unresolved, acute inflammation progresses to chronic inflammation, which can lead to excessive deposition of ECM proteins and associated fibrosis.

Intestinal fibrosis is common amongst IBD patients and the location and extent of fibrosis is commensurate with the frequency and chronicity of the inflammatory response<sup>52,75,76,77</sup>. Fibrosis occurs in 5% of patients with UC, and typically remains confined to the mucosa and submucosa, and is associated with motility disorders and colonic shortening<sup>78</sup>. In CD, fibrosis extends throughout the depth (thickness) of the bowel and can lead to strictures and intestinal obstruction. Fibrosis arises in greater than 30% of patients with CD and this prevalence is likely due to extensive ECM deposition<sup>52,75,76,77</sup>.

Fibrosis is the downstream consequence of an altered balance between ECM production and ECM degradation. In the intestine, multiple cell types have been proposed as potential

precursors of ECM-producing myofibroblasts including mesenchymal cells, epithelial and endothelial cells, and stem cells, among others<sup>78</sup>. Myofibroblasts are activated by paracrine and autocrine factors, pathogen associated molecular patterns (e.g., enteric microbiota), and damage associated molecular pattern molecules (e.g., DNA, RNA, ECM fragments)<sup>79-82</sup>. These ECM-producing cells act in concert and in response to biologic mediators of fibrosis. Intestinal healing depends upon restoration of the balance between pro-fibrotic and anti-fibrotic mediators. The most widely studied pro-fibrotic factor, TGF- $\beta$ , is critical for fibrogenesis in multiple organs, including the intestine, and TGF- $\beta$  has been shown to be highly up regulated in fibrotic CD<sup>79,83</sup>.

Fibrosis progression is characterized by the coupling of increased number of ECM-producing cells with increased cell proliferation and decreased apoptosis<sup>79-81</sup>. Altered ECM degradation (e.g., imbalance of MMPs and TIMPs) is another factor contributing to fibrosis<sup>60</sup>. TIMP-1, for example, is overexpressed in CD fibrosis and plays a combined role in preventing ECM degradation and inhibiting myofibroblast apoptosis<sup>84</sup>.

Despite advances during the past two decades in development of anti-inflammatory drugs, the prevalence of fibrosis in IBD patients has remained largely unchanged. While chronic inflammation triggers fibrosis, it is likely that other cellular and molecular pathways exist that contribute to the fibrotic response. It is noteworthy that certain chronic inflammatory diseases of the intestine, such as celiac disease or lymphocytic colitis, are not complicated by fibrosis. The regulation of ECM remodeling in these non-fibrotic diseases, in comparison to IBD, may provide clues as to the pathogenesis of intestinal fibrosis and identification of potential therapeutic targets.

### 1.4.3 **Cancer**

Extracellular components of the cancer microenvironment play a critical role in tumor initiation, progression and invasion<sup>85</sup>. The highly regulated temporal and spatial deposition of ECM during embryonic development and tissue/organ homeostasis is markedly altered during cancer progression as changes in the biochemical composition and ultrastructure of ECM strongly influence both tumor and stromal cell properties<sup>86,87</sup>. As with fibrosis and IBD, the inflammatory response in the tumor microenvironment has been shown to facilitate neoplastic progression in GI tissues. Chronically inflamed tissue in the GI tract, such as with Barrett's Esophagus (BE), and chronic intestinal or gastric inflammation are highly susceptible to tumor formation due to the increased expression of ECM remodeling enzymes<sup>88,89</sup>. The integrity of the BM has been shown to be extensively impaired in digestive cancers, and is affected by both the synthesis of new components from contributing epithelial and stromal cells, and degradation from proteolytic factors. These breaches in the BM are often located at the invasive front and are associated with epithelial–mesenchymal transition<sup>90,91</sup>. Numerous studies have shown that the increased expression and activity of ECM-degrading enzymes are critical determinants of cell migration and metastasis, as the BM forms an early natural barrier in the process of tumor cell invasion<sup>92,93</sup>. As a result, proteolytic degradation of the BM is one of the main mechanisms of malignant tumor metastasis. This process is orchestrated by the increased expression of MMPs, thereby facilitating the invasion of tumor cells. For instance, studies have shown that compared to normal colorectal tissue, expression of MMP-2 and -9 are elevated in colorectal cancer, and are characteristic of a high invasion and metastatic potential associated with advanced stages of malignancy<sup>94</sup>. Similarly, increased expression of MMP-1, -3, -7, and -10 have been shown to be increased in the progression BE to esophageal adenocarcinoma<sup>195</sup>.

The effect of stromal cells on the tumor microenvironment are most evident in Scirrhus Gastric Carcinoma (SGC) which, when diagnosed, has the worst prognosis of all gastric cancer types due to rapid expansion and peritoneal dissemination. In SGC, cancer-associated fibroblasts have been shown to play a crucial role in ECM remodeling<sup>96</sup>. *In vitro* experiments have shown that SGC cells and fibroblasts form aggregates capable of inducing extensive contraction and mechanical remodeling of the ECM, an event associated with increased actomyosin-mediated mechanical remodeling of ECM<sup>97</sup>. Other innate characteristics of stromal fibroblasts, including expression of  $\alpha$ -smooth muscle actin and increased contractility, contribute to fibrosis in tumor tissue resulting in remodeling and strengthening of the stromal ECM, events which are favorable for invasion and metastasis of carcinoma cells<sup>98-100</sup>. Overall, these results underscore the critical role that ECM plays in GI developmental processes, and in the progression of disease states.

## 1.5 FUTURE PERSPECTIVES

### 1.5.1 *Role of ECM in Tissue Engineering of the GI Tract*

ECM signaling molecules mediate rapid and functional remodeling of GI tract tissues. Preclinical and human clinical studies conducted during the past 15 years have shown that various forms ECM can facilitate a constructive and functional regeneration in the GI tract, specifically, the esophageal mucosa<sup>101,102</sup>. ECM bioscaffolds were shown to prevent scarring/stricture, restore epithelial and submucosal tissue, and preserve/restore normal esophageal motility in both preclinical animal models and human patients<sup>101</sup>. The results of this clinical concept pilot study strongly suggest that ECM signaling molecules induce a fundamental change in the default

healing response from the expected inflammation/scarring response toward a restorative “tissue formation” paradigm. At least two mechanisms contribute to this positive outcome: stem/progenitor cell recruitment (including proliferation, mobilization, and differentiation) and modulation of macrophage phenotype toward an anti-inflammatory/regulatory effector cell type. ECM materials therefore exhibit promising therapeutic properties for pathologies of the GI tract, especially inflammatory conditions such as IBD where immunomodulation and tissue healing are critical for positive outcomes<sup>103</sup>.

Biomaterials derived from decellularized tissues represent naturally occurring ECM-based scaffolds consisting of molecules secreted by the resident cells of all tissues and therefore, the composition of ECM scaffolds varies depending on tissue source. ECM scaffolds have been prepared from multiple regions of the GI tract, including esophagus<sup>104</sup>, small intestine<sup>105</sup>, and colon<sup>106</sup>. There are a number of potential therapeutic benefits of ECM scaffold materials derived from homologous tissue versus heterologous tissue<sup>107-113</sup>. The necessity or preference for site-specific ECM remains unknown for many tissue engineering applications, including those in the GI tract. While tissue specificity may not be necessary for all therapeutic applications<sup>114,115</sup>, studies have shown that site-specific ECM can preferentially maintain tissue-specific cell phenotypes<sup>107-109</sup>, promote cell proliferation<sup>109-110</sup>, induce tissue-specific differentiation<sup>111,116</sup>, and enhance the chemotaxis of lineage-directed progenitor cells<sup>112,113,117</sup>. In the esophagus, site-specific ECM has favorable characteristics that enhance the migration of esophageal stem cells and supports the formation of 3D esophageal organoids to a greater extent than heterologous ECMs<sup>118</sup>. ECM scaffolds derived from GI tissues therefore provide a novel platform for studying mechanisms of tissue repair and can inform future regenerative medicine therapies.

## 1.6 CONCLUSIONS

The ECM plays both permissive and instructive roles during gut morphogenesis, maintenance of healthy tissue, and in the response to injury in adults. The concept of dynamic reciprocity which describes the continuous cross talk between cells and matrix, and the influence of external factors that affect the microenvironmental niche, is central to the understanding of the role of the ECM in GI tract health and disease. While most interest in the GI tract has been cell-centric, the ECM component of the gut offers opportunities for understanding development and disease, identification of biomarkers of disease, and potential therapeutic targets. Tissue engineering/regenerative medicine efforts have shown promising early results in the esophagus. Possible applications of ECM scaffolds for the remainder of the GI tract remain to be explored.

## 2.0 THE ECM AS A BIOLOGIC SCAFFOLD FOR TISSUE ENGINEERING APPLICATIONS<sup>1</sup>

### 2.1 ABSTRACT

With advancements in biological and engineering sciences, the definition of an ideal biomaterial has evolved over the past 50 years from a substance that is inert to one that has select bioinductive properties and integrates well with adjacent host tissue. Tissue engineering (TE) combines the principles of engineering and biology and generally involves the use of some combination of the following: biomaterials, cells, and bioactive molecules<sup>2</sup>. The appropriate contribution of each factor depends upon the application in question, the strategy for tissue replacement, and patient variables such as age, co-morbidities, and other factors. Biomaterials are a fundamental component of tissue engineering, which aims to replace diseased, damaged, or missing tissue with reconstructed functional tissue. This chapter focuses on the role of extracellular matrix as a biomaterial for tissue engineering applications.

---

<sup>1</sup> Portions of this chapter were adapted from the following publication:  
**Keane TJ**, Badylak SF. Biomaterials for Tissue Engineering Applications. Seminars in Pediatric Surgery, June 2014. DOI:10.1053/j.sempedsurg.2014.06.010

## 2.2 INTRODUCTION

Scaffold materials for tissue engineering/regenerative medicine can be broadly classified as either synthetic or naturally occurring in origin. Regardless of their origin, such scaffold materials are intended to support the attachment, maintenance, proliferation, and on occasion the differentiation of selected cell populations. In addition, the scaffold must provide adequate form and structural support for the intended anatomic site. These requirements are non-trivial and to make matters even more challenging, the host response to the presence of the material within the mammalian body must be one that allows for functional replacement of the injured or missing tissue over the life of the patient. This is particularly important in pediatric patients in whom the scaffold must adapt to the growth and development of the surrounding tissues and organs.

It can be argued that the most important measure of a scaffold material is not its composition, shape, mechanical properties, porosity, or ability to support cell growth, but rather the host response to the scaffold material. Regardless of how ideal the material looks and feels at the time of implantation, the true measure of success is how the material looks and feels 1, 5, and 10 years after implantation. There are pros and cons for each material and the optimal scaffold material for each clinical application will vary. Stated differently, one size does not fit all. The present chapter provides a brief overview of common strategies for scaffold design and development in the field of tissue engineering/regenerative medicine, with emphasis on the role of the ECM in tissue engineering applications.

## 2.3 BIOMATERIALS FOR TISSUE ENGINEERING

Tissue engineering (TE) combines the principles of engineering and biology and generally involves the use of some combination of the following: biomaterials, cells, and bioactive molecules<sup>2</sup>. The appropriate contribution of each factor depends upon the application in question, the strategy for tissue replacement, and patient variables such as age, co-morbidities, and other factors. TE strategies can include both in-vitro and in-vivo approaches, and the optimal approach for each clinical application will continue to evolve as advances in stem cell biology, biomaterial science, and bioreactor technology occur. Biomaterials play an important, in fact indispensable, role in the field of TE. Biomaterials have been used for centuries for applications such as intraocular lens replacement and dental fillings, but advancements in cell and molecular biology, chemistry, materials science, and engineering have provided much broader opportunities for clinical use.

The definition of the ideal biomaterial has changed considerably during the past 50 years and, in fact, will vary between given applications<sup>3</sup>. In early biomaterial design, the goal was to match mechanical and material properties, and to achieve a level of functional outcome that adequately matched the native tissue without invoking tissue damage or a deleterious host response. For example, bone cement, stainless steel, and Dacron were used extensively in early biomaterials because they were considered to be relatively inert and incited a predictable but tolerable foreign body response. Furthermore, these materials had favorable mechanical properties. Second-generation biomaterials included materials such as titanium, bioglass, PLGA, and collagen. These materials were engineered for biologic use and have bioactive properties that include osseointegration (titanium, hydroxyapatite), tissue integration (Bioglass), and biodegradation (PLGA, collagen). Many of the aforementioned materials maintain clinical relevance, but the field of TE is rapidly moving toward the use of biomaterials that integrate with

adjacent tissue and are bioinductive; that is, materials that enhance the regenerative or reconstructive capacity of a given tissue or organ. Stated differently, these materials are polar opposite to the “inert” biomaterials of 50 years ago.

A number of biomaterials for TE are available for various clinical applications (**Table 1**). The use of biomaterials should be used in an application-specific nature; that is, a biomaterial that achieves success in one application should not necessarily be expected to perform well in an application that is very different. For example, with pediatric patients a biomaterial should degrade over time or have the capability change shape and size so the engineered tissue can grow with surrounding tissue. Further, if a scaffold is biodegradable the biomaterial must provide adequate mechanical support during the time of scaffold remodeling <sup>4</sup>.

### ***2.3.1 Improving Synthetic Biomaterials***

Given the advantage of manufacturing reproducibility with synthetic materials, a large amount of research has been directed at methods enhance bioactivity. One such approach is to mimic the biochemical composition of native ECM. Many of the remodeling functions are associated with a number of protein motifs. A variety of ECM-derived adhesion peptides have been incorporated within scaffolds for improved cell adhesive properties. These peptides are derived mainly from ECM proteins, including fibronectin <sup>5-9</sup>, laminin <sup>10-14</sup>, collagen <sup>14-20</sup>, and elastin <sup>6,21,22</sup>. A peptide sequence commonly used to modify a scaffold's cell adhesion properties is RGD, a binding domain present in laminin, collagen, and fibronectin <sup>23,24</sup>. By controlling the spatial arrangement of cell binding domains, such as RGD, materials can have cell specific adhesion properties that are essential for tissue regeneration.

**Table 1. Clinically Available Biomaterials for Tissue Engineering**

<b>Product</b>	<b>Description</b>	<b>Application</b>	<b>Company</b>
Apligraf®	Allogeneic fibroblasts on a bovine collagen I matrix with upper keratinocyte cell layer	Skin	Organogenesis
Oasis® Wound Matrix	Decellularized porcine small intestinal submucosa	Skin	Cook Biotech
Integra® Bilayer Wound Matrix	Type I bovine collagen with chondroitin-6-sulfate and silicone	Skin	Integra Life Sciences
Epicel®	Autologous keratinocyte cell sheets	Skin	Genzyme
REGRANEX®	PDGF within a hydrogel	Skin	Healthpoint Biotherapeutics
Carticel®	Autologous chondrocytes	Cartilage	Genzyme
NeoCart®	Autologous chondrocytes on type I bovine collagen	Cartilage	Histogenics
Pura-Matrix™	Hydrogel composed of a self-assembling peptide (RADA)	Bone	3DMatrix
INFUSE® Bone Graft	Recombinant human BMP-2 absorbed in a bovine type I collagen sponge	Bone	Medtronics
Omniflow® II	Polyester mesh with cross-linked ovine collagen	Blood vessels	Binova
Anginera™	Allogeneic fibroblasts on vicryl mesh	Cardiac	Theregen
CardioWrap®	Membrane composed of a copolymer of 70% L-lactide and 30% D,L-lactide	Cardiac	MAST Biosurgery, Inc.
CryoValve® SynerGraft Pulmonary Heart Valve	Decellularized allogeneic pulmonary valve	Cardiac	Cryolife
Encapsulated Cell Technology implant	Polysulfone capsule with PET scaffold containing immortalized retinal epithelial cells	Retinal	Neurotech Pharmaceuticals

Another important functional cue provided by ECM is proteolytic degradation. An optimal rate of scaffold degradation, which will vary between tissues, should be slow enough to provide a support for cellular growth but fast enough to not impede the reconstructive process. A biochemical method employed for altering biomaterial degradation profiles involves incorporation of peptides sensitive to cleavage by enzymes<sup>25</sup>. These peptides have been designed with cleavage sites that are recognized by enzymes including matrix metalloproteinases<sup>26-34</sup>, plasmin<sup>28,29</sup>, and elastase<sup>35</sup>.

Processes vital to tissue regeneration, such as cell migration, differentiation, and proliferation, are dependent on both the presence of specific growth factors as well as their spatial and temporal distribution. Growth factors and peptides derived from growth factors have been coupled to biomaterials to promote nerve regeneration<sup>36,37</sup>, cell proliferation and migration<sup>38</sup>, osteogenesis<sup>39,40</sup>, enhanced cell viability, and angiogenesis in ischemic tissues<sup>41</sup>. A number of biomaterials for growth factor delivery are commercially available. Some examples include INFUSE® Bone Graft (Medtronic) which delivers bone morphogenetic protein 2 (BMP2) for degenerative disc disease, and REGRANEX® (Healthpoint Biotherapeutics), which delivers a recombinant human platelet-derived growth factor (PDGF) known as becaplermin in a hydrogel vehicle for treating diabetic ulcers in lower limbs.

A number of physics-based approaches have been investigated for controlling biologic processes. Micro- and nanofabrication technologies made it possible to pattern surfaces with very detailed features<sup>42-45</sup> including controlled shape<sup>46-48</sup>, mechanical properties<sup>49,50</sup>, and surface topology<sup>51</sup>. The physical characteristics of particles, in turn, have been linked to many essential cellular processes. For example, particle shape at the point of initial contact with macrophages determines whether or not a macrophage initiates phagocytosis<sup>46</sup>. In addition, the size of features on patterned substrates has been shown to determine whether cells undergo

apoptosis<sup>52</sup> or directed cell differentiation<sup>53</sup>. These examples show that even in the absence of biologic activity, particle shape, patterning, and surface topology can direct cellular processes.

The mechanical properties of a tissue have an important role in tissue morphogenesis<sup>54</sup>. Likewise, substrate mechanical properties have a profound effect on cell and tissue behavior. Changing the elastic properties of the substrate that mesenchymal stem cells were cultured upon can facilitate neuronal, myogenic, or osteogenic differentiation dependent upon substrate stiffness<sup>55</sup>. In addition, mechanical properties have been shown to alter immune functions, such as macrophage phagocytosis<sup>56</sup> and dendritic cell activation<sup>57</sup>.

Clearly, improvements in micro and nano-scale manufacture have led to an improved understanding of cellular processes. However, the mechanism that mediates cell recognition of material cues is still poorly understood. Therefore, the possibility to display a single signal or an array of signals at the cell–material interface to elicit a given cell response is still a distant goal<sup>58</sup>.

### **2.3.2 Naturally Derived Biomaterials**

Naturally derived materials include polymers such as silk and chitosan, purified ECM-based molecules including collagen, elastin, and GAGs. While clinical use of biomaterials from natural materials, such as alginate (PhytaCare™) and chitosan (HemCon™) as wound dressings and silk (Ethicon) as suture material, these biomaterials alone lack the signaling functions and mechanical and spatial cues that native ECM contain.

### 2.3.3 *The ECM as a Bioscaffold for Tissue Repair*

Rather than attempting to mimic the native ECM physical and biochemical composition by synthetic methods, an alternative is to decellularize tissues and use the resulting ECM as biologic scaffold. By definition, allogeneic and xenogeneic biologic scaffold materials are composed of ECM. The ECM represents the secreted product of the constituent cells in every tissue. The composition and ultrastructure of ECM is a function of the factors that influence the phenotype of these resident cells such as mechanical forces, biochemical milieu, oxygen concentration, and inherent gene expression patterns. The ECM is in a state of dynamic reciprocity with the cells that reside within it; that is, the ECM provides biosignaling and biophysical cues which influence the resident cells that, in turn, adjust their gene and protein expression patterns to produce a secretome that optimizes the surrounding matrix for cell survival and function<sup>59,60</sup>. This complex mixture of structural and functional molecules is arranged in an ultrastructure that is tissue specific. These molecules comprise the ligands that are arranged in patterns that are ideally suited for the particular cell types present within each tissue. Stated differently, the ECM represents Mother Nature's ideal scaffold material.

The most abundant protein within mammalian ECM is collagen. Over 20 forms of collagen have been described but Type I collagen, the major structural protein present in tissues, is the most prevalent form of collagen in ECM<sup>61</sup>. Other forms of collagen, such as Type III, Type IV and Type VII are present in lesser quantities and provide distinct mechanical and physical properties. Second to collagen in quantity within the ECM is fibronectin. Fibronectin is a dimeric molecule and exists in soluble and insoluble isoforms. The insoluble isoform is an important ECM component that regulates the adhesion, migration, growth, and differentiation of many cell types and mediates processes such as wound healing<sup>62</sup>. Another protein with a well-recognized role in cell-matrix interactions is laminin<sup>63</sup>.

In addition to proteins, the ECM contains various mixtures of glycans. Glycans, including glycosaminoglycans and proteoglycans, are molecules which swell in the aqueous spaces between protein fibrils and allow diffusion of nutrients<sup>64</sup>. Finally, ECM serves as a reservoir for a variety of signaling molecules and growth factors such as vascular endothelial growth factor, transforming growth factor beta, basic fibroblast growth factor, among others. These factors typically exist in inactive forms in the ECM and are preserved to a different extent in most bioscaffolds composed of ECM<sup>65</sup>. When the ECM scaffold degrades, these signaling molecules and growth factors are released. These degradation products have been shown to attract<sup>66</sup> and affect the proliferation of stem cells<sup>67</sup>. However, the specific roles of these various ECM components in remodeling and host response outcomes following ECM scaffold implantation are completely unknown.

The constituent molecules of ECM are highly conserved amongst mammalian species. Basement membrane components, for instance, are among the most highly evolutionarily conserved proteins<sup>68-70</sup>. Basement membranes represent ECM structures which are composed of polymeric sheets of laminin, collagen IV, and associated proteins. Basement membrane structures are found on the basal surface of epithelia and provide both a substrate for cell attachment and a barrier to cell mixing during embryonic development<sup>71</sup>. High cross-species homology has been shown for collagens<sup>72,73</sup>, fibronectin<sup>74</sup>, as well as certain glycosaminoglycans<sup>74,75</sup> and growth factors<sup>76</sup>. Stated differently, ECM constituents in mammalian species are very similar and therefore elicit a similar response when implanted as an allogeneic or xenogeneic bioscaffold.

ECM scaffolds derived from decellularized tissues provide a natural structure that has proven successful in a number of TE applications<sup>77-79</sup>. The ECM from varying species and tissue

sources has been used to repair or replace tissues including vascular<sup>80-83</sup>, tracheal<sup>84,85</sup>, cardiac<sup>86-89</sup>, skeletal muscle<sup>90,91</sup>, and esophageal tissues<sup>92-96</sup>, among others<sup>97-99</sup>. Such allogeneic or xenogeneic sources are commercially available (Table 2), and as expected the composition of ECM scaffolds varies depending on tissue source<sup>100</sup>.

## **2.4 TISSUE SPECIFICITY OF ECM**

Tissue sources from which ECM scaffolds are prepared include humans (allografts) and porcine, bovine, or equine tissue (xenografts). Whether the ECM is derived from allogeneic or xenogeneic species, the composition of ECM constructs is affected by donor state (e.g., age, disease state). Further, the anatomic site of the raw material source has a strong influence upon the device mechanical and material properties, the methods required for adequate decellularization and sterilization, and the eventual host response.

The composition, ultrastructure, and mechanical properties of ECM derived from different tissues/organs are distinct; a logical finding since each tissue/organ has a unique function. For example, ECM derived from small intestinal submucosa has a preferred collagen alignment that leads to anisotropic mechanical behavior of the scaffold, with the preferred (longitudinal) fiber direction showing greater stiffness and strength than the circumferential direction<sup>101</sup>. The collagen fiber alignment of the urinary bladder submucosa and tunica propria, in contrast, shows a much more isotropic fiber alignment than SIS<sup>102</sup>. An understanding of the mechanical properties from different tissues may be an important consideration for matching the choice of ECM source tissue with a specific clinical application.

**Table 2.** Source tissue and species of commercial biologic scaffold materials

Product	Species	Tissue	Application	Company
<b>AlloMax™</b>	Human	Dermis	Soft tissue	Bard Davol
<b>AlloPatch HD™</b>	Human	Dermis	Tendon, breast	Musculoskeletal Transplant Foundation
<b>NeoForm™</b>	Human	Dermis	Breast	Mentor Worldwide LLC
<b>GraftJacket®</b>	Human	Dermis	Soft tissue	KCI
<b>Axis™</b>	Human	Dermis	Pelvic organ prolapse	Coloplast
<b>Strattice™</b>	Porcine	Dermis	Soft tissue	Lifecell Corp.
<b>TissueMend®</b>	Bovine	Dermis	Soft tissue	Stryker Corp.
<b>Avaulta®, CollaMend®</b>	Porcine	Dermis	Soft tissue	Bard Davol
<b>Veritas®, Dura-Guard®, Peri-Guard®</b>	Bovine	Dermis	Soft tissue	Synovis Surgical
<b>Suspend™</b>	Human	Fascia lata	Pelvic organ prolapse	Coloplast
<b>Hancock® II, Mosaic®, Freestyle®</b>	Porcine	Heart valve	Valve replacement	Medtronic Inc.
<b>Prima Plus</b>	Porcine	Heart valve	Valve replacement	Edwards Lifesciences LLC
<b>Epic, SJM Biocor®</b>	Porcine	Heart valve	Valve replacement	St. Jude Medical Inc.
<b>IOPatch™</b>	Human	Pericardium	Ophthalmology	IOP Inc.
<b>OrthAdapt®, Unite®</b>	Equine	Pericardium	Soft tissue, chronic wounds	Synovis Orthopedic and Woundcare Inc.
<b>CopiOs®</b>	Bovine	Pericardium	Dentistry	Zimmer Inc.
<b>Lyoplant®</b>	Bovine	Pericardium	Dura mater	B. Braun Melsungen AG
<b>Perimount®</b>	Bovine	Pericardium	Valve replacement	Edwards Lifesciences LLC
<b>Permacol™</b>	Porcine	Porcine dermis	Soft tissue	Tissue Science Laboratories
<b>Oasis®, Surgisis®</b>	Porcine	Small intestine	Soft tissue	Cook Biotech Inc
<b>Restore®</b>	Porcine	Small intestine	Soft tissue	DePuy Orthopaedics
<b>FortaFlex®</b>	Porcine	Small intestine	Soft tissue	Organogenesis Inc.
<b>CorMatrix ECM®</b>	Porcine	Small intestine	Pericardium, cardiac tissue	CorMatrix® Cardiovascular Inc.
<b>CuffPatch™</b>	Porcine	Small intestine	Rotator cuff	Athrotek
<b>Surgisis®, Durasis®, Stratasis®</b>	Porcine	Small intestine	Soft tissue	Cook SIS
<b>MatriStem®</b>	Porcine	Urinary bladder	Soft tissue	Acell Inc.

The properties of biologic scaffolds also vary with the age of the source animal from which the tissue is harvested. Fetal and neonatal mammals have greater wound healing and regenerative capacity compared to adult mammals <sup>103</sup>. The composition of fetal and neonatal ECM is distinctly different from that of adults and plays an important role in tissue development <sup>104</sup>. In fact, distinct remodeling characteristics exist that are attributable to source animal age. Biologic scaffolds harvested from neonatal animals have been shown to promote a more robust constructive remodeling response when compared to scaffolds derived from market weight and older animals <sup>105</sup>.

The ECM is said to be in a state of dynamic reciprocity with the resident cells; that is, the ECM provides signaling and biophysical cues that influence the cell morphology and phenotype. In turn, the cells modify their secreted ECM products in response to microenvironmental signals including mechanical stimuli, oxygen and nutrient concentration, and all factors that contribute to the microenvironmental niche <sup>59</sup>. Dynamic reciprocity between ECM and resident cells can also be involved in disease progression. For example, healthy colon ECM and CRC-derived ECM have been shown to differentially regulate tissue homeostasis and tumorigenesis <sup>106</sup>. The presence of 'healthy ECM,' therefore, is essential to normal tissue functions. Similarly, in patients with IBD, changes in quantity and distribution of matrix metalloproteinases (MMPs) has been reported in previous studies. For example, MMP2 and MMP9 are upregulated in the colon of individuals with IBD <sup>107</sup>. However, a separate study has shown that 'healthy' ECM is able to downregulate MMP2 and MMP9 production in macrophages <sup>108</sup>. It is plausible that such a mechanism may remediate negative effects of colitis.

Recent work has described potential benefits of ECM scaffold materials derived from homologous tissue versus heterologous tissue when used in selected anatomic locations <sup>109-118</sup>. However, the necessity or preference for site-specific ECM remains unknown for many therapeutic applications. While tissue specificity may not be necessary for all therapeutic

applications <sup>92,119,120</sup>, some studies have shown that site-specific ECM can preferentially maintain tissue-specific cell phenotypes <sup>109-112</sup>, promote cell proliferation <sup>111,113</sup>, induce tissue-specific differentiation <sup>114</sup>, and enhance the chemotaxis of lineage-directed progenitor cells <sup>115-117</sup>. Zhang et al have shown that ECM derived from liver, skin, and skeletal muscle increases the proliferation and differentiation potential for site-matched cell types <sup>113</sup>. Sellaro and colleagues have shown that ECM derived from liver improves the maintenance of sinusoidal endothelial cell phenotype <sup>109</sup> and the function of hepatocytes in-vitro <sup>110</sup>. More recently, porcine myocardial ECM has been shown to improve cardiac progenitor cell function in-vitro <sup>112</sup>. Seif-Naraghi et al have shown that injection of a hydrogel form of cardiac ECM after myocardial infarct improves cardiac function and results in increased cardiac muscle mass <sup>89</sup>.

## **2.5 MECHANISMS OF ECM MEDIATED CONSTRUCTIVE REMODELING**

The fundamental role of a biomaterial in tissue remodeling is to provide structural support and a microenvironmental niche that modulates cell attachment and cell behavior. Nature's template for such a biomaterial is the extracellular matrix (ECM); the material secreted by resident cells in every tissue and organ. Once thought to exist for the primary purpose of providing structural support to tissues, the ECM is now known to consist of a complex milieu of both structural and functional molecules that have a dramatic effect upon cell behavior <sup>59,121</sup>. The ECM provides not only physical support and spatial organization, but also a bioactive microenvironment that directs and influences cell functions. The ECM consists of structural proteins (e.g., collagen and elastin), cell adhesion proteins (e.g., fibronectin and laminin), and glycans (e.g., glycosaminoglycans (GAGs) and proteoglycans). Glycans swell in the aqueous spaces between protein fibrils, allowing the diffusion of nutrients and providing a reservoir for signaling molecules

and growth factors <sup>64</sup>. During tissue regeneration or in response to injury, the ECM is subject to extensive and continuous remodeling. Proteolytic degradation of the ECM, as part of the remodeling process, provides morphogenic cues in the form of cryptic peptides which influence cell survival, proliferation, migration, polarization, and differentiation <sup>59,122-125</sup>. Inductive scaffolds composed of ECM promote functional tissue remodeling by providing structural support and cell signaling cues.

### ***2.5.1 ECM-mediated remodeling of the Gastrointestinal Tract***

Implantation of biologic scaffolds has led to constructive remodeling in various regions of the GI tract. Dramatic advancements have come through study of the esophagus. In both preclinical and clinical studies, biologic scaffolds composed of ECM have been shown to facilitate reconstitution of normal mucosa in the esophagus. In a preclinical model, critically sized, circumferential defects were repaired with minimal stricture formation and near-normal restitution of the esophageal histomorphology when adjacent autologous muscle tissue was placed in direct contact with an ECM scaffold at the time of surgery <sup>93</sup>. A follow-up preclinical study of esophageal transection, designed to reinforce the anastomosis of a “gastric pull-up” procedure, showed restoration of a mature epithelium and regeneration of muscle tissue that bridged the gap between the native muscle tissue on both sides of the surgical site <sup>94</sup>. The successful use of ECM was then extended to a preclinical model of aggressive endoscopic resection <sup>95</sup>. Based upon these preclinical findings, five human patients with diseased esophageal mucosa (i.e., Barrett's esophagus and high grade dysplasia and/or mucosal adenocarcinoma) were subjected to a long segment, circumferential resection of the mucosa and submucosa of the esophagus, and an ECM scaffold material was placed over the site of the resected tissue. The ECM scaffold induced restoration of normal mature squamous epithelium,

and allowed return to a normal diet without significant dysphagia for all patients. This most recent study provided proof of concept in the clinical setting. We found that a minimally invasive endoscopic procedure for treatment of diseased mucosa is possible when combined with the use of a biologic scaffold material to promote reconstruction of functional mucosa<sup>92,126</sup>.

## **2.6 INJECTABLE VS. IMPLANTABLE ECM**

Historically, ECM has been largely used as an implantable physical scaffolding to bridge a defect site. In these cases, diseased or defective tissue is removed and the ECM scaffold is subsequently placed at the site of tissue resection to induce remodeling of new tissue. However, recent studies suggest that this paradigm is only one means by which ECM scaffolds can be utilized. Hydrogels can be prepared from ECM scaffolds by enzymatic digestion followed by physiologic balancing of salt and pH. Such hydrogels have been shown to be deliverable by non-invasive methods and serve as a template for tissue repair. The work of Christman et al. indicates that injectable ECM hydrogels can serve as a template for cardiac repair following myocardial infarct (MI). During MI, a blockage in a coronary artery causes cell death followed by an acute inflammatory response. The ECM hydrogel was able to mitigate the harsh inflammatory milieu following MI, providing an appropriate environment and a physical scaffold to encourage repair and regeneration. This concept—mitigating inflammation and promoting remodeling—serves as the foundation to support the use of an ECM hydrogel as a non-invasive method to treat UC

### 3.0 PREPARING BIOMATERIALS FROM DECELLULARIZED TISSUES<sup>2</sup>

#### 3.1 ABSTRACT

Biologic scaffolds composed of extracellular matrix (ECM) are widely used in both preclinical animal studies and in many clinical applications to repair and reconstruct tissues. Recently, 3-dimensional ECM constructs have been investigated for use in whole organ engineering applications. ECM scaffolds are prepared by decellularization of mammalian tissues and the ECM provides natural biologic cues that facilitate the restoration of site appropriate and functional tissue. Preservation of the native ECM constituents (i.e., three-dimensional ultrastructure and biochemical composition) during the decellularization process would theoretically result in the ideal scaffold for tissue remodeling. However, all methods of decellularization invariably disrupt the ECM to some degree. Decellularization of tissues and organs for the production of ECM bioscaffolds requires a balance between maintaining native ECM structure and the removal of cellular materials such as DNA, mitochondria, membrane lipids, and cytosolic proteins. These remnant cellular components can elicit an adverse inflammatory response and inhibit constructive remodeling if not adequately removed. Many variables including cell density, matrix density, thickness, and morphology can affect the extent of tissue and organ decellularization and thus the integrity and physical properties of the

---

<sup>2</sup> Portions of this chapter were adapted from the following publication:  
**Keane TJ**, Swinehart I, Badyak SF. Methods of Tissue Decellularization Used for Preparation of Biologic Scaffolds and In-vivo Relevance. *Methods*, March 2015. DOI:10.1016/j.ymeth.2015.03.005

resulting ECM scaffold. This chapter reviews currently used processing techniques for preparation of ECM scaffolds.

### 3.2 INTRODUCTION

Biologic scaffold materials composed of extracellular matrix (ECM), and derived via decellularization of source mammalian tissues, are widely used for clinical applications that involve repair and reconstruction of musculoskeletal tissues, cardiovascular structures, lower urinary tract, gastrointestinal tract, and central nervous system, among others<sup>89,92,127-130</sup>. Such scaffold materials have the potential to promote and facilitate “constructive remodeling” processes that form vascularized, innervated, functional tissue. Mechanisms by which these constructive remodeling events occur include the recruitment and differentiation of stem/progenitor cells<sup>66,67,110,131</sup> and modulation of the innate immune response<sup>132-134</sup>. The effector molecules responsible for these processes represent a combination of sequestered cytokines and chemokines within the matrix, and matricryptic peptides generated or exposed during the process of ECM degradation<sup>67,135-137</sup>. Thorough decellularization of source tissues to generate the ECM scaffolds is critical for realization of the full potential of these ECM mediated events. Failure to effectively decellularize the tissue results in retained cell remnants, which can act in a manner similar to damage associated molecular pattern molecules (DAMPs) following tissue injury. Ineffective decellularization has been shown to be associated with an intense inflammatory response which can mitigate or completely inhibit a constructive remodeling outcome<sup>138</sup>.

All methods of decellularization disrupt the structure and composition of the ECM. The goal of tissue decellularization is thorough removal of cells and cell remnants while retaining the three dimensional ultrastructure and composition of the native ECM to the extent possible. Optimal methods of decellularization vary among tissues and organs due to tissue-specific factors such as cell density, matrix density, and geometric considerations including tissue thickness and shape. Complete removal of all cell remnants is not possible, and decellularization processes inevitably and invariably cause some disruption of matrix architecture, orientation, and surface ligand landscape. The specific cellular elements that elicit adverse and proinflammatory responses are only partially known. One objective of the present manuscript is to provide guidance as to the effects of various decellularization methods upon both the resulting biologic scaffold and the associated host remodeling response and outcome. Decellularization methods described include mechanical, chemical, detergent, and enzymatic techniques, or combinations thereof. **Table 3** provides an overview of decellularization processes used for various tissues and organs and the effects of those processes on ECM constituents and the host response.

**Table 3.** Decellularization techniques used for various tissues

<b>Tissue/Organ Type</b>	<b>Decellularization Technique</b>	<b>Effects on ECM and Host Response</b>	<b>References</b>
<b>Laminate</b>			
Pericardium Urinary Bladder Intestine Amnion Dermis	Freeze/thaw, mechanical removal of undesirable layers, brief exposure to acids/bases, rinse. Thicker laminates may require longer exposure to remove cellular debris.	Cellular remnants can elicit an adverse immune response. Microstructure and ultrastructure will be altered. Increased exposure times may damage collagen, reduce GAG and growth factor content.	139-142
<b>Amorphous Organs</b>			
Adipose Brain	Freeze/thaw, mechanical disruption, alcohol/solvent treatment, exposure to acid/base, rinse.	Alcohols required for lipid solubilization crosslink collagen and increase tissue stiffness.	116,143,144
<b>Composite Tissues/Organ Fragments</b>			
Trachea Nerve Testes Uterus	Freeze/thaw, osmotic solutions, detergent treatment, enzymatic treatment, rinse.	Detergents can reduce growth factor content, denature and loosen collagen network. Residual detergent may effect cell migration and remodeling.	145-150
<b>Whole Vital Organs</b>			
Liver Lung Kidney Pancreas	Freeze/thaw, perfusion of decellularization solutions.	Pressure associated with perfusion can disrupt ECM. Vascular basement membranes will be affected by solutions used for decellularization.	151-156

### 3.3 DECELLULARIZATION AGENTS AND TECHNIQUES

Decellularization protocols have been described for nearly every tissue in the body. The decellularization methods must be tuned to the tissue of interest and ultimately the intended use of the decellularized tissue. It is not uncommon for vastly different protocols, with varied detergents and delivery methods, to be described for decellularization of the same tissue.

### 3.3.1 **Physical methods**

3.3.1.1 **Freeze-thaw:** Numerous studies have used multiple freeze-thaw cycles as a method for cellular disruption. This technique can minimize the amounts of chemical agents required for effective decellularization. It has been shown that freeze-thaw cycles do not significantly alter the mechanical properties of the ECM <sup>157,158</sup>. Freeze-thaw cycles produce minor disruptions in the tissue ultrastructure. To minimize adverse effects on tissue architecture without impeding cell lysis, the use of a cryoprotectant such as 5% trehalose has been suggested <sup>159</sup>.

3.3.1.2 **Agitation and immersion:** One of the most commonly used techniques for tissue decellularization is immersion in chemical, detergent, and/or enzymatic solutions with mechanical agitation. Protocols have been described for numerous tissues, including urinary bladder <sup>160,161</sup>, esophagus <sup>162,163</sup>, trachea <sup>84,164</sup>, skeletal muscle <sup>165,166</sup>, heart valves <sup>167,168</sup>, peripheral nerve <sup>169</sup>, spinal cord <sup>116,170</sup>, cartilage <sup>171,172</sup>, and dermis <sup>173,174</sup>. The length of time for each protocol is dependent upon factors such as the degree of agitation and mechanical disruption, the concentration and type of chemical/detergent/enzyme used, and the source tissue thickness and density. Thin tissues such as the urinary bladder or small intestine may be readily decellularized by agitation over a short period of time (e.g., 1-2 hours) of exposure to relatively mild peracetic acid. For thin tissues in particular, the degree of cellular removal is a function of the aggressiveness of agitation <sup>175</sup>. More dense tissues such as dermis and trachea require much longer exposure (e.g., 12-72 hours) to combinations of solutions of enzymes, alcohols, and/or detergents with constant agitation.

**Table 4.** Esophageal tissue decellularization protocols

<b>Species</b>	Rats (Fischer)	Pig (newborn)	Rats (Wistar)	Pig	Pig
<b>Form</b>	Intact full thickness	Intact full thickness	Intact full thickness	Intact full thickness esophagus	Mucosa and submucosa
<b>Method of delivery for decellularization agent</b>	Immersion and agitation rate = N/A	Immersion	Immersion and agitation rate = N/A	Luminal perfusion, rate = 0.6mL/min	Immersion and agitation on rotating shaker rate = 300 rpm
<b>Summary of decellularization protocol</b>	<b>48h</b> 10mM Tris <b>48h</b> 1% Triton X-100 <b>6h</b> 400 U/ml DNase-I/ .125 mg/ml RNase-A <b>48h</b> .5% SDS	5 cycles of: <b>72h</b> distilled water, <b>4h</b> 4% deoxycholic acid, <b>3h</b> 2,000 kU DNase-I	<b>24h</b> 4% deoxycholic acid, <b>12h</b> .2 mg/ml DNase-1	3 cycles of: <b>24h</b> deionized water, <b>4h</b> 4% deoxycholic acid, <b>3h</b> 2,000 kU DNase-I	<b>1h</b> 1% trypsin/ .05% EDTA, <b>30min</b> 1M sucrose, <b>48h</b> 3% Triton X-100, <b>4h</b> 10% deoxycholic acid <b>2h</b> .1% peracetic acid/4% Ethanol <b>2h</b> 100 U/ml Dnase-I
<b>Evaluation of decellularization efficacy</b>	<ul style="list-style-type: none"> <li>No nuclei present on H&amp;E-stained section</li> </ul>	<ul style="list-style-type: none"> <li>No nuclei present on H&amp;E-stained section</li> <li>Lack of MHC antigens</li> </ul>	<ul style="list-style-type: none"> <li>No nuclei present on H&amp;E-stained section</li> <li>DNA concentration: 140 ng/mg</li> </ul>	<ul style="list-style-type: none"> <li>No nuclei present on H&amp;E-stained section</li> <li>DNA concentration: 500 ng/mg</li> </ul>	<ul style="list-style-type: none"> <li>No nuclei present on H&amp;E- and DAPI-stained sections</li> <li>DNA concentration: 50 ng/mg</li> </ul>
<b>Reference</b>	Bhrany, 2006	Marzaro, 2006	Ozeki, 2006	Totellini, 2012	Keane, 2012

A number of protocols have been described to achieve decellularization of esophageal tissue. These protocols have varied combinations of detergents and enzymes to achieve the same goal of decellularization (Table 4). Ionic detergents are used in each of the published protocols. Bhrany et al <sup>176</sup> used an SDS-based solution while Marzaro et al. <sup>163</sup>, Ozeki et al <sup>177</sup>, Totonelli et al <sup>178</sup>, and Keane et al <sup>162</sup> used a 4% sodium deoxycholate solution as the main

decellularization agent. Each of the protocols also required an endonuclease (DNase and/or RNase) to remove residual nucleic acids. It is noteworthy that the measurement of decellularization efficacy used in each study was unique and common criteria were not used. Decellularization efficacy is discussed in more detail in a later section. Undoubtedly, the resultant esophageal ECM for each protocol was distinct and unique. The “optimal” technique will depend upon the intended use of the ECM scaffold and upon factors such as cytocompatibility and intended clinical application.

**Table 5.** Effects of decellularization on tissue mechanical properties

Tissue source species	Pig	Pig	Rat
<b>Delivery method of decellularization agent</b>	Immersion	Immersion and agitation on rotating shaker at 300 RPM	Immersion
<b>Summary of protocol</b>	17 cycles of: <b>48h</b> Deionized water <b>4h</b> 4% deoxycholic acid <b>4h</b> 2,000 kU DNase-I	<b>48h</b> 3% Triton X-100 <b>2h</b> .1% peracetic acid/4% Ethanol	2 cycles of: <b>4h</b> 4% deoxycholic acid <b>3h</b> 50kU/ml DNase-1 <b>41h</b> Deionized water
<b>Measured effects on mechanical properties</b>	<ul style="list-style-type: none"> <li>Maintained strain ability similar to native trachea</li> <li>Decrease in tracheal volume compared to native trachea</li> </ul>	<ul style="list-style-type: none"> <li>Increased tissue compliance compared to native trachea</li> </ul>	<ul style="list-style-type: none"> <li>Maintained strain ability similar to native trachea</li> <li>Decreased elastic modulus compared to native trachea</li> </ul>

Immersion and agitation protocols have also been investigated for the decellularization of tracheal tissue. However, compared to the esophagus, effective decellularization of the trachea is challenging due to the presence of hyaline cartilage rings. As a result, the protocols described by Remlinger et al.<sup>84</sup>, Jungebluth et al.<sup>179</sup>, Zang et al.,<sup>180</sup> and Haykal et al.<sup>181</sup> result in a tracheal matrix that contains residual chondrocyte material within the tracheal rings. These groups propose that decellularization reduces antigenicity (measured by the reduction or loss of

MHC antigens) of the scaffold to a degree that allows tissue remodeling to occur. Each of the protocols also results in measureable alternations to the tissue mechanics (Table 5). Whether these effects are critical to the clinical use is debatable as Macchiarini et al <sup>182</sup> adapted the protocol described by Jungebluth et al <sup>179</sup> and showed that implantation of decellularized human tracheal ECM reseeded with autologous airway epithelial and bone marrow cells provides for mechanical properties that allow relatively normal function in the immediate post operative period and absence of evidence for classic tissue rejection. Elliott et al <sup>183</sup> also reported the successful use of a similar construct in a pediatric patient. At two years post-surgery, the patient had a functioning airway with the construct exhibiting appropriate growth thereby eliminating the need for future surgical interventions <sup>183</sup>.

**3.3.1.3 Use of pressure for decellularization:** Pressure gradients can be applied to tissue during decellularization to accelerate and improve the efficiency of delivering cell-lysing agents into the tissue and forcing cellular debris out of the tissue. For hollow tissues such as blood vessels and the intestinal tract, luminal perfusion with a pressure gradient can be useful. Montoya et al <sup>184</sup> compared the use of luminal perfusion vs. agitation alone in the decellularization of umbilical veins. The study showed that the pressure-based decellularization process with a flow rate of 50 mL/min with pulse frequency of 2 Hz removed all cells from the tissues as determined by histologic examination. In contrast, traditional rotary agitation (100 RPM) showed retention of whole cells and cellular components. This study also showed that the use of a pressure gradient compared to passive diffusion techniques has only minor effects on the mechanical properties and molecular components of the resulting ECM construct. Bolland et al <sup>185</sup> have used a pressure gradient to decellularize urinary bladder tissue by combining immersion and agitation with cyclic bladder distension. The authors showed that cytoskeletal

components of the smooth muscle cells are maintained but the basement membrane components are removed during the decellularization process.

High hydrostatic pressure has been reported as a method that can eliminate or reduce exposure time to harsh detergents in the decellularization of tissues. At a controlled temperature, Funamoto et al <sup>186</sup> decellularized porcine blood vessels by immersion in saline and subsequent exposure to increasing pressure up to 980 MPa. Normal atmospheric pressure was then reestablished by step-wise reduction of pressure. Sasaki et al <sup>187</sup> similarly decellularized porcine cornea using high hydrostatic pressure of over 1,000 MPa. Both studies showed that the use of high pressure led to more effective removal of cellular components when compared to detergent-based methods under normal atmospheric conditions. DNA content in tissues decellularized by detergent-based methods ranged from 0.3-2.3 µg/mg, but after high hydrostatic pressure decellularization, corneas and blood vessels contained 0.1 µg/mg and undetectable levels of DNA, respectively <sup>186,187</sup>. High hydrostatic pressure has been shown to reduce GAG content to a greater degree than immersion/agitation methods <sup>188,189</sup>. It is necessary to avoid the freezing phase when using high hydrostatic pressure in order to maintain native ECM structure. Studies have shown that the pressurization effect damages both collagen and elastin fibers and alters their mechanical properties <sup>190</sup>.

**3.3.1.4 Supercritical fluids for decellularization:** A recently described method of tissue decellularization utilizes the unique properties of a supercritical fluid. The low viscosity and high transport characteristics of a supercritical fluid allow for simple and short decellularization protocols. The advantages of supercritical decellularization include the use of an inert substance (e.g. carbon dioxide) for cell removal and minimal alteration of ECM mechanical properties. Further, tissues can be obtained in a dry condition following decellularization and thus eliminate

the need for lyophilization; a commonly used technique to facilitate long term storage. Carbon dioxide forms a critical fluid under moderate conditions (at a temperature of 32°C and pressure of 7.4 MPa) and has been shown to effectively remove cells from aortic tissue after only 15 minutes when placed in an ethanol solution <sup>191</sup>. The widespread applicability of supercritical fluids for decellularization of other tissues remains to be determined.

### 3.3.2 *Chemical and biologic agents for decellularization*

**3.3.2.1 Alkalines and Acids for decellularization:** Solutions at an extreme pH can increase the efficacy of cell removal but can impart substantial changes to the ECM constituents.

Tomoshi et al <sup>192</sup> have shown that increasing the pH of an 8 mM CHAPS solution during lung decellularization increases the effectiveness of cell and cytoskeletal protein removal. However, highly alkaline CHAPS (pH 12) disrupted ECM architecture and resulted in a more fibrotic response compared to the lungs (less effectively) decellularized in 8mM CHAPS at pH 8 and pH 10 following subcutaneous implantation. The use of acidic or alkaline solutions during decellularization therefore requires a balanced approach to achieve effective decellularization without severe detriment to the ECM constituents.

Alkaline bases denature chromosomal and plasmid DNA. Commonly used alkaline bases include ammonium hydroxide, sodium sulphide, sodium hydroxide, and calcium hydroxide <sup>173,193-196</sup>. Such compounds have been used in the decellularization of dense tissues such as dermis <sup>173,193</sup>, but alkalines are likely to degrade structural component of the matrix including collagen to some degree. Sheridan et al <sup>195</sup> used 0.5M NaOH and sonication to controllably degrade small collagen fibrils of decellularized pig arterial tissue to increase access of cells during the recellularization process. Mendoza-Novela et al <sup>197</sup> showed that a calcium oxide treatment results in a dramatic reduction in GAG content and altered viscoelastic

properties of pericardial tissue. The use of bases in a decellularization procedure can also eliminate growth factors from the resulting ECM and reduce mechanical properties of dermal ECM constructs <sup>142</sup>.

Acids are used to dissociate DNA from the ECM by solubilizing cytoplasmic components and disrupting nucleic acids. Acids can also denature ECM proteins including GAGs, collagen, and growth factors. It is important to optimize the dose and exposure time when acids are used for decellularization. Peracetic acid, applied at 0.1% (v/v) in a single wash for 2 hours, and combined with appropriate mechanical methods and rinsing, can thoroughly decellularize thin tissues such as small intestinal submucosa and urinary bladder matrix (UBM). Acids commonly used for decellularization include deoxycholic acid and acetic acid <sup>177,198</sup>. However, acetic acid has been shown to cause damage and removal of collagens from ECM with a corresponding reduction in construct strength <sup>199</sup>.

**3.3.2.2 Non-ionic detergents:** Non-ionic detergents are generally considered to be gentle detergents that solubilize proteins while maintaining native protein structure and enzymatic activity. However, success in achieving effective decellularization varies with non-ionic detergents such as X-100 <sup>196,200-206</sup>, likely as a result of differences in source tissue composition and architecture. For example, in attempts to decellularize aortic valve tissue, Grauss et al <sup>207</sup> reported little to no cell removal for 1-5% Triton X-100 treated rat aortic valve, while Liao et al <sup>208</sup> showed effective decellularization of porcine aortic valve using 1% Triton X-100. These results highlight the fact that differences in tissue density and cellularity require a decellularization process that is adapted to the tissue of interest and there is no “one size fits all” decellularization process. While commonly considered to be preferred detergent for decellularization procedures <sup>209 210</sup>, like all decellularization agents, Triton X-100 alters properties of ECM, including the

formation of a more open collagen network in anterior cruciate ligament ECM <sup>211</sup> and removal of GAGs in pericardial tissue <sup>212</sup>.

**3.3.2.3 Ionic detergents:** Ionic detergents are strong detergents that can completely disrupt cell membranes and fully denature proteins. Sodium dodecyl sulfate (SDS), sodium deoxycholate, and Triton X-200 are among the most commonly used ionic decellularization agents because they effectively solubilize cytoplasmic membranes, lipids, and DNA <sup>184,213-216</sup>. SDS is commonly used to denature and unravel proteins for polyacrylamide gel electrophoresis (SDS-PAGE) and will also disrupt covalent bonds between proteins when used in decellularization procedures. To minimize adverse effects on the remaining matrix constituents of the decellularized tissue, protocols that use SDS would ideally use multiple low-concentration washes with short exposure time, or apply SDS at a decreased temperature <sup>200</sup>. SDS can achieve adequate cell removal and retain collagens, glycoproteins, and fiber orientation for rat thick aortic heart muscular tissue <sup>217</sup>, monkey kidney <sup>200</sup>, and rat tendon <sup>201</sup>. Other reports suggest SDS reduces GAGs by 50% <sup>97</sup>, and significantly reduces growth factor content <sup>173</sup>. Some denaturation of collagen has been reported, but SDS also targets the cytoskeletal protein vimentin, to completely remove the tethered nuclear envelopes <sup>202</sup>. It should be noted that SDS can be difficult to completely remove from the remaining matrix and can adversely affect cytocompatibility.

**3.3.2.4 Zwitterionic detergents:** The net zero electrical charge on the hydrophilic groups of zwitterionic detergents protects the native state of proteins during the decellularization process. Examples of zwitterionic detergents include 3-[(3-cholamidopropyl) dimethylammonio]-1-propanesulfonate (CHAPS), sulfobetaine-10 (SB-10) and SB-16 <sup>213</sup>. SB-10 and SB-16 show greater ECM preservation and better cell removal than non-ionic detergents <sup>215</sup>, and CHAPS

retains more collagen, GAGs, and elastin <sup>99,218,219</sup> than SDS ionic detergent while still removing 95% of nuclear material. However, the efficiency of cell removal of zwitterionic detergents has been disputed <sup>220</sup>. The use of detergents for retaining the basement membrane complex of urinary bladder was assessed using various detergents and surprisingly the zwitterionic detergent (8 mM CHAPS) were destructive to the collagen network. The basement membrane integrity of CHAPS treated bladders was disrupted to a similar extent as those treated with 1% SDS, whereas the basement membrane complex was less disrupted when other ionic detergents (4% sodium deoxycholate) and non-ionic detergents (3% Triton X-100) were used <sup>209</sup>.

**3.3.2.5 Alcohols:** If cell membranes are permeabilized, the polar hydroxyl groups of alcohols can diffuse into the cell where alcohols replace intracellular water, and lyse the cell by dehydration <sup>221,222</sup>. Ethanol or methanol may be used as a final wash to remove residual nucleic acids from tissue. Moreover, the nonpolar carbon chain of alcohols dissolves nonpolar substances such as lipids <sup>184</sup>. Ethanol and isopropanol delipidize tissue and are used to remove phospholipids in liver, adipose tissue, and cornea <sup>193,223-225</sup>. However, Levy et al <sup>226</sup> showed ethanol pretreatment of tissue alters the collagen structure by crosslinking the ECM. Lumpkins et al <sup>216</sup> used a 75% ethanol/-25% acetone mixture to decellularize the porcine temporomandibular joint disc. After 24 hours, the tissue had no visible cell nuclei, but was three times as stiff as the native tissue.

**3.3.2.6 Enzymatic agents:** Enzymatic agents include proteases (e.g., trypsin, dispases), esterases (phospholipase A2), and nucleases (e.g., DNase, RNase), and are advantageous because of their specificity for biologic substrate. Trypsin selectively cleaves cell adherent proteins on the carboxyl side of the amino acids arginine or lysine to detach cells from the tissue

surface. Trypsin has been shown to be effective for decellularizing adjuvant, but long exposure times damage the collagen matrix <sup>193,204,224</sup>. Meyer et al <sup>204</sup> showed 0.5% trypsin causes extensive damage to aortic valve ECM following 48h exposure. Brown et al <sup>224</sup> used 0.02% trypsin for 1h with negligible change in tissue architecture for porcine adipose decellularization. Prasertsung et al <sup>193</sup> suggest 1% trypsin not be used longer than 24h to prevent collagen damage in porcine dermis.

Dispase II is a bacterial protease that selectively cleaves fibronectin and collagen IV in the basement membrane, and is used to separate epithelial sheets from the substratum <sup>227,228</sup>. Dispase II is used in the initial steps of decellularization for many tissues, including porcine skin and corneas, but requires subsequent treatment with other agents to achieve adequate decellularization <sup>193,229</sup>. The decellularization agents that are used in conjunction with Dispase depend upon tissue specific factors. For example, porcine corneas can be decellularized with 4 mg/ml Dispase II for 45 min followed exposure to hypertonic (12h in 1.5 M NaCl at 200rpm) or, more effectively, ionic detergent (12h in 0.1% SDS at 200rpm) <sup>228</sup>. Dispase II (0.24 mg/ml for 3h) was also used to decellularize porcine skin but required pretreatment in strongly alkaline 20% sodium sulfide, hypertonic 1M NaCl, 85% glycerol, and 2/1 (v/v) chloroform/methanol for hair, epidermis, and fat removal <sup>193</sup>.

DNase and RNase are endonucleases that hydrolyze deoxyribonucleotide and ribonucleotide chains, respectively. Typically, these enzymatic agents are added to detergent treatments if effective decellularization is not achieved with detergents alone, to help remove residual DNA <sup>205,206,230,231</sup>. When a 24-hour SDS treatment of rat aortic valves still had remaining nuclei, Grauss et al <sup>230</sup> added an additional 1 hour step of DNase (20 ug/mL) and RNase (0.2 mg/mL) to produce a completely acellular material based on hematoxylin and eosin staining. Likewise, phospholipase A2 is often added to detergent treatments. Phospholipase A2 can

hydrolyze the phospholipid component of tissues such as cornea, which preserves the collagen ultrastructure and proteoglycans, but can result in reduction in GAGs <sup>232,233</sup>.

A special consideration when using enzymatic methods for decellularization is activity inhibition by natural protease inhibitors released from lysed cells. Prasertsung et al <sup>193</sup> found the activity of trypsin to decrease by 60% after 12 hours, and cell removal percentage significantly increased with more frequent enzyme refreshments. The addition of certain protease inhibitors (e.g., phenylmethylsulfonyl fluoride (PMSF), aprotonin, leupeptin) may partially ameliorate this limitation <sup>175</sup>.

**3.3.2.7 Chelators and toxins:** Ethylenediaminetetraacetic acid (EDTA) and ethylene glycol tetracetic acid (EGTA) are commonly used chelating agents that bind divalent metal cations at cell-adhesion sites of the ECM. This sequestering causes cell dissociation from the ECM. EDTA and EGTA can be used with trypsin <sup>118,206,221,234</sup> or detergents <sup>99</sup> to ensure complete removal of cell nuclei while retaining the major constituents of the ECM. However, this procedure may leave some cellular remnants <sup>206,221</sup>. Because the successful applications of EDTA and EGTA are typically used in combination with other decellularization agents, the direct effect of these chemicals on ECM has not been determined.

Latrunculin B, a marine toxin, offers an alternative to detergent methods as a powerful disruptor of the actin cytoskeleton. When latrunculin B was applied to skeletal muscle with hypertonic solutions and DNase, no intact nuclei remained in the tissue. GAGs were reduced by 40%, but collagen content and fibrillar ultrastructure remained largely unchanged <sup>166</sup>.

### **3.4 PERFUSION DECELLULARIZATION OF WHOLE ORGAN CONSTRUCTS**

Vascular perfusion is a technique that is intended to preserve the three-dimensional architecture of an organ while eliminating the parenchymal cell population. Since all cells are in close

proximity to a vascular network, perfusion through the vasculature is an efficient method for delivery of decellularizing agents. For obvious reasons however, effects of these agents upon the components of the vascular basement membrane must be considered when perfusion techniques are used.

Decellularization of the heart via vascular perfusion has been used to generate a three-dimensional scaffold that preserves the geometry of the native organ. By cannulating the aorta, Ott et al <sup>235</sup> have shown that retrograde perfusion of decellularization agents, including 1% SDS and 1% Triton X-100, is an effective method for removal of cell material from a rat heart with the vascular network remaining intact throughout the process. Recellularization with cardiomyocytes showed that the ECM was compatible with cell growth and the recellularized tissue had a small degree of contractility. Wainwright et al <sup>87</sup> have shown that the vascular perfusion can be scaled up to larger organs using a porcine heart. While still using retrograde coronary perfusion, the decellularization of the porcine heart required the successive perfusion of trypsin and detergents, and a progressive increase of perfusion pressure.

Perfusion decellularization, alone or in combination with tracheal flushing, has been applied to lung tissue by a number of investigators <sup>236-240</sup> These groups have demonstrated that perfusion decellularization is effective both in small animal models as well as large animal and human lungs. However, the methodology has varied significantly among studies as outlined in. Several groups began decellularization procedures with freeze/thaw cycles. Cortiella et al demonstrated that freezing was necessary to completely remove nuclei and DNA <sup>241</sup>. Perfusion with detergent solutions is common in lung decellularization procedures, however the type of detergent and length of exposure time vary dramatically. Ott et al <sup>242</sup> used vascular perfusion of 1% SDS at physiologic pressure to decellularize rat lungs in 2 hours. Another method published by Peterson et al <sup>99</sup> utilized the zwitterionic detergent, CHAPS, and perfused the airway compartment via the trachea rather than the vasculature. Price et al <sup>243</sup> perfused both the airway

and vascular compartments but did not use continuous perfusion techniques. Instead, the lungs were repeatedly incubated under static conditions in solutions of Triton X-100, sodium deoxycholate, DNase, and bleach. Cortiella et al <sup>114</sup> perfused lungs via the airway compartment with 1% SDS while the tissue was circulated in a bioreactor system for approximately five weeks. Nichols et al perfused lungs with 1% SDS for five days following a freeze/thaw cycle <sup>244</sup>. All five groups showed that the lung ECM could be repopulated with cells. Cortiella et al <sup>114</sup> used a homogenous mouse embryonic stem cell population for reseeding and showed that the ECM was capable of promoting site-appropriate differentiation without the addition of further growth factors. After reseeding the decellularized lungs with cells, orthotopic transplantation was performed by Ott et al <sup>242</sup> and Peterson et al <sup>99</sup>. Vascular leakage was evident upon implantation in recipient rats in both studies, and these lung constructs did not function for more than a few hours. Despite significant differences in decellularization techniques, all groups have shown removal of nuclei and reduction in DNA content as well as preservation of lung microstructure together with the major components of the ECM such as collagen, laminin, elastin, and GAGs. Further studies are necessary, however, to compare the effects of each protocol on the ECM composition and, more importantly, on the suitability for recellularization and the host response following implantation.

**Table 6.** Results and considerations for varying decellularization methods

Method/Agent	Result	Considerations
<b>Freeze/thaw</b> 149,245-247	<ul style="list-style-type: none"> <li>Not required for complete decellularization</li> </ul>	<ul style="list-style-type: none"> <li>May be useful for tissue storage</li> <li>Effects of freeze/thaw vs. fresh have not been examined</li> </ul>
<b>SDS</b> 149,153,245,248-253	<ul style="list-style-type: none"> <li>Improves removal of cytoplasmic and nuclear material</li> <li>Effective for cellular removal when used alone</li> </ul>	<ul style="list-style-type: none"> <li>Concentration and exposure time vary widely among protocols and for different source animals</li> <li>More detrimental to mechanical properties than other detergents</li> <li>Residual SDS is harmful</li> </ul>
<b>Triton X-100</b> 149,153,245-248,250-253	<ul style="list-style-type: none"> <li>Only effective for cellular removal when used in conjunction with other agents</li> </ul>	<ul style="list-style-type: none"> <li>Concentration and exposure time vary widely among protocols</li> <li>Effective for removal of residual SDS</li> </ul>
<b>Sodium Deoxycholate</b> 149,251	<ul style="list-style-type: none"> <li>Not sufficient for cellular removal when used without additional decellularization agents</li> </ul>	<ul style="list-style-type: none"> <li>Ionic detergents damage matrix components</li> </ul>
<b>Trypsin</b> 246,251	<ul style="list-style-type: none"> <li>Only effective for cellular removal when used in conjunction with other agents</li> </ul>	<ul style="list-style-type: none"> <li>May be used to reduce amount or time of exposure to harsh detergents</li> <li>Can damage collagen structure</li> </ul>
<b>Peracetic Acid</b> 246,Wang, 2014 #357,251	<ul style="list-style-type: none"> <li>Not effective for cellular removal when used alone</li> </ul>	<ul style="list-style-type: none"> <li>Can denature ECM proteins, damaging collagen and reducing growth factor content</li> </ul>
<b>Ethanol</b> 246	<ul style="list-style-type: none"> <li>Not effective for cellular removal when used alone</li> </ul>	<ul style="list-style-type: none"> <li>Can alter ECM structure by crosslinking collagen</li> </ul>
<b>Ammonium Hydroxide</b> 247,251	<ul style="list-style-type: none"> <li>Effective for cellular removal when used in conjunction with Triton X-100</li> </ul>	<ul style="list-style-type: none"> <li>The combination of ammonium hydroxide and Triton X-100 is effective for decellularization and maintains mechanical properties better than SDS/Triton X-100</li> </ul>

The liver is another example of an organ that has been decellularized by perfusion. Antegrade perfusion via the portal vein has resulted in a decellularized tissue with maintained vascular networks. **Table 6** highlights the techniques and agents that have been used for perfusion-based liver decellularization along with considerations for the use of each agent. Uygun et al <sup>97</sup> used increasing concentrations of SDS (0.1-1%) followed by 1% Triton X-100 to

achieve decellularization of rat liver whereas the protocol published by Shupe et al <sup>254</sup> used increasing concentrations of Triton X-100 followed by 0.1% SDS. Shupe et al also demonstrated that perfusion with Triton X-100 alone was not sufficient for decellularization and SDS was required for complete nuclear removal. The protocol used by Uygun et al was optimized by DeKock et al <sup>250</sup> who decellularized rat liver with 1% Triton X-100 followed by 1% SDS in 1 hour. Soto-Gutierrez et al <sup>255</sup> published an effective decellularization protocol that, unlike those previously reported, excludes the use of harsh detergents, such as SDS. Using this method they report that growth factor content retained within the matrix was 30-50% of the native tissue. Kajbafzadeh et al <sup>251</sup> compared the protocol developed by Uygun et al to 4 other protocols for the decellularization of sheep liver. The authors determined that increasing concentrations of SDS followed by Triton X-100 achieve effective decellularization, however, the mechanical properties of the resulting ECM are poor compared to protocols that do not use SDS. They suggest that the best protocol to completely decellularize the liver while maintaining mechanical properties is perfusion with 0.05% ammonium hydroxide followed by 0.5% Triton X-100. Following decellularization, similar to other tissues, the liver is a translucent and white acellular matrix. The vascular network is maintained and can be visualized by perfusion of a colored dye (Figure 3). Multiple studies have shown that integral components of the basement membrane, collagen IV and laminin, remain in the decellularized liver while intact cells are removed <sup>245,246,248-250</sup>. Following decellularization, the matrix has been recellularized, via portal vein perfusion, with rat liver progenitor cells <sup>248</sup>, human fetal liver cells <sup>249</sup>, and human liver progenitor cells <sup>153</sup>. For up to 8 hours following heterotopic transplantation in a rat, the hepatocytes maintained functional synthesis of albumin and lactate dehydrogenase <sup>248</sup>.

Intact renal constructs have been prepared by perfusion decellularization. Ross et al <sup>256</sup> developed a protocol for decellularization of mouse kidney using solutions of Triton X-100, DNase, and SDS. The ECM was supportive of tissue-specific differentiation of embryonic stem

cells. Song et al<sup>257</sup> used SDS to perfuse cadaveric rat kidneys at a pressure of 40 mm Hg. Renal ECM components were maintained including the glomerular and tubular basementmembrane, which serve essential roles in renal filtration and reabsorption. The scaffolds were recellularized with endothelial cells and a heterogeneous neonatal kidney cell population. In vitro, the recellularized construct produced urine and cleared creatine nearly 20% as well as cadaveric kidney, with urine production also demonstrated following orthotropic transplantation. For more information on perfusion decellularization of whole organ constructs refer to<sup>258</sup> and<sup>77</sup>.

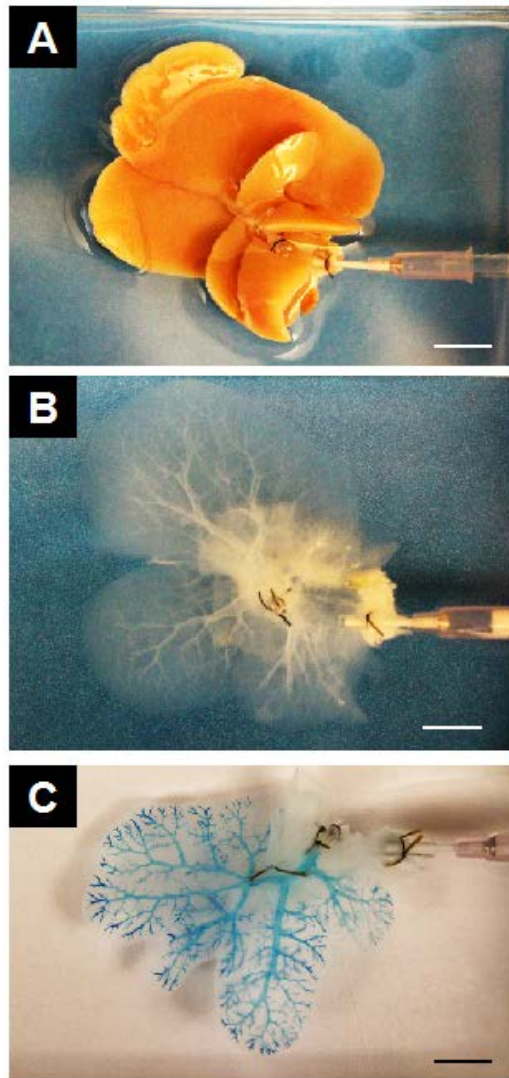


**Figure 3. Perfusion decellularization of rat liver.** The cadaveric rat liver (A) is cannulated through the portal vein. Following the decellularization protocol, the matrix is devoid of cells and has a white/translucent appearance (B). Perfusion decellularization allows for the maintenance of an intact vascular network, visualized by injection of a colored dye (C). Scale bar = 1 cm.

### 3.5 EFFECTS OF RESIDUAL DETERGENTS FROM DECELLULARIZATION

It has been suggested that the presence of residual SDS within ECM biomaterials has severe cellular toxicity and may be responsible for discouraging cellular ingrowth<sup>149,206</sup>. Rieder et al<sup>206</sup> demonstrated that scaffolds decellularized using SDS were unable to be recellularized due to

the toxic effects of the ionic detergent, whereas, scaffolds prepared with 0.25% tert-octylphenyl-polyoxyethylen in combination with sodium-deoxycholate enabled host recellularization.

Cebotari et al <sup>157</sup> examined detergent levels remaining in the wash solution following decellularization with SDS or a combination of SDS and SDC using solid phase extraction and high performance liquid chromatography (HPLC). They determined that a detergent concentration of <50 mg/L in the wash solution did not influence the receptiveness of the matrix to reseeding with endothelial cells. The authors also showed that the combination of SDS and SDC was more easily washed out from the tissue.

Another method for quantification of residual SDS takes advantage of the fact that SDS and methylene blue produce blue compounds under acidic conditions. This colorimetric assay allows for quantification of residual SDS in the ECM scaffold. The lower cytotoxic threshold for SDS is approximately 10 ug/mg dry weight. Wang et al showed that following SDS perfusion with BSA or PBS reduces the residual SDS to well below this level and washing with Triton X-100 results in almost complete removal of residual SDS.

Sansoto et al <sup>259</sup> assessed the effects of the SDS compared to high hydrostatic pressure on the decellularization of uterine tissue and their subsequent effects on tissue regeneration *in vivo*. Their methods achieved effective decellularization as shown by H&E staining and quantification of residual DNA. Analysis of the *in vivo* host response showed that cells migrated into the area surrounding the grafts but only the sample that was decellularized using high hydrostatic pressure stimulated cell migration into the graft. Cells did not migrate into decellularized grafts generated using SDS treatment.

Decellularization methods can clearly affect the host response to biologic scaffolds. However, it remains possible that these effects are due to differences in structure and composition as a result of the decellularization process rather than due to residual detergent in

the material after processing with SDS. Gratzner et al <sup>260</sup> found that the level of repopulation and viability of cells were the same regardless of washing technique and resulting level of residual SDS in the tissue. These data suggest that alterations in tissue matrix biochemistry or structure from SDS treatment are responsible for low cell repopulation observed in SDS decellularized anterior cruciate ligament. Additional studies are necessary to determine if this holds true for other tissues.

### **3.6 ESTABLISHING METRICS FOR EFFECTIVE DECELLULARIZATION**

While it is unlikely that any decellularization protocol will completely remove all cell remnants, cell components that do remain (e.g., DNA, phospholipids) can be quantitatively assayed. Until recently, no quantitative metric has been suggested to evaluate the efficacy of a decellularization protocol <sup>175</sup>. It is important to note that for most studies reviewed in the present manuscript, no objective criteria were used to assess degree of decellularization. Only one study to date has related quantitative degree of decellularization to host remodeling outcome <sup>138</sup>.

Commercially available scaffolds are regulated by the FDA and therefore are subject to sterility guidelines (see section 5) and endotoxin amounts. Endotoxin is a complex lipopolysaccharide (LPS) that is a major part of the gram-negative bacteria cell wall. Endotoxins are especially abundant in the gut, the tissue source for small intestine submucosa. The FDA standard for a biologic scaffold eluate is 0.5 EU/mL, and 0.06 EU/mL for cerebrospinal devices. While the exact level of endotoxin concentration necessary to elicit an adverse reaction is unknown, dermal matrices spiked with 20 times the FDA limit had similar immune responses to devices below the FDA standard suggesting that the current endotoxin standard may fall well

below the levels required to elicit an acute proinflammatory response <sup>261</sup>. While strict guidelines for some metrics do exist, the FDA does not yet have guidance related to remnant cellular content in commercially available decellularized tissues.

The definition of effective decellularization varies greatly across published reports. Decellularization has been defined as a lack of positive staining for intact nuclei and cellular antigens (e.g., MHC-1). Other definitions include a “significant” reduction in dsDNA content compared to native tissue as criteria for decellularization. The increased clinical use of ECM-based scaffolds is prompting the need for established decellularization guidelines. A recent report recommended tissue decellularization criteria that utilize nucleic acid content as a basis. The three-part criteria include: 1) No visible nuclei upon histologic evaluation via hematoxylin and eosin and DAPI stains, 2) The remaining double stranded DNA (dsDNA) content should not exceed 200 base pair in length, and 3) the amount of dsDNA should not exceed 50ng per mg of dry weight of the material <sup>175</sup>. These criteria were shown to make a difference in the host response in a separate study <sup>138</sup>.

The criteria referenced above may be too stringent, sufficient, or too liberal; and these criteria may not be appropriate for all source tissues from which such bioscaffolds are prepared. It is unknown but likely that the threshold level of cellular content necessary to elicit a proinflammatory host response will vary depending on anatomic location. In addition to nucleic acid content, it may be necessary to assay cellular components such as remnant mitochondria. Mitochondria are evolutionarily derived from bacteria, bear damage associated molecular patterns (DAMPs) and may elicit a proinflammatory host response if present above some threshold level <sup>262</sup>. As a greater understanding of the association between specific cellular components and the host response is achieved, the criteria may need to be revised or supplemented.

### 3.7 TERMINAL STERILIZATION OF DECELLULARIZED TISSUES

There are many examples of biologic scaffold products composed of decellularized tissues. These include dermis, small intestine, urinary bladder, mesothelium, pericardium, and heart valve. These products are used for repair applications in soft tissue, tendon, chronic wounds, breast reconstruction, ophthalmology, dentistry, valve replacement and others. Biologic scaffolds from decellularized xenogenic source tissue are typically regulated by the Food and Drug Administration (FDA) as medical devices. This classification requires that the methods used to terminally sterilize ECM products are adherent to directed guidelines regarding bacterial load (e.g., ISO/DIS 1135-1, ISO/DIS 1137-1). Incubation with peracetic acid has been used as a decellularization agent for biologic scaffolds and has also been shown to be an effective sterilization method for polymeric scaffolds<sup>263</sup>. However, incubation with acid may not provide sufficient penetration of ECM bioscaffolds to achieve satisfactory sterilization. Terminal sterilization methods such as ethylene oxide exposure, gamma irradiation, and electron beam irradiation achieve effective sterilization but are known to alter ECM ultrastructure and mechanical properties. The effect of terminal sterilization on ECM structure is a particular concern for hydrogel forms of ECM because sterilization methods can have significant effects on the rheologic properties of the hydrogel. While all biologic scaffolds must pass sterility testing prior to their approval for clinical use, it will be important for regulatory agencies to consider the effects of terminal sterilization on the structure and biologic activities of these materials. For more information on terminal sterilization, see Appendix 12.4 (page 211).

## 4.0 THE HOST RESPONSE TO ECM<sup>3</sup>

### 4.1 ABSTRACT

The clinical use of biologic scaffold materials has become commonplace. Such scaffolds are composed of extracellular matrix (ECM), or components of ECM, derived from allogeneic or xenogeneic tissues. Such scaffold materials vary widely in their source tissue, processing methods, and sterilization methods. The success or failure of an ECM scaffold for a given application is dependent on the host response following implantation; a response that is largely mediated by the innate immune system and which is influenced by a numerous factors, including the processing methods used in the preparation of biologic scaffolds. The present chapter reviews various aspects of the host response to biologic scaffolds and factors that affect this response. In addition, some of the logistical, regulatory, and reconstructive implications associated with the use of biologic scaffolds are discussed.

---

<sup>3</sup> Portions of this chapter were adapted from the following publication:  
**Keane TJ**, Badylak SF. The Host Response to Allogeneic and Xenogeneic Biologic Scaffold Materials. *Journal of Tissue Engineering and Regenerative Medicine*, February 2014. DOI:10.1002/term.1874

## 4.2 INTRODUCTION

Scaffolds and surgical mesh materials composed of mammalian extracellular matrix (ECM) are commonly used for the repair and reconstruction of a variety of tissues including musculoskeletal tissues<sup>90,264</sup>, cardiovascular structures<sup>265,266</sup>, esophagus<sup>92,96</sup>, lower urinary tract<sup>267,268</sup>, and body wall<sup>269,270</sup>. These materials are typically prepared by the decellularization of a source tissue such as dermis, small intestine, or urinary bladder, among others (Table 1). Scaffolds are derived from allogeneic or xenogeneic source tissues and can have unique regulatory considerations that are dependent upon the tissue of origin.

Clinical outcomes vary from excellent<sup>1,92,271,272</sup> to poor<sup>271,273</sup> and the reasons for this disparity in clinical performance are partially understood. Processing methods play a prominent role in the host response to biologic scaffold materials. For example, inadequate decellularization of the source tissue results in retained cellular debris within the extracellular matrix and elicits a proinflammatory response<sup>138</sup>. Similarly, sterilization methods<sup>161</sup> and lyophilization<sup>274</sup> affect mechanical and material properties and the associated clinical performance. Age of the animal from which the tissue is harvested has been shown to affect mechanical and compositional properties of porcine derived xenogeneic scaffold material<sup>105</sup>. Finally, and the main focus of this manuscript, a factor that would logically play a prominent role in the clinical outcome is the host immune response to these allogeneic and xenogeneic materials. With the exception of studies focused upon the Gal $\alpha$ 1-3Gal $\beta$ 1-4GlcNAc-R (Gal) epitope<sup>275-277</sup>, there has been surprisingly little attention given to this issue.

The number of biologic scaffolds composed of allogeneic and xenogeneic ECM implanted during the past 15 years worldwide exceeds several million, including many cases of individual patients receiving repeated implants. No documented report of zoonotic infection exists following xenogeneic whole organ or tissue transplants. Therefore the use of these

materials can clearly be considered safe from the standpoint of infectious disease. There have been suggestions of an immune-mediated cause of unfavorable outcomes<sup>278,279</sup>, but evidence based support of such a phenomenon in the clinical setting is lacking. It should be noted however that the recipient uniformly and immediately responds to presence of these materials following implantation. In fact, such a response is not only acceptable but necessary for a constructive remodeling outcome<sup>280</sup>. The present manuscript describes various aspects of the host response to allogeneic and xenogeneic scaffold materials and the factors that affect this response.

#### **4.3 RAW MATERIAL SOURCE OF BIOLOGIC SCAFFOLDS**

Tissue sources from which ECM scaffolds are prepared include humans (allografts) and porcine, bovine, or equine tissue (xenografts). Whether the ECM is derived from allogeneic or xenogeneic species, the composition of ECM constructs is affected by donor state (e.g., age, disease state). Further, the anatomic site of the raw material source has a strong influence upon the device mechanical and material properties, the methods required for adequate decellularization and sterilization, and the eventual host response.

The composition, ultrastructure, and mechanical properties of ECM derived from different tissues/organs are distinct; a logical finding since each tissue/organ has a unique function. For example, ECM derived from small intestinal submucosa has a preferred collagen alignment that leads to anisotropic mechanical behavior of the scaffold, with the preferred (longitudinal) fiber direction showing greater stiffness and strength than the circumferential direction<sup>101</sup>. The collagen fiber alignment of the urinary bladder submucosa and tunica propria,

in contrast, shows a much more isotropic fiber alignment than SIS <sup>102</sup>. An understanding of the mechanical properties from different tissues may be an important consideration for matching the choice of ECM source tissue with a specific clinical application.

The properties of biologic scaffolds also vary with the age of the source animal from which the tissue is harvested. Fetal and neonatal mammals have greater wound healing and regenerative capacity compared to adult mammals <sup>103</sup>. The composition of fetal and neonatal ECM is distinctly different from that of adults and plays an important role in tissue development <sup>104</sup>. In fact, distinct remodeling characteristics exist that are attributable to source animal age. Biologic scaffolds harvested from neonatal animals have been shown to promote a more robust constructive remodeling response when compared to scaffolds derived from market weight and older animals <sup>105</sup>.

#### **4.4 INNATE AND ADAPTIVE RESPONSE TO BIOLOGIC SCAFFOLD MATERIALS**

The innate and acquired immune response to whole organ transplantation is well recognized and understood. However, the response to acellular xenogeneic or allogeneic biologic scaffold materials has been studied much less and is poorly understood compared to that of the response to whole organs. Preformed circulating antibodies and/or T cell activation are central phenomena to whole organ rejection. Tissue destruction occurs as a result of complement activation or direct T cell-mediated lysis of donor cells, activation of accessory cells, and/or alloantibody production <sup>281</sup>. As the genetic difference between host and donor cells increases, the severity of the adverse immune response increases. Xenografts (i.e., tissue or organ transplants between different species) are not used clinically because such grafts (i.e., the

resident cells) evoke a robust and hyperacute or acute rejection response. Ultimately, whether mediated by humoral or cellular mechanisms, the host immune recognition of donor antigens present on transplanted cells incites a response that, in the absence of immunosuppression, results in graft rejection.

The host response to biologic scaffold materials composed of (acellular) ECM involves both the innate and acquired immune system but is distinct and different from the response to whole organs which contain donor cells. By definition, materials composed of ECM are devoid of cells. The immune response is affected by ECM device-specific variables including the intended clinical application (e.g., anatomic site of implantation), the source of the raw material/tissue from which the ECM is harvested, and the processing steps involved in manufacturing an approved medical device. The implantation of an ECM scaffold is inevitably coupled with tissue injury at the surgical site. The default mammalian host response following tissue injury includes a well-documented series of overlapping events (hemostasis, inflammation, proliferation, and remodeling) that culminates in the deposition of dense fibrous connective tissue (i.e., scar)<sup>282</sup>. The clinical success of a biologic scaffold is largely attributed to its ability to modulate this default wound healing response toward the mitigation of scar tissue deposition and the formation of site-specific functional tissue (i.e., constructive remodeling)<sup>283</sup>. The mechanisms by which ECM constructs promote constructive remodeling are only partially understood.

An adaptive immune response to biologic scaffolds has been described previously; specifically, a correlation between T helper (Th) cell response and constructive remodeling outcomes has been shown following implantation of an ECM scaffold derived from porcine small intestinal submucosa (SIS-ECM)<sup>284,285</sup>. T cells are classified as either cytotoxic or helper T cells. Further, Th cells are phenotypically divided into Th1 or Th2 effector cells, which have a distinct immune response with respect to cytokine and chemokine expression and effector action. Th1

polarization is associated with a pro-inflammatory response, whereas Th2 polarization is associated with a regulatory, anti-inflammatory, wound healing and constructive remodeling response. In a mouse model of abdominal wall defect, SIS-ECM elicited Th2 cytokine expression but not Th1 cytokine expression and constructive remodeling<sup>285</sup>. Similarly, a clinical study with the use of SIS-ECM showed that a Th2 polarized cytokine and antibody isotype profile was associated with tissue acceptance<sup>286</sup>. Repeat exposure to xenogeneic ECM failed to cause sensitization or a Th1 type response in a mouse model, and in fact, accentuated the Th2 response<sup>284</sup>. Although recipients of SIS–ECM scaffolds recognize the material as “non-self” and produce antibodies, these antibodies appear to be limited to the Th2 profile, a finding consistent with their ability to induce constructive remodeling and avoid a classic tissue rejection response<sup>287</sup>. In fact, this response may be one of the primary mechanisms by which ECM scaffolds produce constructive tissue remodeling.

#### **4.5 MACROPHAGE PARTICIPATION IN ECM MEDITATED TISSUE REMODELING**

While a humoral response is elicited following allogeneic or xenogeneic ECM implantation, a robust cellular response also occurs. This cellular response, which consists mainly of macrophages, represents the innate arm of the immune system and in large part determines the downstream events which occur following recognition of the implanted ECM material. Several studies have shown the determinant role of macrophages in constructive remodeling outcomes<sup>280</sup>. In fact, although it may not be immediately intuitive, constructive remodeling outcomes are delayed or inhibited when there are deficiencies in macrophage number and/or their function<sup>288,289</sup>. Interestingly, it has recently been shown that amphibian tissue regeneration is dependent upon a macrophage presence and participation<sup>290</sup>.

Similar to the Th1/Th2 polarization schemes for lymphocytes described above, phenotypic macrophage polarization has been described.<sup>291-294</sup> Macrophage phenotypes exist along a spectrum that ranges from M1 to M2. The pro-inflammatory M1 phenotype is characterized by pathogen killing and facilitates classic signs of inflammation via secretion of proinflammatory cytokines such as IL12 and TNF- $\alpha$ . In contrast, the anti-inflammatory M2 macrophage promotes immunoregulation, tissue repair, matrix deposition and constructive tissue remodeling. The concept of macrophage phenotype has been evaluated in the context of the host response to implanted ECM scaffold materials and has been shown to be a strong predictor of bioscaffold remodeling and functional outcome<sup>132,133,295</sup>. ECM scaffolds that promote constructive remodeling are associated with a prevalence of M2 macrophages. The default host response to tissue injury is characterized by an early M1 macrophage predominance followed by a late switch to M2, occurring concurrently with the resolution of inflammatory processes and generally results in the formation of localized scar tissue. However, certain biologic scaffolds have been shown to modulate the default immune response. During ECM-facilitated remodeling, the early macrophage response is predominantly M1 with a relatively quick shift to M2 prevalence after about 72 hours<sup>133</sup>. As remodeling continues, the M2 macrophage phenotype is sustained and is usually associated with a site-appropriate tissue remodeling outcome rather than scar tissue formation.

It is noteworthy that chemical crosslinking of ECM scaffolds which inhibits bioscaffold degradation is associated with an M1 proinflammatory macrophage response. Furthermore, remnant cellular material within ECM scaffolds (i.e., ineffective decellularization) will alter the host response and promote an M1 macrophage response<sup>138,296</sup>. Although much remains to be understood regarding the innate immune response to ECM based biologic scaffolds, it is clear that such a response is not only desirable, but required if constructive and functional remodeling outcomes are to be expected.

#### **4.6 XENOGENEIC VS. ALLOGENEIC TISSUE SOURCE: LOGISTICAL AND REGULATORY CONSIDERATIONS**

There are limited studies that directly compare allogeneic vs. xenogeneic scaffolds for specific applications. Although allogeneic scaffold materials may be intuitively superior to xenogeneic materials because of genetic similarities, there are other considerations which mitigate their clinical utility. For example, allograft tissues and organs are in limited supply and have a greater risk of disease transmission than tissues of xenogeneic origin. In contrast, xenogeneic tissues are typically in abundant supply through the agricultural supply chain and, as previously noted, the constituents of the extracellular matrix are highly conserved across species boundaries. The choice of allogeneic vs. xenogeneic scaffold materials is also influenced by factors that extend beyond biology such as regulatory, cost reimbursement, and logistical considerations, some of which are discussed below. Regardless of tissue origin, the importance of effective decellularization<sup>175</sup> of these ECM scaffolds, while not directly regulated, cannot be overstated for good remodeling outcomes.

In the United States, the Food and Drug Administration (FDA) regulates human tissue products and the tissue banks that supply allografts. Tissue banks can voluntarily gain accreditation of the American Association of Tissue Banks (AATB) and the AATB sets industry standards to regulate the retrieval, processing, storage, and distribution of human tissue products.

Allografts are procured from individuals whose families have consented to tissue donation. The tissue bank prescreens donors and the recovery of tissue occurs in hospital operating rooms and other settings regulated by the FDA including morgues and funeral homes. Donors should be relatively healthy, prescreened for HIV, Hepatitis, and any behavior that may compromise the integrity of the donor tissue. The FDA provides minimum requirements for donor screening while additional recommendations are provided by the AATB. However, the

ultimate responsibility of setting minimum requirements and validating procedures is the responsibility of the tissue bank or company marketing the product. Allogeneic biologic scaffold processing methods are generally proprietary, but the design and validation of processing methods must be in accordance with FDA Good Tissue Practices. The methods, packaging, and storage of the allogeneic biologic scaffolds vary widely. The FDA classifies most allogeneic tissue as a Human Cell and Tissue/Product (HCT/P) and not as a medical device. As a result, unlike xenogeneic scaffolds, there are not specific sterilization techniques or requirements for sterility levels for most allogeneic ECM scaffolds.

Xenogeneic biologic scaffolds have historically been classified as medical devices by the FDA and must meet the requirements for a medical device. This classification has proven effective since safety of these materials has been established. Processing techniques used in the production of xenogeneic ECM scaffolds are also proprietary and include methods of decellularization and terminal sterilization. The device must meet a sterility assurance level that is appropriate for the given application. Patient-related considerations for the use of xenogeneic scaffolds should also be considered prior to use. For example, certain social and religious groups may oppose the use of animal tissue in any form <sup>297</sup>.

## 5.0 OBJECTIVES

Ulcerative colitis (UC) is the most common form of inflammatory bowel disease, and represents a significant global health problem. Since the 1930s, the fundamental approach to treatment has not changed. Pharmacologic treatment (e.g., 5-amino salicylic acid, immunosuppressives), and/or surgical intervention (e.g., colectomy) have been the two basic tenets of patient care. Almost a century later, these two approaches remain the clinical standard of care even though results are unacceptable. More than 50% of patients suffer from severe systemic side effects and disease recurrence. We propose a distinctly different, nonsurgical/ nonpharmacologic approach which will: (1) abate the inflammatory “flares” not by immunosuppression but rather by promoting alternative activation of the local innate immune cell population, and (2) induce rapid replacement of the colonic mucosal barrier function not by providing a physical barrier between the denuded colonic submucosa and luminal contents, but rather by local stem cell recruitment, mitogenesis, and differentiation to restore a normal mucosal epithelial structure.

This two-pronged approach will be tested by local delivery (enema) of naturally occurring signaling molecules present within a hydrogel form of mammalian extracellular matrix (ECM).

This proposal attempts to determine whether diseased mucosa can be successfully remodeled into healthy mucosa using an ECM scaffold based regenerative medicine approach. Developing a regenerative medicine strategy to repair or replace native colonic mucosal tissue is central to the improvement of UC and IBD therapy, as repair of the diseased tissue and replacement with new, healthy tissue would essentially cure an affected patient. In stark contrast to current

surgical intervention, a regenerative medicine approach utilizing an ECM hydrogel would be non-invasive and would result in colon preservation. If successful, this therapeutic strategy would represent a quantum leap forward for the millions of patients affected by UC, and potentially identify new diagnostic and therapeutic targets for a wide variety of chronic inflammatory diseases.

## 6.0 CENTRAL HYPOTHESIS AND SPECIFIC AIMS

**Central Hypothesis:** ECM hydrogels will support constructive remodeling of GI tissue by modulation of the microenvironment and local immune cells.

**Specific Aim 1:** To prepare, quantitatively describe, and compare gastrointestinal extracellular matrix (GI-ECM) bioscaffolds derived from porcine esophagus and colon.

*Corollary Hypothesis:* GI tissue can be effectively decellularized while retaining tissue-specific properties.

Rationale: The composition and structure of ECM are directly attributed to the cell population of the tissue from which the ECM is derived. The use of ECM derived from a heterologous tissue source has been shown to enhance remodeling outcomes in a number of tissues; however several unsuccessful outcomes have also been reported. Advantages of site-specific ECM (i.e., ECM derived from the tissue to be treated) have been recently described. It is plausible that, in contrast to heterologous ECM, an ECM derived from GI tissue would contain the appropriate biochemical constituents to support remodeling of GI tissue. Quantitatively characterizing the biochemical composition of different ECMs may highlight one or more molecular cues necessary for the maintenance of lower vs. upper GI tissue.

**Specific Aim 2:** To characterize the effect of GI-ECM on the remodeling and inflammatory response of intestinal epithelial cells and macrophages, respectively.

*Corollary Hypothesis:* Exposure of IECs to ECM will enhance their barrier function.

Macrophages exposed to degradation products of GI-ECM will polarize towards M2.

Rationale: Effective treatment of UC requires (1) a reduction in inflammatory state and (2) rapid reformation of a robust epithelial barrier. The body's largest reservoir of macrophages is found in the mucosa of the GI tract<sup>298</sup>. These macrophages are positioned in the lamina propria (LP) and are uniquely suited to protect against bacteria/pathogens that have breached the mucosa and to clear dead cells and debris while maintaining a secretome that is largely devoid of inflammatory cytokines<sup>299</sup>. With UC, a defect in the integrity of the mucosal barrier leads to excessive uptake of luminal contents and disrupts the regulatory nature of the mucosal immune system. LP macrophages are increased in number in UC with enhanced production of inflammatory cytokines (e.g., IL1b, TNF, IL6). ECM hydrogels have been shown to induce a shift in macrophage phenotype towards an anti-inflammatory secretome profile (TNF $\alpha$ <sup>low</sup>/IL-1 $\beta$ <sup>low</sup>/IL-1RA<sup>high</sup>). Therefore, it is feasible that solubilized ECM could similarly down-regulate macrophage production of pro-inflammatory cytokines that are known to have deleterious effects on the epithelial barrier<sup>300</sup>.

**Specific Aim 3:** To determine the efficacy of ECM in treating inflamed colonic mucosal tissue.

*Corollary Hypothesis:* Topical application of ECM hydrogels will mitigate the inflammatory response in colitic rats by modulating the microenvironmental milieu towards an anti-inflammatory state and thereby facilitating constructive remodeling of colonic mucosa.

Rationale: Inflammation mitigation and remodeling (i.e., restoration of colonic epithelial barrier) is central to effect treatment of UC. Preclinical and clinical studies have shown that ECM can facilitate the repair of neo-esophageal tissue following mucosal resection in both healthy and diseased subjects. While the mechanisms that governs ECM-mediated remodeling are not fully understood, positive remodeling outcomes are consistently accompanied by a temporal modulation of the local immune response. In-vivo, a shift towards an M2, immunomodulatory macrophage phenotype accompanies ECM scaffold implantation in muscle defect models.

Preliminary in-vitro data suggest the GI ECM degradation products also drive an M2 macrophage bias. Preclinical studies will determine whether the effects of degraded ECM are robust enough to alter the tissue microenvironment from a pro-inflammatory state to one that is not only anti-inflammatory but also supportive of functional tissue remodeling in vivo.

## 7.0 PREPARATION AND CHARACTERIZATION OF A BIOLOGIC SCAFFOLD FROM ESOPHAGEAL MUCOSA<sup>4</sup>

### 7.1 ABSTRACT

Biologic scaffolds composed of extracellular matrix (ECM) are commonly used to facilitate a constructive remodeling response in several types of tissue, including the esophagus. Surgical manipulation of the esophagus is often complicated by stricture, but preclinical and clinical studies have shown that the use of an ECM scaffold can mitigate stricture and promote a constructive outcome after resection of full circumference esophageal mucosa. Recognizing the potential benefits of ECM derived from homologous tissue (i.e., site-specific ECM), the objective of the present chapter was to prepare, characterize, and assess the in-vivo remodeling properties of ECM from porcine esophageal mucosa. The developed protocol for esophageal ECM preparation is compliant with previously established criteria of decellularization and results in a scaffold that maintains important biologic components and an ultrastructure consistent with a basement membrane complex. Perivascular stem cells remained viable when seeded upon the esophageal ECM scaffold in vitro, and the in-vivo host response showed a pattern of constructive remodeling when implanted in soft tissue.

---

<sup>4</sup>Portions of this chapter have been adapted from the following publication:  
**Keane TJ**, Londono R, Carey RM, Carruthers CA, Reing JE, Dearth CL, D'Amore A, Medberry CJ, Badylak SF. Preparation and Characterization of a Biologic Scaffold from Esophageal Mucosa. *Biomaterials*, September 2013. DOI:10.1016/j.biomaterials.2013.05.052

## 7.2 INTRODUCTION

The default mechanism of mammalian tissue repair typically results in scar tissue deposition, a protective and favorable response in most tissues. However, this scar tissue formation is associated with adverse clinical consequences including stricture in select anatomic locations such as the esophagus. Preclinical studies have shown that placement of an extracellular matrix (ECM) scaffold derived from heterologous tissue is capable of restoring a functional esophagus with minimal stricture and normal esophageal motility following circumferential mucosal resection<sup>93</sup>. A clinical report involving patients with stage 1 esophageal adenocarcinoma corroborated this finding and provided proof-of-concept in the clinical setting<sup>92,126</sup>. While heterologous ECM was successful in reducing stricture formation, the remodeled tissue did not fully reconstitute all components of normal esophageal tissue; for example, glandular tissue was absent. Delivery of the scaffold also required temporary placement of an intraluminal stent to allow integration of the scaffold with the subjacent tissue. A possible advantage of a site-specific, homologous ECM could be more rapid integration and faithful remodeling of the esophageal mucosa.

Recent work has described potential benefits of ECM scaffold materials derived from homologous tissue versus heterologous tissue when used in selected anatomic locations<sup>109-118</sup>. While tissue specificity is not necessary for all therapeutic applications<sup>92,119,120</sup>, some studies have shown that site-specific ECM can preferentially maintain tissue-specific cell phenotypes<sup>109-112</sup>, promote cell proliferation<sup>111,113</sup>, induce tissue-specific differentiation<sup>114</sup>, and enhance the chemotaxis of lineage-directed progenitor cells<sup>115-117</sup>. It is plausible therefore that a site-specific esophageal mucosal ECM may promote similar effects and further improve clinical outcomes in esophageal mucosa repair. The harvesting and preparation of an ECM scaffold requires tissue specific methodologies for optimal outcomes<sup>274,301-304</sup>.

Biologic scaffolds composed of ECM, when prepared by methods designed to preserve structure and composition of the native source tissue, contain bioactive molecules including growth factors (e.g., vascular endothelial growth factor (VEGF)<sup>136</sup>, basic fibroblast growth factor (bFGF)<sup>65</sup>) and glycosaminoglycans (GAGs)<sup>135</sup>. The composition, ultrastructure, and mechanical properties of an ECM construct are affected by the methods used to decellularize the source tissue as well as the methods of sterilization and storage of such bioscaffolds<sup>161,175,274</sup>. Therefore, the methods of preparing ECM scaffolds intended for use in the repair and reconstruction of the esophageal mucosa must be carefully considered as regenerative medicine strategies are developed for this intended therapeutic application.

The objective of this chapter was to prepare, characterize, and determine the in-vitro cytocompatibility and in-vivo host response of ECM derived from porcine esophageal mucosa (emECM). Esophagi were collected and decellularized by a method sufficient to meet stringent decellularization criteria: specifically no visible intact nuclei by hematoxylin and eosin staining, remnant DNA concentration less than 50 ng/mg dry weight, and DNA fragment length less than 200 basepairs<sup>175</sup>. Biochemical and mechanical properties of the ECM were then characterized by quantitative and qualitative measures.

## **7.3 MATERIALS AND METHODS**

### **7.3.1 *Harvest and preparation of ECM from porcine esophagus***

Esophagi were harvested from market weight (240–260 lbs) pigs and split longitudinally. The mucosa and submucosa were isolated by mechanical separation from the muscularis propria. The luminal surface was gently abraded to remove squamous epithelium. The tissue

that remained was composed primarily of the basement membrane, lamina propria, muscularis mucosa, and submucosa. This tissue was then subjected to a series of immersion treatments as follows: 1% trypsin/0.05% EDTA (Invitrogen, Carlsbad, CA) for 1 h at 37°C on a rocker plate, deionized water for 15 min, 1.0 M sucrose (Fisher Scientific, Pittsburgh, PA) for 30 min, deionized water for 30 min, 3.0% Triton X-100 (Sigma Aldrich, St. Louis, MO) for 48 h, deionized water for 15 min, PBS (Fisher Scientific) for 15 min, 10% deoxycholate (Sigma Aldrich) for 4 h, deionized water for 30 min, 0.1% peracetic acid (Rochester Midland Corp., Rochester, NY) in 4.0% ethanol for 4 h, 100 U/ml DNase (Invitrogen) for 2 h on a rocker plate, followed by 15 min washes with PBS, deionized water, PBS, and deionized water. All treatments were performed at room temperature with agitation on a shaker plate at 300 RPM unless otherwise stated. For cytocompatibility evaluation and in-vivo remodeling evaluation, chemically cross-linked emECM (XL-emECM) scaffolds were used as negative controls. Chemically cross-linked bioscaffolds have been shown to consistently inhibit a constructive remodeling response<sup>270,305</sup>. Cross-linking was achieved by immersion in 0.01 M carbodiimide for 24 hours with multiple subsequent washes in PBS over 48 hours. All devices were lyophilized and sterilized using ethylene oxide.

### **7.3.2 Assessment of DNA content**

DNA was extracted from representative samples (n=6) of emECM. For DNA extraction, lyophilized ECM scaffolds were powdered using a Wiley Mill and filtered through a 60-mesh screen. One hundred milligrams of lyophilized, powdered emECM was digested with proteinase K digestion buffer (100 mM NaCl, 10 mM Tris-HCl (pH = 8), 25 mM EDTA (pH = 8), 0.5% SDS, 0.1 mg/mL proteinase K) at 50 °C for 24 hr. The digest was extracted twice using 25:24:1 (v/v/v) phenol/chloroform/isoamyl alcohol. DNA was precipitated from the aqueous phase at -20 °C

with the addition of 2 volumes of ethanol and 0.1 volume of 3 M sodium acetate (pH = 5.2). The DNA was then centrifuged at 10,000 g for 10 min and resuspended in 1 mL of TE buffer (10 mM Tris (pH = 8), 1 mM EDTA).

The concentration of each extracted DNA sample was determined using Quant-iT PicoGreen dsDNA Assay Kit (Invitrogen) following the manufacturer's recommended protocol. A standard curve was constructed by preparing samples of known DNA concentrations from 0 to 1000 ng/mL and concentration of DNA was found by linear interpolation of the standard curve. Samples were read using SpectraMax M2 Plate Reader (Molecular Devices, Sunnyvale, CA). DNA samples were diluted to ensure their absorbance properties fell within the linear region of the standard curve.

To determine the fragment size of remnant DNA, equal concentrations of extracted DNA from each sample were separated on a 2% agarose gel containing 0.5% ethidium bromide and visualized with ultraviolet transillumination using a reference 100 bp ladder (New England BioLabs, Ipswich, MA). All assays were performed in quadruplicate.

### **7.3.3 Immunolabeling and histochemistry**

A set of slides (n=6) was stained to visualize the extent of cell removal with a standard hematoxylin and eosin (H&E) protocol. Antigen retrieval was performed for immunolabeling studies using a 0.01 M citrate buffer (pH=6) heated to 95-100°C. Slides were placed in the hot buffer for 20 min and subsequently rinsed in PBS (3 × 5 min). Sections were placed in pepsin solution (0.05% pepsin/0.01 M HCl) at 37°C for 15 minutes. After rinsing in PBS (3 × 5 min), the samples were blocked in blocking buffer (2% goat serum/1% bovine serum albumin/0.1% Triton X-100/ 0.1% Tween) for 1 hr at room temperature. The sections were then incubated in the

blocking buffer with rabbit polyclonal collagen IV antibody (1:500 dilution, Abcam, Cambridge, UK), rabbit polyclonal laminin antibody (1:200 dilution, Abcam), or mouse monoclonal fibronectin (1:200 dilution, Abcam) overnight at 4°C in a humidified chamber. Sections were subsequently rinsed in PBS (3 × 5 min). Endogenous peroxidase activity was quenched by rinsing sections in a 3% hydrogen peroxide in methanol solution for 30 min followed by rinsing in PBS (3 × 5 min). Biotinylated goat anti-rabbit or goat anti-mouse secondary antibodies (Vector Laboratories, Burlingame, CA) were diluted 1:200 in blocking buffer and added to the sections for 30 min at 25 °C and sections were subsequently rinsed in PBS (3 × 5 min). The slides were then incubated in detection solution (VectaStain® Elite ABC Reagent, Vector Laboratories) for 30 minutes at 37°C. After rinsing the slides, peroxidase substrate, 3,3'-diaminobenzadine (ImmPACT™ DAB, Vector Laboratories) was prepared as per manufacturer instructions and sections were incubated while being visualized under a microscope to time the color change for subsequent section staining intensities. Tissues were rinsed in water (3 × 5 min). Sections were dipped in hematoxylin (Thermo Shandon, Pittsburgh, PA) for 1 min for a nuclear counterstain and subsequently rinsed in PBS (3 × 5 min).

#### **7.3.4 Sulfated glycosaminoglycan assay**

Sulfated glycosaminoglycan (sGAGs) concentration in esophageal ECM samples was determined using the Blyscan Sulfated Glycosaminoglycan Assay Kit (Biocolor Ltd, Belfast, Northern Ireland). For extraction of sGAGs, lyophilized ECM scaffolds were powdered using a Wiley Mill and filtered through a 60-mesh screen. Samples were prepared by digestion of 50 mg/ml dry weight of each sample with 0.1 mg/ml proteinase K in buffer (10 mM Tris–HCl, pH 8, 100 mM NaCl, 25 mM EDTA) for 48 hr at 50°C. Digested samples were assayed following the

manufacturer's protocol, and the assay was performed in duplicate on three different emECM sample.

#### **7.3.5 Growth factor assay**

The concentration of basic fibroblast growth factor (bFGF) and vascular endothelial growth factor (VEGF) in urea-heparin extracts of emECM samples was determined with the Quantikine Human FGF basic Immunoassay, Human VEGF Immunoassay (R&D Systems, Minneapolis, MN). Each assay for bFGF and VEGF was performed in quadruplicate. The ELISA assays are cross-reactive with porcine growth factors and do not measure activity.

#### **7.3.6 Scanning electron microscopy**

Scanning electron micrographs were taken to examine the surface topology of emECM. Prior to final lyophilization, samples were fixed in cold 2.5% (v/v) glutaraldehyde (Electron Microscopy Sciences, Hatfield, PA) in PBS for at least 24 hr, followed by three washes in PBS. Fixed samples were then dehydrated using a graded series of alcohol (30, 50, 70, 90, 100%) for 15 min each, followed by 15 min in hexamethylenediamine (Fisher) and subsequent air-drying. The dried samples were sputter coated with a 3.5 nm layer of gold/palladium alloy using a Sputter Coater 108 Auto (Cressington Scientific Instruments, Watford, UK) and imaged with a JEOL JSM6330f scanning electron microscope (JEOL, Peabody, MA) at 100× and 500× magnifications.

### 7.3.7 *Perivascular stem cell (PVSC) culture*

Perivascular stem cells isolated by flow cytometry from fetal muscle<sup>306,307</sup> were used in all experiments. These cells (CD146<sup>+</sup>/NG2<sup>+</sup>/CD34<sup>-</sup>/CD144<sup>-</sup>/CD56<sup>-</sup>) have been previously shown to represent a distinct population of perivascular cells obtained after positive selection and stringent exclusion of hematopoietic, endothelial, and myogenic cells, and which are able to differentiate into mesodermal lineages<sup>307,308</sup>. Isolated cells were cultured in high-glucose Dulbecco's modified Eagle's medium (Invitrogen) containing 20% fetal bovine serum (Thermo), 100 U/mL penicillin, and 100 µg/mL streptomycin (Sigma Aldrich) at 37°C in 5% CO<sub>2</sub>.

In-vitro cell viability assays were performed using single layer sheets of ECM. PVSCs (0.5×10<sup>6</sup>) were cultured for 48 hr on 2cm diameter circular sheets of emECM or XL-emECM. Cell viability was compared to growth on tissue culture plastic (TCP) using LIVE/DEAD<sup>®</sup> Viability/Cytotoxicity Kit (Invitrogen) following manufacturer's guidelines. Capturing 4 random fields across the emECM scaffold, the live and dead cells were imaged with green fluorescent calcein-AM (cAM) and red fluorescent ethidium homodimer-1 (EtH1), respectively. Quantification of live and dead cells was achieved using a custom image analysis algorithm developed using the cell profiler image analysis package<sup>309,310</sup>. This custom algorithm identified and quantified the number of cAM<sup>+</sup> (live) and EtH1<sup>+</sup> (dead) cells present on the emECM scaffolds. These results were then expressed as a percentage of total cells.

### 7.3.8 *In-vivo cytocompatibility*

All procedures were performed in accordance with the National Institute of Health (NIH) guidelines for care and use of laboratory animals and with approval of the Institutional Animal Care and Use Committee (IACUC) at the University of Pittsburgh. Sprague Dawley rats (female; 250-350g) were anesthetized with 1.5-3% isoflurane and maintained at a surgical plane of anesthesia. The surgical site was shaved, disinfected with a betadine solution, and an incision was made into the ventrolateral abdominal wall. Bilateral partial thickness abdominal body wall defects<sup>261</sup> were created by excision of a 1cm<sup>2</sup> piece of tissue comprising the internal and external oblique muscles but leaving the transversalis muscle intact<sup>270</sup>. Size matched emECM or XL-emECM scaffolds were then sutured into the defect site using nonresorbable 4-0 proline sutures at each of the 4 corners of the device. The skin was closed using 3-0 resorbable vicryl sutures. Rats were euthanized at 14 or 35 days post-implantation and implant sites were identified by nonresorbable sutures. The implant site containing emECM devices and adjacent tissue site were isolated and placed in 10% neutral buffered formalin. Fixed samples were paraffin embedded and cut into 6 µm sections. The sections from 14 and 35 days post-op were stained with H&E for a qualitative and semiquantitative histomorphologic analysis that evaluated cell infiltration, multinucleated giant cells, vascularity, connective tissue, encapsulation, and scaffold degradation. Two blinded investigators scored the sections according to a previously established and validated semi-quantitative scoring method<sup>132,270</sup>. Using quantitative scoring criteria (Table 7) biologic scaffolds can be grouped according to chronic inflammation and foreign body response (quantitative score < 5), early inflammatory cell infiltration with decreased cellularity and little evidence of constructive remodeling at later time points (5 < quantitative score < 10), and early infiltration by inflammatory cells and signs of constructive remodeling at a later time point (quantitative score > 10).

**Table 7.** Semiquantitative scoring criteria for day 14 and day 35 explants

<b>Day 14</b>				
<b>Scoring Criteria</b>	<b>3</b>	<b>2</b>	<b>1</b>	<b>0</b>
<i>Cellular Infiltration</i> (per 40x field)	>150 cells	75-150 cells	1-75 cells	0 cells
<i>Connective Tissue Organization</i>	Highly organized connective tissue present	Moderately organized connective tissue present	Unorganized connective tissue throughout disrupted original scaffold	Original scaffold intact
<i>Degradation</i>	No scaffold present	Some scaffold present	Mostly present	No degradation
<i>Encapsulation</i>	No encapsulation	Minimal encapsulation	Moderate encapsulation	Dense encapsulation
<i>Multinucleated Giant Cells</i> (per 40x field)	0 cells	1 cell	2-5 cells	>5cells
<i>Vascularity</i> (per 40x field)	>10 vessels	6-10 vessels	2-5 vessels	0-1 vessel
<b>Day 35</b>				
<b>Scoring Criteria</b>	<b>3</b>	<b>2</b>	<b>1</b>	<b>0</b>
<i>Connective Tissue Organization</i>	Highly organized connective tissue present	Moderately organized connective tissue present	Unorganized connective tissue throughout disrupted original scaffold	Original scaffold intact
<i>Degradation</i>	No scaffold present	Some scaffold present	Mostly present	No degradation
<i>Encapsulation</i>	No encapsulation	Minimal encapsulation	Moderate encapsulation	Dense encapsulation
<i>Multinucleated Giant Cells</i> (per 40x field)	0 cells	1 cell	2-5 cells	>5cells
<i>Muscle Ingrowth</i>	Organized muscle throughout scaffold	Muscle cells present in scaffold center	Muscle cells present at scaffold periphery	No muscle ingrowth

Immunolabeling of macrophages was performed on tissue sections from day 14 explants. Paraffin embedded sections were deparaffinized with xylene and rehydrated through a graded ethanol series. Heat-mediated antigen retrieval was performed with 0.01 M citrate buffer (pH=6) at 95-100 °C for 25 min. The tissue sections were subjected to Tris-Buffered Saline Tween-20 (TBST) for 15 min, followed by incubation in blocking buffer (2% horse serum albumin/1% bovine serum albumin/0.05% Tween-20/0.05% Triton X-100) for 1 h. The primary antibodies, diluted in blocking buffer, were added to the slides for 16 hr at 4 °C in a humidified chamber. The slides were then washed three times in PBS prior to the addition of the secondary antibody for 1 hr in a humidified chamber at room temperature. DAPI was used as a nuclear counterstain. The primary antibodies used in this study were mouse anti-rat CD68 (1:150, AbD Serotec, Raleigh, NC), goat polyclonal CD206 (Santa Cruz Biotech, Santa Cruz, CA), rabbit anti-rat CD86 (1:150, Abcam) and mouse anti-rat CD68 (1:50, Serotec, Raleigh NC). The secondary antibodies used were Alexa Fluor® donkey anti-mouse 594 (1:200, Invitrogen), Alexa Fluor® donkey anti-goat 488 (1:200, Invitrogen) and donkey anti-rabbit IgG-PerCP-Cy5.5 (1:300, Santa Cruz). CD68 is a pan-macrophage marker. CD86 is an M1 marker. CD206 is an M2 marker. All primary antibodies were confirmed to cross-react with rat epitopes. The sections were imaged at random fields along the interface of the native tissue and ECM scaffold. Quantification of M1/M2 polarization was achieved using a custom image analysis algorithm developed using the cell profiler image analysis package<sup>309,310</sup>. This algorithm identified and quantified the number of CD68+ CD86+ (M1 phenotype) and CD68+ CD206+ (M2 phenotype) cells present within the tissue sections. Any cells that co-expressed these markers were not counted. These numbers were then expressed as a ratio of M2/M1.

### 7.3.9 **Biomechanical testing**

The passive biaxial mechanical properties were characterized for the native esophageal mucosa and emECM (n=8). A detailed description of the testing device and methods used for planar biaxial testing has been reported previously<sup>311</sup>. Briefly, samples were affixed to 250 g load cells (Model 31, Honeywell, Columbus, OH) with two loops of suture attached to each side with four hooks, and deformation was measured from a four marker array. Samples were tested in PBS at room temperature under an equibiaxial stress protocol from a 0.5 g tare load to 250 kPa after 10 cycles of preconditioning with a cycle time of 30 s. All data was referenced to the post-preconditioned free-float state. The maximum strain for each sample was then defined as the strain at the maximum tested stress of 250 kPa.

The suture retention analysis we performed according to a previously described protocol<sup>312</sup>. Briefly, a 2-0 prolene suture with a taper needle was passed through the specimen with a 2 mm bite depth, and tied with a square knot and the loop attached to an Instron machine, and pulled at a constant rate of 10 cm/min<sup>312</sup>. Two locations were tested per sample and eight samples were tested per group. Samples were thoroughly rehydrated prior to testing.

### 7.3.10 **Statistical analysis**

An independent samples t-test was used to determine whether the DNA, growth factor, and GAG content, and mechanics of the emECM were different than that of native esophagus ( $p < 0.05$ ). A one-way analysis of variance (ANOVA) was used to determine differences in the percentage of viable cells in culture. Macrophage phenotype ratio between XL-emECM and emECM was compared using an independent samples t-test. A two-way ANOVA with post-hoc Tukey test was performed to determine differences in biomechanical properties with the two independent variables being axes and material. All data are reported as mean  $\pm$  standard error.

## 7.4 RESULTS

### 7.4.1 *Decellularization efficacy*

The degree of decellularization following the described method was assessed using previously established guidelines for decellularization <sup>175</sup>. The concentration of remnant DNA in emECM ( $48 \pm 6.4$  ng/mg) was markedly less ( $p < 0.001$ ) than that in native esophageal tissue ( $855 \pm 24$  ng/mg) (Figure 4A). Residual DNA was present only in fragments less than 200 bp in length (Figure 4B).

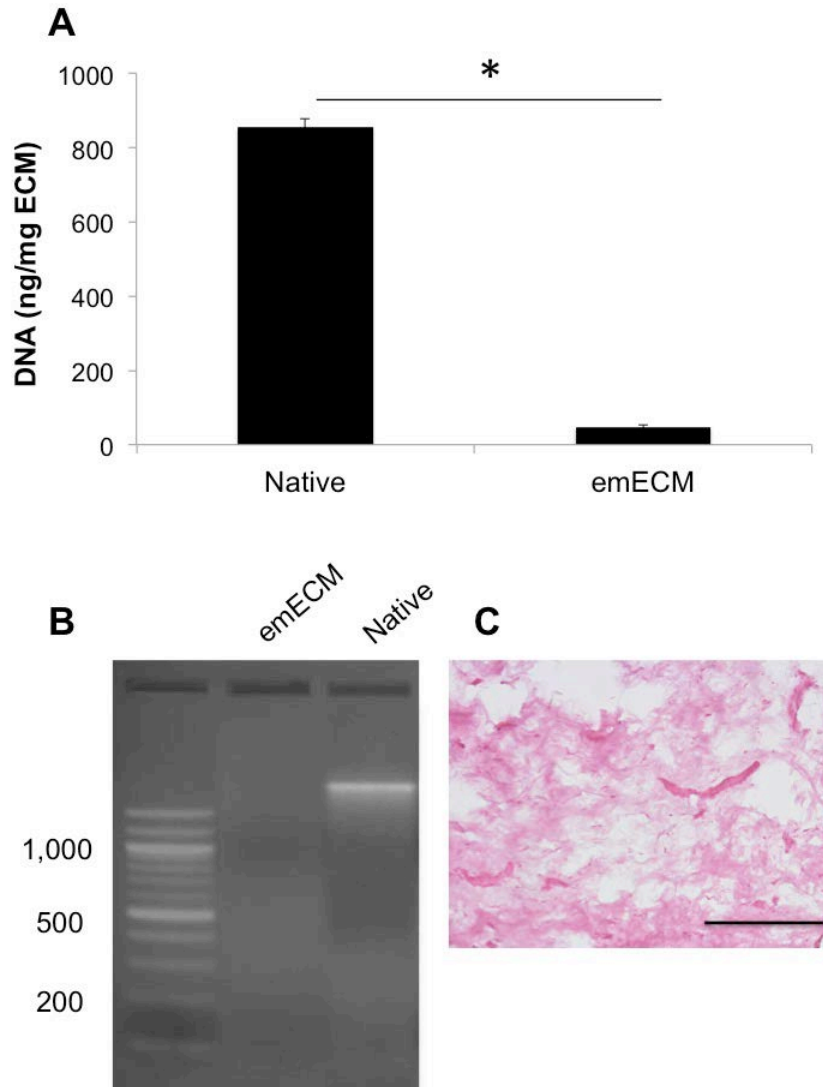


**Figure 4. Decellularization efficacy.** Decellularization of emECM was assessed by the amount and size of remaining DNA and histologically by hematoxylin and eosin (H&E). The amount dsDNA in emECM was less than 50ng/mg, which was significantly less (asterisk;  $p < 0.001$ ) than native tissue (A). DNA fragment length was assessed by gel electrophoresis using a reference 100 bp ladder (B). No intact nuclei were visible after decellularization by H&E staining (C). Data represented as mean  $\pm$  standard error. Scale bar = 100  $\mu$ m.

#### 7.4.2 Biochemical and ultrastructural characteristics of esophageal ECM

The concentration of sGAGs in emECM ( $226 \pm 19$  mg/g) was not different ( $p=0.37$ ) compared to the concentration of sGAGs in native esophagus ( $188 \pm 28$  mg/g) (Figure 5A). Quantification of growth factors showed no detectable levels of VEGF were present following decellularization. However, bFGF was retained after decellularization ( $63 \pm 16$  ng/g) (Figure 5B) in a lesser amount than that in native tissue ( $3585 \pm 100$  ng/g) ( $p<0.001$ ).

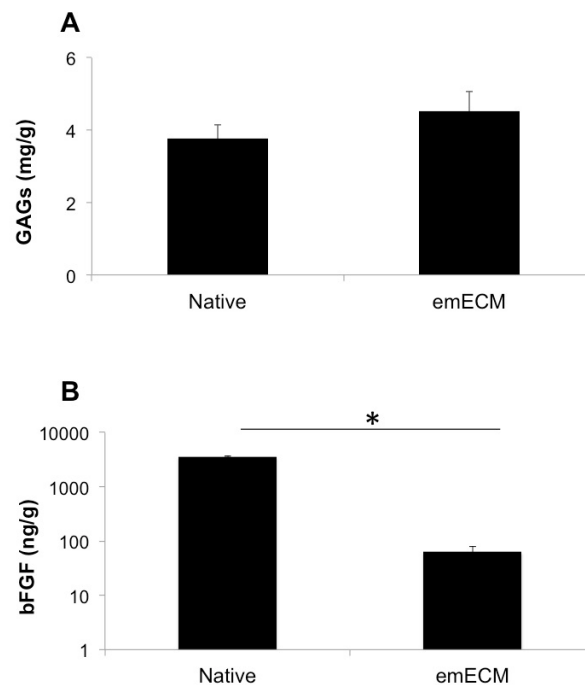


**Figure 5. Retention of biologic components.** Growth factor protein and glycosaminoglycans (GAGs) remain after decellularization. The amount of (A) GAGs and (B) basic fibroblast growth factor (bFGF) remaining after decellularization was measured. Data represented as mean  $\pm$  standard error. Asterisk signifies  $p < 0.05$ .

In addition to measuring the concentration of remaining sGAGs and growth factors, the preservation and spatial distribution of basement membrane proteins, collagen IV and laminin, and a non-basement membrane protein, fibronectin, was examined. Immunolabeling showed the presence of collagen IV (*Figure 6B*) and laminin (*Figure 6D*) that was predominant along the luminal surface of the emECM (marked by “L”). Positive staining for fibronectin was present and distributed throughout the emECM scaffold (*Figure 6F*).

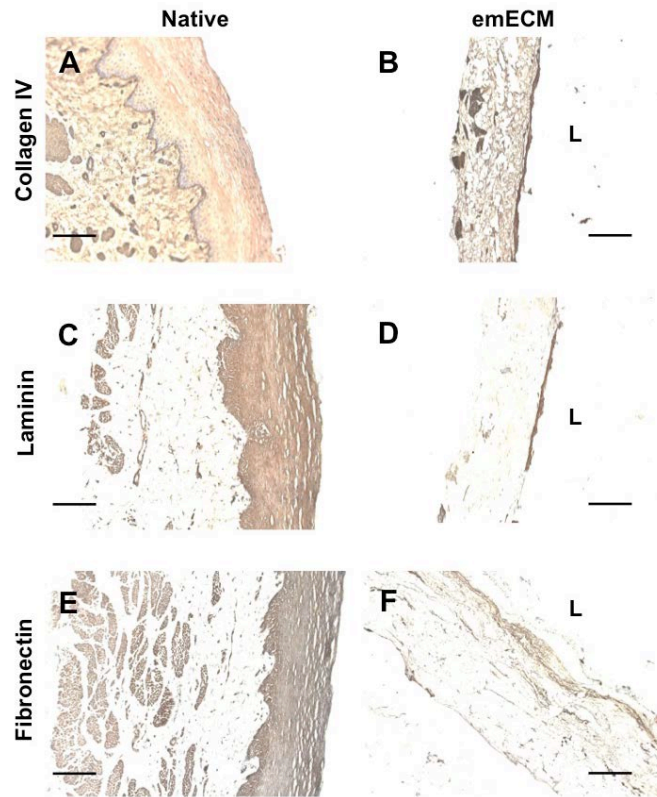


**Figure 6. Immunolabeling of collagen IV, laminin, and fibronectin in emECM samples.** Dark brown indicates positive stain. Immunolabeling of native tissue (A,C,E) is shown as a comparison to emECM (B,D,F). L indicates luminal surface. Scale bar = 200  $\mu$ m.

Lastly, SEM images of the luminal and abluminal surface of emECM showed a smooth surface on the luminal surface of the emECM (Figure 7A,C). The abluminal surface, however, had a more textured and fibrous structure (Figure 7B,D).

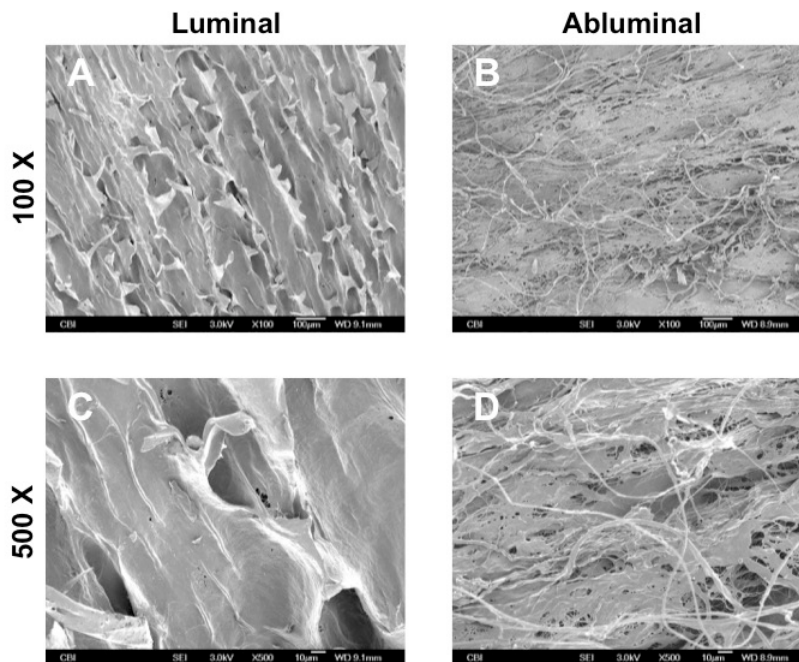


**Figure 7. Scanning electron micrographs (SEM) of emECM surface.** The luminal surface of the emECM scaffold was characterized by a smoother surface (A,C) compared to the abluminal surface which was more textured and fibrous (B,D)

#### 7.4.3 Biomechanical properties

The equibiaxial stress response of the native esophagus showed anisotropic behavior with a maximum strain of 83% and 18% in the circumferential and longitudinal direction, respectively (Figure 8A,B). The emECM showed similar anisotropy, but had a lower compliance along both

axes, with the circumferential strain reaching only 10.5% (Figure 8A,B). The decellularized tissue had 30% lower suture retention strength than the native esophagus (**Table 8**).

**Table 8. Native esophagus and emECM suture retention test**

	<i>Treatment</i>			
	<i>Native</i>		<i>emECM</i>	
	<i>Mean</i>	<i>Standard Error</i>	<i>Mean</i>	<i>Standard Error</i>
<i>Suture Retention Strength (N)*</i>	<i>2.42</i>	<i>0.24</i>	<i>1.73</i>	<i>0.17</i>

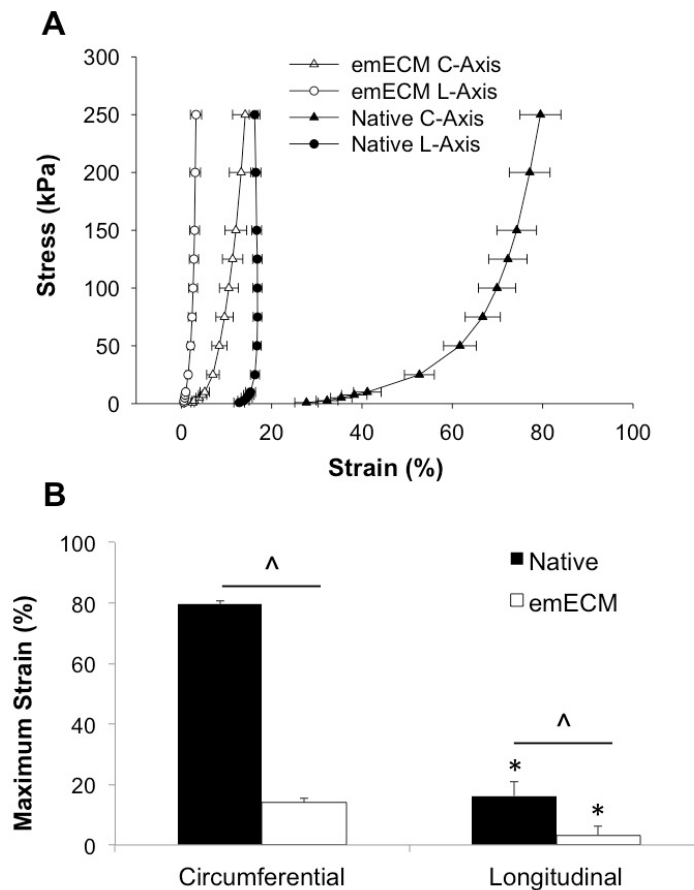


**Figure 8. Native and decellularized esophagus mechanical characterization.** The equibiaxial stress response was characterized along the circumferential and longitudinal axes (A). The maximum strain defined at a stress of 250 kPa for both circumferential (C) and longitudinal (L) axes (B). Significant differences ( $p < 0.05$ ) between the circumferential and longitudinal axes of the same sample are denoted as the following: (\*) as different from circumferential. Significant differences between samples in each axis are denoted as the following: (^) as different from native. Data represented as mean  $\pm$  standard error.

#### 7.4.4 Cytocompatibility

When cultured on emECM and XL-emECM, quantification of PVSC cell viability in-vitro showed no difference when compared to tissue culture plastic ( $p = 0.67$ ). Both conditions resulted in over 98% viability following 48 hours in culture (**Figure 9**).

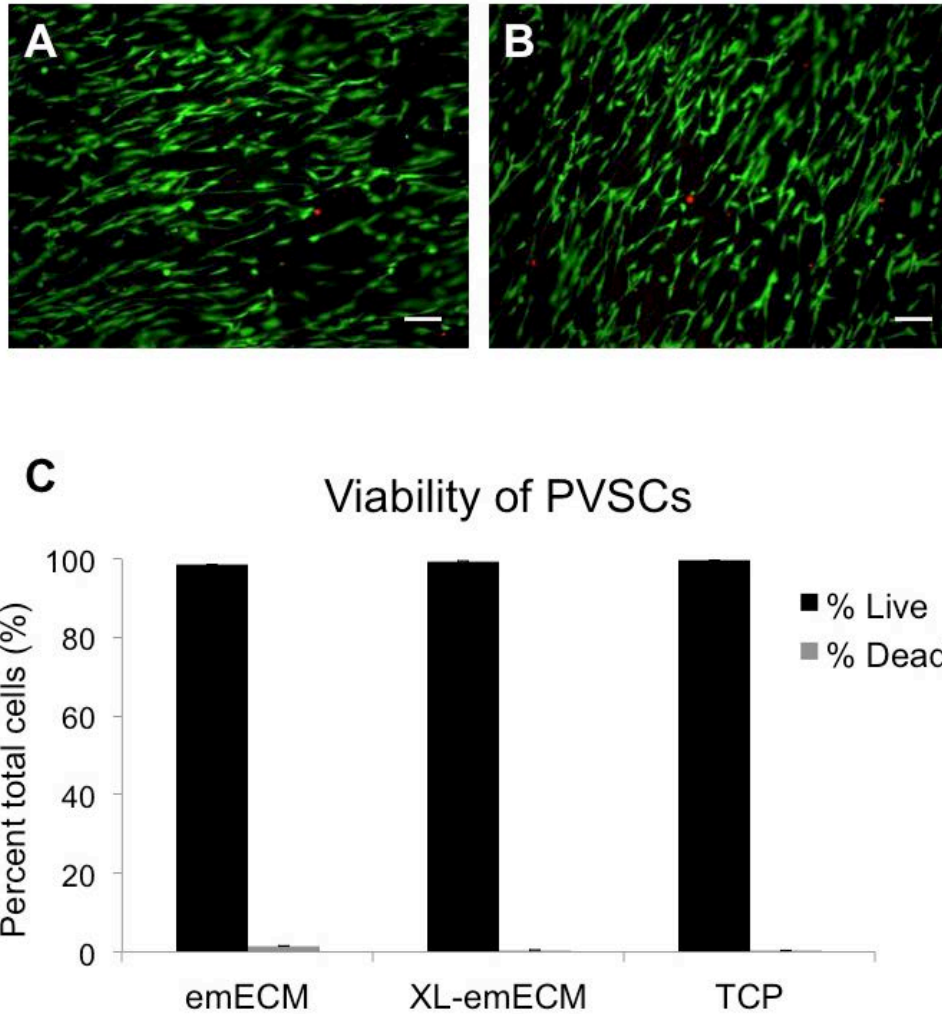


**Figure 9. Cytocompatibility of emECM and XL-emECM.** The viability of perivascular stem cells (PVSCs) after 48 h culture on emECM (A), XL-emECM (B), and tissue culture plastic (TCP) was assessed. Percentage of live cells was quantified and compared across groups (C). Data represented as mean  $\pm$  standard error. Scale bar = 50  $\mu$ m.

In-vivo host response to emECM was examined at both 14 and 35 days post-implantation in a rat abdominal body wall model. The host response to emECM scaffolds showed a robust mononuclear cell response throughout the partially degraded scaffold at 14 days (Figure 10A) and yielded a histologic score of 11.4. Along the interface between the emECM scaffold and native tissue, the macrophage response was predominantly of the M2

phenotype (Figure 11A) with a ratio of M2/M1 macrophages of  $1.29 \pm 0.21$  (Figure 11C). By 35 days post-implantation, the original material was not identifiable by histologic evaluation and the remodeling site was composed of organized host connective tissue and islands of skeletal muscle at the periphery that extended into the center of the remodeling site (Figure 10B).

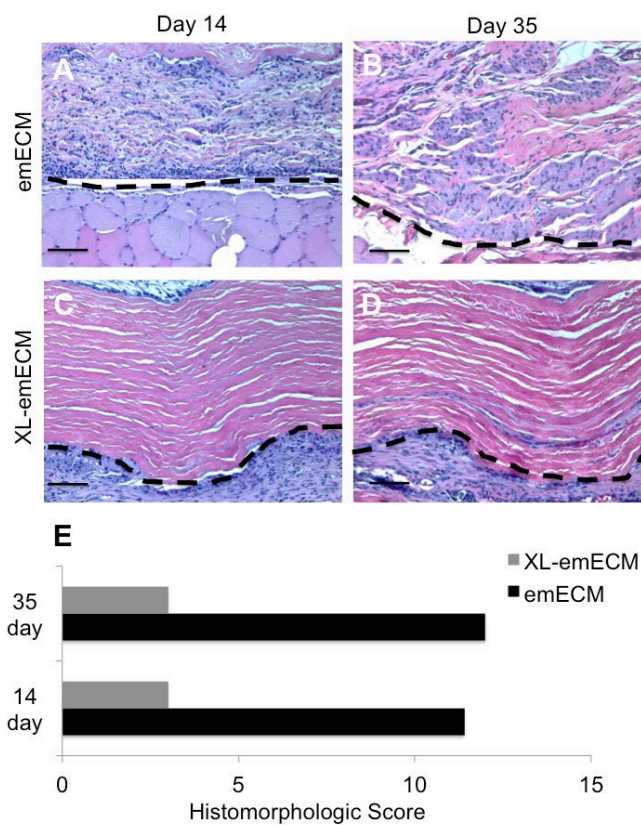


**Figure 10. In-vivo cytocompatibility.** Tissue sections were stained with H&E at 14 and 35 days after implantation of emECM (A,B) and XL-emECM (C,D). Histomorphologic sections were evaluated and scored according to previously established criteria (E). Scale bar= 100  $\mu$ m

Semiquantitative histomorphologic analysis of emECM at day 35 resulted in a total score of 12. In contrast, the host response to XL-emECM was characterized by little to no cellular infiltration or vasculature within the chemically cross-linked bioscaffold, a dense population of mononuclear macrophages at the host-scaffold interface, the deposition of disorganized connective tissues surrounding the implanted test article, and little to no degradation of the material at 14 days (Figure 10C). The cellular response along the scaffold and native tissue interface was shown to be predominantly macrophages of the M1 phenotype (Figure 11B) with an M2/M1 ratio of  $0.19 \pm 0.03$ , which was less than ( $p < 0.001$ ) the M2/M1 ratio in emECM. By 35 days, the XL-emECM was still largely intact and showed no infiltration of skeletal muscle (Figure 10D).

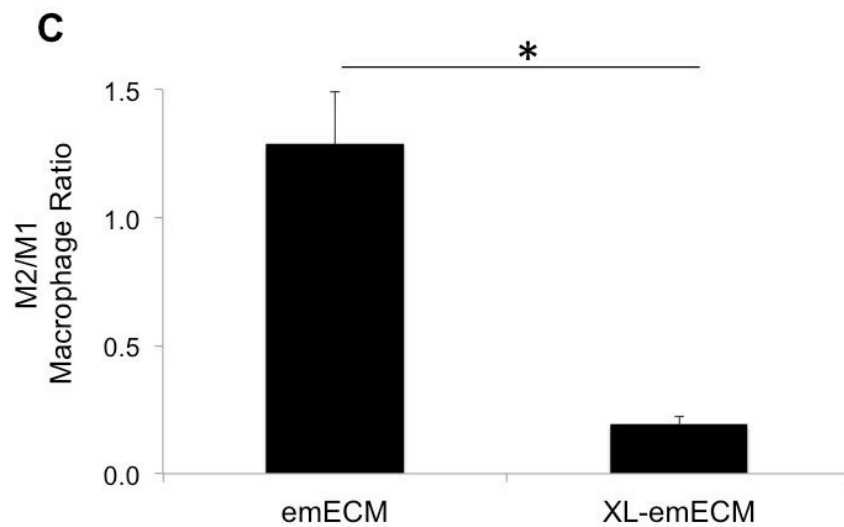
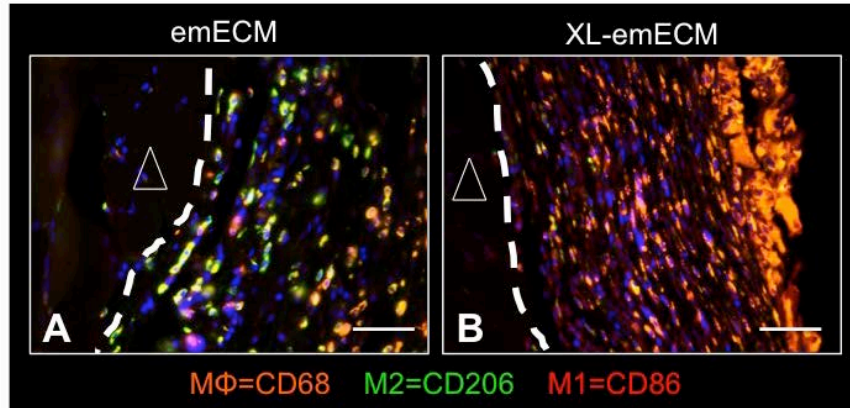


**Figure 11. In-vivo macrophage response.** Macrophage immunolabeling in emECM (A) and XL-emECM (B) in explants 14 d after implantation was quantified and represented as a ratio of M2/M1 phenotype (C). Dashed line indicates the interface of native tissue (marked by a triangle) and the surgical site. Data represented as mean  $\pm$  standard error. Scale bar = 50  $\mu$ m.

## 7.5 DISCUSSION

Although current clinical applications of ECM-based biologic scaffolds have included the use of devices originating from heterologous tissue sources, recent studies have suggested there may be an advantage to using ECM derived from homologous tissue (i.e., site-specific)<sup>109-111,115</sup>. This

concept is based upon the fact that ECM from different tissue sources have distinct and specific properties, including the ultrastructure and composition; i.e., a tissue specific microenvironmental niche.

The necessity or preference for site-specific ECM remains unknown for many therapeutic applications. Zhang et al have shown that ECM derived from liver, skin, and skeletal muscle increases the proliferation and differentiation potential for site-matched cell types <sup>113</sup>. Sellaro and colleagues have shown that ECM derived from liver improves the maintenance of sinusoidal endothelial cell phenotype <sup>109</sup> and the function of hepatocytes in-vitro <sup>110</sup>. More recently, porcine myocardial ECM has been shown to improve cardiac progenitor cell function in-vitro <sup>112</sup>. Seif-Naraghi et al have shown that injection of a hydrogel form of cardiac ECM after myocardial infarct improves cardiac function and results in increased cardiac muscle mass <sup>89</sup>. Although the present study showed that the emECM facilitates a constructive remodeling response in a heterologous location and excellent in-vitro cytocompatibility, any site specific benefit in the esophageal mucosa (homologous) location has not yet been tested.

The importance of effective decellularization is well recognized <sup>138,175</sup>. While protocols for decellularizing the esophagus have been reported, little has been described with focus on the esophageal mucosa. Bhrany et al developed a rat full thickness esophageal scaffold that was able to support epithelial cell growth <sup>176</sup>. Marzaro et al decellularized intact porcine esophagus and seeded with autologous smooth muscle cells for repair of an esophageal muscularis defect <sup>163</sup>. Using a similar protocol, Totonelli et al decellularized intact esophagus using luminal perfusion <sup>313</sup>. These groups reported decellularization of the entire esophagus, including both muscularis externa and mucosa. However, the efficacy of these decellularization protocols, characterization, and cytocompatibility of the scaffold were not investigated in a comprehensive manner.

Protocols for esophageal decellularization have been reported but have been conducted using non-porcine species and/or have used harsh detergents such as sodium dodecyl sulfate (SDS) <sup>176,314</sup>. SDS, as an ionic detergent, destroys the cell membrane and denatures protein—altering the collagen structure in ECM <sup>213</sup>. Thus, SDS has the associated drawback of ultrastructure disruption <sup>242,315,316</sup> and growth factor elimination <sup>173</sup>. A loss of ECM structure is also associated with variability in biomechanical properties <sup>317</sup>. Therefore, the use of SDS was avoided in the present study.

Studies have shown the requirement for retention of at least a portion of the submucosal tissue to promote constructive remodeling of the esophagus over stricture and scarring <sup>93</sup>. The use of emECM would therefore appear a more logical strategy for clinical translation. The methods of the current study thoroughly decellularized esophageal mucosa with the use of mild detergents while preserving the anisotropic mechanical properties and bioactive molecules. The described method effectively removed cellular components while maintaining ECM constituents and basement membrane proteins, collagen IV and laminin, in a contiguous pattern at the surface of the emECM material. Scanning electron micrographs of the luminal surface of emECM showed a smooth contour that was also consistent with an intact basement membrane surface. The basement membrane complex may be of importance to esophageal mucosal remodeling because of its natural function of supporting the growth of epithelial cell populations <sup>318-320</sup>. The emECM scaffold was cytocompatible with perivascular stem cells, which were shown to survive and proliferate when cultured on the scaffold.

The role of the host response to biologic ECM scaffolds is a topic of interest and has been reviewed in detail elsewhere <sup>321</sup>. Briefly, the successful therapeutic efficacy of biologic scaffolds is attributed largely to the ability of these ECM-derived materials to modulate the innate immune response in favor of a constructive remodeling outcome over scarring/encapsulation. Key mediators of the innate immune response are macrophages—a

highly plastic and heterogeneous cell population<sup>292,322</sup>. Appropriately prepared biologic scaffolds have been shown to elicit a macrophage response that is predominantly of an anti-inflammatory (M2) phenotype which has been associated with a downstream constructive remodeling response (i.e., formation of functional, site-appropriate tissue)<sup>132,133,305</sup>. However, when biologic scaffolds are prepared using harsh decellularization methods, are chemically cross-linked, or are inadequately decellularized, a robust proinflammatory (M1) macrophage phenotype is observed at the in-situ interface of host tissue and ECM scaffold and ultimately results in chronic inflammation, encapsulation, and fibrosis<sup>132,314</sup>. In the present study, implantation of emECM scaffolds in an established rodent model was associated with a predominant M2 macrophage response after 14 days and was shown to remodel in a constructive fashion with a histomorphologic score comparable to urinary bladder matrix (UBM-ECM) and small intestinal submucosa ECM (SIS-ECM)<sup>90,132,270</sup>. These findings are consistent with the predictive association of the M2 phenotype with constructive remodeling outcomes<sup>132</sup>.

The objective of this chapter was to develop and characterize an emECM scaffold but was limited by a number of factors. The effects of emECM on esophageal cells were not studied. Instead, perivascular stem cells were used because they are well-characterized<sup>307</sup> and have been used in a number of studies to evaluate the cytocompatibility of a variety ECM scaffolds<sup>308</sup>. In addition, while retention of growth factor proteins was used as an indicator of the relative mildness of the decellularization protocol, the activity of the growth factors was not determined and the effect of the presence of these growth factors in the overall remodeling process is unknown. While the M2/M1 macrophage phenotype ratio has been shown to be strongly associated with a constructive remodeling response in several anatomic locations, a direct cause-effect relationship has yet to be established. Finally, the present study observed the in-vivo compatibility and constructive remodeling response of the emECM scaffold in a well-characterized abdominal wall defect model, a heterologous anatomic site. Thus, the potential

benefits of ECM derived from homologous tissue (i.e., the use of emECM in an esophageal mucosal resection model) remain unknown.

## **7.6 CONCLUSION**

Porcine esophageal mucosa was effectively decellularized with the use of a relatively mild detergent-based protocol. The emECM scaffold maintained structural proteins and an ultrastructure consistent with a basement membrane complex. Likewise, retention of sGAGs and bFGF was shown. Compared to native esophageal mucosal tissue biomechanics, the emECM scaffold was expectedly less compliant but retained similar anisotropy. The emECM biologic scaffold was conducive to stem cell viability in-vitro and was associated with a host innate immune response consisting predominantly of M2 macrophages and a more robust constructive remodeling response when compared to XL-emECM biologic scaffolds in-vivo. Future studies aimed at investigating the specific physical and/or biochemical factors responsible for the constructive remodeling outcome and the utility of an emECM biologic scaffold in an esophageal location are warranted.

## **7.7 ACKNOWLEDGMENTS**

The authors gratefully acknowledge the work of Dr. Jeremy Kelly for the isolation of perivascular stem cells and Deanna Rhodes for histologic processing. Funding for this project was partially provided by NIH Grant: 5T32EB001026-08.

## 8.0 PREPARATION AND CHARACTERIZATION OF A BIOLOGIC SCAFFOLD FROM COLONIC MUCOSA<sup>5</sup>

### 8.1 ABSTRACT

Gastrointestinal pathologies, injuries, and defects affect millions of individuals each year. While there are diverse treatment options for these individuals, no ideal solution exists. The repair or replacement of gastrointestinal tissue therefore represents a large unmet clinical need. Biomaterials derived from extracellular matrix scaffolds have been effectively used to repair or replace numerous tissues throughout the body in both pre-clinical and clinical studies. Such scaffolds are prepared from decellularized tissues and the biochemical, structural, and biologic properties vary depending upon the source tissue from which the ECM is derived. Given the potential benefit of a site-specific ECM scaffolds for some applications, the objective of the present chapter was to prepare, characterize, and determine the *in vitro* and *in vivo* cell response to ECM derived from porcine colon. Results show that porcine colon can be effectively decellularized while retaining biochemical and structural constituents of the source tissue. Two forms of coECM, scaffold and hydrogel, were shown to be cell-friendly and facilitate the polarization of macrophages towards an M2 phenotype both in-vitro and in-vivo.

---

<sup>5</sup> Portions of this chapter were adapted from the following publication:  
**Keane TJ**, Dziki J, Castelton A, Faulk DM, Messerschmidt V, Londono R, Reing JE, Velankar SS, Badylak SF. Preparation and Characterization of a Biologic Scaffold and Hydrogel Derived from Colonic Mucosa. *Journal for Biomedical Materials Research Part B*. October 2015. DOI:10.1002/jbm.b.33556

## 8.2 INTRODUCTION

The gastrointestinal (GI) tract is composed of a series of hollow muscular tubes that perform a variety of functions including mastication, digestion, motility, nutrient absorption, and waste excretion, among others. Such functional diversity requires organization of specialized cell and tissue types, and repair following injury or disease is imperative for the health of the host. Pathologies such as inflammatory bowel disease affect up to 4 million patients per year <sup>323</sup> and short bowel syndrome affects an additional 20,000 individuals in the United States alone <sup>324</sup>. Diseases such as these have very limited therapeutic options and are the cause of tremendous morbidity and health care expenditures. Biomaterials and/or regenerative medicine strategies to address such problems will require the creation of a microenvironment that supports the cultivation, recruitment, differentiation, and maintenance of the specialized cell types required for normal GI function.

Biomaterial-mediated approaches to GI replacement must not only provide a mechanical support structure for cell growth but also be amenable to cell infiltration, allow for gas and nutrient exchange, and be compatible with the host innate immune system. Both synthetic and biologic scaffold materials have been manufactured and studied for GI repair / replacement applications and each are associated with their respective advantages and disadvantages <sup>325,326</sup>. Synthetic scaffolds such as poly-lactic acid or poly-caprolactone allow for tunable materials that can be tailored for specific applications. However, synthetic scaffolds invariably elicit proinflammatory and/or a foreign body response upon implantation that may result in encapsulation, fibrosis, and loss of function <sup>327</sup>. Compatibility of scaffold materials with the host immune system has been shown to be a critical determinant of downstream functional tissue remodeling <sup>328</sup>.

Biologic scaffold materials, such as those composed of extracellular matrix (ECM) derived via decellularization of source tissues, can provide a compatible and instructive template for endogenous cell infiltration and differentiation, recapitulate the natural niche, and degrade to allow for complete host tissue replacement with associated release or exposure of bioactive matricryptic peptide sites. Implanted ECM bioscaffolds promote a favorable host immune response by induction of an M2-like macrophage phenotype. This immune modulation is typically associated with a functional constructive remodeling outcome. However, the properties and composition of ECM bioscaffolds are often variable and are critically dependent on factors such as source tissue anatomic site and age<sup>105</sup>, use of chemical cross-linking agents<sup>67,280</sup>, method of decellularization<sup>138</sup>, manufacturing processes, and terminal sterilization methods<sup>329</sup>, among others. The potential benefits of utilizing ECM scaffolds derived from homologous source tissue include the retention of tissue-specific cell phenotypes<sup>109,110</sup>, enhancing tissue-specific differentiation<sup>118</sup>, and promoting chemotaxis and proliferation of progenitor cells<sup>86</sup>. Previous reports have shown that regions of the porcine GI system such as the small intestine (i.e., SIS) and esophagus can be decellularized and retain essential ultrastructural components, endogenous growth factors, and biomechanical strength<sup>330-336</sup><sup>162</sup>. The suitability of these scaffolds for GI repair applications including treatment of esophageal disease, short bowel syndrome, ulcerative colitis, Crohn's disease, or mucositis, has not been extensively investigated.

The objective of the present chapter was to prepare, characterize, and determine the *in vitro* and *in vivo* cytocompatibility of ECM bioscaffolds derived from porcine colon. DNA content, retention of ultrastructural and biochemical molecules, biomechanical properties, *in vitro* cytocompatibility, and the *in vivo* host macrophage response were examined both quantitatively and qualitatively and compared across sheet, hydrogel, cross-linked, and incompletely decellularized forms of porcine colon ECM.

## 8.3 MATERIALS AND METHODS

### 8.3.1 *Preparation of colonic ECM (coECM)*

Colons were collected from market weight pigs (approximately 6 months of age and 260 lbs) at a local abattoir (Thoma's Meat Market, Saxonburg, PA). The colon was rinsed in water to remove contents and frozen at -20C until use. Colonic submucosa was mechanically isolated from the surrounding tissue and then delipidized and decellularized. Native colonic submucosa prior to delipidization and decellularization was used as a control group. For preparation of coECM, submucosa was subject to agitated washes of 2:1 (v/v) chloroform to methanol (30 min with stirring), 3 washes each of 100%, 90%, and 70% ethanol (5 minutes each), 3 washes of deionized water (5 min), 0.02% Trypsin/0.05% EDTA (1h at 37 °C), twice with deionized water (5 min), 4% sodium deoxycholate (30 min), twice with deionized water (5 min), 4% sodium deoxycholate (30 min), deionized water (2 x 5 min), 0.1% peracetic acid in 4% ethanol (2h), PBS (15 min), deionized water (2 x 15min), and PBS (15 min). Solutions were agitated on a shaker at 300 rpm and room temperature unless otherwise stated.

A subset of coECM scaffolds was subjected to chemical cross-linking (XL) using 10mM carbodiimide for 24h at room temperature with constant stirring. The XL-coECM was then washed extensively in PBS for 48h with stirring and then lyophilized to dry. For in-vitro cell growth, in-vivo implants, and suture retention strength experiments, the colonic submucosa, XL-coECM, and coECM were vacuum pressed to form a 4-layer device. The devices used for cell culture and in-vivo implantation were sterilized by ethylene oxide.

### 8.3.2 *Hydrogel preparation*

Hydrogels were prepared from coECM as previously described<sup>337</sup>. Briefly, lyophilized scaffolds were powdered using a Wiley Mill and filtered through a 60 mesh screen (<250 µm particle size). The comminuted ECM was then digested in 1 mg/mL porcine pepsin (Sigma Aldrich, St. Louis, MO) in 0.01 N HCl for 48 h under constant stir rate at room temperature. Gelation was induced by neutralization at 4°C of pH and salt concentration with the respective addition of one-tenth digest volume of 0.1 N NaOH and one-ninth digest volume of 10x PBS. Gelation was then achieved by placing the neutralized digest in a non-humidified incubator at 37°C for 1 h for in-vitro studies. Gelation of coECM hydrogels for in-vivo studies was accomplished by direct injection of the neutralized digest over the site of abdominal wall defect. ECM concentrations of 4 and 8 mg/mL were evaluated by turbidometric and rheologic assays. Cell culture and in-vivo experiments were conducted with 8 mg/mL coECM hydrogels.

### 8.3.3 *Determining decellularization efficacy*

8.3.3.1 **Histologic analysis:** Scaffolds (native colonic submucosa and coECM) and native colon tissue were fixed in 10% neutral buffered formalin for 24h. The fixed samples were then paraffin embedded and 5µm sections were cut onto slides. Slides were stained with hematoxylin and eosin (H&E) or 4',6-diamidino-2-phenylindole (DAPI) to visualize the presence of nuclear material.

**8.3.3.2 DNA concentration and fragment analysis:** Residual DNA content of the ECM was quantified by powdering samples with a Wiley Mill using a 60-mesh from separate preparations (n = 4) of lyophilized coECM. Samples (100 mg) were digested in 0.1 mg/mL proteinase K digestion buffer at 50 °C for 24 hours. DNA was extracted twice in phenol/chloroform/isoamyl alcohol and centrifuged at 10,000g (10 min at 4 °C). The aqueous phase, containing the DNA, was then mixed with 3 M sodium acetate and 100% ethanol, frozen on dry ice for 20 minutes, centrifuged at 10,000g (10 min at 4 °C), pouring off the supernatant, adding 70% ethanol, repeating centrifugation, removing supernatant, and drying the remaining DNA pellet. When dry, the pellet was resuspended in TE buffer (10mM Tris/1mM EDTA) and the DNA concentration was quantified utilizing a PicoGreen Assay (Invitrogen) following manufacturer's instructions. The fragment length of remnant DNA in the samples was then visualized with gel electrophoresis on a 1% agarose gel with a 100bp ladder (Invitrogen) containing ethidium bromide.

**8.3.3.3 Phospholipid measurement:** Homogenates were prepared from 40 mg of lyophilized and comminuted tissue or ECM in 2 mL of homogenization buffer (50mM Tris pH 7.4/ 20mM CaCl<sub>2</sub>/ 0.5% Triton X-100). Samples were homogenized on ice 5 times for 15 sec using a PowerGen 500 Homegenizer (Fisher Scientific, Pittsburgh, PA). Samples were centrifuged at 2,000×g for 20 min at 4°C and the supernatant extract was collected. A second extraction was completed on the remaining pellet, as above, using 1 mL of extraction buffer. The extracts were combined and measured for phospholipid content using EnzyChrom Phospholipid Assay Kit (BioAssay Systems, Hayward, CA) according to manufacturers instructions.

#### **8.3.4 Glycosaminoglycan and growth factor measurement**

The concentration of sulfated glycosaminoglycan (sGAG) and non-sulfated GAG in coECM samples was determined using the Blyscan Sulfated Glycosaminoglycan Assay Kit (Biocolor Ltd, Belfast, Northern Ireland) and Hyaluronan Quantikine ELISA Kit (R&D Systems, Minneapolis, MN), respectively. The concentration of non-sulfated GAG, hyaluronic acid (HA), was measured using neutralized pepsin digests as described above. Digested samples were assayed following the manufacturer's protocol, and the assay was performed in duplicate on three different coECM samples.

The concentration of basic fibroblast growth factor (bFGF) and vascular endothelial growth factor (VEGF) in urea-heparin extracts of coECM samples was determined with the Quantikine Human FGF basic Immunoassay, Human VEGF Immunoassay (R&D Systems). Each assay for bFGF and VEGF was performed in quadruplicate. The ELISA assays are cross-reactive with porcine growth factors and do not measure activity.

#### **8.3.5 Immunohistochemistry**

Antigen retrieval was performed on de-paraffinized slides with 5 µm sections using a 0.01 M citrate buffer (pH=6) heated to 95-100°C. Slides were placed in the hot buffer for 20 min and subsequently rinsed in PBS (3 × 5 min). Sections were placed in pepsin solution (0.05% pepsin/0.01 M HCl) at 37°C for 15 minutes. After rinsing in PBS (3 × 5 min), the samples were blocked in blocking buffer (2% goat serum/1% bovine serum albumin/0.1% Triton X-100/ 0.1% Tween) for 1 hr at room temperature. The sections were then incubated in the blocking buffer with rabbit polyclonal laminin antibody (1:200 dilution, Abcam), or mouse monoclonal fibronectin

(1:200 dilution, Abcam) overnight at 4°C in a humidified chamber. Sections were subsequently rinsed in PBS (3 × 5 min). Endogenous peroxidase activity was quenched by rinsing sections in a 3% hydrogen peroxide in methanol solution for 30 min followed by rinsing in PBS (3 × 5 min). Biotinylated goat anti-rabbit or goat anti-mouse secondary antibodies (Vector Laboratories, Burlingame, CA) were diluted 1:200 in blocking buffer and added to the sections for 30 min at 25 °C and sections were subsequently rinsed in PBS (3 × 5 min). The slides were then incubated in detection solution (VectaStain® Elite ABC Reagent, Vector Laboratories) for 30 minutes at 37°C. After rinsing the slides, peroxidase substrate, 3,3'-diaminobenzadine (ImmPACT™ DAB, Vector Laboratories) was prepared per manufacturer instructions and slides were incubated while being visualized under a microscope to time the color change for subsequent section staining. Tissues were rinsed in water (3 × 5 min). Sections were dipped in hematoxylin (Thermo Shandon, Pittsburgh, PA) for 1 min for a nuclear counterstain and subsequently rinsed in PBS (3 × 5 min).

### **8.3.6 Scanning electron microscopy**

Scanning electron microscopy was used to examine the surface topology of the luminal and abluminal sides of native porcine colonic tissue, submucosal tissue, and colonic ECM. Samples were fixed in 2.5% glutaraldehyde in 1X PBS for 60 min, cut into blocks of 8 mm<sup>3</sup>, and washed thoroughly in 1X PBS three times at 15 min each. Samples were then fixed in 1% OsO<sub>4</sub> in 1X PBS for 15 min each, dehydrated in graded series of alcohol (30–100%) baths for 15 min each. Samples were then critically point dried with hexamethyldisiloxane, mounted on studs, sputter coated and stored in a desiccator until imaged. SEM images were captured using a JEOL 6335F Field Emission SEM instrument with a backscatter detector.

### 8.3.7 **Mechanical testing of coECM scaffolds**

8.3.7.1 **Planar biaxial testing:** Planar biaxial mechanical testing was performed as previously described<sup>338</sup>. Briefly, a 15 mm x 15 mm sample of each tested material was acquired. Thickness was measured from the center of each material using a Starret® caliper model 1010. Four fiducial markers were placed in the center of the square on the luminal surface after the removal of excess loose connective tissue and fat. Deformations were measured optically by tracking this four marker array. Two loops of suture of equal length were attached to each side of the specimens with four stainless steel hooks, and 500 g Model 31 load cells (Honeywell) were used to acquire load values. Biaxial testing was conducted with the circumferential and longitudinal specimen axes aligned with the device axis and submerged in a bath at room temperature. The biaxial testing system was automated, allowing the marker locations and axial forces to be continuously recorded with custom marker tracking and data acquisition software<sup>311</sup>.

Specimens were first preconditioned by cyclically loading the specimens to the desired maximum equibiaxial stress of 250 kPa for ten cycles using a cycle time of 30 s per cycle to quantify the quasi-static response. Immediately following the preconditioning cycles, the specimen was completely unloaded and imaged in its post-preconditioned free-floating configuration. The stress-stretch plot reported in this study start from a 5 g preload that is referenced to the post-precondition free float state, which was used to ensure test response repeatability. The response of the eight samples from each group was averaged after a three point linear interpolation at representative stress values and reported with standard error. The maximum strain for each sample was then defined as the strain at the maximum tested stress of 250 kPa.

**8.3.7.2 Suture retention testing:** The suture retention test has been previously described <sup>339</sup>.

The suture retention strength was performed according to ANSI/AAMI VP20-1994 Guidelines for Cardiovascular Implants-Vascular Prostheses. The suture retention strength was defined as the force required to pull a suture through the full thickness of the material. A 2-0 Prolene suture with a SH taper needle was passed through the test article with a 2-mm bite depth using a simple suture technique. The specimen was clamped at one end while the suture was attached to the uniaxial mechanical testing machine (Instron Model 3345 single column materials testing system) and pulled at a constant rate of 10 cm/min according to the aforementioned standard. Two tests were performed 1.5 cm apart on the same edge of the test article and the maximum load was recorded for each test.

**8.3.7.3 Rheologic testing of coECM hydrogels:** The rheological characteristics of coECM hydrogels at 4 and 8 mg/mL were determined with a rheometer (AR2000, TA instruments, New Castle, DE) operating with a 40 mm parallel plate geometry. The temperature was controlled within 0.1 °C using a Peltier plate. Pre-gels were pH neutralized on ice and were immediately loaded onto the rheometer plate pre-cooled to 10 °C. Mineral oil was spread along the edge (i.e. the free surface of the hydrogel) to minimize evaporation. After loading, the steady shear viscosity was measured by applying a stress of 1 Pa at a frequency of 0.159 Hz. The temperature was then increased to 37 °C to induce gelation and a small amplitude oscillatory strain of 0.5% was imposed to track the gelation kinetics. After complete gelation, a creep test (1 Pa for 20 s) was performed to verify that there was no slip between the ECM hydrogels and rheometer plates.

**8.3.7.4 Turbidometric gelation kinetics:** The gelation kinetics of coECM hydrogels was evaluated turbidometrically <sup>337,340</sup>. Briefly, neutralized pre-gel solutions of coECM at 4 and 8 mg/mL concentrations were prepared on ice. For each ECM concentration, 100 µL/well was

added to a 96-well plate and placed into a plate reader (Spectramax M2, Molecular Devices, Sunnydale, CA) pre-warmed to 37°C. Absorbance at 405 nm was read every 2 min for 60 min and the readings were scaled from 0 (initial absorbance) to 100% (maximum absorbance). The time to half gelation ( $t_{1/2}$ ) was defined as the time at 50% absorbance. Gelation rate was defined as the slope of the linear region of the gelation curve. The lag time ( $t_{lag}$ ) was defined as the intercept of the linear region of the gelation curve with 0% absorbance.

**8.3.7.5 In-vitro cytocompatibility:** In vitro cytocompatibility was determined using a Live/Dead Viability/Cytotoxicity Kit (Invitrogen) following the manufacturer's directions. Briefly, 1 cm<sup>2</sup> multilaminates of colonic ECM (coECM), cross linked colonic ECM (XL-coECM), or scraped native colon were sterilized with ethylene oxide. 8 mg/ml coECM hydrogels were prepared as described above. Intestinal epithelial cells (IEC6; ATCC) were cultured and maintained in complete growth media consisting of 5% fetal bovine serum (FBS) (Gibco), 0.1 U/ml bovine insulin, 100 ug/ml penicillin, 100 U/ml streptomycin. IECs were seeded at  $1 \times 10^6$  cells/scaffold for 48 h. Cell viability was compared to growth on tissue culture plastic (TCP). Cells were stained with 4 mM green fluorescent calcein-AM (cAM) and 2 mM red fluorescent ethidium homodimer-1 (EthD-1) to detect viable and dead cells, respectively. Images were taken with a Zeiss Axiovert microscope capturing 3 random fields across the scaffold. Quantification of percentage of live and dead cells was completed using a custom CellProfiler pipeline. Cell-seeded scaffolds were then fixed in 2% paraformaldehyde and formalin, embedded in paraffin, and sectioned for hematoxylin and eosin (H&E) staining.

### 8.3.8 In-vitro macrophage response

Primary murine bone marrow derived macrophages were isolated as described previously<sup>134</sup>. Briefly, bone marrow was isolated from the femur and tibia of C57bl/6 mice and cultured for 7 days in 100 ng/ml MCSF to derive naïve (MΦ) macrophages. Macrophages were then activated with 20 ng/ml IFN $\gamma$  and 100 ng/ml lipopolysaccharide (LPS) to derive M1 macrophages, 20 ng/ml IL-4 to derive M2 macrophages, or 200 ug/ml of solubilized colonic ECM for 18 hours. Macrophages were then fixed with 2% paraformaldehyde for immunolabeling or lysed for western blot analysis. Cells were incubated in blocking buffer consisting of 0.1% Triton-X 100, 0.1% Tween-20, 2% bovine serum albumin (BSA), and 4% goat serum for 1 hour at room temperature. Following blocking, cells were incubated in the following primary antibodies diluted in blocking buffer for 16 h at 4 °C: (1) anti-F4/80 (abcam) at 1:200, (2) anti-iNOS (abcam) at 1:100, or<sup>37</sup> anti-RELM $\alpha$  (Fizz1, Peprotech) at 1:200. Cells were washed with phosphate buffered saline (PBS) and incubated in secondary antibodies diluted in blocking solution for 1 hour at room temperature: (1) Alexa Fluor 488 goat anti-rat at 1:200, (2) AlexaFluor 488 donkey anti-rabbit at 1:200. Cells were then washed with PBS and counterstained with DAPI nuclear stain. The assay was completed on four separate days (n=4) and cells were imaged using a Zeiss Axiovert microscope with exposure times standardized using classically polarized (IFN $\gamma$ /LPS or IL-4) internal controls. Percentage of F4/80, iNOS, and Fizz1 positive cells were quantified using CellProfiler.

Western blotting was performed to analyze an additional marker of M2 macrophages. Cells were lysed and lysates were boiled at 95°C for 5 minutes and loaded at 100 ug/well in a 4-20% gradient polyacrylamide SDS page gel. Separated proteins were transferred to PVDF membranes using a wet-transfer set up and incubated for 16 hours in 3% milk, TBS-T to prevent non-specific antibody binding. Membranes were incubated in the following primary antibodies for 18 h in 3% milk at 4 °C: (1) polyclonal anti-rabbit mannose receptor (Abcam, Cambridge, MA) at

1:714 dilution for an M2 marker or (2) monoclonal anti-mouse  $\beta$ -actin (Santa Cruz, Dallas, TX) at a dilution of 1:1000 as a loading control. Three blots completed on separate days (n=3) and were visualized using a LICOR Odyssey fluorescent imaging scanner. Densitometry of protein expression was standardized to the loading control.

### **8.3.9 *In-vivo* cytocompatibility**

**8.3.9.1 Abdominal wall defect model:** The partial thickness abdominal wall defect model for evaluation of the host response to biomaterials is well established <sup>270,330</sup>. Surgical plane of anesthesia was achieved via inhalation of 2% isoflurane in oxygen. The surgical site was prepared by shaving the lateral abdominal region on both sides of each animal, followed by scrubbing, and draping. Animals were placed in a lateral decubitus position and incisions were made along the midaxillary line. The skin and subcutaneous tissues medial to the incision were separated from the underlying muscle tissues. A 1.5 cm by 1.5 cm section of the external and internal oblique layers of the ventral lateral abdominal wall were excised while the underlying transversalis fascia and peritoneum were left intact. The muscle defect was subsequently repaired with a size-matched piece of the chosen test article or a hydrogel. The test articles were secured in place with 4-0 Prolene at each of the four corners securing the device to the surrounding and underlying musculature allowing for mechanical loading of the test article during the normal abdominal wall activity of daily living, and facilitating identification at the time of explantation. Incisions were closed with 4-0 Vicryl sutures. Animals were recovered from anesthesia, returned to the housing unit, and received 0.02 mg Buprenex (buprenorphine hydrochloride) by subcutaneous injection the day of surgery and for two additional days twice daily. Baytril (20 mg) was administered orally the day of surgery and for two additional days. The dietary habits, general health status, and the surgical site were monitored daily and recorded. The implant site containing test articles and

surrounding adjacent tissue were isolated and placed in 10% neutral buffered formalin (NBF). Samples were then embedded in paraffin and cut into 6  $\mu\text{m}$  sections for histologic studies.

**8.3.9.2 Histomorphologic scoring:** Tissue sections were stained with hematoxylin and eosin (H&E) for qualitative and semiquantitative histomorphologic analysis of remodeling outcomes. Two blinded investigators scored sections according to an established semi quantitative scoring method as shown in **Table 7** (page 82). Scoring criteria were used to group devices according to the following categories: chronic inflammation and foreign body reaction (quantitative score < 5), early inflammatory cell infiltration with decreased cellularity and little evidence of constructive downstream remodeling ( $5 \leq$  quantitative score  $\leq 10$ ), and early infiltration by inflammatory cells and signs of constructive remodeling at later time points (quantitative score > 10).

**8.3.9.3 Host response: macrophage immunolabeling:** To characterize macrophage phenotype following ECM implantation, paraffin-embedded tissue sections were deparaffinized. Heat-mediated antigen retrieval was performed in heated citrate buffer for 20 minutes (10 mM citrate, pH 6.0 at 95-100°C). Tissue sections were allowed to cool and were incubated in blocking solution consisting of 2% goat serum, 1% bovine serum albumin (BSA, Sigma), 0.1% Triton X-100 (Sigma), and 0.1% Tween-20 (Sigma) in PBS to prevent non-specific antibody binding. After blocking, tissue sections were incubated with primary antibodies diluted 1:150 in blocking solution overnight at 4°C. CD68 (mouse anti-rat CD68 clone ED1, AbD Serotec) was used as a pan-macrophage marker, CD86 (rabbit anti-human CD86, clone EP 1158Y, abcam) was used as an M1 macrophage marker, and CD206 (goat anti-human CD206 polyclonal, Santa Cruz) was used as an M2 marker. Following primary incubation, sections were washed in PBS and incubated in the following fluorescently conjugated secondary antibodies for 1 hour at room temperature

diluted in blocking solution: AlexaFluor donkey anti-mouse 594 at 1:200 (Invitrogen), PerCP-Cy5.5 donkey anti-rabbit at 1:300 (Santa Cruz), and AlexaFluor donkey anti-goat 488 at 1:200 (Invitrogen). Tissue sections were washed, counterstained with 4',6-diamidino-2-phenylindole (DAPI), and coverslipped. Multispectral images were acquired with appropriate filter sets using a Nuance microscope and spectrally unmixed to remove tissue auto-fluorescence. Four images were taken along the defect and underlying transversalis interface at 200X magnification. Total cells expressing CD68 and either CD86 or CD206 were quantified using CellProfiler image analysis software. Macrophages were defined as CD68 positive colocalized with nuclei. M1 and M2 cells were defined as macrophages (CD68+) coexpressing CD86 or CD206 respectively. Cells expressing both CD86 and CD206 were subtracted from the M1 and M2 totals, and an M2:M1 ratio was calculated for each image.

### 8.3.10 ***Statistical analysis***

A two-tailed equal variance student's *t*-test was used to determine whether the DNA, phospholipid, GAGs, HA, collagen, growth factor, and mechanics of the coECM were different than that of native colon ( $p < 0.05$ ). A *t*-test was also used to determine differences in turbidometric and rheologic properties of 4 mg/mL vs. 8 mg/mL coECM hydrogels. A one-way analysis of variance (ANOVA) with post-hoc Tukey test was used to determine differences in the percentage of viable cells in culture, percentage of cells expressing macrophage phenotype markers, in-vivo histologic scores, and in-vivo macrophage phenotype ratio. All data are reported as mean  $\pm$  standard error.

## 8.4 RESULTS

### 8.4.1 *Decellularization efficacy*

A protocol for effective decellularization of colonic submucosa was identified with the use of enzyme and detergent washes. Although previously described decellularization protocols for gastrointestinal tissue (e.g., esophageal and small intestine) do not require delipidization<sup>138,162</sup>, the porcine colonic submucosa had high lipid content and thereby required delipidization for effective decellularization. The degree of decellularization following the described method was assessed using previously established guidelines for decellularization<sup>175</sup>. No intact nuclei were visible by H&E or DAPI staining following decellularization (Figure 12A). The concentration of remnant DNA in coECM ( $43 \pm 5.3$  ng/mg) was markedly less ( $p < 0.001$ ) than that in native colonic tissue ( $7435 \pm 420$  ng/mg) and native submucosa ( $998 \pm 31$  ng/mg) (Figure 12B). Residual DNA was present in fragments less than 200 bp in length (Figure 12C). In addition to DNA content, phospholipid concentration in the coECM was used as an indicator of decellularization efficacy. The concentration of phospholipids, a fundamental component of cell membranes, in the coECM was  $876 \pm 105$  nmol/g and was much lower ( $p < 0.001$ ) than the native colon (Figure 12D).

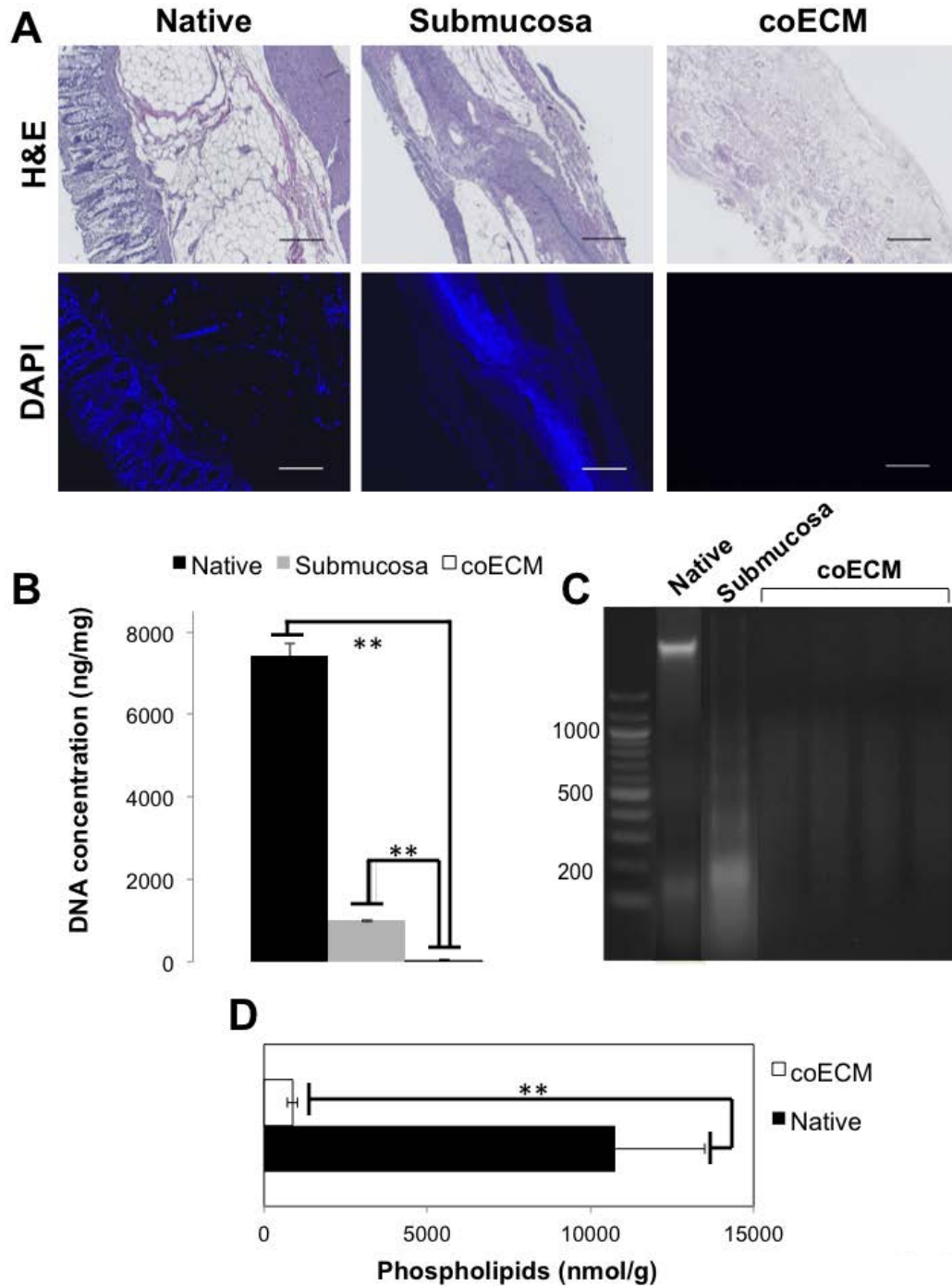


**Figure 12. Decellularization efficacy.** (A) The presence of nuclei in the decellularized tissue was assessed by hemotoxylin and eosin (H&E) staining and 4',6-diamidino-2-phenylindole (DAPI) staining. (B) DNA concentration was quantified using PicoGreen® assay. (C) The fragment length of residual DNA was visualized by gel electrophoresis. (D) Residual cell membrane components were quantified using EnzyChrom™ phospholipid assay. Scale bar = 200  $\mu$ m. \*\* =  $p < 0.01$

#### **8.4.2 Biochemical and structural properties of coECM**

The preservation and spatial distribution of ECM proteins, including basement membrane-associated laminin, and a non-basement membrane protein, fibronectin, were examined. Immunolabeling expectedly showed that laminin was present along the basement membrane of the native colon but this layer was mechanically removed during decellularization and thus laminin was largely absent in the coECM. Similarly, positive staining for fibronectin was present and distributed throughout the native colonic tissue but only diffuse staining for fibronectin was observed in the coECM (Figure 13A). The surface ultrastructure of the coECM scaffold was observed with SEM. SEM images of the luminal and abluminal surface of coECM showed a smooth surface on the luminal surface of the coECM. The abluminal surface, however, had a more textured and fibrous appearance (Figure 13B).

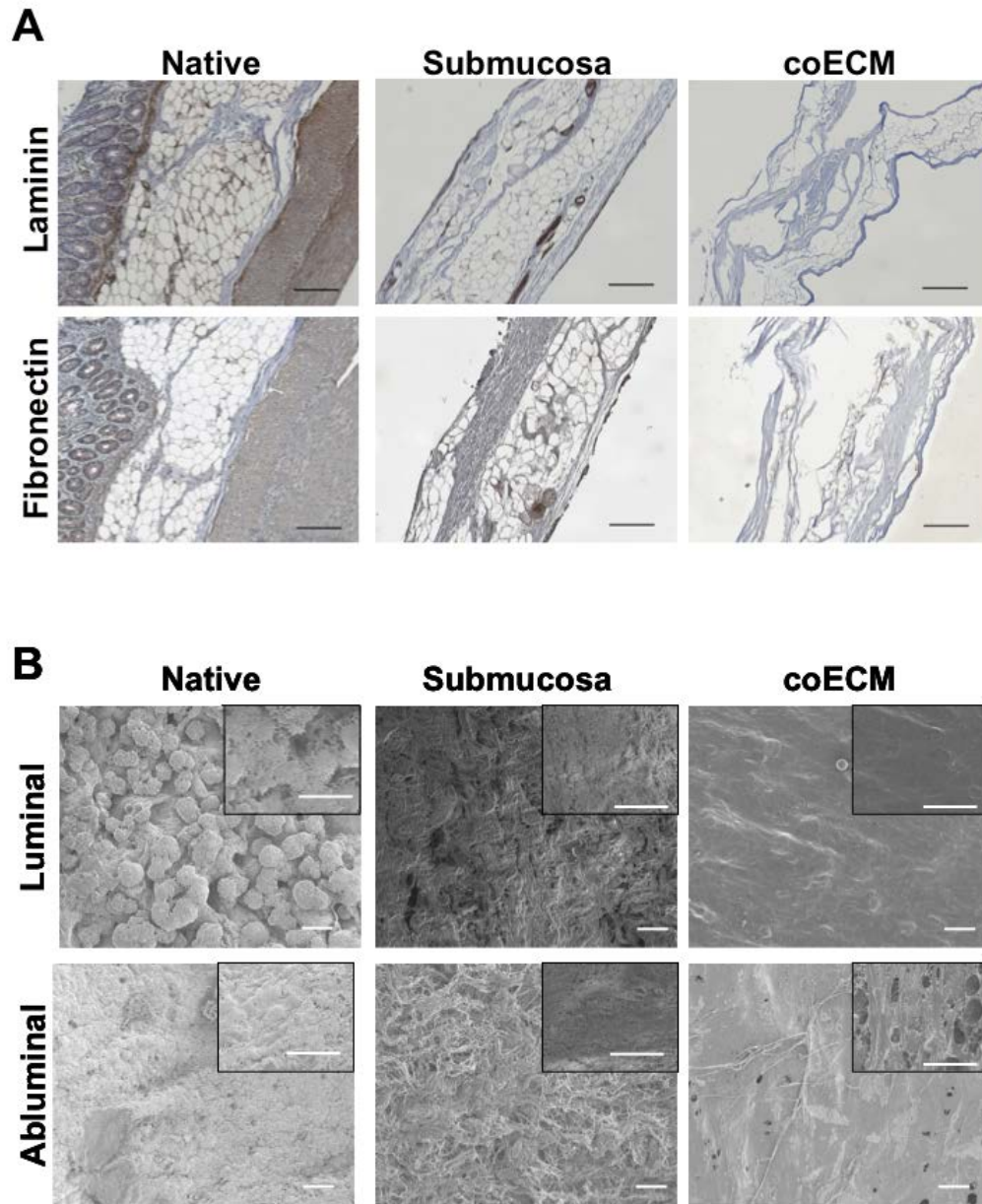


**Figure 13. CoECM composition and ultrastructure.** (A) The presence and distribution of laminin and fibronectin was assessed by immunohistochemical staining. (B) The ultrastructure of the luminal and abluminal surfaces of the scaffold was visualized at low and high (inset) magnification. Scale bar in 2A = 200  $\mu\text{m}$ . Scale bar in 2B = 50  $\mu\text{m}$ .

Biochemical characterization of coECM showed that important ECM constituents are present in the decellularized colonic mucosa. GAGs, both sulfated and non-sulfated, were retained in coECM. A large percentage of sGAGs were preserved in the coECM although the

concentration was less than ( $p=0.012$ ) the native tissue (Figure 14A). Hyaluronic acid, a non-sulfated GAG, was present in the coECM while the concentration was also lower ( $p=0.001$ ) than native tissue (Figure 14B). The amount of fibrillar collagen in the coECM was expectedly greater ( $p=0.039$ ) than native tissue as collagen represents a large proportion of the ECM (Figure 14C). Lastly, although present in reduced levels compared to native tissue, both bFGF (Figure 14D,  $p<0.001$ ) and VEGF (Figure 14E,  $p<0.001$ ) were retained in the coECM.

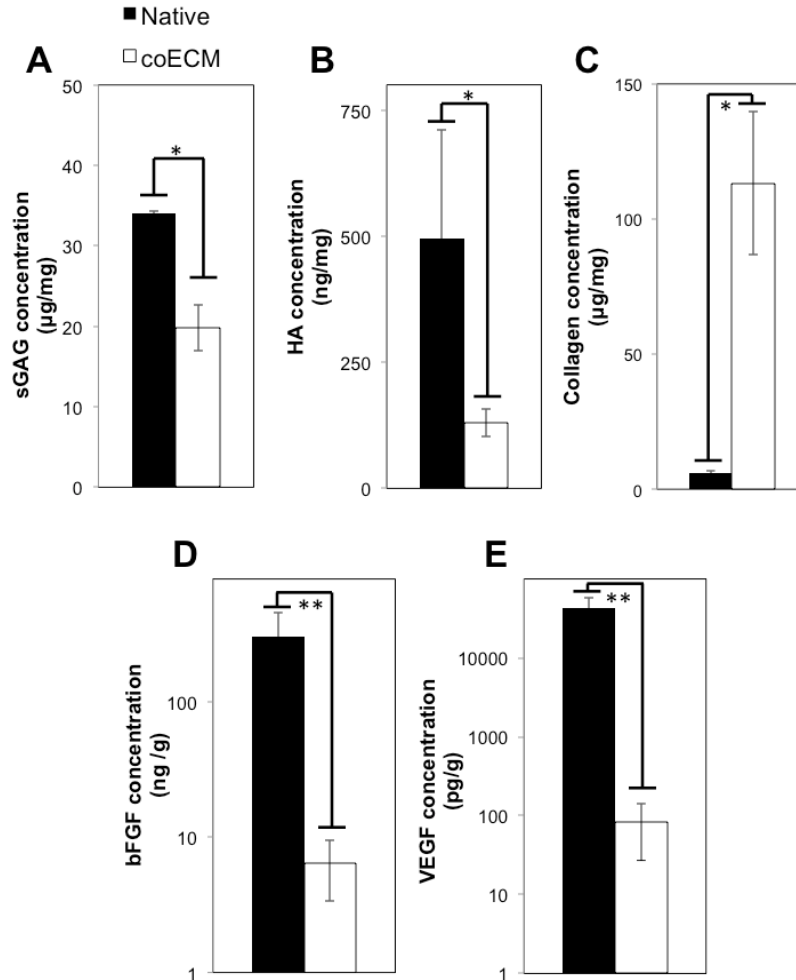


**Figure 14. Biochemical composition.** The retention of biochemical constituents in coECM was compared to native colonic tissue. (A) The concentration of sulfated glycosaminoglycans (sGAGs) was measured using Blyscan™ assay. (B) Non-sulfated GAG hyaluronic acid (HA) content was measured using an ELISA. (C) Fibrillar collagen was quantified using Sircol™ assay. The presence of two growth factors, bFGF (D) and VEGF (E), was detected using ELISA kits. \* =  $p < 0.05$ , \*\* =  $p < 0.01$

#### 8.4.3 Mechanical properties of coECM scaffold

The equibiaxial stress response of the native colon showed anisotropic behavior with a maximum strain of 4.9% and 2.4% in the longitudinal and circumferential direction, respectively (Figure 15A,B). The coECM showed similar anisotropy, but had a lower compliance along both

the longitudinal (1.8%,  $p=0.042$ ) and circumferential (0.5%,  $p=0.023$ ) axes (Figure 15A,B). The multilaminate coECM scaffold, however, had marked increase ( $p<0.001$ ) in suture retention strength compared to the native colon (Figure 15C).

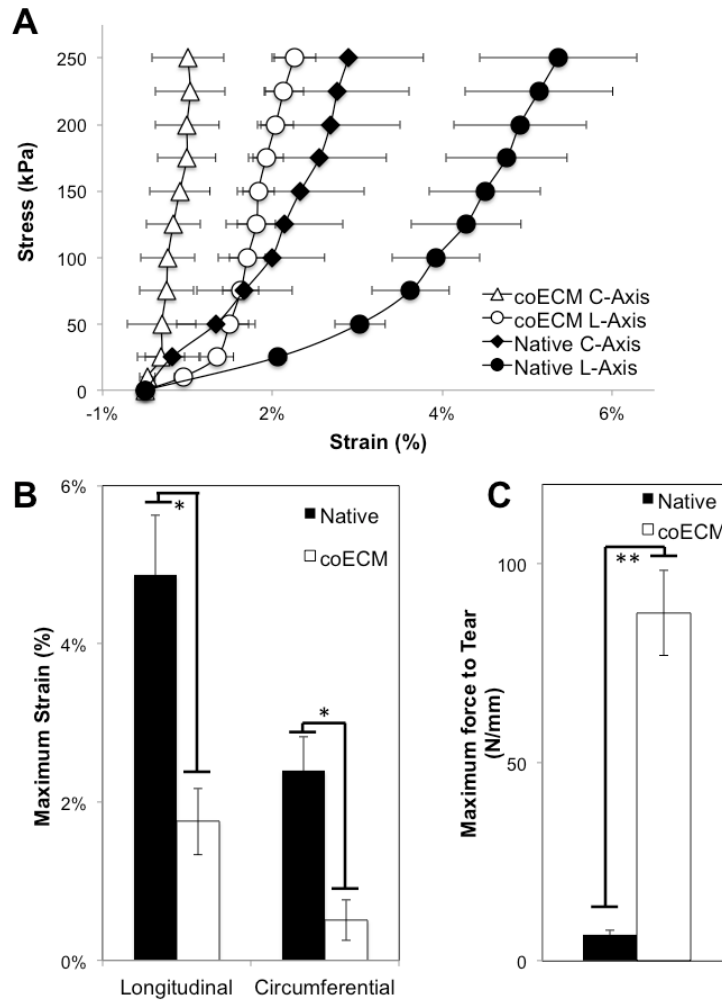


**Figure 15. Scaffold mechanical properties.** (A) The response of the scaffold to equibiaxial stress was assessed using planar biaxial testing. (B) Maximum strain of the scaffold at a stress of 250 kPa was quantified in the longitudinal and circumferential direction. (C) The suture retention strength of multi-laminate scaffolds was compared prior to in-vivo implantation.

\* =  $p<0.05$ , \*\* =  $p<0.01$

#### **8.4.4 Rheologic and turbidometric properties of coECM hydrogel**

The turbidometric and rheological properties of the coECM hydrogel were concentration dependent. Macroscopically, the higher ECM concentration 8 mg/mL hydrogels had a rigid structure with defined edges, and could be handled and manipulated with forceps while the 4 mg/mL hydrogels were softer with rounded edges and not easily handled (Figure 16A).

Compared to the 4 mg/mL hydrogel, the more concentrated 8 mg/mL hydrogel had a shorter lag time ( $17 \pm 0.3$  vs.  $22 \pm 0.8$  min;  $p < 0.001$ ) prior to gelation (Figure 16B), and gelled more rapidly (Figure 16C-D). Results of rheological testing showed that the 8 mg/mL pre-gel was more ( $p = 0.027$ ) viscous (Figure 16E) and the hydrogel that formed was much stiffer ( $p = 0.001$ ) than the 4 mg/mL hydrogel (Figure 16F).

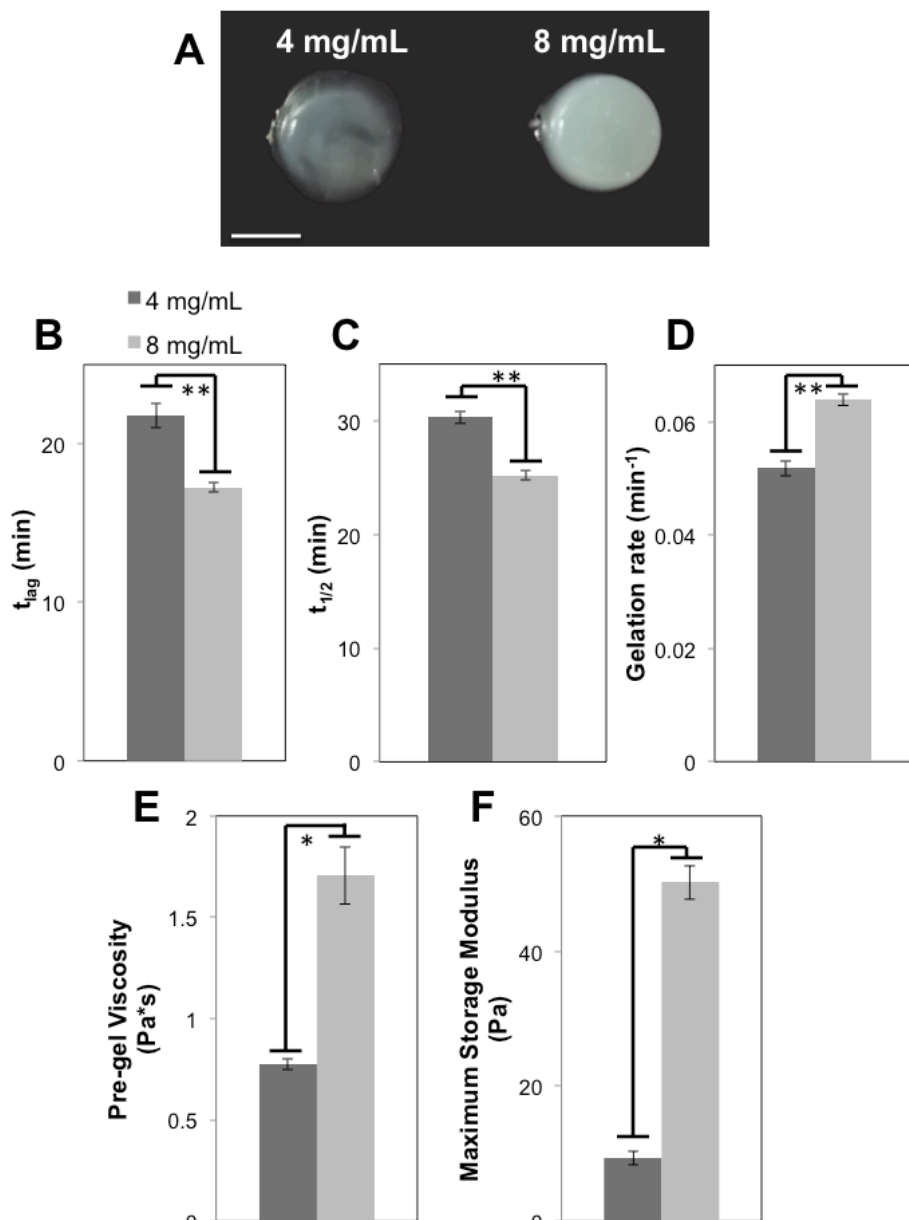


**Figure 16. Hydrogel turbidometric and rheological properties.** (A) Two concentrations of coECM hydrogel, 4 and 8 mg/mL, were formed in a ring mold and compared macroscopically. Turbidometric analysis was used to measure the  $t_{lag}$  (B),  $t_{1/2}$  (C), and rate of gelation (D) of the hydrogel at two different concentrations. Parallel plate rheology was used to measure the viscosity of the pre-gel (E) and maximum storage modulus of the hydrogel (F).

Scale bar = 1cm, \* =  $p < 0.05$ , \*\* =  $p < 0.01$

#### 8.4.5 *In-vitro cell response to coECM*

Intestinal epithelial cells retained nearly 100% viability when seeded on coECM, XL-coECM, coECM gel, and submucosa (Figure 17A). There was no difference between these treatments and when compared to tissue culture plastic after 24 hours in culture (Figure 17B).

Primary murine bone marrow derived macrophages were activated to the M1 (IFN $\gamma$ /LPS) and M2 (IL-4) phenotypes for 18 hours or treated with 200  $\mu$ g/ml of solubilized coECM. All experimental groups showed uniform F4/80 staining with  $93.4 \pm 0.5\%$  of cells expressing the pan-macrophage marker. The controls showed an expected increase ( $p < 0.001$ ) in iNOS when macrophages were treated with IFN $\gamma$ /LPS and an increase ( $p < 0.001$ ) in Fizz1 when treated with IL-4. The coECM treatment was found to promote M2-like macrophage activation, similar to IL-4 treated macrophages as shown by Fizz1 expression accompanied by little iNOS expression (Figure 17C). Results quantified using CellProfiler show a large Fizz1+ cell population and small iNOS+ cell population when treated with coECM, suggesting that coECM directly promotes a constructive, M2-like macrophage phenotype (Figure 17D). The presence of CD206, a cell surface receptor that is indicative of M2 macrophage phenotype, was assessed using western blot analysis and normalized to a  $\beta$ -actin loading control. Similar to above with Fizz1 expression, the ratio of CD206: $\beta$ -actin was on average greatest in macrophages following IL-4 ( $1.8 \pm 0.4$ ) and coECM treatment ( $1.2 \pm 0.2$ ) compared to IFN $\gamma$ /LPS treatment ( $0.6 \pm 0.2$ ) or the pepsin control, although not significant.

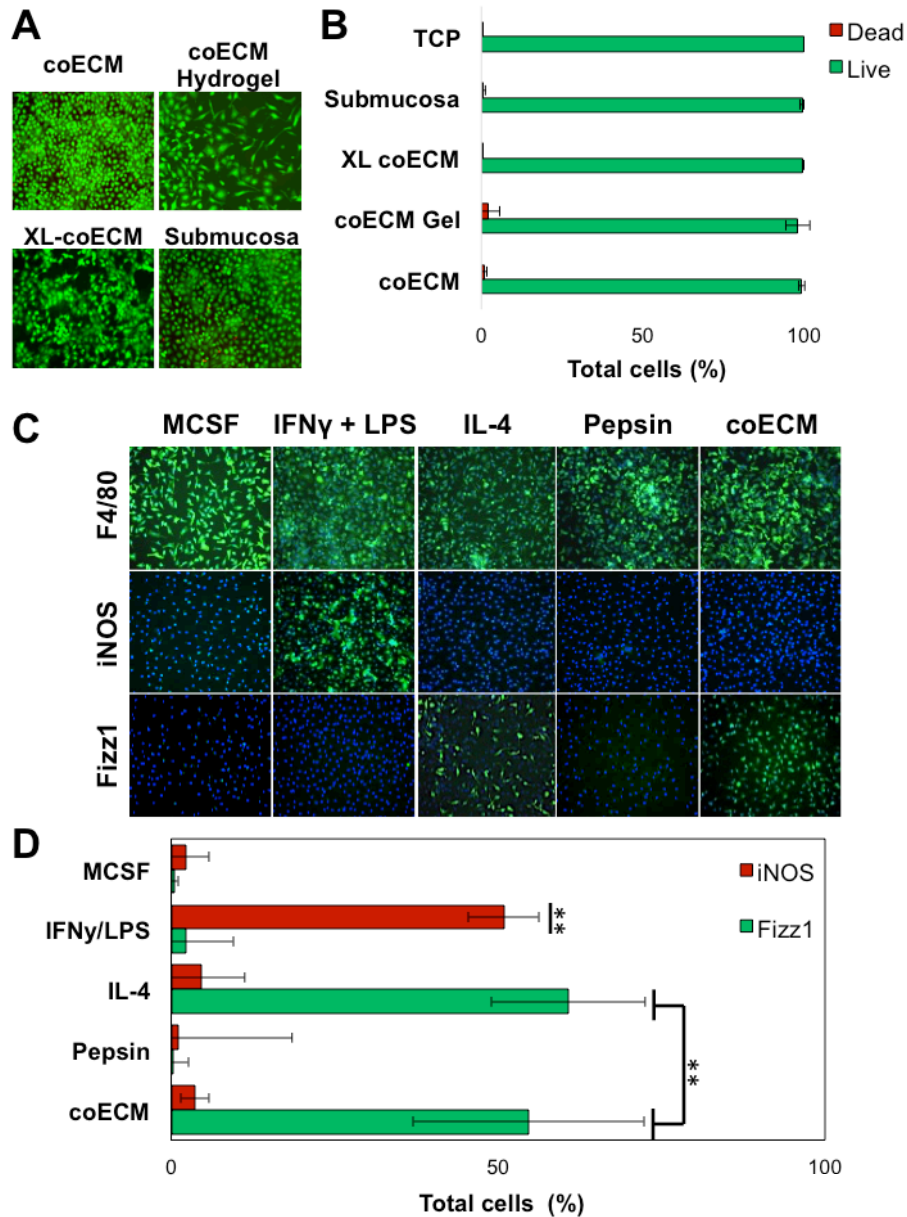


**Figure 17. In-vitro cell response.** (A) Intestinal epithelial cells cultured on coECM scaffold, coECM hydrogel, XL-coECM, and native submucosa were stained with LIVE/DEAD® cell viability dye and (B) the percentage of live and dead cells were quantified. (C) Bone marrow derived macrophages were cultured in the presence of enzymatically digested coECM and immunolabeled for F4/80 (pan macrophage), iNOS (M1), and Fizz1 (M2). Controls included MCSF (baseline), IFN $\gamma$  +LPS (M1), IL-4 (M2), and pepsin (digestion buffer). (D) The percentage of cells expressing the markers indicative of M1 and M2 phenotypes was quantified and compared. \*\* =  $p < 0.01$

#### 8.4.6 *In-vivo host response*

The in vivo host response to coECM was examined in a rat abdominal wall defect model at both 14 and 35 days following implantation. In addition to coECM and coECM hydrogel, two additional groups were used as negative controls. Native colonic submucosa was used as a control to validate the necessity for effective decellularization<sup>138</sup>. Cross-linked coECM was used to validate the need for scaffold degradation<sup>328</sup>. By 14 days, coECM sheet and gel implants showed histologic evidence of a robust cell infiltrate and partial scaffold degradation shown by hematoxylin and eosin staining (Figure 18A) with an average histologic score of 12.9 and 12.1, respectively (Figure 18B). In contrast, cross-linked coECM and native colonic submucosa implants were characterized by very little cellular infiltration and vessel formation and minimal scaffold degradation (Figure 18A). Disorganized connective tissue was present along the interface of XL-coECM and submucosa with the native underlying muscle. The average histologic scores for XL-coECM and native submucosa was 9.4 and 8.8, respectively (Figure 18B), which were both significantly less ( $p < 0.05$ ) than the coECM and coECM hydrogel. By 35 days, coECM sheets and gels were completely degraded while XL-coECM and native colonic submucosa remained almost completely intact (Figure 18A). The histologic scores for both coECM and coECM hydrogel were greater ( $p < 0.05$ ) than both XL-coECM and native submucosa (Figure 18B).

Macrophage immunolabeling at 7 days post surgery (Figure 18C) showed a predominant CD68+CD206+ M2 macrophage population in coECM sheet and gel treated groups when compared to a predominant CD68+CD86+ proinflammatory M1 macrophage phenotype following XL-coECM or colonic submucosa implantation as shown in Figure 18C. The ratio of the M2:M1 macrophages in the coECM scaffold was  $1.46 \pm 0.3$  which was greater ( $p < 0.01$ ) than the XL-coECM and native submucosa (Figure 18D). The M2:M1 ratio in the coECM gel was on average also greater than the XL-coECM and native submucosa, although not significant ( $p = 0.055$ )

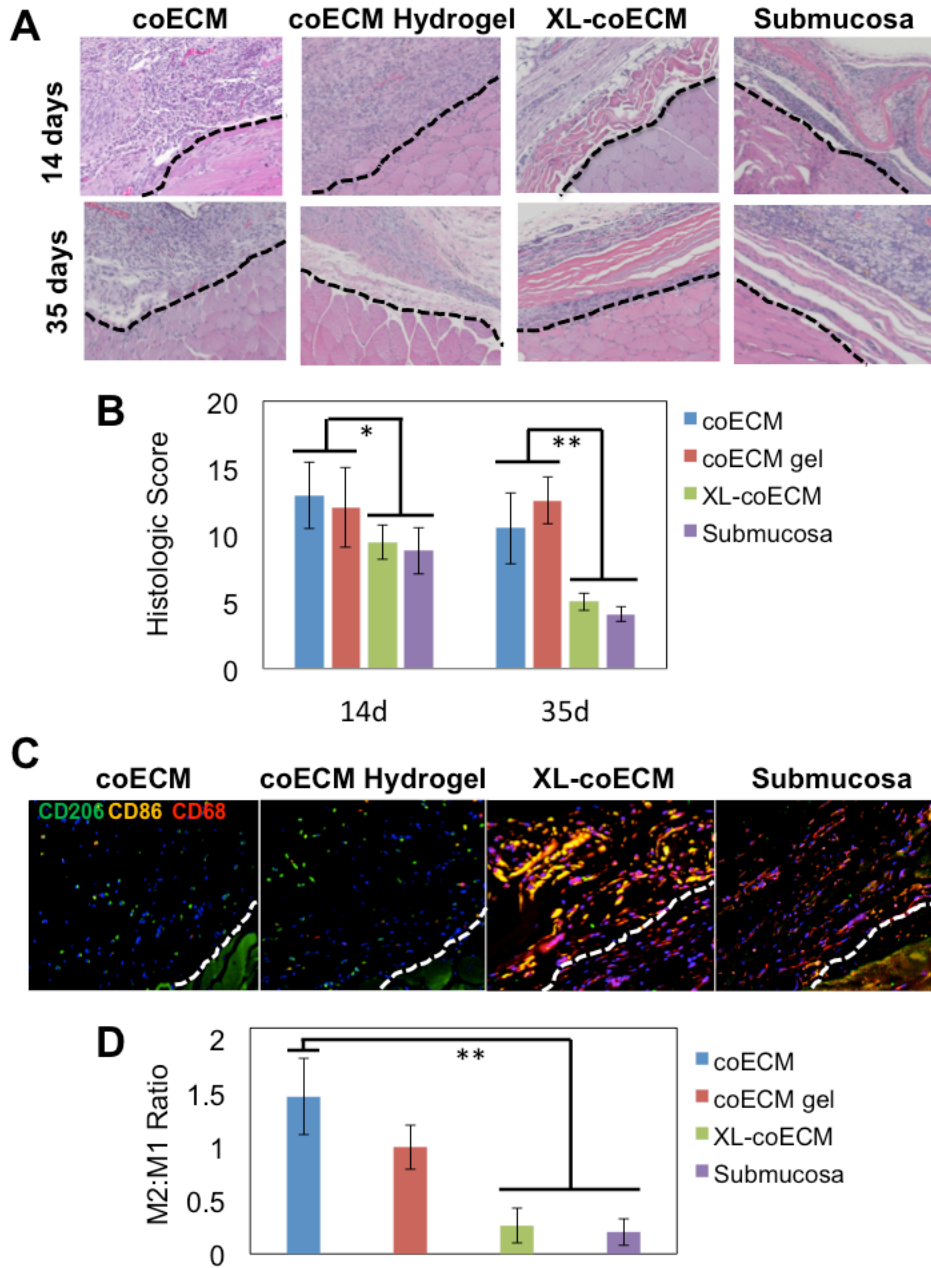


**Figure 18. Host response.** The host response to coECM scaffold and hydrogel was compared in-vivo to XL-coECM and native submucosa in a rat abdominal defect model. (A) Representative H&E images show the histologic response at 14 and 35 days. (B) The combined histologic score at each time point was quantified and compared across groups. (C) The macrophage response at 14 days post surgery was analyzed by immunofluorescent staining for M2 indicator CD206 (green), M1 indicator CD86 (orange), and pan-macrophage CD68 (red). (D) The ratio of M2 (CD68+/CD206+) to M1 (CD68+/CD86+) was quantified and compared across groups. Dashed lines indicate interface between scaffold and underlying muscle. \* =  $p < 0.05$ , \*\* =  $p < 0.01$

## 8.5 DISCUSSION

Functional replacement of injured or missing GI tissue requires a diverse tool set to promote the growth and differentiation of specialized cell types and tissue layers that vary from esophagus to small intestine to colon. The present study represents a thorough characterization of an ECM bioscaffold derived from porcine colon (coECM). The coECM scaffold was shown to be decellularized—meeting previously established stringent criteria<sup>175</sup>. The decellularization protocol effectively removed native DNA while preserving essential structural and biochemical ECM components including sGAGs, hyaluronic acid, collagen, bFGF, and VEGF. The coECM scaffold was shown to retain similar mechanical properties and anisotropy as native colon. *In vitro* and *in vivo* coECM is cytocompatible and promotes a constructive, M2-like macrophage phenotype when compared to its ineffectively decellularized or cross-linked counterparts. Such properties make coECM promising for use as an “off-the-shelf” gastrointestinal repair biomaterial.

Regions of the GI tract, specifically the small intestinal submucosa (SIS) and esophageal mucosa, have been successfully decellularized previously<sup>4,162</sup>. Just as the native GI tract is a highly complex and variable organ, the composition and properties of each of these bioscaffolds are also variable. Such properties are largely dependent on the method of decellularization utilized and the source tissue from which they are derived. SIS-ECM is prepared primarily by mechanical delamination and exposure to peracetic acid. Esophageal ECM (eECM), on the other hand, is exposed to a series of enzymatic and chemical detergent treatments after mechanical delamination methods, similar to coECM preparation<sup>162</sup> though an additional delipidization step is necessary for coECM decellularization. Each of these protocols results in scaffolds with unique properties and compositions. For example, when compared to eECM, coECM has a lower maximum strain along the longitudinal axis<sup>162</sup>. Differences in these values could be important determinants of *in vivo* remodeling outcomes. Previous studies have shown that tensile strength

increases from proximal to distal intestine <sup>341</sup>, likely stemming from the need of distal colon to accommodate changes in higher stress as fecal pellets become more solid. Distinguishing the mechanics of different regions of the gut and a thorough comparison and understanding of the similarities and differences between ECMs derived from different source tissues could have important implications for application-specific selection of bioscaffolds, particularly in gastrointestinal repair applications which are also inherently diverse and complex and require individualized mechanics for peristalsis, digestion, absorption, and gastric motility.

While heterologous ECM bioscaffolds have been used with success in multiple anatomic locations for constructive tissue remodeling, a subset of studies have indicated that it may be advantageous to utilize site-specific ECM <sup>109,110,113,114,172</sup>. Each tissue has a distinct composition of ECM in which the appropriate signaling molecules and structural components are present to allow for cell growth and differentiation and synergized tissue function. It is reasonable to assume, therefore, that decellularization of site-specific tissue would provide the optimal inductive template for tissue engineering in its respective anatomic location. Whether or not site-specific ECM use is relevant in all therapeutic applications, however, is not fully understood. Results of the present study show coECM facilitated constructive tissue remodeling in a heterologous location. Design of a tissue-engineered intestine should take into consideration gut function such as contractility. Biomaterials for gut replacement should allow for regeneration of functional muscle and directional self-organization of functionally distinct layers that perform a variety of functions including nutrient absorption, mucus secretion, and motility. Future studies are warranted to determine the efficacy of coECM as a bioscaffold in gastrointestinal, or specifically colon, disease / injury models.

Although the mechanism(s) of action of ECM-mediated tissue remodeling are only partially understood, the activation/polarization of infiltrating macrophages at the remodeling site from a pro-inflammatory, cytotoxic M1 phenotype to an immunoregulatory, constructive M2 macrophage

phenotype has been shown to be a predictor of favorable downstream remodeling outcomes <sup>132</sup>. The present study shows that coECM promotes a predominant M2 (CD68+CD206+) macrophage phenotype when compared to native colonic submucosa and XL-coECM following implantation. The immunomodulatory properties of coECM may prove beneficial in cases of inflammatory bowel disease treatment in which it is postulated that the host lamina propria macrophages fail to polarize toward a more tolerant M2-like phenotype <sup>342,343</sup>. The present study shows that coECM can also be prepared in a hydrogel form with unique and concentration-dependent viscoelastic properties, providing flexibility for *in vivo* applications such as injectable or enema administration.

Biologic scaffolds are preferred over synthetic scaffolds for many tissue repair applications because of their degradability *in vivo*. It is now well accepted that cross-linking biologic scaffolds results in slower degradation and often encapsulation and fibrosis. Such inhibition of scaffold degradation prevents the release or exposure of matricryptic peptides and is consistently associated with less than desirable outcomes <sup>90,270</sup>. Hematoxylin and eosin (H&E) staining of abdominal wall explants shows that coECM sheet and hydrogel formulations are characterized by a robust cellular infiltrate at 14 days and are largely degraded by 35 days, unlike the native (non-decellularized) submucosa and XL-coECM which were characterized by mostly disorganized connective tissue and some encapsulation as reflected by a lower histomorphologic score. This score differential is likely due to the incomplete decellularization of the submucosa graft and the inability of XL-coECM to degrade. Ineffective decellularization has been shown to be a crucial factor in provoking a foreign body reaction from the host following bioscaffold implantation<sup>138,344</sup> (See Appendix 12.3, page 188 for more information). Degradation products of coECM have been shown to not only promote a predominant F480+/Fizz1+ macrophage population *in vitro*, but previous work has also shown that degradation products of ECM are chemotactic and mitogenic for progenitor cells both *in vitro* and *in vivo* <sup>67,134,345</sup>. These results emphasize the importance for effective decellularization and scaffold degradation.

The present chapter has limitations. While coECM was shown to be conducive to intestinal epithelial cell survival *in vitro*, the tissue-specific effects of coECM on colonic progenitor cells and in a colonic repair animal model were not evaluated. Additionally, while retention of growth factors bFGF and VEGF protein were measured, their bioactivity was not measured. The role of these growth factors in constructive remodeling is not understood. Previous work shows that vascularization has been, to this point, a limiting step in tissue engineered construct survival<sup>325</sup>. Future studies should determine whether coECM-retained VEGF remains active to promote an angiogenic response. While a high M2:M1 macrophage ratio has been shown to be a predictor of downstream remodeling outcomes in ECM-mediated tissue repair, macrophage phenotype polarizes along a spectrum. The present study utilizes CD206 and CD86 for M2 and M1 macrophage markers, respectively; however, a more thorough characterization of macrophage activation phenotype would result from analyzing additional markers.

## 8.6 CONCLUSION

A biologic scaffold was successfully prepared from porcine colon. The coECM scaffold was effectively decellularized and retained important ECM constituents. The decellularized tissue was prepared in hydrogel or lyophilized sheet forms to address diverse gastrointestinal repair applications. Both forms of ECM were conducive to intestinal epithelial cell growth and were shown to promote a constructive macrophage phenotype *in-vitro*. Surgically implanted coECM scaffold and hydrogel also promote an immunomodulatory host response and site appropriate tissue deposition. Given the large unmet clinical need for repair of GI tissue, further work is warranted to examine the specific effects of coECM upon colonic stem / progenitor cells and *in vivo* remodeling in a gastrointestinal disease model to assess site-specific effects of ECM bioscaffolds.

## **8.7 ACKNOWLEDGMENT**

Funding was provided in part by the National Science Foundation (NSF) graduate research fellowship program to TJK and DMF (1247842). SSV was also supported by the NSF (NSF-BET grant no. 09320901 and 1336311).

## 9.0 TISSUE-SPECIFIC EFFECTS OF ESOPHAGEAL EXTRACELLULAR MATRIX<sup>6</sup>

### 9.1 ABSTRACT

Biologic scaffolds composed of extracellular matrix (ECM) have been used to facilitate repair or remodeling of numerous tissues, including the esophagus. The theoretical ideal scaffold for tissue repair is the ECM derived from the particular tissue to be treated; i.e., site-specific or homologous ECM. The preference or potential advantage for the use of site-specific ECM remains unknown in the esophageal location. The objective of the present chapter was to characterize the in-vitro cellular response and in-vivo host response to a homologous esophageal mucosal ECM (eECM) vs. non-homologous ECMs derived from small intestinal submucosa and urinary bladder. The in-vitro response of esophageal stem cells was characterized by migration, proliferation, and 3D organoid formation assays. The in-vivo remodeling response was evaluated in a rat model of esophageal mucosal resection. Results of the study showed that eECM retains favorable tissue-specific characteristics that enhance the migration of esophageal stem cells and supports the formation of 3D organoids to a greater extent than heterologous ECMs. The in-vivo response to eECM was also positive. However,

---

<sup>6</sup> Portions of this chapter were adapted from the following publication:

**Keane TJ**, DeWard A, Londono R, Saldin L, Carey L, Castelton A, Nieponice A, Lagasse E, Badylak SF. Tissue-Specific Effects of Esophageal Extracellular Matrix. *Tissue Engineering Part A*. August 2015. DOI: 10.1089/ten.tea.2015.0322

implantation of eECM facilitates the remodeling of esophageal mucosa following mucosal resection but no distinct advantage vs. heterologous ECM could be identified.

## 9.2 INTRODUCTION

Scaffolds derived from extracellular matrix (ECM) have been investigated for their ability to support tissue remodeling in nearly every body system, including parts of the gastrointestinal tract. Similarly, ECM scaffolds have been isolated from tissues ranging from urinary bladder and small intestine to spinal cord and brain<sup>82,116,346</sup>, among others. Implantation and subsequent degradation of ECM scaffolds leads to the release or exposure of cryptic peptide fragments that affect cell behavior and tissue remodeling events. However, the necessity or preference for homologous ECM remains unknown for many therapeutic applications.

The ECM represents the structural and functional molecules secreted by the resident cells of a tissue or organ. The biochemical composition and mechanical and ultrastructural characteristics of an ECM scaffold therefore vary according to the tissue source from which the ECM is isolated. Logically, the ideal substrate for cell survival, proliferation, differentiation, and functional tissue remodeling is the native ECM of the homologous tissue or organ. Recent work has described potential benefits of ECM scaffold materials derived from homologous tissue versus heterologous tissue when used in selected anatomic locations<sup>109-116,118</sup>. Homologous ECM can preferentially maintain tissue-specific cell phenotypes<sup>109-112</sup>, promote cell proliferation<sup>111,113</sup>, induce tissue-specific differentiation<sup>114</sup>, and enhance the chemotaxis of stem cells<sup>115-117</sup>. However, the preference or necessity for tissue-specific ECM has not been shown for all therapeutic applications<sup>92,119,120</sup>.

The objective of the present chapter was to compare the cellular response to esophageal ECM (eECM) versus small intestinal submucosa (SIS-ECM) and urinary bladder matrix (UBM) in-vitro and in-vivo. The chemotaxis, proliferation, and capacity for eECM to support the formation of three dimensional (3D) organoids of esophageal stem cells, which are a candidate cell population that may play a role in functional tissue remodeling of the esophagus, was investigated. The eECM scaffold was then implanted in a rat esophageal mucosal defect model to determine the ability of the scaffold to facilitate remodeling of esophageal mucosa.

### **9.3 MATERIALS AND METHODS**

#### **9.3.1 *Overview of experimental design***

Porcine esophageal mucosa was decellularized to produce eECM. Using a population of murine-derived esophageal stem cells<sup>347</sup>, the ability for eECM to promote migration, proliferation, and 3D organoid formation was evaluated and compared to two benchmark ECM scaffolds; specifically urinary bladder matrix (UBM) and small intestinal submucosa (SIS). Subsequently, eECM and UBM scaffolds were implanted into a rat model of esophageal mucosa resection and the remodeling response was evaluated at 14 days post surgery.

### 9.3.2 *Mice and rats*

Transgenic EGFP C57BL/6 mice were bred and housed in the Division of Laboratory Animal Resources facility at the University of Pittsburgh McGowan Institute for Regenerative Medicine. Female Sprague Dawley rats (350 – 400 g at implantation) were purchased from Harlan Laboratories and housed in the Division of Laboratory Animal Resources facility at the University of Pittsburgh McGowan Institute for Regenerative Medicine. Experimental protocols followed NIH guidelines for animal care and were approved by the Institutional Animal Care and Use Committee at the University of Pittsburgh.

### 9.3.3 *Harvesting and preparation of ECM and hydrogels*

The esophagus, urinary bladder, and small intestine were isolated from market weight pigs and frozen at -20 °C until use. All ECM scaffolds were prepared according to established decellularization protocols (Fig 1). Briefly, esophageal mucosal ECM (eECM) was prepared by mechanically separating the mucosa and submucosa from the muscularis externa and subjecting the mucosal layers to 1% trypsin/0.05% EDTA (Invitrogen, Carlsbad, CA) for 1 h at 37 °C on a rocker plate, deionized water for 15 min, 1 M sucrose (Fisher Scientific, Pittsburgh, PA) for 30 min, deionized water for 30 min, 3.0% Triton X-100 (Sigma Aldrich, St. Louis, MO) for 48 h, deionized water for 15 min, PBS (Fisher Scientific) for 15 min, 10% deoxycholate (Sigma Aldrich) for 4 h, deionized water for 30 min, 0.1% peracetic acid (Rochester Midland Corp., Rochester, NY) in 4.0% ethanol for 4 h, 100 U/mL DNase (Invitrogen) for 2 h on a rocker plate, followed by 15 min washes with PBS, deionized water, PBS, and deionized water<sup>162</sup>. All washes were at 300 rpm unless otherwise specified.

Small intestinal submucosa (SIS) was prepared by mechanically removing the superficial layers of the tunica mucosa, tunica serosa, and tunica muscularis externa from the intact small intestine, leaving the submucosa, muscularis mucosa, and basilar stratum compactum intact. Urinary bladder matrix (UBM) was prepared by mechanically removing the tunica serosa, tunica muscularis externa, the tunica submucosa, and majority of the tunica muscularis mucosa from the intact bladder, leaving the lamina propria and basement membrane intact. The SIS and UBM were then subjected to 0.1% peracetic acid in 4.0% ethanol for 4 h, followed by 15 min washes with PBS, deionized water, PBS, and deionized water as described above. All treatments were performed at room temperature with agitation on a shaker plate at 300 RPM unless otherwise stated.

For implantation studies, the ECM scaffolds were lyophilized using an FTS Systems Bulk Freeze Dryer (Model 8-54) and sterilized with ethylene oxide. For studies using a hydrogel form of the ECM, the decellularized ECM sheets were lyophilized and comminuted to a particulate form using a Wiley Mini Mill. One gram of lyophilized ECM powder and 100 mg of pepsin (Sigma) were mixed in 100 ml of 0.01 M HCl and kept at a constant stir for 48 h at room temperature.

#### **9.3.4 SDS gel chromatography**

Pepsin solubilized (0.1% pepsin) forms of SIS, UBM, and eECM were diluted 1:1 in 2x Laemmli sample buffer (Bio-Rad, Hercules, CA) and boiled at 95 °C for 8 minutes. Samples were diluted and protein concentrations were approximated using a bovine serum albumin (BSA) with a Pierce BCA Protein Assay (Thermo Fisher, Waltham, MA) according to the manufacturer's instructions. Samples (5 µg) were run on a 10%, 12-well SDS PAGE gel (Bio-Rad, Hercules,

CA) at 50V until the tracking dye moved below the stacking gel. The gel was then run at 150 V for 50 min, until the dye reached the end of the gel. After running, the gel was washed and fixed with 30% ethanol/10% acetic acid in a rocking staining dish. Silver stain was applied according to manufacturer's instructions (Silver Stain Plus Kit, Bio-Rad) and developed for 15 minutes. The developed gel was imaged using a Nikon D7000 over a light table.

### **9.3.5 Isolation and culture of esophageal stem cells**

The esophagus was removed from transgenic EGFP C57BL/6 mice (Jackson Laboratories) followed by physical separation of the mucosa using forceps. The mucosa was minced into small pieces and digested with 0.25 % Trypsin for 60 minutes. Cells and remaining tissue were passed through a 70  $\mu\text{m}$  filter to obtain a single cell suspension. Cells were then placed in tissue culture flasks that were previously seeded with irradiated LA7 feeder cells. LA7 cells have been shown to select for esophageal epithelial cells with stem cell properties<sup>347</sup>. Esophageal epithelial cells were expanded by passaging cells to flasks coated with irradiated LA7 cells.

### **9.3.6 Migration assay**

Migration assays were performed using a 48 well chemotaxis chamber with polycarbonate filters containing 5  $\mu\text{m}$  pores (Neuro Probe, Gaithersburg, MD). The filters were coated with 20  $\mu\text{g/ml}$  laminin (Sigma) and dried prior to use. The bottom wells of the chamber were loaded with 30  $\mu\text{l}$  containing 25 or 100  $\mu\text{g/ml}$  of ECM digest and the top wells were loaded with 50  $\mu\text{l}$  containing  $7 \times 10^4$  esophageal stem cells. Control wells consisted of serum free media and media containing

10% FBS. Following 6 h incubation, the top filter surface (non-migratory) was scraped and the bottom of the filter was fixed in 95% methanol for 5 min and then mounted on a glass slide with mounting media containing DAPI (Vector Laboratories Inc, Burlingame, CA) and imaged.

Migrated cells were quantified using ImageJ (NIH) to set the threshold and count cells, with binning to resolve cell clusters of various counts. The same ImageJ macro was used to analyze all images. Experiments were performed using 4 technical replicates with 4 separate biologic replicates (n=4).

### **9.3.7 Generation of 3D organoids**

Esophageal cells were suspended in ECM hydrogels and were placed as a droplet in a tissue culture plate. Cells were incubated at 37° C for 30 minutes to allow for solidification of the hydrogels. Growth medium was added to the plate to initiate organoid formation. Growth medium consisted of Advanced Dubecco's modified Eagle's medium/F12, 1x N2, 1x B27 Supplements, 1x Glutamas, 1x HEPES, 1x penicillin/streptomycin, 1 mM N-acetyl-L-cysteine, 100 µM gastrin, 10 mM nicotinamide, 10 µM SB202190, 50 ng/mL epidermal growth factor, 100 ng/mL Noggin, 100 ng/mL Wnt3A, 100 ng/mL R-Spondin 2, and 500 nM A8301. Media was changed every 2-3 days.

### **9.3.8 Proliferation assay**

Esophageal organoids were generated followed by the addition of 5-ethynyl-2'-deoxyuridine <sup>212</sup> to the culture media. Cells were exposed to EdU for 2 hours to allow incorporation of EdU into dividing cells. Organoids were fixed in 4% paraformaldehyde and embedded in gelatin.

Organoids were sectioned at 10  $\mu\text{m}$  and EdU was detected using the Click-iT Alexa Fluor 594 EdU labeling kit. Cells were counterstained with Hoechst to detect cell nuclei. EdU positive cells was counted to determine the number of proliferating cells per organoid.

### **9.3.9 *Surgical procedure and ECM implantation***

All surgical procedures were approved by the Institutional Animal Care and Use Committee at the University of Pittsburgh and the animal care complied with the National Institutes of Health Guidelines for the Care and Use of Laboratory Animals. Induction and surgical plane of anesthesia were achieved with 2% inhaled isoflurane and the animals were placed on a warming pad in supine position. The cervical skin was shaved and aseptically prepared with ethanol and betadine. A midline cervical incision was performed above the clavicle and the esophagus exposed via blunt dissection. A transverse incision of the muscularis externa layer was performed, and a window of full thickness mucosa extending 5-10 mm length including 70% of the circumference was resected. Animals treated with ECM received a single layer sheet that was placed over the denuded area and secured in place with interrupted 10.0 prolene sutures (Ethicon, Somerville, NJ). The denuded mucosa was left exposed in non-treated control animals. Skin was closed with 4.0 Vicryl (Ethicon) and buprenorphine (0.5 mg/kg, Benckiser Healthcare (UK) Ltd, Hull, England) was administered intramuscularly immediately postoperatively and twice a day for 3 days. Animals were placed on a soft diet for 5 days post operatively.

### 9.3.10 *Histology and immunolabeling*

Two histology and immunolabeling studies were performed: 1) on the 3D organoids and 2) on the explanted esophageal tissue sections. Organoids were collected upon digestion of the hydrogel using 0.2% Dispase, 0.1% collagenase type II, and 20 ug/mL DNase I in 1x HBSS containing 1% HEPES. Organoids were embedded in 5% gelatin, fixed in 4% paraformaldehyde for 1 h, and embedded in paraffin. Explanted esophageal tissue sections were fixed in 10% neutral buffered formalin and paraffin embedded.

Serial sections (5 µm) of the organoids and tissue sections were stained with hematoxylin and eosin or immunolabeled. Organoid and tissue sections were deparaffinized with xylene and rehydrated through a graded ethanol series. Antigen retrieval was performed by heating a citrate antigen retrieval buffer (10 mM citric acid with 0.05% Tween 20, pH 6) until boiling, and incubating the slides in the solution until returning to room temperature. Three washes in phosphate buffered saline (PBS) for five minutes at room temperature were performed. Organoid and tissue sections were permeabilized with 1x Tris-Buffered Saline with Tween 20 (TBST) for 10 minutes at room temperature. The slides were incubated in a blocking solution (5% BSA in 1x PBS) at room temperature to prevent non-specific binding. The slides were incubated in primary antibody blocking solution at 4°C overnight. Five washes in PBS were performed for 5 minutes at room temperature. Slides were incubated in secondary antibody in blocking buffer at room temperature for 1 hour. Five washes in PBS were performed for 5 minutes at room temperature. The primary antibodies used for the immunolabeling studies were cytokeratin 13 (1:250; Ab92551, Abcam) and cytokeratin 14 (1:500; Ab7800, Abcam) for the organoids, and cytokeratin 14 (1:200; NBP1-67606, Novus Biologicals, Littleton, CO) for tissue sections. The secondary antibodies used were Alexa Fluor 488 (1:200; A-11034, Invitrogen) and Alexa Fluor 594 (1:200; A21203, Invitrogen). Sections were counterstained with 4',6-diamidino-

2-phenylindole (DAPI) and mounted in fluorescence mounting medium (Dako). Stained sections were visualized on Nikon E600 fluorescence microscope with Cri Nuance FX multispectral imaging system.

### 9.3.11 **Statistical analysis**

Data sets were analyzed with a one-way analysis of variance (ANOVA) using SPSS Statistical Analysis Software (SPSS Inc., IBM, Chicago, IL). A student t-test was used to identify the differences between means when the observed F ratio was statistically significant ( $p < 0.05$ ). Data are reported as mean  $\pm$  standard error.

## 9.4 RESULTS

### 9.4.1 **ECM characteristics**

Esophagus, small intestine, and urinary bladder were decellularized according to established methods of decellularization. The attributes (thickness, cellularity, density, etc.) of each tissue are unique and therefore require different protocols for decellularization (Figure 19A). Effective decellularization, as defined by previously described metrics<sup>175</sup>, was achieved for each tissue. Each ECM scaffold had a unique protein banding pattern and eECM had a prevalent band at approximately 30 kDa that was absent in both UBM and SIS (Figure 19B).

**A**

UBM	SIS	eECM
<ul style="list-style-type: none"> <li>• Mechanically isolate urinary bladder basement membrane and tunica propria</li> <li>• Peracetic acid</li> </ul>	<ul style="list-style-type: none"> <li>• Mechanically isolate small intestinal submucosa</li> <li>• Peracetic acid</li> </ul>	<ul style="list-style-type: none"> <li>• Mechanically isolate esophageal mucosa and submucosa</li> <li>• Trypsin/EDTA</li> <li>• Sucrose</li> <li>• Triton X-100</li> <li>• Deoxycholic acid</li> <li>• Peracetic acid</li> <li>• DNase</li> </ul>

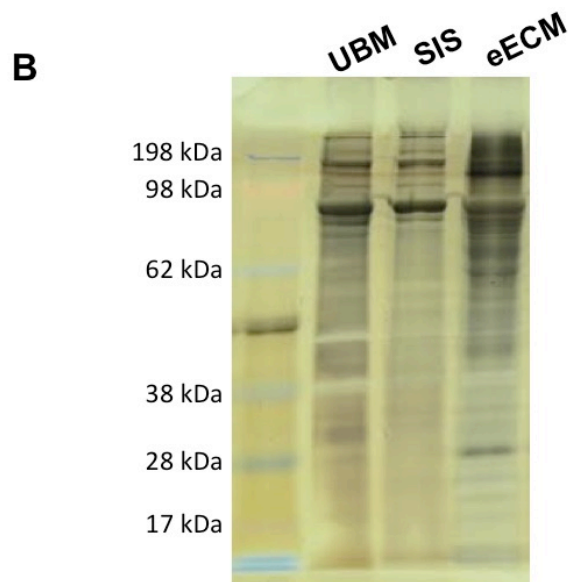


**Figure 19. Preparation and characteristics of ECM scaffolds. (A)** Overview of decellularization process for preparing UBM, SIS, and eECM. **(B)** Gel chromatography of ECM materials showing features in banding patterns of different ECM materials.

#### 9.4.2 *Esophageal stem cell characteristics*

The chemotaxis of esophageal stem cells was evaluated using a Boyden chamber assay. Two concentrations of ECM were chosen to determine whether a migration dose response existed. The stem cells did not migrate toward serum free media or 10% FBS. Representative images of

migratory cells after DAPI staining (Figure 20A) showed an increased migration response of the esophageal stem cells toward eECM and SIS, but not UBM, versus the pepsin control.

Quantification of migrating cells (Figure 20B) showed that eECM enhanced migration of esophageal stem cells at both 25  $\mu\text{g/ml}$  ( $p = 0.01$ ) and 100  $\mu\text{g/ml}$  ( $p = 0.04$ ). The SIS-ECM enhanced stem cell migration at 100  $\mu\text{g/ml}$  ( $p < 0.01$ ) but not at 25  $\mu\text{g/ml}$ .

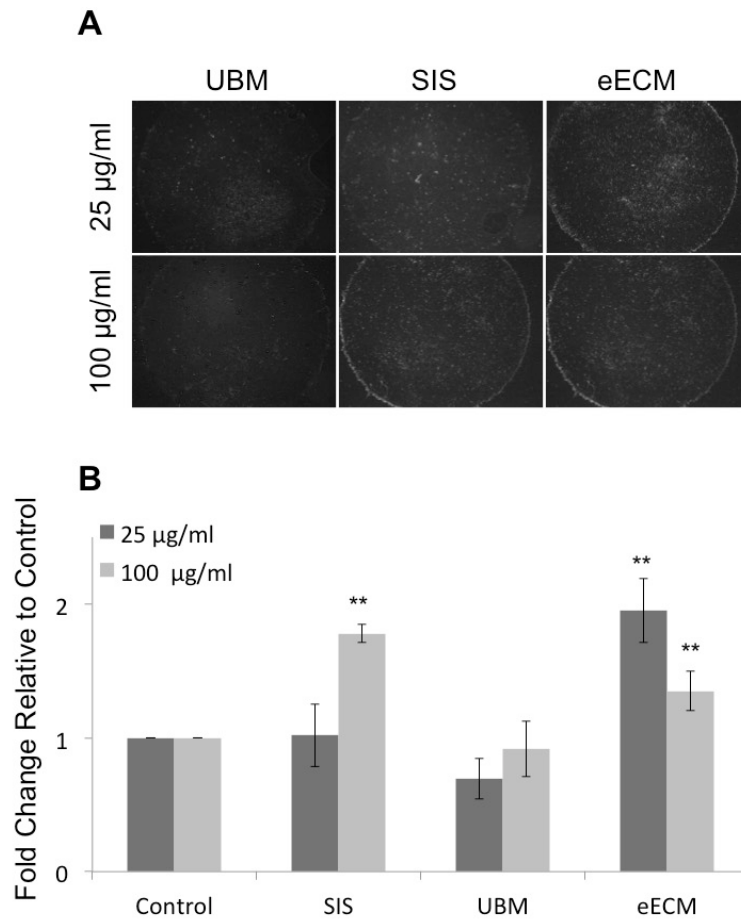


**Figure 20. Migration of esophageal stem cells.** (A) Representative images of DAPI stained migrating cells towards varying concentrations of ECM. (B) Quantification of migrated cells in response to ECM scaffolds.

#### 9.4.3 Organoid forming capacity of ECM hydrogels

The ability of ECM hydrogels to support the formation of esophageal organoids was tested using two concentrations of ECM: 2 mg/ml and 6 mg/ml (Figure 21A). The number of organoids formed in eECM was greater than those formed in SIS and UBM at both 2 mg/ml ( $p = 0.04$ ) and 6 mg/ml ( $p=0.04$ ). Interestingly, the lower concentration hydrogel (2 mg/ml) better supported the

formation of organoids compared to the 6 mg/ml ECM hydrogel (Figure 21B). Furthermore, SIS consistently performed the poorest among the ECM hydrogels in the ability to support organoid formation. Based upon these results, only the 2 mg/ml ECM hydrogels were used for subsequent proliferation studies and only eECM and UBM were used for *in-vivo* studies.

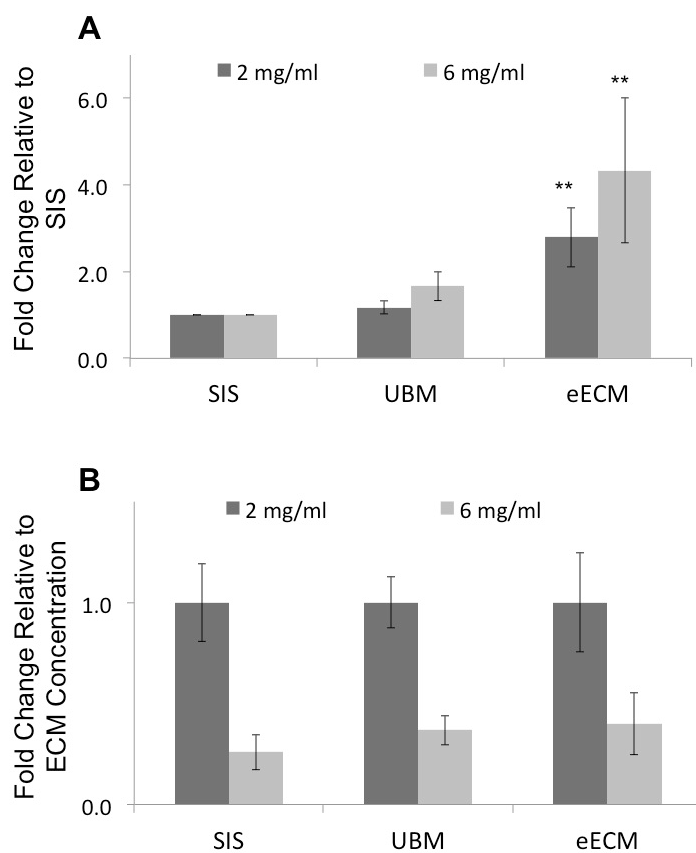


**Figure 21. Capacity of ECM hydrogels to support organoid formation.** (A) Comparison number of organoids formed in different ECM types. Data are normalized to the number of organoids formed in SIS. (B) Comparison of number of organoids formed in ECM at 2 mg/ml and 6 mg/ml. Data are normalized to the number of organoids present at 2mg/mL concentration of ECM

Only eECM was able to support the growth of a substantial number of organoids necessary for histologic processing. Organoids that formed in eECM were sectioned and immunolabeled for cytokeratin 14 (CK14), a marker of basal epithelium, and CK13, a marker of suprabasal differentiated epithelial cells (Figure 22A)<sup>347</sup>. Compared to native esophageal mucosa (Figure 22B), the organoids largely maintained the CK14<sup>+</sup> phenotype at the periphery of the organoid while the cells at the organoid center exhibited a more differentiated CK13<sup>+</sup> phenotype.

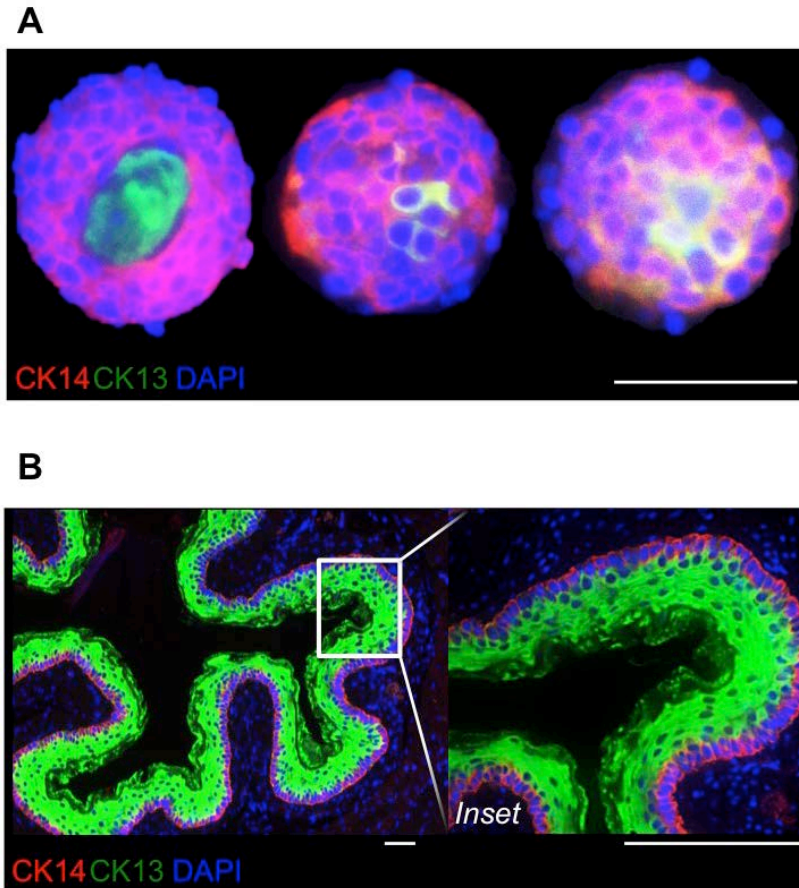


**Figure 22. Cytokeratin immunolabeling.** (A) Representative images of organoids formed in eECM. (B) Representative image of normal esophageal mucosa. Cytokeratin 14, a basal epithelial cell marker, is stained red. Cytokeratin 13, a marker of suprabasal epithelial cells, is stained green. Nuclei (DAPI) is shown blue. Scale bars = 50  $\mu$ m.

#### 9.4.4 Proliferation of esophageal stem cells

Proliferating cells were identified by incorporation of EdU and immunolabeling (Figure 23A). Proliferating cells within organoids were present in numbers similar to that in native tissue<sup>347</sup> and there was no difference among the values for proliferating cells in organoids formed in UBM and eECM (Figure 23B). Similarly, the size of organoids (i.e., number of cells per organoid) were equivalent in the UBM and eECM hydrogels.

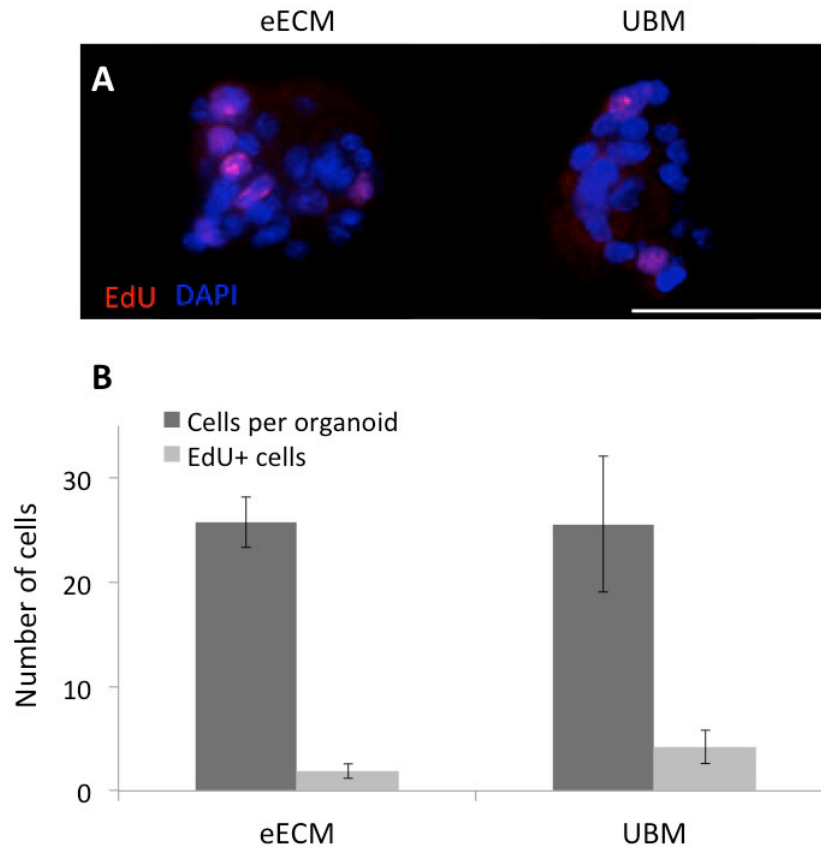


**Figure 23. Proliferation of organoid cells.** (A) Representative images of EdU stained organoids following 2h EdU exposure. EdU+ cells are shown in red. (B) Quantification of number of cells per organoid and number of EdU+ cells per organoid. Scale bar = 50  $\mu$ m.

#### 9.4.5 Esophageal mucosal remodeling

The ability of ECM to mediate tissue repair in the esophageal mucosa was tested in a rat model of mucosal resection. Following resection of approximately 7 mm length of esophageal mucosa consisting of 70% of the circumference, a size-matched ECM scaffold was placed at the site of tissue resection. Rats weighed  $228 \pm 2.5$ g prior to operation, and all animals lost weight following mucosal resection. The ECM treated rats gradually gained weight over time. Eighty-three percent (5 out of 6) of the untreated control animals showed anorexia and complications

secondary to anastomotic leaks and stricture formation that required removal from the study prior to the predetermined experimental endpoint. The remaining control rat showed no signs of mucosal coverage of the implant site (Figure 24A). The eECM treated rats lost  $-7.4 \pm 1.3\%$  vs.  $-11.9 \pm 2.5\%$  for the UBM treated rats by 3 days post surgery compared to the UBM treated rats although the difference was not significant ( $p=0.243$ ). By 14 days post surgery both groups had recovered from the weight loss and exceeded their initial weight (eECM  $+2.4 \pm 2.7\%$  vs UBM  $+1.4 \pm 2.6\%$ ). All of the ECM treated rats recovered from surgery and survived to the experimental endpoint (14 days) without complications. Representative images show that remodeling of the esophageal mucosa was indistinguishable in rats treated with UBM (Figure 24B) vs. eECM (Figure 24C). Positive staining for CK14, a marker of basal esophageal epithelium, was absent in the control animals (Figure 24D) but was shown in cells lining the basement membrane of the esophageal mucosa in rats treated with both UBM (Figure 24E) and eECM (Figure 24F).

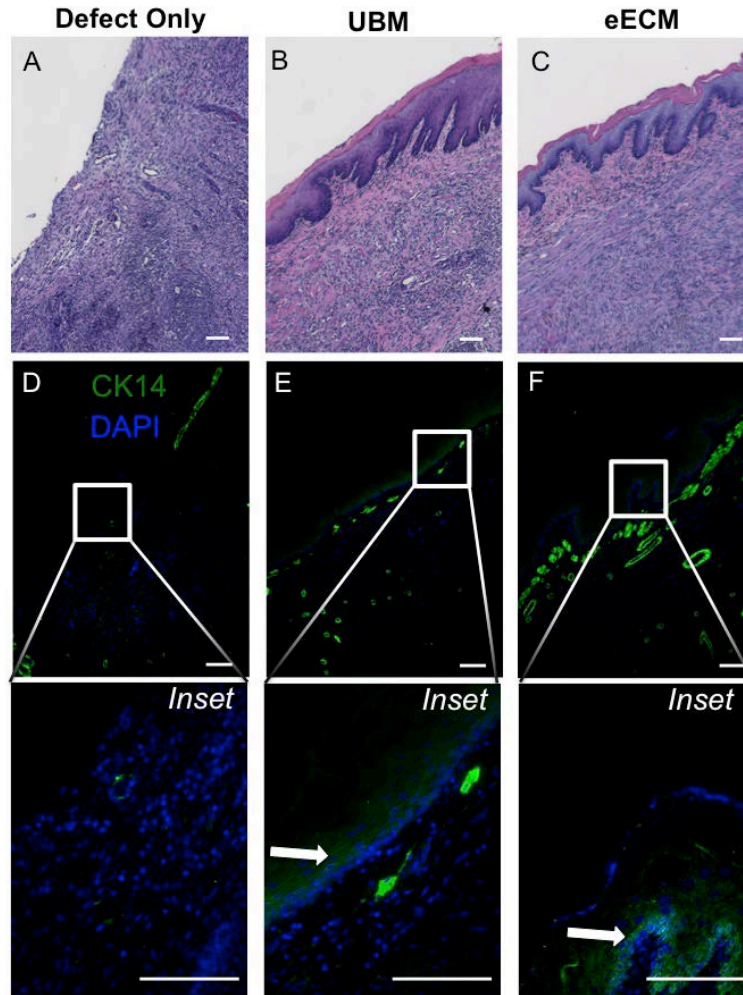


**Figure 24. Histology and immunolabeling of explants at 14 days post-surgery.** The in-vivo host response to no treatment (A, D), UBM scaffold (B, E), and eECM (C, F) was assessed histologically with hematoxylin and eosin (H&E) staining and by immunolabeling for stratified squamous epithelium (cytokeratin 14, green). Blood vessel endothelial cells stain positive for cytokeratin 14. Arrows indicate positive staining and scale bars = 100  $\mu$ m.

## 9.5 DISCUSSION

Results of the present study show that a homologous eECM preferentially enhances the migration of esophageal stem cells and supports the formation of 3D organoids in culture but in-vivo remodeling of the esophageal mucosa was similar with the use of heterologous (UBM) vs.

homologous (eECM) scaffolds. These collective results suggest that the mucosa of the esophagus contains favorable tissue-specific properties that are retained following the decellularization process but the contribution to these properties to the overall in-vivo remodeling process are either not identifiable in this model or are not required for a constructive remodeling outcome.

While the cells that contribute to esophageal remodeling following mucosal resection in the present study are not completely identified, the resident esophageal stem cell population represents a plausible and logical candidate<sup>348</sup>. These cells are present in the basal layer of the esophageal mucosa and following tissue resection must migrate the length of the mucosal resection to aid in tissue repair. Results of the present study show that ECM constituents facilitate the migration and differentiation of esophageal stem cells and that eECM in particular support these processes. Interestingly, the present study showed an inverse dose response of migrating cells toward esophageal ECM. It is known that chemoattractants often exhibit a bell shaped dose response curve<sup>349</sup>. It is plausible tissue-specific chemoattractant molecule(s) are present in eECM and similar findings may be true for other tissues and organs<sup>115,307</sup>. A unique gel chromatography protein-banding pattern in eECM was identified in the present study but the identities and biologic activity of the proteins have not yet been characterized.

A key indicator of the success or failure of an ECM scaffold to facilitate constructive and functional tissue repair is the host response to the material following implantation. While a distinct and tissue-specific ECM-dependent cellular response was observed in-vitro in the present study, the in-vivo remodeling outcome at 14 days post surgery yielded an indistinguishable constructive outcome regardless of which ECM scaffold was used for repair. The fate of the control animals clearly indicated that the mucosal defect was critically sized and both ECM scaffolds promoted a constructive remodeling response compared to the healing

response of the untreated control animals. Whether the temporal remodeling response differed between UBM and eECM is unknown since only a single post-operative time point was studied.

Previous studies in the esophagus have shown constructive outcomes with the use of UBM and SIS<sup>92-94</sup>, both heterologous forms of ECM. The heterologous ECMs were successful in reducing stricture formation but the remodeled tissue did not fully reconstitute all components of normal esophageal tissue; for example, glandular tissue was absent. The present study showed that heterologous source ECM scaffolds were inferior to site-specific ECM in-vitro but in-vivo differences in outcomes in eECM vs. UBM at 14 days post mucosectomy were not identified. Species differences in the rat and human esophageal histology, namely the lack of submucosal glands in the rat esophagus, would require testing in a large animal model to determine whether eECM may have clinical benefits.

A variable in the present study that should be noted is that the ECM materials were derived from xenogeneic tissues. However, this is quite representative of the clinical scenario, where a large majority of commercial scaffolds composed of ECM are from a porcine source<sup>350</sup>. Practical considerations favor the use of xenogeneic tissues as they are in abundant supply through the agricultural supply chain. More importantly, the constituent molecules of ECM are some of the most highly evolutionarily conserved proteins across species<sup>68-70</sup>. The present study shows that porcine eECM regulates murine esophageal stem cell behavior and also mediates esophageal remodeling in the rat, consistent with known species homology of ECM constituents.

There were limitations to the present study. First, the response of only one cell type was evaluated. Esophageal stem cells are not the only cell population that may contribute to remodeling of the esophageal mucosa. Another potential contributing cell population is the multipotent perivascular stem cell<sup>66,307</sup>. Perivascular stem cells are found surrounding

endothelium of normal tissue and are likely to be present in the vasculature within the esophagus. A number of studies have reported the chemotactic and mitogenic potential of ECM for the perivascular stem cell population<sup>66,308</sup>. Another limitation of the present study was the use of different decellularization protocols for preparing the ECM scaffolds. Decellularization protocols are typically dictated by tissue-specific characteristics, which almost always differ to achieve effective decellularization. Use of a single decellularization protocol for all tissues in the present study would have resulted in ECM scaffolds with a different content of cell remnants and thus would have added a major variable. The effects of the different decellularization protocols upon the results in the present study are unknown, but protocols similar or identical to those in the present study would likely be used in the clinical setting and therefore have potential clinical relevance.

## **9.6 CONCLUSION**

In conclusion, the present chapter showed a superior in-vitro response of esophageal stem cells to homologous ECM vs. heterologous ECM. Surgical placement of the scaffold into a rodent mucosal defect, however, showed no differences in remodeling response for homologous vs. heterologous ECM. A single time point limited conclusions from the in-vivo portion of the present chapter and the preference of homologous ECM in the esophageal location is worthy of further investigation considering the unmet clinical need for therapeutic options for esophageal pathology.

## **10.0 RESTORING MUCOSAL BARRIER FUNCTION AND MODIFYING MACROPHAGE PHENOTYPE WITH AN EXTRACELLULAR MATRIX HYDROGEL: POTENTIAL THERAPY FOR ULCERATIVE COLITIS**

### **10.1 ABSTRACT**

Despite advances in therapeutic options, more than half of all patients with ulcerative colitis (UC) do not achieve long-term remission, many require colectomy, and the disease still has a major negative impact on quality of life. Extracellular matrix (ECM) bioscaffolds facilitate the functional repair of many tissues by mechanisms that include the mitigation of pro-inflammatory macrophage phenotype and mobilization of endogenous stem/progenitor cells. The aim of the present study was to determine if an ECM hydrogel therapy could influence outcomes in an inducible rodent model of UC. The dextran sodium sulfate (DSS)-colitis model was used in male Sprague Dawley rats. Animals were treated via enema with an ECM hydrogel and the severity of colitis was determined by clinical and histologic criteria. Lamina propria cells were isolated and the production of inflammatory mediators was quantified. Mucosal permeability was assessed in-vivo by administering TRITC-dextran and in-vivo using transepithelial electrical resistance (TEER). ECM hydrogel therapy accelerated healing and improved outcome. The hydrogel was adhesive to colonic tissue, which allowed for targeted delivery of the therapy, and resulted in a reduction in clinical and histologic signs of disease. ECM hydrogel facilitated functional improvement of colonic epithelial barrier function and the resolution of the pro-

inflammatory state of tissue macrophages. The present chapter shows that a nonsurgical and nonpharmacologic ECM-based therapy can abate DSS-colitis not by immunosuppression but by promoting phenotypic change in local macrophage function and rapid replacement of the colonic mucosal barrier.

## 10.2 INTRODUCTION

Ulcerative colitis (UC) is one of the most common forms of inflammatory bowel disease, and represents a significant global health problem<sup>351</sup>. Since the 1930s, the fundamental approach to treatment has been pharmacologic (e.g., 5-amino salicylic acid, immunosuppressive therapy) and/or surgical intervention (e.g., colectomy). Nearly a century later, the basic tenets of patient care remain unchanged despite inadequate and less than acceptable results. Each year more than 50% of UC patients suffer from active flares and associated systemic effects. Overall, greater than 20 percent of patients diagnosed with UC will eventually require radical tissue resection (i.e. colectomy)—an alarming incidence that has remained unchanged over the last 50 years<sup>352</sup>.

UC is a chronic relapsing disease consisting of acute flares followed by periods of remission and healing<sup>353</sup>. Active disease is characterized by chronic inflammation of the colon and defects in intestinal epithelial cell (IEC) barrier function<sup>354</sup>. Based upon observations that scaffolds composed of extracellular matrix (ECM) were shown to mitigate inflammation and support functional reconstruction of tissues including the gastrointestinal tract<sup>92,93,96,355</sup>, we hypothesized that a similar approach to UC therapy will (1) abate inflammatory flares not by immune suppression but rather by promoting alternative activation of the local immune cell

population, and (2) induce rapid restoration of the colonic mucosal barrier function not by simply providing a physical barrier between colonic submucosa and luminal contents but rather by promoting proliferation and replacement of the colonic mucosal epithelium. This two-pronged approach was tested by local delivery (enema) of an ECM hydrogel in a rodent model of UC.

The common mechanism associated with the successful clinical application of ECM bioscaffolds has been modulation of the innate immune response via embedded signaling molecules. Intact and solubilized/hydrogel forms of ECM have been shown to facilitate a rapid and dramatic transition away from an M1-like, pro-inflammatory macrophage phenotype toward an M2-like, pro-healing/regulatory macrophage phenotype<sup>108,134</sup>. Simultaneously, naturally occurring cryptic peptide motifs released or exposed during in-vivo degradation of the ECM material, combined with the secreted products of ECM-exposed alternatively activated macrophages, promote stem/progenitor cell chemotaxis, proliferation, and differentiation<sup>66,241</sup>. The objective of the present study was to determine if the above-mentioned ECM-induced biologic effects could influence outcomes in an inducible rodent model of UC.

## **10.3 MATERIALS AND METHODS**

### ***10.3.1 Experimental design***

Ulcerative colitis was induced in male Sprague Dawley rats and treated with a daily enema of ECMH or vehicle (pepsin buffer) only for 7 days to determine the effect of an extracellular matrix hydrogel (ECMH) on colonic inflammation and barrier function. Animals were sacrificed at 7 days and 14 days post-DSS to evaluate the temporal response (n = 14 per time point per

treatment) as shown in Figure 1. Healthy control rats, which did not receive DSS, were included for comparison at both 7 and 14 days (n = 6 per time point). The study endpoints included clinical response, histologic scores of colon pathology, characterization of the inflammatory response, and barrier function. The effect of ECMH on cell phenotype and epithelial barrier function was also measured in-vitro with lamina propria mononuclear cells (LPMCs) and intestinal epithelial cells, respectively.

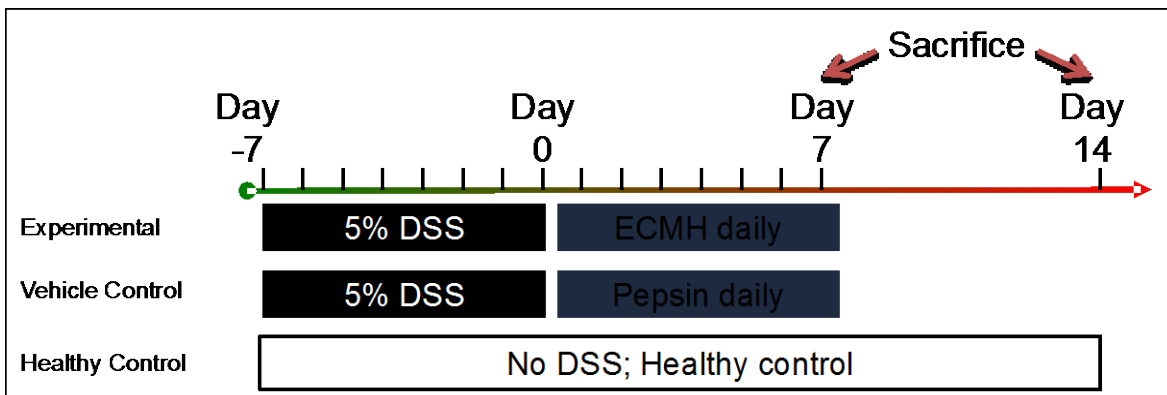


**Figure 25. Schematic of experimental overview.** Rats were administered 5% DSS in drinking water for 7 days to induce ulcerative colitis followed by daily enema treatments with either ECMH or the vehicle buffer (pepsin). Animals were sacrificed at days 7 and 14.

### 10.3.2 ECM hydrogel preparation and formulations

ECM composed of porcine small intestinal submucosa (SIS) was prepared according to a standard protocol<sup>83</sup>. In brief, porcine small intestine was harvested immediately following euthanasia, rinsed of contents in deionized water, and frozen. The tissue was thawed and the tunica mucosa, the tunica serosa, and tunica muscularis externa were mechanically removed,

leaving behind the tunica submucosa and basilar portions of the tunica mucosa (termed SIS). Decellularization of the SIS material was conducted by rinsing in deionized water for 24-72h prior to treatment with 0.1% peracetic acid / 4% ethanol and subsequent saline and water rinses. SIS-ECM was frozen, lyophilized, and comminuted with a Wiley Mill using a #60-mesh screen, and digested at 10 mg/mL dry weight with 1 mg/mL pepsin (Sigma, St. Louis, MO) in 0.01N HCl while stirring for 20-26 h at 21-23°C. Digest was stored in aliquots at -20°C and pH neutralized with 0.1M NaOH prior to use. Hydrogel formation was induced by the neutralization step and an accompanying temperature increase to approximately 37°C following administration of the enema. All in-vivo studies used an ECM hydrogel (ECMH) concentration of 8 mg/mL and all in-vitro studies used an ECMH concentration of 500 µg/mL.

<sup>14</sup>C-labeled ECMH was prepared as stated above with the intestines of pigs that were injected with <sup>14</sup>C-tagged proline, as previously described<sup>356</sup>. FITC-labeled ECMH was prepared with a protein labeling kit (Thermo PierceNet) per manufacturer's instructions<sup>66</sup>.

### **10.3.3. Characterization of ECM hydrogel**

Decellularization efficiency was determined by the absence of nuclei by H&E and DAPI staining. Remnant DNA was measured via PicoGreen assay (Invitrogen) and DNA fragmentation was determined using gel electrophoresis. Sulfated glycosaminoglycan content in the ECM was measured using a Blyscan Sulfated Glycosaminoglycan Assay (Biocolor Ltd.) per manufacturer's guidelines. The rheological characteristics of ECMH were determined with a rheometer (AR2000, TA instruments, New Castle, DE) operating with a 40 mm parallel plate geometry and the steady shear viscosity was measured by applying a stress of 1 Pa at a

frequency of 0.159 Hz, as described previously. All characterization assays were completed on 4 independent preparations of ECM (n = 4).

#### **10.3.4. ECM adhesion testing**

The mucoadhesion strength of ECMH was measured using a modified detachment force technique<sup>357</sup>. A uniaxial tensile testing machine (MTS Insight; MTS Systems Corp., Eden Prairie, MN) equipped with a 10 N load cell was used for all tensile strength measurements. Two colon sections were glued to steel washers (diameter 12.7 mm) with mucosa facing outward and one washer was glued to the bottom of a 24-well plate (diameter 15.6 mm). The ECMH was prepared by neutralizing with one tenth volume of 0.1M NaOH and one ninth volume of 10x PBS then 0.5 mL of ECMH was added onto the bottom tissue and the top tissue was added and allowed to penetrate into the gel to a predetermined depth before incubating at 37°C for 1 hour. After incubation, the upper washer was slowly withdrawn at a constant speed of 5 mm/min until a failure occurred between the surfaces.

#### **10.3.5 Animals and husbandry**

All procedures and animal studies were approved and conducted in compliance with the University of Pittsburgh Radiation Safety Committee and the Institutional Animal Care and Use Committee. Male Sprague Dawley rats, 8-12 weeks of age, were obtained from standard vendor (Harlan) and were housed and environmentally acclimated for 7-10 days. Animals were housed

in standard laboratory conditions with a temperature of 21-23 °C and 12 hr dark/light cycles.

Rats were allowed ad libitum access to food and water throughout the study.

### 10.3.6 *Disease induction and monitoring*

Five percent dextran sulfate sodium (DSS) salt (36,000-50,000 MW; MP Biomedical) was prepared daily in deionized water and administered to rats by ad libitum drinking for 7 days and the animals were monitored daily. Animal weight and consumption of food and water were tracked for each animal. Disease activity (i.e., stool consistency, presence of blood in stool, and weight loss) was measured every other day (i.e., days 1, 3, 5, 7, etc.) and scored on a range of 0 to 4 as shown in **Table 9**. Stool was scored for consistency (0=normal, 2=loose, 4=diarrhea) and presence of blood (0=none, 2=occult, 4=gross bleeding). Stool was tested for the presence of blood using ColoScreen ES Lab Pack Fecal Occult Tests. Weight loss compared to baseline was scored as follows: 0=none, 1= 1-5%, 2= 5-10%, 3= 10-20%, and 4= >20%.

**Table 9.** Criteria for clinical symptom scoring

<b>Score</b>	<b>Weight loss</b>	<b>Stool consistency</b>	<b>Stool Blood</b>
0	None	Normal	None
1	1-5%		
2	5-10%	Loose stools	Occult
3	10-20%		
4	>20%	Diarrhea	Gross bleeding

### **10.3.7 Enema administration**

Rats were anesthetized with 2-4% inhaled isoflurane and enemas were delivered using a flexible Surflo winged infusion catheter (Terumo, OD= 2mm). Enemas (5mL) were administered at 3 sites along the colon utilizing a syringe attached to the catheter (approximately 1.7 mL per site), starting at 8 cm proximal to anus and at 5 cm and 3 cm while gradually removing the catheter with approximate total infusion time of 60 seconds (i.e., 20 sec per site).

### **10.3.8 ECM retention studies with FITC- and <sup>14</sup>C-ECMH**

To determine hydrogel retention time, rats were administered FITC-labeled or <sup>14</sup>C-labeled ECMH via enema following disease induction. Eighteen rats were divided into 2 groups based on ECMH formulation (FITC- and <sup>14</sup>C-ECMH) and sacrificed at 2 hr, 12 hr, and 24 hr post enema (n = 3 per time point per ECMH formulation). Explanted colons from FITC-ECMH treated rats were processed to be optically clear such that the luminal contents were visible by fluorescent imaging. Immediately following sacrifice all samples were protected from light to prevent photo bleaching of the FITC conjugate. Optical clearing of the colons was initiated by incubating in Dent's fixative (1:4 dimethyl sulfoxide (DMSO): acetone) for 2 hours. Colons were then permeabilized and bleached in Dent's bleach (1:4:1 DMSO: acetone: H<sub>2</sub>O<sub>2</sub>) for 1 hour. Optically cleared colons were then imaged on a Fluorescent gel imager (Chemidoc Touch, Biorad). Exposure time was set to a control sample of FITC-ECMH and kept constant for all subsequent images.

For <sup>14</sup>C measurements, the entire colon of each rat was individually flash frozen in liquid nitrogen and homogenized. The frozen tissue was ground with mortar and pestle and mixed

until homogenous. Approximately 40 mg of tissue samples was analyzed by accelerated mass spectrometry (AMS). Non-treated controls were used to subtract the background  $^{14}\text{C}$  levels in native tissue.

### ***10.3.9 Explanting and scoring colonic tissue***

Animals were sacrificed at predetermined time points as described previously. Euthanasia was achieved by  $\text{CO}_2$  inhalation and subsequent cervical dislocation in accordance with the guidelines of the American Veterinary Medical Association (AVMA). Following euthanasia, the colon was resected following a ventral abdominal midline incision. A continuous colon segment was collected, spanning from the rectum to the cecum, and photographed. Colon length was measured as an indicator of disease activity. The colon was opened longitudinally and assessed grossly by investigators blinded to the treatment group for damage according to the metrics outlined in **Table 10**.

**Table 10.** Criteria for gross anatomical scoring of colon specimens

Score	Appearance
0	Normal
1	Localized hyperemia, no ulcers
2	Ulceration without hyperemia or bowel wall thickening
3	Ulceration with inflammation at one site
4	Two or more sites of ulceration and inflammation
5	Ulceration at multiple sites or extending >1 cm along the length of the colon
6-10	When an area of damage extended >2 cm along the length of colon, the score was increased by 1 for each additional cm of involvement

The distal region of colon, 9 cm in length, was cut into thirds and opened longitudinally. Specimens were then collected for histologic examination, ex-vivo organ culture, and myeloperoxidase measurement. The colon specimens were paraffin embedded and tissue sections (5  $\mu$ m) that were obtained from 2 to 8 cm from distal to proximal colon were stained with hematoxylin and eosin (H&E) for representative histologic scoring. The distal and proximal tissue sections were separated onto 2 slides and histologic scoring was performed according to **Table 11** by six blinded investigators.

**Table 11.** Criteria for histologic scoring of colon specimens

<b>Feature</b>	<b>Score</b>	<b>Description</b>
Inflammation extent	0	No inflammation
	1	Mild inflammation in mucosa
	2	Moderate-severe inflammation in mucosa
	3	Mild inflammation into the submucosa
	4	Moderate-severe inflammation into the submucosa
Ulceration	0	0%
	1	1-25%
	2	26-50%
	3	51-75%
	4	76-100%

#### 10.3.10 *TRITC-Dextran permeability assay*

Colonic mucosal permeability was assessed by enteral administration of TRITC-dextran (molecular mass 4.4 kDa; Sigma). Rats were administered TRITC-dextran (1mL, 10 mg/mL) 4 h before sacrifice. Whole blood was obtained at the time of sacrifice in serum collection tubes and allowed to clot undisturbed at room temperature for at least 30 minutes. The clot was removed by centrifuging at 1,000 x g for 10 minutes at 4°C. TRITC-dextran concentration in the serum were determined in triplicate on a SpectraMax plate reader (Molecular Devices), with serial dilutions of TRITC-dextran used as a standard curve.

### 10.3.11 **Organ cultures**

Full thickness biopsies were obtained following sacrifice from the explanted colon of each experimental and control animal at day 7 and day 14 using a 3 mm dermal punch as described previously<sup>358</sup>. Tissue specimens were cultured at 37°C with 5% CO<sub>2</sub> for 48 h. The supernatants were then harvested and stored at -80°C until the amount of TNFα and PGE2 was measured using ELISA assays.

### 10.3.12 **LPMC isolation and culture**

Lamina propria mononuclear cells (LPMCs) were isolated from rats following colitis induction with DSS as described above. The colon was explanted, cleared of mesenteric fat tissue, and regions of Peyer's patches were excised. The colon was then split in half longitudinally, cut into pieces, and dissociated into single cell suspensions using a lamina propria dissociation kit (Miltenyi) according to manufacturer's instructions. The suspension was then separated along a 40/70% Percoll gradient. The cells were suspended in RPMI 1640 containing 10% FBS and 100 U/mL penicillin and streptomycin, and then placed in 96-well plates at  $2 \times 10^5$  cells per well with or without the addition of 500 µg/mL ECMH or vehicle (i.e., pepsin buffer). After 48 hours incubation, the supernatant was collected and stored at -80°C until assayed for TNFα and PGE2 with ELISAs.

### 10.3.13 ***IEC culture***

For in-vitro barrier function assays, IECs (Caco-2, passages 24-28, ATCC) were cultured to approximately 80% confluence in MEM containing non-essential amino acids, 1mM sodium pyruvate, and 20% FBS. The functional response of IECs to ECMH was evaluated using rapid differentiation system (Corning Biocoat HTS Caco-2 Assay) per manufacturer's instructions. Confluent and differentiated cell monolayers were challenged with 100 ng/mL LPS for 2 hours and then treated with ECMH for 48 hours.

### 10.3.14 ***Trans-epithelial electrical resistance (TEER) measurement***

TEER of Caco-2 monolayers was measured with an Epithelial Voltohmmeter (EVOM2, World Precision Instruments). Before seeding Caco-2 cells, electrical resistance of the supporting filter and buffer medium was measured and subtracted from the total electrical resistance determined with the monolayer to calculate the TEER of the monolayer. Only differentiated monolayers with TEER values greater than  $300 \Omega \times \text{cm}^2$  were used in the study.

### 10.3.15 ***Immunolabeling***

To determine the macrophage response following ECMH treatment, paraffin embedded histologic sections were deparaffinized and immunolabeled for a pan-macrophage marker (CD68) and indicators of the M1-like ( $\text{TNF}\alpha$ ) and M2-like (CD206) macrophage phenotypes. All primary antibodies were confirmed to cross-react with rat epitopes. For visualizing the presence of Caco-2 adhesion proteins, sections were imaged at five random fields per

tissue section. Quantification of localized staining was achieved using a custom image analysis algorithm developed using CellProfiler Image Analysis Software.

For macrophage immunolabeling, tissue sections were deparaffinized using xylene and rehydrated using a graded ethanol series. Heat-mediated epitope retrieval was performed using 0.01 M citrate buffer (pH=6) at 95°C for 20 minutes. Tissue sections were subjected to Tris-Buffered Saline Tween-20 (TBST) for 15 min, followed by incubation in blocking buffer (2% horse serum / 1% bovine serum albumin/0.05% tween-20/0.05% Triton X-100) for 1 hour. The primary antibodies, diluted in blocking buffer, were added to the slides for 16 h at 4 C in a humidified chamber. The slides were then washed three times in TBS prior to the addition of secondary antibody for 1 h in a humidified chamber at room temperature. Slides were counterstained 4'6-diamidino-2-phenylindole (DAPI) to visualize nuclei. Primary antibodies used were mouse anti-rat CD68 (AbD Serotec, Raleigh, NC) at a 1:150 dilution as a pan macrophage marker, rabbit polyclonal to TNF $\alpha$  (abcam) at a 1:200 dilution as an M1-like marker, and goat polyclonal CD206 (Santa Cruz Biotech, Santa Cruz , CA) at a 1:100 dilution. The secondary antibodies used were Alexa Fluor donkey anti-mouse 594 (1:200, Invitrogen), Alexa Fluor donkey anti-goat 488 (1:200, Invitrogen), and Alexa Fluor donkey anti-rabbit 546 (1:200, Invitrogen). All primary antibodies were confirmed to cross-react with rat epitopes.

For Caco-2 immunolabeling, the primary antibodies were diluted in blocking solution and added to trans-well inserts for 16 h at 4°C in a humidified chamber. The slides were then washed three times in PBS prior to the addition of the secondary antibody for 1 h in a humidified chamber at room temperature. DAPI was used as a nuclear counterstain. The primary antibody used was rabbit anti-E-cadherin (Abcam, AB15148. 1:50). The secondary antibody used was Alexa Fluor® goat anti-rabbit 488 (Invitrogen, A11008, 1:400). The primary antibody was confirmed to cross-react with human epitopes.

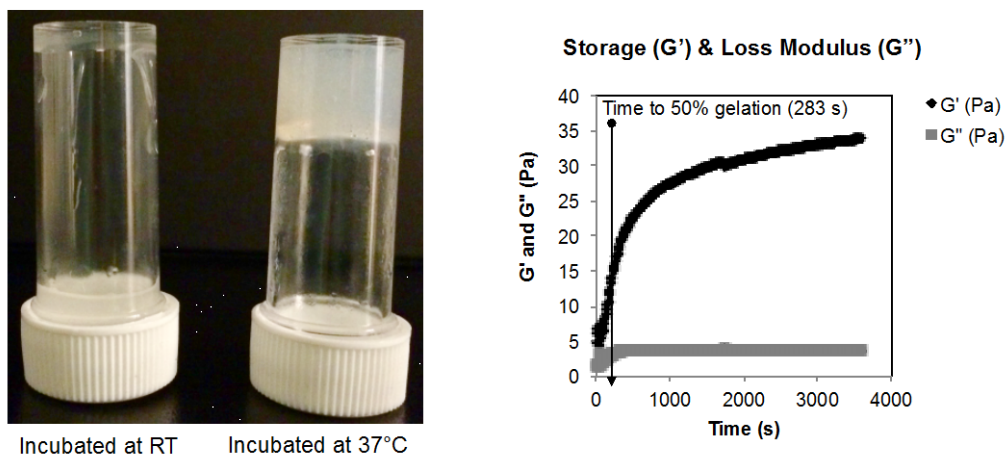
#### 10.3.16 **Statistical analysis**

The sample size used in the present study was determined based on a power analysis using pilot study data in combination with previously published relevant studies. All animals were numbered and randomly assigned to a treatment. All investigators responsible for scoring were blinded to the experimental groupings. Quantitative outcomes were compared with a one-way or two-way analysis of variance (ANOVA) and post-hoc Tukey test to determine differences between groups. All statistical analysis was performed using SPSS Statistical Analysis Software (SPSS, IBM). Data are reported as mean  $\pm$  standard deviation unless otherwise stated.

## 10.4 RESULTS

### 10.4.1 **ECMH is adhesive to colon tissue**

The therapeutic efficacy of ECMH is reliant upon its ability adhere to the colon wall and interface with the resident cells. ECMH has the distinctive property of reverse thermal gelation and the hydrogel properties are dependent upon material characteristics (Figure 26).



ECMH Characteristic	
DNA concentration	465.90 ± 43.88 ng/ mg ECM
Sulfated glycosaminoglycan concentration	18.74 ± 2.26 µg/ mg ECM
Pre-gel viscosity	1.00 ± 0.01 Pa *s
Maximum Hydrogel Stiffness (i.e., $G'$ )	33.85 ± 0.43 Pa
Time to 50% Gelation	4.72 ± 0.25 min

**Figure 26. Material properties of ECMH.** (A) ECMH material properties allow injection as a liquid and the subsequent gelation at 37°C ensures that the treatment remains localized. (B) Viscoelastic properties of ECMH, including storage modulus ( $G'$ ) and loss modulus ( $G''$ ), were measured with parallel plate rheology. (C) The biochemical and hydrogel properties were measured in 6 separate batches of ECMH.

Results of adhesion testing show that ECMH is mucoadhesive, with a dose-dependent increase in adhesion strength when tested on healthy colon (Figure 27A). Importantly, the 8 mg/mL ECMH dose used in the present study maintains equivalent adhesion strength in colitic rat colon when compared to healthy tissue (Fig 2B). It is noteworthy that mucosal adherence is not simply a property of thermoreversible gels. For example, Pluronic F-127 (20%; Sigma) did not show adhesion strength greater than the negative control (data not shown). When delivered via enema to colitic rats, the residence time of the ECMH is greater than 24 hours. Two hours after administering the enema, about 50% of the  $^{14}\text{C}$ -ECMH remains in the colon and approximately 10% of the initial ECMH enema remained after 24 hours (Figure 27C). These results were corroborated by visualization of FITC-ECMH (Figure 27D). Together the results

show that ECMH material properties allow injection as a liquid and the subsequent gelation ensures that the treatment remains localized for at least 24 hr. Based on these data, a daily enema treatment was used to measure the therapeutic efficacy of ECMH.

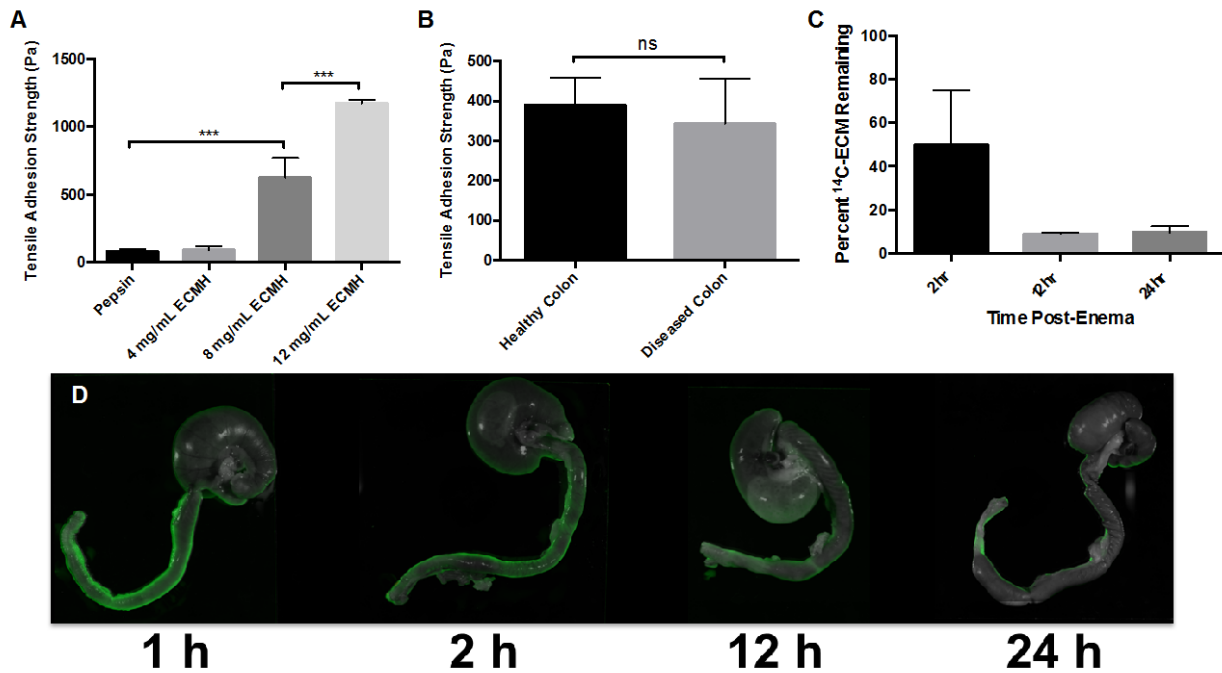


**Figure 27. ECMH is Mucoadhesive.** Tensile tests show dose-dependent increase in adhesion strength of ECMH to healthy colon (A) and equivalent adhesion in healthy vs. diseased colon (B). The resident time of ECMH following enema delivery was tested with <sup>14</sup>C (C) and FITC-labeled ECMH (D).

#### 10.4.2 ECMH treatment mitigates disease state

The DSS experimental model is a well-accepted UC-like self-limiting colitis phenotype with epithelial barrier defects<sup>359</sup>. Clinical signs of colitis (e.g., weight loss, stool blood, and stool

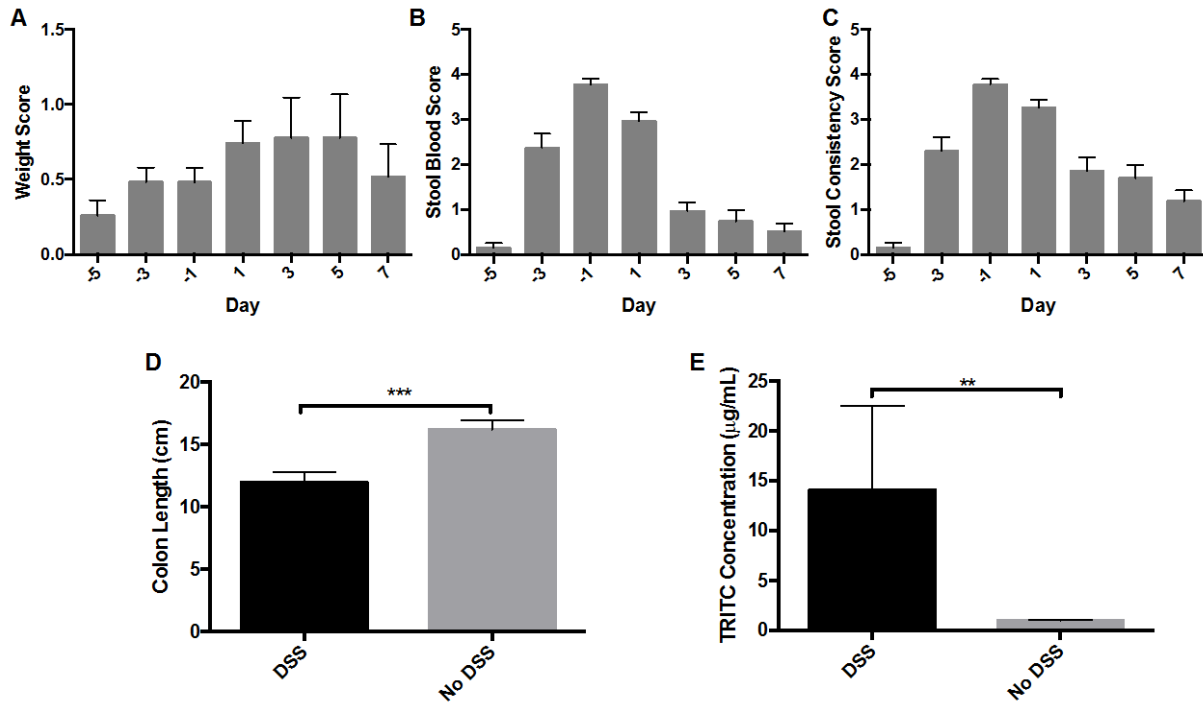


**Figure 28. DSS-colitis model effectively induces disease.** Weight change (A), the presence of blood in stool (B), and stool consistency (C) were tracked as clinical indicators of disease. Following 7 days of exposure to DSS, colon length (D) was measured as an indicator of disease severity and barrier dysfunction was measured by TRITC-dextran permeability (E).

consistency) were present following 3 days of exposure to 5% DSS in drinking water and reach their peak following 6 days (Figure 28). ECMH treatment diminished clinical symptoms of UC in this rodent model. ECMH treated animals did not lose as much weight (at days 1 and 3) and had less blood in stool (at days 3 and 5) compared to the vehicle control. The shortening of the colon that was present at day 0 (Figure 28D) was no longer evident by days 7 and 14 across all groups (Figure 29D). ECMH treatment resulted in a reduction in the gross score compared to the vehicle at day 7 (Figure 29E).

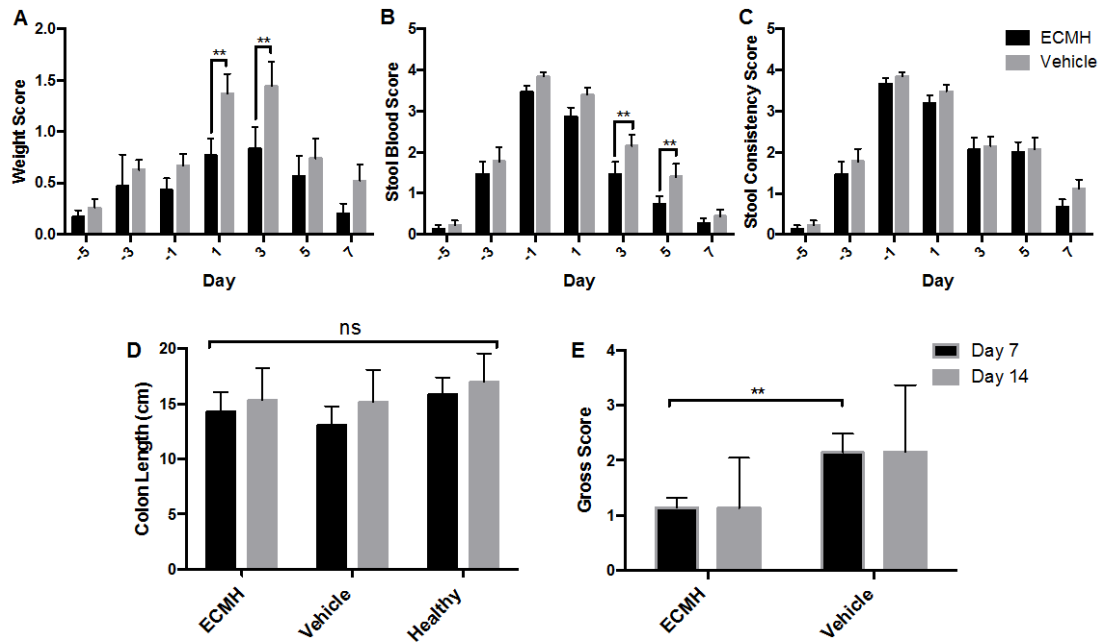


**Figure 29. ECMH Treatment Reduces Disease Activity.** The effect of ECMH treatment on clinical symptoms (A-C), colon length (D), and gross score at explant (E) was tracked and compared to the vehicle (i.e., pepsin buffer) alone.

Histomorphologic analysis also showed that ECMH is therapeutic in the present model as evident in representative images (Figure 30). ECMH treatment resulted in diminished signs of inflammation and a lower the degree of ulceration at 7 and 14 days in both distal and proximal tissue sections (Figure 31).

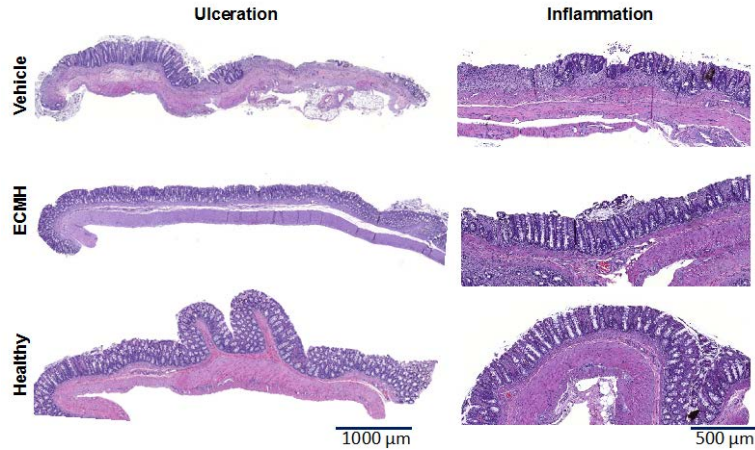


**Figure 30. Histologic Response to ECMH.** Histomorphologic scoring of hematoxylin and eosin stained tissue sections was used to assess the effect of ECMH treatment on ulceration and inflammation extent.

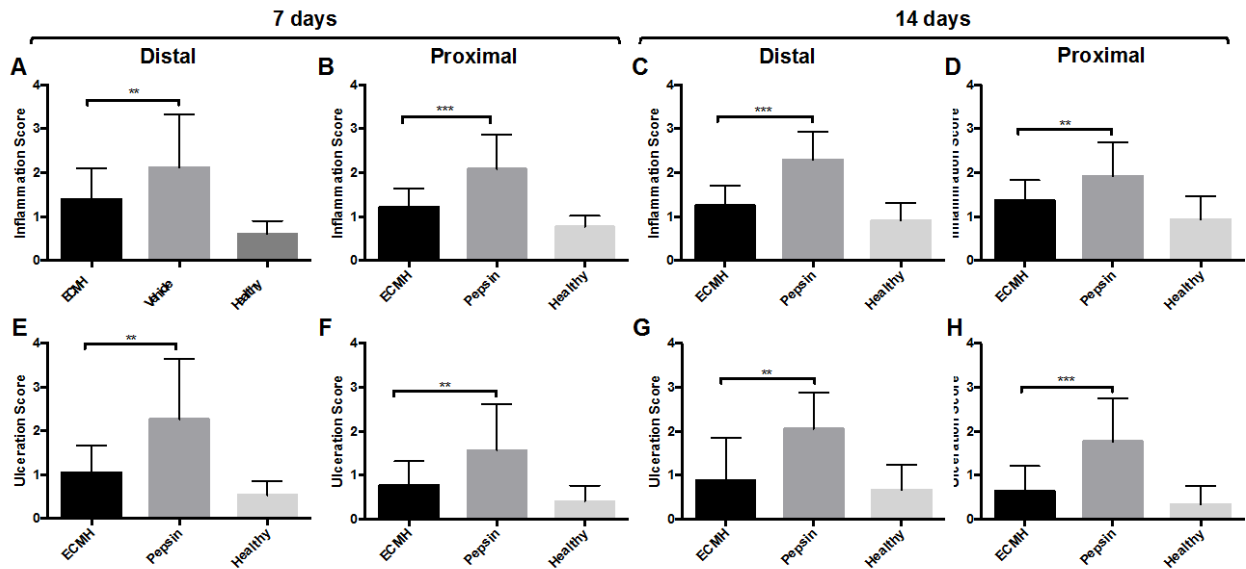


**Figure 31. ECMH Treatment Lowers Histologic Score.** Distal and proximal tissue sections stained with hematoxylin and eosin were scored by blinded investigators and compared with vehicle/pepsin buffer. The extent of inflammation and degree of ulceration were quantified at 7 days (A,B,E,F) and 14 days (C,D,G,H).

### 10.4.3 *ECMH restores epithelial barrier function*

A defect in gut barrier function and increased permeability can lead to inflammatory bowel disease even in the presence of an intact immune system<sup>360</sup>. Results of the TRITC-Dextran permeability assay showed that the barrier function of ECMH-treated animals is similar to healthy animals at 7 days while the colonic epithelial barrier in the vehicle-treated control group remain impaired compared to the healthy control (Figure 32A). Differentiated and LPS-damaged monolayers of IECs respond to ECMH treatment in-vitro with functional recovery as shown by TEER readings (Figure 32B). The increased barrier function was associated with an increased presence of E-cadherin, one of the most important cell-cell adhesion proteins in the gut. ECMH treatment leads to approximately 50% increase in E-cadherin positive cells compared with negative controls (Figure 32C-D).

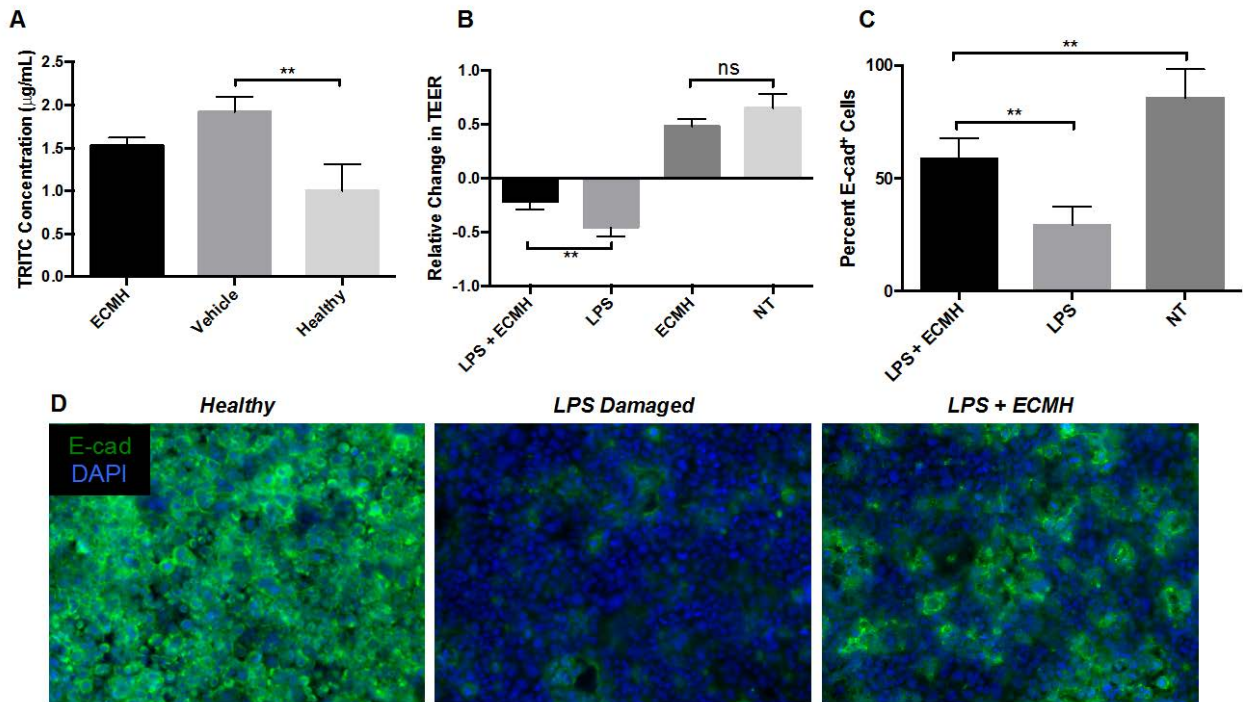


**Figure 32. ECM Restores Barrier Function.** TRITC-Dextran permeability assay show that the barrier function of ECMH-treated animals is similar to healthy animals while the colonic epithelial barrier in the vehicle-treated control group remain impaired compared to the healthy control (A). Differentiated and LPS-damaged monolayers of IECs respond to ECMH treatment in-vitro with functional recovery as shown by TEER readings (B). The increased barrier function is associated with an increased presence of E-cadherin compared with negative controls (C-D).

#### 10.4.4 ECMH mitigates the inflammatory response

Recognized inflammatory mediators of IBD (i.e., TNF $\alpha$  and PGE2) were measured in the present study. LPMCs isolated from colitic rats were plated and exposed to ECMH. The ECMH treatment resulted in a substantial reduction in the production of TNF $\alpha$  (Figure 33A) by the LPMCs but had no effect on PGE2 production (Figure 33B). Organ cultures of biopsies collected from rats following ECMH or vehicle control treatment showed secreted PGE2 was similar to healthy controls in the ECMH treated animals while the vehicle controls had significantly

elevated levels of mucosal PGE2 (Figure 33C). Secreted levels of  $\alpha\alpha$  were below detection in the organ cultures regardless of experimental condition at the time points studied.

The effect of ECMH on macrophage phenotype in DSS-colitis was evaluated by quantifying the number of CD68<sup>+</sup> macrophages in the colon that co-express TNF $\alpha$  or CD206. Interestingly, the absolute number of individually labeled CD68<sup>+</sup>, CD206<sup>+</sup>, and TNF $\alpha$ <sup>+</sup> cells was the same across all treatment groups (data not shown) but ECMH treatment resulted in a reduction in the number of co-labeled CD68<sup>+</sup>/TNF $\alpha$ <sup>+</sup> inflammatory macrophages at day 7 (Figure 33D). The fact that ECMH did not affect the amount of global TNF $\alpha$ <sup>+</sup> cells but did reduce the number of CD68<sup>+</sup>/TNF $\alpha$ <sup>+</sup> cells suggests a direct role for ECMH in modulating the macrophage response by reducing the number of inflammatory macrophages present in the colonic tissue.

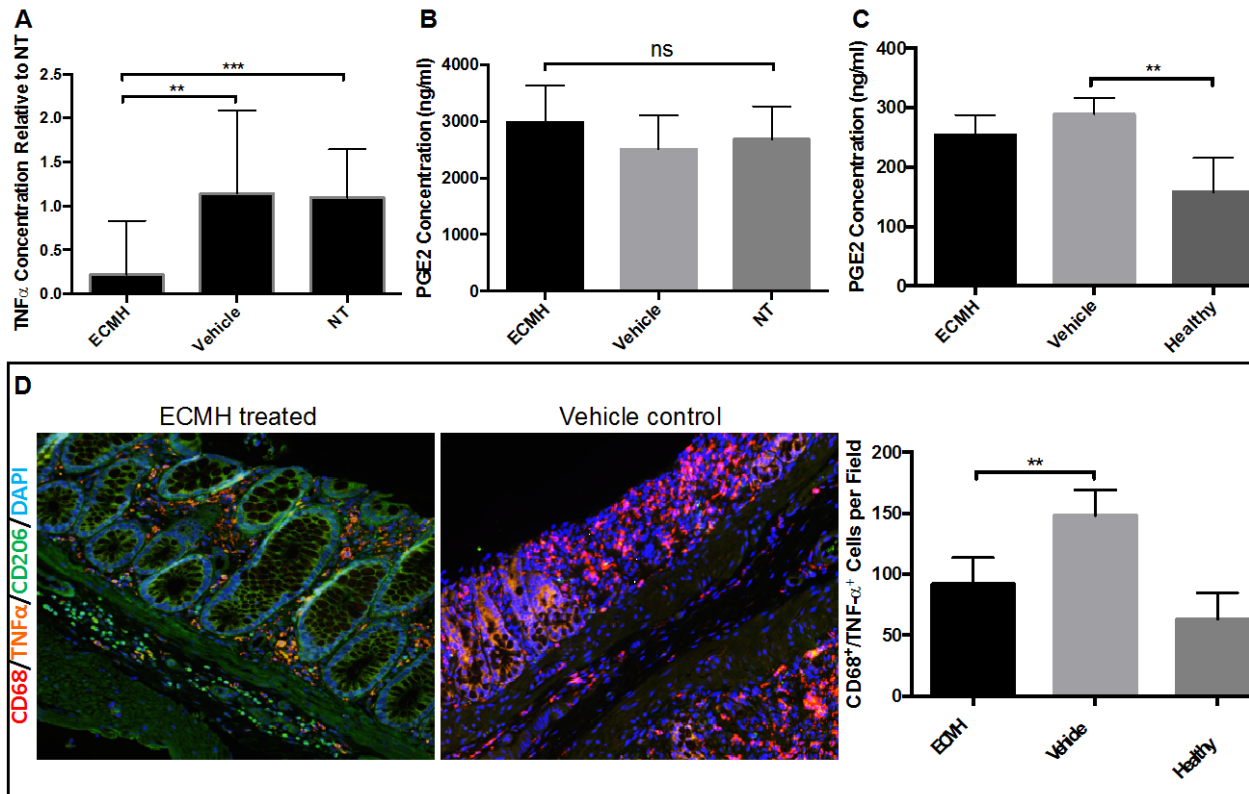


**Figure 33. ECMH Mediates Inflammation.** Lamina propria cells exposed to ECMH results in lowered levels of TNF $\alpha$  (A) but didn't affect PGE2 production (B). Organ cultures, however showed ECMH had a significant impact on PGE2 levels (C). ECMH treatment led to a decrease in total number of M1, TNF $\alpha$  expressing macrophages (D).

## 10.5 DISCUSSION

The present study shows that an ECM hydrogel composed of ECM mitigates the proinflammatory macrophage phenotype and restores barrier function in a rodent model of UC. It is noteworthy that the total number of macrophages was not changed by ECMH treatment, but rather the phenotype of this cell population was changed. In addition, the barrier function was not restored by the physical presence of the hydrogel but rather by the restoration of an

effective mucosal epithelium. These effects are a distinct departure from the immunosuppressive (defensive) and surgical (salvage) methods currently used to treat UC in humans. More than half of all patients with UC do not achieve long-term remission and many require colectomy.

The findings of the present study are consistent with, and analogous to, the known mechanisms by which ECM-based approaches facilitate the constructive remodeling of injured tissues in other anatomic locations<sup>87,89,92,129,361,362</sup>. Specifically, ECM materials derived via decellularization of a variety of allogeneic or xenogeneic source tissues have been shown to induce a phenotypic transition from the proinflammatory macrophage and lymphocyte phenotype toward a regulatory, “anti-inflammatory” and healing phenotype<sup>132,134,305,363</sup>, and to promote endogenous stem/progenitor cell activation and recruitment<sup>66,67,345,362</sup>. Furthermore, the findings are similar to the results in patients with esophageal adenocarcinoma who were subjected to surgical removal of the affected esophageal mucosa and placement of a solid (i.e., not hydrogel) form of an ECM bioscaffold. These patients showed a rapid restoration of the esophageal mucosa without recalcitrant stricture, and normal esophageal function.

The combination of promoting a shift in macrophage function from inflammation to wound healing and facilitating the restoration of an intact colonic mucosa is a departure from current therapeutic strategies for UC. Current therapies are focused upon immune suppression (e.g., corticosteroids and anti-TNF $\alpha$  compounds) with the associated local and systemic effects. Immune suppression is clearly different than maintaining complete functionality of the immune system while redirecting its’ biologic objectives. In fact, a robust immune system is necessary for a healthy, functional gastrointestinal tract<sup>364-367</sup>.

The use of immunosuppressive and/or anti-inflammatory compounds has a limited effect on mucosal healing<sup>368,369</sup> and yet the disrupted mucosal barrier integrity is a key component in

the pathogenesis of UC. Barrier dysfunction enables the ingress of luminal antigens and pathogens, continuous immune cell activation in the lamina propria, and the associated chronic inflammation that is the hallmark of UC. Restoration of barrier function is therefore an important therapeutic target in UC. In the present study, ECMH therapy had a protective effect on the epithelial cells of the colonic mucosa. Results show that ECMH facilitates functional improvement of the epithelial barrier function and suggest that ECMH acts therapeutically either by limiting epithelial cell damage and/or by actively salvaging mucosal integrity. Given the mucoadhesive properties of ECMH it would also be feasible to use ECMH as a carrier for local delivery of pharmacologics.

Recognition that effector cells of the immune system, such as the macrophages and T-helper cells, not only promote classic inflammatory processes but also orchestrate the temporal inhibition of inflammation and initiation of functional tissue remodeling <sup>132,291,370-373</sup> provides the opportunity to re-examine immunosuppressive strategies for treatment of diseases such as UC. Although the signaling molecules that influence macrophage and lymphocyte phenotype transition are not fully understood, there is suggestive evidence that at least some of these regulators reside within the ECM <sup>108,134,370</sup>. Results of the present study suggest that ECMH modulates the innate immune response not by directly promoting an M2-like macrophage phenotype but rather by reducing the number of M1-like pro-inflammatory macrophages, thus shifting the microenvironmental milieu from inflammation to repair.

Limitations of the present study include the use of one animal model and only 2 surface markers for macrophage phenotype. The DSS-colitis model was chosen because the model features innate immunity and epithelial barrier defects that are central to the present study's hypothesis. The outcomes in the DSS-colitis model can also be effective in predicting clinical treatment of IBD <sup>359</sup>. While only two markers for macrophage phenotype were used for immunolabeling, we chose the most representative marker of UC-like inflammation (TNF $\alpha$ ) and

for M2-like macrophages (CD206). Macrophages are a heterogeneous cell population and the use of a single marker to delineate phenotype can result in ambiguity.  $\text{TNF}\alpha$ , in particular, was chosen for the present study because of its integral role in the pathogenesis of UC<sup>374</sup>, however it is logical and plausible that the use of other markers could provide additional insight into the effects of ECMH treatment upon the resident macrophage population in the colitic microenvironment.

## **10.6 CONCLUSION**

Despite limitations, the present study shows that ECMH restores epithelial barrier function and modulates macrophage phenotype away from a pro-inflammatory state. Two physiologic processes, the colonic barrier function and pro-inflammatory response, were positively influenced by ECMH therapy. One benefit of ECMH, in addition to the therapeutic efficacy, is that the well-accepted safety profile of ECM products may allow for accelerated transition to the clinic.

## 11.0 SUMMARY OF MILESTONES AND FUTURE DIRECTIONS

The central hypothesis addressed in this thesis is that ECM hydrogels support constructive remodeling of GI tissue by modulation of the microenvironment and local immune cells. The following milestones were achieved:

**Milestone 1:** Gastrointestinal extracellular matrix (GI-ECM) bioscaffolds derived from porcine esophagus and colon were decellularized and quantitatively described.

Summary Milestone 1: The composition and structure of ECM are directly attributed to the cell population of the tissue from which the ECM is derived. The esophageal mucosa is a smooth dense tissue has anisotropic mechanical properties with 83% and 18% maximal strain in the circumferential and longitudinal direction, respectively. Decellularized esophageal mucosa retains similar anisotropy (but with lower compliance along both axes) and retains biochemical constituent's bFGF and GAGs (see Chapter 7 for more details). In contrast, the colonic mucosa is a loose thin permeable tissue that, while also shows anisotropy, is much weaker than the esophageal mucosa with 5% and 2% maximal strain in the longitudinal and circumferential direction. The anisotropy is similarly retained following decellularization and the biochemical constituents are retained following decellularization, although the concentrations of GAGs and bFGF are lower in the colonic mucosa when compared to the esophageal mucosa (see Chapter

8 for more details). Interestingly, esophageal mucosal ECM retains tissue-specific characteristics that enhance the migration of esophageal stem cells and supports the formation of 3D organoids to a greater extent than heterologous-derived ECM (see Chapter 9 for more details).

Future Directions Milestone 1: Future experiments should focus on determining if either esophageal- or colon-derived biologic scaffolds can be used to treat diseases of the GI tract. In particular, it would be interesting to characterize the response to these GI-derived ECM scaffolds to site-specific diseases. While some site-specific effects of esophageal ECM were shown in the present study, future experiments could examine the effects of colonic ECM on colonic cells to determine if there are tissue-specific benefits with the use of site-specific ECM.

**Milestone 2:** The effect of GI-ECM on the remodeling and inflammatory response of intestinal epithelial cells and macrophages, respectively, was characterized.

Summary Milestone 2: Effective treatment of UC requires (1) a reduction in inflammatory state and (2) rapid reformation of a robust epithelial barrier. The body's largest reservoir of macrophages are positioned in the lamina propria (LP) of the GI tract and are increased in number in UC with enhanced production of inflammatory cytokines (e.g., TNF $\alpha$ ) in IBD. Discovery work in the Badylak lab over the past 2 decades has identified the modulation of the innate immune response as a contributing mechanistic factor for ECM-induced tissue remodeling. ECM derived from esophageal and colonic mucosal tissues were cell-friendly in-vitro, and supported a constructive response when implanted in a partial thickness abdominal wall defect in-vivo. The macrophage response to ECM from the GI tract was activated towards and M2-like phenotype in-vitro and promoted an M2 predominance (i.e., the M2/M1 ratio at the scaffold-tissue interface was equal to 1.3 for eECM and 1.5 for coECM at 14 days post-surgery)

in-vivo compared to controls (see Chapters 7 and 8 for more details). The inflammatory state of mononuclear cells isolated from the LP of colitic rats is also affected by GI ECM, showing about 75% reduction in TNF $\alpha$  production following ECM treatment (see Chapter 10, Figure 33 for more details). The epithelial cell response to GI ECM was also constructive and showed a functional healing response in-vitro. Differentiated monolayers of epithelial cells had increased TEER values and E-cad staining when treated with ECM hydrogel in-vitro (see Chapter 10, Figure 32 for more information).

Future Directions Milestone 2: The cellular response to the GI-ECM scaffolds can be largely responsible for improved therapeutic outcomes in-vivo. Future experiments should focus on determining what component(s) of ECM elicit a cellular response. In addition, while the present thesis shows that the ECM materials promote a shift in innate immune cell phenotype, future experiments should aim to determine the effect of these materials on the adaptive immune response that also contributes to disease.

**Milestone 3:** The efficacy of ECM hydrogel in treating inflamed colonic mucosal tissue was determined.

Summary Milestone 3: Inflammation mitigation and remodeling (i.e., restoration of colonic epithelial barrier) is central to effect treatment of UC. Chapter 10 shows that topical application of ECM hydrogels mitigate the inflammatory response in colitic rats by modulating the microenvironmental milieu towards an anti-inflammatory state and thereby facilitating constructive remodeling of colonic mucosa. This constructive response resulted in functional improvement in the epithelial barrier function as shown with decreased mucosal permeability (see Figure 32). This combination of immune activation and restoration of the colonic mucosa is a distinct departure from current therapeutic strategies for treating IBD. Whereas current

therapies focus on immune suppression (i.e., lowering total number of immune cells in the tissue), the ECM hydrogel therapy maintains complete functionality of the immune system but redirects the pro-inflammatory response to a pro-remodeling one. Together these effects, if successful on the clinical scale, could create a paradigm shift in the approach to IBD treatment away from the immunosuppressive and surgical methods currently used.

Future Directions Milestone 3: Future experiments should be designed to further elucidate the mechanisms by which ECM is able to facilitate tissue repair. Determining the mechanisms of tissue repair could allow for improvements and optimization of therapies to treat ulcerative colitis. Further study is also necessary to determine whether ECM hydrogels can be used to treat diseased tissue at the opposite end of the GI tract (i.e., esophageal tissue). Development of therapies to treat other inflammation-mediated disease (e.g., rheumatoid arthritis, necrotizing enterocolitis) should be the focus of future studies.

## APPENDIX A

### CONSEQUENCES OF INEFFECTIVE DECELLULARIZATION OF BIOLOGIC SCAFFOLDS ON THE HOST RESPONSE

#### A.1 Abstract

Despite known variations in tissue remodeling outcomes, no systematic evaluation of the host response to cell remnants has been conducted. As a result, the amount of retained cellular material varies widely among commercial products. The objective of the present chapter was to evaluate the consequences of ineffective decellularization on the host response. Three different methods of decellularization were used to decellularize porcine small intestinal ECM (SIS-ECM). The amount of cell remnants was quantified by the amount and fragmentation of DNA within the scaffold materials. The M1/M2 phenotypic polarization profile of macrophages, activated in response to these ECM scaffolds, was assessed *in vitro* and *in vivo* using a rodent model of body wall repair. The results of this study show that, *in vitro*, more aggressive decellularization is associated with a shift in macrophage phenotype predominance from M1 to M2. While the macrophage phenotype shift was not quantitatively apparent *in vivo*, notable differences were found in the distribution of M1

vs. M2 macrophages within the various scaffolds. A clear association between macrophage phenotype and remodeling outcome exists and effective decellularization remains an important component in the processing of ECM-based scaffolds.

## A.2 Introduction

The use of biologic scaffolds derived from decellularized mammalian tissues is commonplace. Such scaffolds are composed of extracellular matrix (ECM) and have been used to repair or replace a variety of damaged or diseased tissues including cardiac<sup>375-377</sup>, esophageal<sup>378,379</sup>, dermal<sup>380</sup>, and musculotendinous tissues<sup>90,381-384</sup>, among others. These materials are typically regulated as devices and marketed as surgical mesh products; however, these ECM-based scaffolds can also serve as an inductive template for tissue repair and regeneration<sup>385,386</sup>. Numerous commercial products composed of allogeneic or xenogeneic ECM are now available for clinical use.

Results of preclinical and clinical studies with biologic scaffolds have varied from very successful<sup>387-391</sup> to complete failure<sup>392-395</sup>. The host response to these materials can be attributed to factors such as the source species (e.g., human, porcine, equine, or bovine), the tissue from which the ECM is isolated (e.g., dermis, small intestine, or pericardium), mechanical loading<sup>396,397</sup>, and the niche factors to which the scaffold is exposed following implantation. The decellularization, disinfection, and sterilization methods used during the manufacturing process can markedly influence the tissue remodeling response and functional outcome<sup>175,213</sup>. Despite these known variations in functional outcome, no quantitative criteria by which decellularization can be assessed have been suggested until recently<sup>175</sup> and as a result, the amount of retained cellular material varies widely among commercial products composed of decellularized tissues

<sup>398</sup>. The consequences of ineffective or incomplete decellularization upon the host response have not been systematically investigated.

The innate and acquired immune response to non-autologous cells is well established and understood by the tissue and organ transplantation community. However, the response to acellular xenogeneic or allogeneic biologic scaffold materials is less well understood. The macrophage represents a key component of the host response. Macrophages are activated in response to tissue damage, infection, or the presence of foreign antigens and subsequently release a variety of cytokines and chemokines <sup>399</sup>. Macrophages are now recognized to assume a variety of phenotypes characterized by distinct functional properties, surface markers, and their secreted cytokine profile <sup>400</sup>. Polarized macrophages are referred to as either M1 or M2 cells, mimicking the Th1/Th2 nomenclature. Classically activated, M1 proinflammatory macrophages express IL-12<sup>high</sup>, IL-23<sup>high</sup>, IL-10<sup>low</sup>; metabolize arginine; produce high levels of inducible nitric oxide synthetase <sup>228</sup>; secrete toxic reactive oxygen and nitric oxygen intermediates and inflammatory cytokines such as IL-1 $\beta$ , IL-6, and TNF. M1 macrophages are inducer and effector cells in Th1 type inflammatory responses. In contrast, M2, alternatively activated macrophages are induced by exposure to a variety of signals including the cytokines IL-4, IL-13, and IL-10, immune complexes, and glucocorticoid or secosteroid (vitamin D3) hormones. M2 activated macrophages express IL-12<sup>low</sup>, IL-23<sup>low</sup>, and IL-10<sup>high</sup>; have high levels of scavenger, mannose, and galactose receptors; produce arginase in the place of arginine which results in the secretion of ornithine and polyamines; are involved in polarized Th2 reactions; and possess the ability to facilitate tissue repair and constructive remodeling <sup>399,401,402</sup>.

It is known that cell death incites a series of events that typically results in the classic cascade of inflammatory processes including polymorphonuclear leukocyte (PMN) and mononuclear cell infiltration, edema, fibroblast infiltration, and eventual scar tissue formation <sup>403-405</sup>. The presence of cells within a biologic scaffold material has been shown to elicit a greater

proinflammatory response than use of the acellular biologic scaffold alone<sup>133</sup>. It is logical, therefore, that cell remnants within a partially decellularized tissue could elicit a proinflammatory response that would adversely affect a constructive tissue remodeling outcome. In fact, it has been shown that the presence of intact cells within implanted scaffolds can be associated with adverse remodeling through stimulation of a pro-inflammatory M1 macrophage response<sup>133</sup>. In contrast, thoroughly decellularized biologic ECM scaffolds are known to promote a host response that is polarized towards the M2 macrophage phenotype and is associated with constructive tissue remodeling<sup>133,406-408</sup>. These two responses sit at the extremes of the normal cellular response to an implanted biologic scaffold. Little is known about which cellular components stimulate an M1 macrophage response or if a threshold level for cellular material exists below which the M2 macrophage phenotype predominates. It has been suggested that the presence of mitochondria may be a stimulator of M1 macrophages given their primitive bacterial origin<sup>262</sup>. In light of the heterogeneity with regard to the amount and efficacy of decellularization in commercially available ECM-scaffolds<sup>398</sup>, a more thorough understanding of the effects of cell remnants upon the host response is needed.

The objective of the present study was to evaluate the effect of cell remnants (i.e., ineffective tissue decellularization) within biologic scaffolds upon *in vitro* and *in vivo* outcome measures. Three different methods were used to decellularize porcine small intestinal submucosal ECM (SIS-ECM). The amount of cellular material remaining was quantified by the amount and fragmentation of DNA. The polarization profile of activated macrophages in response to these ECM-scaffolds was then assessed *in vitro* and *in vivo* using a rodent model of body wall repair.

### A.3 Materials and Methods

**A.3.1 Harvest and preparation of ECM from porcine small intestine:** Preparation of small intestinal submucosa (SIS) ECM has been previously described<sup>409,410</sup>. Briefly, jejunum was harvested from market weight (240-260 lbs.) pigs and split longitudinally for processing. The superficial layers of the tunica mucosa were mechanically removed. Likewise, the tunica serosa and tunica muscularis externa were mechanically removed, leaving the tunica submucosa and basilar portions of the tunica mucosa. To produce ECM with differing amounts of remnant cellular material, three different chemical treatments were performed on the tissue. In rank order of most to least decellularization, the SIS material was treated with: (1) 0.1% peracetic acid (PAA) for two hours with mechanical agitation and subsequent 15 min washes with phosphate buffered saline (PBS), deionized water, PBS, and deionized water; (2) As above, but with the PAA treatment limited to 1hr; or<sup>37</sup> PBS for two hours followed by subsequent 15 min washes with PBS, deionized water, PBS, and deionized water. For *in vivo* studies the prepared ECM was vacuum pressed to form a 4-layer laminate. *In vitro* assays were performed on single layer sheets of SIS-ECM. All devices were lyophilized and sterilized using ethylene oxide.

**A.3.2 Histologic assessment of decellularization:** Representative samples of SIS with each amount of decellularization were fixed in 10% neutral buffered formalin and embedded in paraffin. Sections were cut at 5 $\mu$ m thickness and stained with hematoxylin and eosin (H&E) and 4', 6-diamidino-2-phenylindole (DAPI) to identify the presence of any residual intact nuclei within the tissue samples.

**A.3.3 Quantification of DNA content:** DNA was extracted from representative samples of SIS prepared by each of the three decellularization protocols. One hundred mg of lyophilized, powdered SIS-ECM was digested with proteinase K digestion buffer [100 mM NaCl, 10 mM Tris-HCl (pH=8), 25 mM EDTA (pH=8), 0.5% SDS, 0.1 mg/mL proteinase K] at 50°C for 24 hours. The digest was extracted twice using 25:24:1 (v/v/v) phenol/chloroform/isoamyl alcohol. DNA was precipitated from the aqueous phase at -20°C with the addition of 2 volumes of ethanol and 0.1 volume of 3M sodium acetate (pH=5.2). The DNA was then centrifuged at 10,000 g for 10 minutes and resuspended in 1mL of TE buffer [10mM Tris (pH=8), 1mM EDTA].

The concentration of each extracted DNA sample was determined using Quant-iT PicoGreen dsDNA Assay Kit (Invitrogen #P7589) using the manufacturer's recommended protocol. A standard curve was constructed by preparing samples of known DNA concentrations from 0-1000 ng/mL. Samples were read using SpectraMax M2 Plate Reader. DNA samples were diluted to ensure their absorbencies that fell into the linear region of the standard curve.

To determine DNA fragment size, equal concentrations of extracted DNA from each sample were separated on a 2% agarose gel containing 0.5% ethidium bromide and visualized with ultraviolet transillumination using a reference 100bp ladder (New England BioLabs). All assays were performed in triplicate. A quantitative comparison of the specimens prepared by the three different decellularization methods was then completed using recently established guidelines <sup>175</sup>.

**A.3.4 In-vitro culture of macrophages on SIS-ECM devices:** Characterization of the macrophage response to devices with varying amounts of cell remnants was performed by *in-vitro* culture of mouse monocyte macrophage cells (RAW 264.7 from ATCC) on single layer

sheets of SIS-ECM prepared using the three described methods of decellularization. Cells were maintained in Dulbecco's Modified Eagle Medium (DMEM Invitrogen) supplemented with 20% fetal bovine serum (FBS, Hyclone), 2mM -glutamine (Invitrogen), 100 units/ml penicillin, 100 µg/ml streptomycin (Invitrogen) at 37°C in a humidified atmosphere with 5% CO<sub>2</sub>.

At confluency, the cells were passaged and seeded onto 1.5 cm × 1.5 cm sheets of lyophilized SIS-ECM at a density of 1×10<sup>6</sup> cells/scaffold in 12-well plates (N=4 per scaffold type). At 4 days post-seeding, the scaffolds were fixed with 4% paraformaldehyde and snap frozen in OCT embedding media for frozen sectioning.

**A.3.5 In-vivo macrophage response to SIS-ECM scaffolds:** All procedures were performed in accordance with the National Institute of Health (NIH) guidelines for care and use of laboratory animals, and with approval of the Institutional Animal Care and Use Committee (IACUC) at the University of Pittsburgh. Twelve adult female Sprague–Dawley rats weighing approximately 300 g (Charles River Laboratory, Wilmington, MA) were randomly assigned to 3 separate groups (N=4/group) based on scaffold type: (1) acellular (2hr PAA) (2) partially decellularized (1hr PAA) and <sup>37</sup> cellular (PBS). A partial thickness abdominal wall defect model <sup>406,407</sup> was used to evaluate the host response to each scaffold type.

Each animal was anesthetized by inhalation with 2% isoflurane in oxygen, and the ventral abdominal wall was prepared for sterile surgery. A ventral midline abdominal skin incision was created, and the skin and subcutaneous tissue were separated from the underlying muscle tissues on one side of the midline. A 1cm × 1cm section of the external and internal oblique muscles on the ventral lateral abdominal wall was excised leaving the underlying transversalis fascia and peritoneum intact. The defect was repaired with a size-matched piece of the chosen test scaffold. A single 4–0 Prolene suture was placed at each of the four corners

of the test article to secure the device to the surrounding musculature, allow for mechanical loading of the test article during the normal abdominal wall activity of daily living, and to demarcate the implant for identification at the time of necropsy. A subcuticular placement of 4–0 Vicryl suture was used to close the skin incision. Each animal was recovered from anesthesia and was returned to the housing unit. Each animal was housed individually in shoebox cages. The rats were fed a diet of Purina Isopro rodent chow ad libitum (LabDiet ProLab Isopro RMH 3000, PMI Nutrition International, St. Louis, MO). The housing environment was maintained at 68° to 76 °C for 24 h a day and with a light:dark cycle of 12:12 h. Each rat received 0.02 mg Buprenex (buprenorphine hydrochloride) by subcutaneous injection the day of surgery and for two additional days. Baytril (20 mg) was given orally the day of surgery and for two additional days. The dietary habits, general health status, and the surgical site were monitored daily and recorded.

Animals were sacrificed at 14 post surgery. Each rat was euthanized with 5% isoflurane in oxygen followed by an intracardiac injection of 5 mL of potassium chloride to induce cardiac arrest. The implant site, including the surrounding native abdominal wall tissue was excised, mounted on a fixed support structure to maintain the size and shape of the *in situ* tissue, and placed in 10% neutral buffered formalin (NBF). The sections were then processed for routine paraffin sectioning.

#### A.3.6 Immunolabeling

Immunolabeling of both *in vitro* and *in vivo* tissue samples was performed on 5 µm sections. Frozen sections were fixed in ice cold 50:50 acetone: methanol (v/v) for 5 minutes and rinsed 3 times in PBS. Paraffin embedded sections were deparaffinized with xylene and rehydrated

through a graded ethanol series. Heat-mediated antigen retrieval was performed with 0.1 mM EDTA buffer at 95–100 °C for 25 min.

The tissue sections were subjected to Tris-Buffered Saline Tween-20 (TBST) for 15 minutes, followed by incubation in blocking buffer (1% bovine serum albumin/0.05% Tween-20/0.05% Triton X-100) for 1 hour. The primary antibodies, diluted in blocking buffer, were added to the slides for 16 hours at 4°C in a humidified chamber. The slides were then washed three times in PBS prior to the addition of the secondary antibody for 1 hour in a humidified chamber at room temperature. The primary antibodies used in this study were Alexa Fluor® 488 anti-mouse CD206 (1:50, BioLegend #123008), goat polyclonal CD206 (Santa Cruz Biotech), rabbit monoclonal CCR7 (1:100, Epitomics #2059-1) and mouse anti-rat CD68 (1:50, Serotec). The secondary antibodies used were Alexa Fluor® goat anti-rabbit 568 (Invitrogen), Alexa Fluor® donkey anti-goat 488 (Invitrogen) and Alexa Fluor® donkey anti-mouse 350 (Invitrogen). CD68 is a pan-macrophage marker. CCR7 is an M1 marker. CD206 is an M2 marker. For *in vitro* studies, 4',6-diamidino-2-phenylindole (DAPI) was used as a nuclear counterstain. For *in vivo* studies, Draq5 (Cell Signaling Technologies) was used as a nuclear counterstain by the manufacturers recommended protocol. All primary antibodies were confirmed to cross-react with either mouse or rat epitopes.

**A.3.7 Quantification of M1/M2 macrophage staining:** All tissue sections were imaged using a Zeiss Axiovert Z1 microscope with appropriate brightfield and fluorescent filter sets. For analysis of *in vitro* macrophage polarization, 5 x320 magnification fields of view per scaffold were obtained at random intervals along the length of the scaffold. For analysis of *in vivo* macrophage polarization, 10 random x320 magnification fields of view were obtained which spanned the area between the anastomoses with the native tissue.

Quantification of M1/M2 polarization was achieved using a custom image analysis pipeline developed using the cell profiler image analysis package<sup>309,411</sup>. This custom pipeline identified and quantified the number of CD68+CCR7+ (M1 phenotype) and CD68+CD206+ (M2 phenotype) cells present within the tissue sections. These numbers were then expressed as a ratio of M1/M2.

**A.3.8 Statistical analysis:** Analysis of variance was used to determine statistical significance of the difference in scaffold decellularization using M1/M2 ratio. Where samples variances were found to be non-homogenous, the Kruskal-Wallis analysis was used as an alternative. The Tukey multiple comparison procedure was used to determine which pairs of decellularization methods were significantly different when a main effect was statistically significant.

#### **A.4. Results**

**A.4.1 DNA concentration and fragmentation in scaffolds:** The amount of tissue decellularization following the three preparation methods was assessed using previously established guidelines for decellularization<sup>175</sup>. Intact nuclei were visible by H&E and DAPI staining on samples prepared with PBS washing only (Figure 34A & B). No intact nuclei were seen by H&E staining on samples treated with PAA for either 1hr (Figure 34C) or 2 hrs (Fig 1E) although potential fragments of DNA were seen attached to the ECM fibers in DAPI stained samples following 1hr PAA protocol (Figure 34D). No nuclear material was seen in samples following the 2hr PAA protocol (Figure 34F).

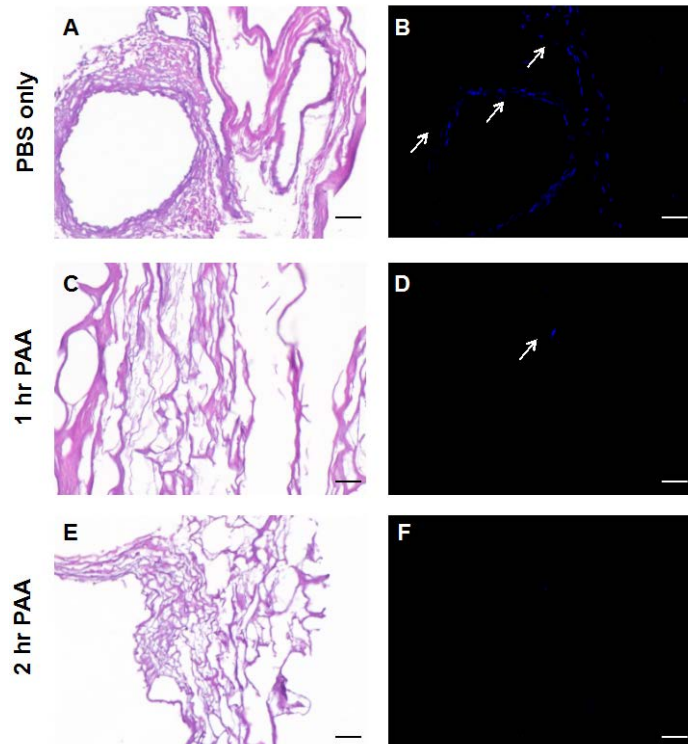


**Figure 34. Histologic images of SIS-ECM scaffolds.** Decellularization of ECM devices was assessed histologically by hematoxylin and eosin (H&E) and 4',6-diamidino-2-phenylindole (DAPI) staining. Scaffolds prepared by the PBS protocol contained intact nuclei visible by H&E and DAPI staining (A,B). No intact nuclei were seen on scaffolds prepared following the 1 hr PAA protocol and 2 hr PAA protocol by H&E staining (C,E). While no DNA fragments were seen by DAPI staining in samples following the 2 hr PAA protocol (F), small fragments were seen in scaffolds following the 1 hr PAA protocol (D).

The concentration of remaining DNA within the ECM materials was used as a measure of remaining cellular material. ECM prepared using the 1hr PAA protocol contained the greatest concentration of DNA with  $959 \pm 9.2$  ng/mg ECM. Interestingly, ECM prepared using the PBS only protocol showed a lesser concentration of DNA ( $p < 0.05$ ) with  $423 \pm 29.7$  ng /mg ECM. Both of these concentrations were greater ( $p < 0.05$ ) than those of the ECM prepared using the 2hr PAA protocol which had an average DNA concentration of  $62 \pm 16.4$  ng/mg ECM. The isolated DNA was assessed for fragment size using agarose gel electrophoresis. In samples prepared using the 1hr or 2hr PAA protocols, all residual DNA was less than 500bp in length. In

contrast, scaffolds prepared using the PBS only protocol showed the residual DNA to range from 100bp to greater than 1500bp and most likely included intact full length DNA (Figure 35).

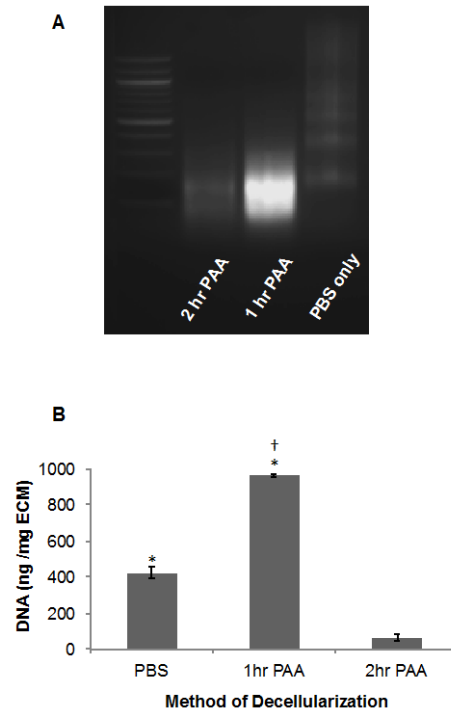


**Figure 35. Concentration of remnant DNA in ECM scaffolds.** The amount of DNA remaining in the ECM scaffolds prepared by varying methods was quantified as a marker of remaining cellular material. Dagger symbol indicates ECM prepared using the 1 hr PAA protocol contained the highest DNA concentration while, interestingly, ECM prepared using the PBS protocol showed lower levels of DNA. Asterisk indicates both of these levels were significantly higher ( $p < 0.05$ ) than ECM prepared using the 2 hr PAA protocol (B). DNA fragment length was assessed by gel electrophoresis using a reference 100bp ladder (A).

**A.4.2 In-vitro macrophage response:** The response of macrophages to the ECM scaffolds with differing amounts of residual DNA was assessed *in vitro* using the RAW 264.7 macrophage cell line. Immunolabeling for CCR7 (M1 marker) and CD206 (M2 marker) showed

a distinct pattern of macrophage polarization depending on the method of ECM preparation. On scaffolds prepared using the PBS protocol 90.3%  $\pm$  16.9% were CCR7+ (Figure 36A). On ECM prepared using the 1hr PAA protocol the phenotype of CCR7+ macrophages decreased to 55.0%  $\pm$  17.1% (Figure 36C). ECM prepared using the 2hr PAA protocol showed only 25.2%  $\pm$  15% of macrophages with a CCR7+ marker (Figure 36E). The percentage of CD206+ cells on each scaffold was 18.0%  $\pm$  9.2% (Figure 36B), 28.0%  $\pm$  15.9% (Figure 36D) and 46.0%  $\pm$  6.1% (Figure 36F) for scaffolds prepared using PBS, 1hr PAA and 2hr PAA, respectively. Since CD68+ macrophages were present on the scaffolds and some of these cells did not stain positive for surface markers indicative of polarization, it is logical that the percentage of CCR7+ and CD206+ cells does not add to 100%. Calculation of the M1/M2 ratio for each ECM showed that scaffolds prepared using the PBS protocol promoted a strong M1 polarization while scaffolds prepared using the 1hr PAA and 2hr PAA protocols had a significantly lower ( $p < 0.05$ ) M1/M2 ratio.

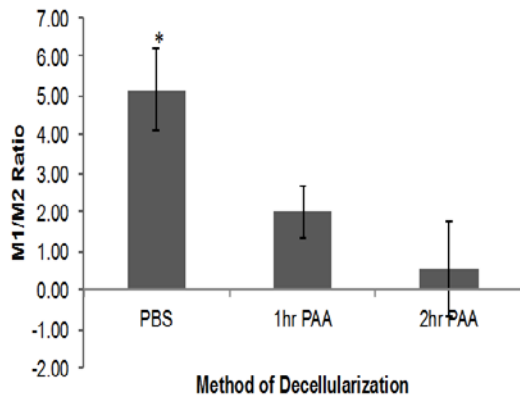
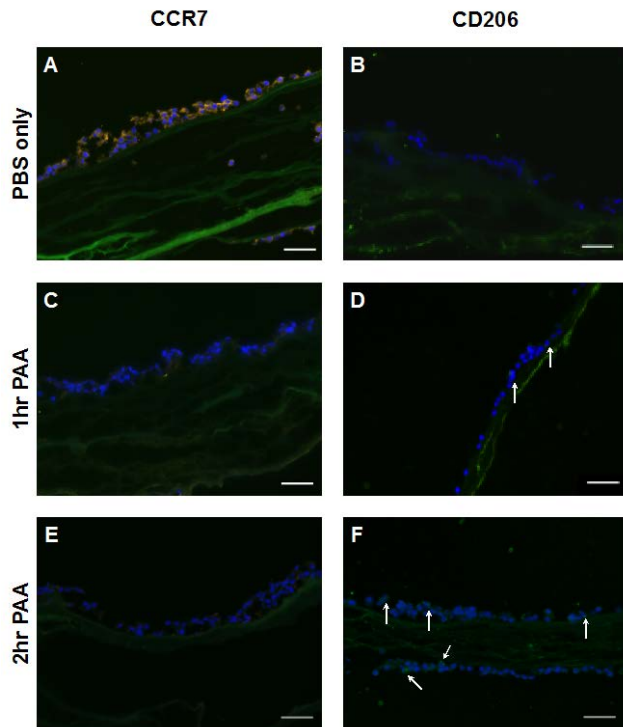


**Figure 36. Macrophage response in-vitro.** *In vitro* immunolabeling images of macrophage phenotype. The macrophage response to ECM scaffolds was assessed *in vitro* using the RAW 264.7 macrophage cell line. Immunolabeling for M1, CCR7+, macrophages (orange) and M2, CD206+, macrophages (green) showed that macrophages show distinct polarization profiles depending on the method of decellularization. On scaffolds prepared following the PBS and 1hr PAA protocols, macrophages showed high levels of CCR7+ staining (A, C) and lower levels of CD206+ staining (B, D). However, macrophages responded with a predominant M2 phenotype on scaffolds prepared using the 2hr PAA protocol with high levels of CD206+ staining (F) and little CCR7+ staining (E). Arrows indicate positive staining and scale bars= 50  $\mu$ m.

**A.4.3 Macrophage response In-vivo:** Four-layer multilaminar scaffolds prepared with sheets of ECM from each of the decellularization protocols were implanted for 14 days in the rat partial thickness abdominal wall defect model. All of the animals survived the surgical procedure and post-operative period without complications. The host response to the implanted scaffolds was assessed by macroscopic examination and by both qualitative and quantitative histologic methods. Macrophage phenotype was characterized by immunolabeling methods. All scaffolds showed a robust macrophage presence although there were distinct differences in the density and distribution M1 vs. M2 phenotype dependent upon the decellularization method. CD68+ macrophages were present within the wound site, some of which did not stain positive for either M1 or M2 surface markers. These macrophages may have just arrived at the site and not yet express polarization towards an M1 or M2 phenotype. Macrophages that have not been polarized would not show markers indicative of polarization (i.e., CCR7 or CD206). Therefore it is logical that the percentages of CCR7+ and CD206+ cells would not equal 100%.

**A.4.3.1 Macrophage response to PBS-treated scaffolds:** Devices prepared using the PBS protocol showed the highest density of mononuclear cell infiltration. Macroscopically the implant sites all showed swelling and seroma formation that were not present in either the 1hr PAA or 2hr PAA treated scaffolds. The mononuclear cells formed dense accumulations particularly within the middle of the implant site (Figure 37A-B). A strong angiogenic response was present with large numbers of blood vessels present within the implant site. The device was clearly distinguishable and mononuclear cells surrounded the scaffold fibers in a dense layer. Immunolabeling studies showed that these scaffolds had the highest value for concentration of macrophages with the mean of  $455 \pm 82.7$  CD68+ cells per field of view. However, this value was not statistically different from the 1hr PAA or 2hr PAA treated scaffolds. The M1 macrophage phenotype predominated in a cell layer immediately surrounding the ECM scaffold

(Figure 37C), and M2 cells were mainly located near the anastomoses with the native tissue and in areas of remodeling peripheral to the ECM scaffold. Quantitative analysis of macrophage phenotype showed that the percentages of M1 and M2 over the entire implant site (scaffold plus adjacent tissue) were similar with  $53.7 \pm 9.6\%$  and  $57.4\% \pm 6.6\%$  respectively. As a result, the M1/M2 ratio slightly favored the M2 phenotype with a ratio of  $0.93 \pm 0.17:1$ .

**A.4.3.2 Macrophage response to 1hr PAA treated scaffolds:** Devices prepared using the 1hr PAA protocol showed an intense mononuclear cell response at 14 days. Macroscopically, there was a slight swelling at the implant site but no sign of seroma formation. Small and scattered remnants of the ECM device were visible and mononuclear cells were distributed more evenly throughout the individual layers of the multi-laminate device than was observed in the PBS only treated samples. A robust angiogenic response was present and there was abundant neomatrix deposition (Figure 37D-E). Immunolabeling studies showed large numbers of CD68+ macrophages throughout the scaffold with an average of  $395.4 \pm 83.9$  CD68+ cells per field. The macrophages surrounding the scaffold fibers predominately expressed the M1 marker CCR7. However, some CD206+ M2 macrophages were also observed immediately adjacent to the scaffold and the distribution of M2 cells was more uniform than was observed in the PBS treated scaffold (Figure 37F). Quantitative analysis of polarized macrophages over the entire implant site showed that M1 macrophage percentage was similar to that found in the PBS only treated devices with  $56.3\% \pm 16.0\%$  CCR7+ and  $65.0\% \pm 7.6\%$  CD206+ with a M1/M2 ratio of  $1.02 \pm 0.23:1$ .

**A.4.3.3 Macrophage response to 2hr PAA treated scaffolds:** Devices prepared using the 2hr PAA protocol showed a strong mononuclear cell response at 14 days. Macroscopically there was no sign of swelling or seroma. Histologic examination showed mononuclear cells present throughout the scaffold and between layers of the multi-laminate device similar to the 1hr PAA treatment (Figure 37G-H). Remnants of the device were still visible along with deposition of a neomatrix and a strong angiogenic response. Immunolabeling studies showed that these scaffolds had similar numbers of macrophages to the 1hr PAA scaffolds with an average of  $407 \pm 100.7$  CD68+ cells per field. The spatial distribution of polarized macrophages showed that M1 macrophages were still the predominant phenotype immediately adjacent to the scaffold fibers. However, M2 macrophages were more evenly distributed throughout the implant site rather than being limited to the periphery of the implant site as was seen with the PBS treated scaffolds (Figure 37I). Quantitative analysis of M1 and M2 phenotype showed no difference to either the PBS or 1hr PAA treated scaffolds with an average  $53.7\% \pm 15.8\%$  of macrophages expressing the M1 marker and  $61.2\% \pm 7.6\%$  of macrophages expressing the M2 marker. Overall the M1/M2 ratio slightly favored the M2 phenotype with a ratio of  $0.87 \pm 0.22:1$  although this value was not significantly different to the values for either the 1hr PAA or PBS only treated scaffolds (Figure 37J).

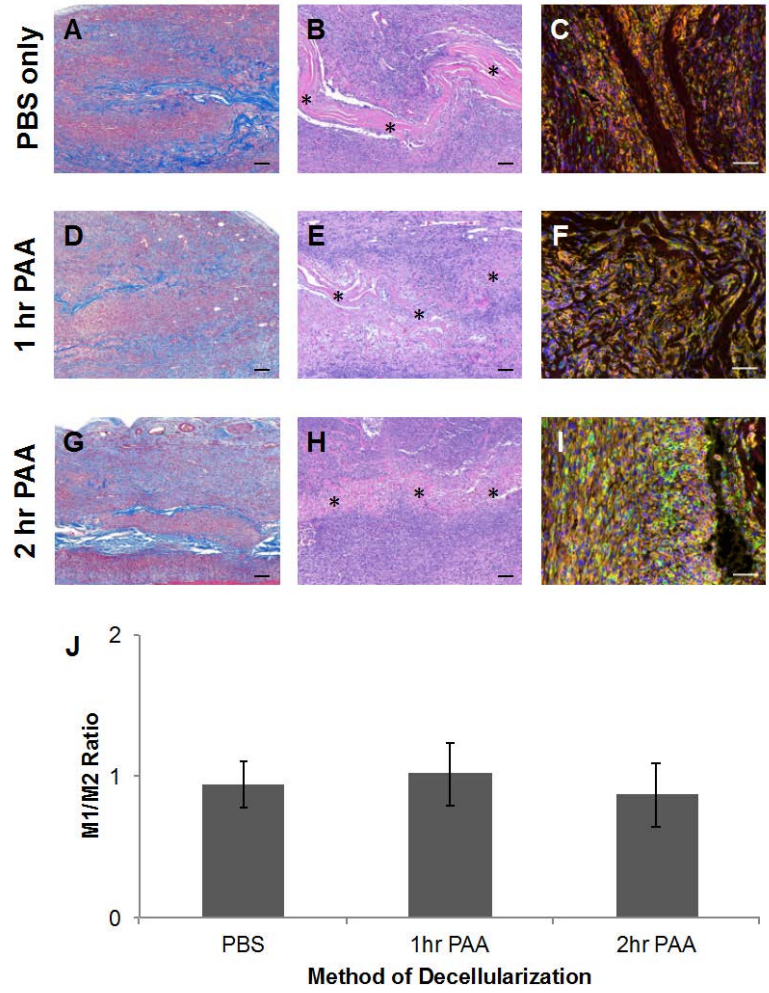


**Figure 37. Histologic and immunolabeling images of the tissue surrounding implant site at 14 weeks post-surgery.** The *in vivo* host response to scaffolds prepared using varying methods of decellularization was assessed histologically with Masson's Trichrome and hematoxylin and eosin (H&E) staining and by the immunolabeling of macrophages. Devices prepared using the PBS protocol (A-C) showed the highest levels of mononuclear cell infiltration with M1 cells (orange) predominating in a layer surrounding the ECM scaffold, while M2 cells were mainly located toward the anastomoses and in areas surrounding the ECM scaffold. Devices prepared using the 1hr PAA protocol (D-F) showed a similar distribution of macrophages, however, some M2 cells were observed surrounding the scaffold and the M2 cell distribution was more even than the PBS treated scaffold. Characterization of the polarized macrophages in the 2hr PAA treated scaffolds (G-I) showed that while M1 macrophages still predominated around the scaffold fibers, M2 macrophages were more evenly distributed throughout the scaffold rather than being limited to the margins of the wound as seen with PBS scaffolds. Immunohistochemical staining showed the presence of macrophages (red) in all scaffolds and used DRAQ5 (blue) as a nuclear stain. Calculation of the M1/M2 ratio (J) for PBS and 2hr PAA showed the macrophage response favored M2 while 1hr PAA favored M1 slightly. However, no treatment resulted in a significantly different macrophage profile. A M1/M2 value of 1 indicates equal amounts of cells expressing CCR7 and CD206. M1/M2 ratios above 1 indicates an M1 majority and below 1 is an M2 majority. Scale bars=50  $\mu$ m, asterisks=scaffold

## A.5 Discussion

The present study is the first attempt to determine the association between decellularization efficacy and host response by qualitative and quantitative methods. Quantitative criteria of decellularization have not been described until recently<sup>175</sup>. The presence of xenogeneic DNA within biologic scaffold materials has been suggested as a possible cause of an “inflammatory response”<sup>392</sup> in patients. Indeed, many commercial biologic scaffolds contain varying amounts of remnant DNA<sup>398,412</sup>. This remnant DNA is typically present as small fragments less than 300 bp in length<sup>398</sup>, and it is therefore unlikely to play any substantive role in an adverse tissue remodeling response. However, the question remains as to whether there is a threshold level of cellular “debris” that will elicit an adverse remodeling outcome.

The negative effects of the presence of intact allogeneic or xenogeneic cells within a biologic scaffold are widely recognized; therefore, it is logical that the effective removal of antigenic epitopes and intracellular components of source tissues and organs is necessary to minimize an adverse immune response by recipients of an ECM scaffold device. It has been shown that the presence of cells within a scaffold is associated with increased amounts of pro-inflammatory cytokines, increased macrophage M1 polarization, and a poor remodeling outcome in a primate model<sup>413</sup>. Previous studies have shown that the implantation of a xenogeneic ECM scaffold containing a cellular component results in the classic cascade of inflammatory processes with mononuclear cell infiltration, including macrophages predominantly of an M1 phenotype at 3 days post implantation, with eventual scar tissue formation<sup>133</sup>. Furthermore, when the same scaffold materials are prepared by methods that remove the

cellular component, the mononuclear cell response is marked by macrophages primarily of an M2 phenotype<sup>133</sup>.

The current chapter used DNA content as a quantitative marker of cellular remnants. The decellularization protocols developed resulted in three distinct levels of decellularization; one which retained intact cells and full length DNA, one with large amounts of small fragment DNA, and one that contained small amounts of small fragment DNA. While all three protocols were effective at removing or lysing intact cells and cellular material with only 1 or 2 isolated nuclei detected per field, even with in the PBS alone protocol, the aggressiveness of the decellularization process had a marked *in vitro* effect on macrophage polarization and was associated with a more favorable macroscopic host tissue response *in vivo*, including less swelling and absence of seroma formation. While ECM treated with the 1hr PAA protocol contained a greater amount of DNA compared to the PBS treated ECM, more M2 macrophage polarization was seen suggesting that DNA content alone is not the sole determinant of the host response. This study also demonstrated that PAA treatment, rather than mechanical agitation, is the key factor in the dissociation of DNA and most likely other cellular components from the remaining ECM. The dissociated cell remnants can then be effectively removed by the mechanical agitation process. It is important to note that DNA was used in this study as an indicator of the presence of cell remnants and it is almost certain that other cell components capable of causing an adverse response are retained in the scaffold through the process of decellularization. For example, mitochondria are known to release damage associated molecular patterns (DAMPs) that promote a pro-inflammatory response<sup>262</sup>. It is unknown if DNA quantification is the best indicator, or even a good indicator, of “decellularization” but alternative sensitive and quantitative methods of assessing the presence of cell remnants were not available or used in this study. The results of the present study clearly show that less complete removal of the cell remnants and increased DNA fragment size are associated with a

more proinflammatory macrophage phenotype *in vitro* and that more thorough removal of cell remnants and effective fragmentation of cellular material are associated with a more liberal and widespread distribution of the constructive M2 phenotype.

Analysis of the macrophage response to these biological scaffold materials *in vitro* examined the response of macrophages at a relatively early time point. The devices containing significantly more cellular material, prepared by the PBS only and 1hr PAA protocol, showed a predominantly M1 macrophage response while the device containing less amounts of DNA, prepared using the 2hr PAA protocol, resulted in a macrophage response predominantly of an M2 phenotype. This data supports the findings of previous studies using an *in vivo* model where a cellular scaffold promoted a clear M1 phenotype macrophage response at 3 days whereas the equivalent acellular scaffold promoted a strong M2 phenotype<sup>133</sup>. Rieder et al have shown that decellularization can reduce the chemotactic potential of heart valve tissue for macrophages but does not inhibit the activation of macrophages although they did not study macrophage polarization<sup>414</sup>. In addition, Ariganello et al. have shown that *in vitro* exposure of a macrophage cell line to decellularized tissue elicited lower esterase and phosphatase activity consistent with a subdued inflammatory response comparable to the M2 phenotype observed in the present study<sup>415</sup>.

Interestingly, the significant differences seen with the *in vitro* assays were not quantitatively apparent when the macrophage response *in vivo* was evaluated 14 days after implantation. All the scaffold materials elicited a mixed macrophage response with no significant differences observed in total number of macrophages or M1/M2 ratio. The notable and perhaps more important differences were found in the distribution of macrophages within the various scaffolds. Scaffolds treated with only PBS contained dense accumulations of M1 cells within the scaffolds and especially at the scaffold interface with native tissue whereas the M2 macrophages were mainly located peripheral to the ECM scaffold. As the method for

decellularization became more aggressive, M1 macrophages still were the dominant phenotype immediately adjacent to the scaffold fibers but the distribution of M2 cells became more uniformly and widely distributed throughout the implant site. It is unknown whether certain regions, such as the interface between the ECM implant and the native tissue, are a more important determinant of downstream tissue remodeling outcomes than regions more peripheral to the implant. In addition, macrophage phenotype may not be a strong indicator of remodeling outcomes at all time points and it may be necessary to examine macrophage phenotypes only at early times after surgery to predict the remodeling outcome.

There were several limitations in the present study. Only 1 time point, 14 days after implantation, was examined because it has been shown to be a useful time point in previous studies with this model <sup>90,133,416</sup>. Another limitation was that macrophage phenotype was determined solely upon cell surface markers. The present study used CCR7 and CD206 as markers of M1 and M2 macrophages respectively. Neither is specific for macrophages alone and co-staining with CD68 was used to identify polarized macrophages. However, the polarized macrophages can be subdivided into a number of subgroups <sup>400</sup> and these subgroups may not have been accurately counted using just two markers. A more complete picture of macrophage phenotype may have been provided by concomitant cytokine analysis. Finally, any systemic effect of the ECM scaffolds was not accessed and only the local tissue response was evaluated. Circulating DNA has been associated with clinical signs of sepsis <sup>417</sup>, may be the cause of a sepsis-like systemic response <sup>418</sup>, and is present in patients with chronic inflammatory diseases <sup>419</sup>. Although there are limitations, this study represents the first systematic effort to determine the relationship between decellularization efficacy and host response to the implantation of a biologic scaffold material.

## **A.6 Conclusion**

The results of this chapter show that decellularization efficacy of biologic scaffold materials is at least one determinant of the macrophage phenotype response. Although a cause-effect relationship between macrophage phenotype and remodeling outcome has not been definitely shown, a clear association exists. Effective decellularization remains an important component in the production of ECM-based scaffolds for therapeutic applications.

## **A.7 Acknowledgement**

Funding for this study was provided through a grant from the National Institutes of Health (R01 AR054940).

## APPENDIX B

### THE EFFECT OF TERMINAL STERILIZATION ON THE MATERIAL PROPERTIES AND IN-VIVO REMODELING OF A PORCINE DERMAL BIOLOGIC SCAFFOLD

#### *B.1* Abstract

The Food and Drug Administration typically regulates biologic scaffolds as medical devices, thus requiring terminal sterilization prior to clinical use. The objective of the present study was to characterize the effect of sterilization on the material properties and the host remodeling response of a porcine dermal biologic scaffold. Outcome measures included biochemical, structural, and mechanical properties as well as cytocompatibility in vitro. The host response to each experimental group was determined by quantitative histologic methods and by immunolabeling studies. Results showed that increasing irradiation dosage resulted in changes in the collagen fiber architecture and a dose dependent decrease in mechanical properties compared to untreated controls. Ethylene oxide-treated porcine dermal ECM resulted in decreased DNA content and bFGF content compared to untreated controls. All ETO treated, gamma irradiated, and e-beam irradiated samples had similar cytocompatibility scores

in-vitro. In-vivo results showed an increased rate of degradation of the biologic scaffold material following 14 and 35 days in the high dose irradiated samples compared to the other groups.

## **B.2 Introduction**

Biologic scaffolds composed of extracellular matrix (ECM) are commonly used in a variety of surgical applications to reinforce soft tissue, particularly in the abdominal wall and pelvic floor and in reconstructive breast surgery<sup>420</sup>. ECM scaffolds are produced by decellularization of source mammalian tissues and organs, including small intestine, urinary bladder, and dermis, among others. Over the last decade, a wide array of manufacturing protocols have been described for ECM scaffold materials, each of which vary widely in their use of chemical, enzymatic, and/or physical methods of decellularization. While it is inevitable that all processing methods used to prepare biologic scaffold materials will adversely affect the mechanical, biochemical, and cell signaling properties of the resulting ECM to some degree, the preferred methods will mitigate these effects as much as possible. Preservation of native ECM composition and ultrastructure in biologic scaffolds has been shown to facilitate beneficial constructive remodeling outcomes<sup>175</sup>. Specifically, the host response to biologic scaffold materials has been shown to be directly related to the efficacy of decellularization<sup>138</sup>. These findings have led to the proposal of standard criteria for defining effective decellularization<sup>175</sup>. While much progress has been made to this end, relatively little has been studied regarding preferred methods of terminal sterilization.

The Food and Drug Administration (FDA) regulates biologic scaffolds derived from xenogeneic source tissue, including materials derived from decellularized porcine dermis, as medical devices; thus requiring these products to be terminally sterilized prior to clinical use. Common methods of terminal sterilization include electron beam (e-beam) and gamma ( $\gamma$ )

irradiation and ethylene oxide (ETO) <sup>421</sup>. While it is known that each method exerts its sterilizing effect by modifying the structure or function of the critical components (e.g. proteins and nucleic acids) of target microorganisms and has directed guidelines regarding bacterial load (e.g., ISO/DIS 11135-1, ISO/DIS 11137-3), each method also has the potential to alter material properties of the ECM, including mechanics, susceptibility to degradation, biocompatibility, and ultimately the elicited *in vivo* remodeling response <sup>422</sup>. In contrast to the aforementioned decellularization criteria, currently no consensus exists for the most effective yet minimally destructive sterilization protocol for any biologic scaffold material. The objective of the present study was to characterize the effect of several types and doses of terminal sterilization on the material properties and elicited *in vivo* remodeling response of a biologic scaffold material derived from porcine dermis.

### **B.3 Methods**

**B.3.1 Experimental Design:** The effect of terminal sterilization on a porcine dermal biologic scaffold was examined using *in vitro* and *in vivo* test systems. Porcine dermal ECM scaffold materials were exposed to one of three terminal sterilization methods – ETO,  $\gamma$ -irradiation, and e-beam irradiation. The  $\gamma$ -irradiation and e-beam irradiation groups were further subdivided into three dosage levels – 10, 25, and 40 kGy. Two non-sterilized control groups (non-sterilized porcine dermal ECM and non-sterilized intact porcine dermis) were also evaluated. All materials were evaluated for biochemical (DNA, sulfated glycosaminoglycan, & bFGF content), structural (scanning electron microscopy), and mechanical (thickness, porosity index, ball burst, suture retention) properties as well as cytocompatibility with human microvascular endothelial cells (HMEC-1). In the *in vivo* experiments, a rodent 1.5 cm x 1.5 cm bilateral partial thickness

abdominal wall defect model was used to examine the host response to the materials following 7, 14, or 35 days (n=4 / group / time point). The host response to each experimental group was determined by quantitative histologic methods and by immunolabeling for macrophage polarization (M1/M2) within explanted specimens.

**B.3.2 Preparation and Sterilization of Dermal ECM Scaffolds:** Porcine full thickness skin from the dorsolateral flank of market weight pigs was harvested and processed immediately after euthanasia as previously described<sup>142</sup>. All full thickness skin sheets were cut into 35-cm × 50-cm rectangles. All samples were then mechanically delaminated to remove subcutaneous fat, excess connective tissue and the epidermis. The harvested sheets of porcine dermis were immediately frozen at -80 °C. Porcine dermis sheets designated to be treated with decellularization protocols were removed from the freezer and cut into sections measuring 3–7 cm × 3–7 cm. Dermis sections were decellularized as described previously<sup>142</sup>. Briefly, dermis was treated on a vortex shaker at 300 RPM at room temperature in the following solutions: 0.25% trypsin for 6 h, 1x; deionized water, 15 min, 3x; 70% ethanol, 10–12 h, 1x; 3% H<sub>2</sub>O<sub>2</sub>, 15 min, 1x, deionized water, 15 min, 2x; 1% Triton X-100 in 0.26% EDTA/0.69% Tris, 6 h, 1x and then overnight, 1x; deionized water, 15 min, 3x; 0.1% peracetic acid/4% ethanol, 2 h, 1x; PBS, 15 min, 2x; and finally deionized water, 15 min, 2x. Following decellularization, all dermal ECM sheets were lyophilized. Lyophilized dermal sheets were sterilized with ETO gas (16 h cycle at 50 °C in a Series 3plus EOGas Sterilizer, Anderson Sterilizers, Inc., Haw River, NC), γ-10 kGy, γ-25 kGy, γ-45 kGy, e-beam 10 kGy, e-beam 25 kGy, or e-beam 45 kGy.

**B.3.3 Assessment of Cellular Content:** Decellularization efficacy of dermis samples was assessed by three previously published criteria: (1) the absence of visible nuclear material on hematoxylin and eosin (H&E) stained and 40,6-diamidino-2-phenylindole (DAPI) stained sections;

(2) a Quant-iT Pico-Green assay (Invitrogen, Carlsbad, CA) for quantification of double-stranded DNA; and (3) evaluation of a 2% agarose gel to determine the size of remaining DNA fragments

175.

**B.3.4 Measuring DNA content:** Scaffolds were digested in 0.6% proteinase K solution for at least 24 h at 50°C, until no visible tissue remained. Phenol/chloroform/isoamyl alcohol was added, and samples were centrifuged at 10,000g for 10 min at 4°C. The top aqueous phase containing the DNA was transferred into a new tube. Sodium acetate and ethanol was added to each sample, and the solution was mixed and placed at -80°C overnight. While still frozen, the samples were centrifuged at 4°C for 10 min at 10,000g. The supernatant was discarded, and all residual alcohol was removed. The pellet was suspended in TE (10 mM Tris / 1 mM EDTA) buffer. Double stranded DNA was quantified using Quant-iT PicoGreen Reagent (Invitrogen Corp., Carlsbad, CA) according to the manufacturer's instructions. The dsDNA assay was performed twice (n=2) with two technical replicates per assay.

**B.3.5 DNA Fragmentation Analysis:** To determine the fragment size of remnant DNA, equal concentrations of extracted DNA from each sample were separated on a 2% agarose gel containing 0.5% ethidium bromide and visualized with ultraviolet transillumination using a reference 100-bp ladder (New England BioLabs, Ipswich, MA).

**B.3.6 Sulfated Glycosaminoglycan Assay:** Sulfated glycosaminoglycan concentrations of porcine dermis samples were determined using the Blyscan Sulfated Glycosaminoglycan Assay Kit (Biocolor Ltd., Carrickfergus, Co Antrim, United Kingdom). Samples were prepared by digestion of 50 mg/ml dry weight of each sample with 0.1 mg/ml proteinase K in buffer (10 mM Tris-HCl, pH 8, 100 mM NaCl, 25 mM EDTA) for 48 h at 50 °C. Digested samples were assayed

following the manufacturer's protocol, and the assay was performed in duplicate on three different samples.

**B.3.7 Growth Factor Quantification:** Three hundred (300) mg of ECM powder was suspended in 4.5 ml of urea–heparin extraction buffer. The extraction buffer consisted of 2 M urea and 5 mg/ml heparin in 50 mM Tris with protease inhibitors (1 mM phenylmethylsulfonyl fluoride, 5 mM benzamidine and 10 mM N-ethylmaleimide) at pH 7.4. The extraction mixture was rocked at 4°C for 24 h and then centrifuged at 3000g for 30 min at 4°C. Supernatants were collected, and 4.5 ml of freshly prepared urea–heparin extraction buffer was added to each pellet. Pellets with extraction buffer were again rocked at 4°C for 24 h, centrifuged at 3000g for 30 min at 4°C, and supernatants were collected. Supernatants from first and second extractions were dialyzed against Barnstead filtered water (three changes, 80–100 vol. per change) in Slide-A-Lyzer Dialysis Cassettes, 3500 MWCO (Pierce, Rockford, IL). The concentration of total protein in each dialyzed extract was determined by the bicinchoninic acid (BCA) Protein Assay (Pierce, Rockford, IL), following the manufacturer's protocol, and extracts were frozen in aliquots until time of assay.

Concentrations of basic fibroblast growth factor (bFGF) in urea–heparin extracts of dermis samples were determined with the Quantikine Human FGF basic Immunoassay (R&D Systems, Minneapolis, MN). Manufacturers' instructions were followed. Assays were performed in duplicate with two biologic replicates per sample ( $n = 2$ ). The ELISA assay is cross-reactive with porcine growth factors and does not measure growth factor activity.

**B.3.8 Scanning Electron Microscopy:** Scanning electron micrographs were taken to examine ECM surface topology. Sterilized dermis samples were sputter coated with a 3.5 nm layer of gold/palladium alloy using a Sputter Coater 108 Auto (Cressington Scientific Instruments,

Watford, UK) and imaged with a JEOL JSM6330f scanning electron microscope (JEOL, Peabody, MA) according to methods established in multiple previously reported studies.

**B.3.9 Thickness Measurements of Sterilized Samples:** Each experimental samples was measured for thickness by a blinded operator applying equivalent compressive force ( $8.5 \pm 0.5$  N) to all samples. Thickness after rehydration was measured by subjecting the specimens to lyophilization and then fully rehydrating the samples by soaking for at least 48 h before measurement by the same operator in the same fashion. Fourteen samples were measured for each material.

**B.3.10 Porosity Index:** The hydrostatic porosity index (PI) measurement has been previously described<sup>337</sup>. Briefly, the test specimens were placed on the top orifice of the porosity testing apparatus. Distilled water was added to the upper reservoir and a hydrostatic pressure head of 120 mmHg was maintained throughout the duration of the test (3 min). To achieve this pressure head, a height of 163.2 cm was sustained between the water surface and the test specimen. A graduated cylinder was placed beneath the hydrostatic permeability testing apparatus and the clamp was released to allow passage of water to the test specimen. The clamp was closed after 3 min and the volume collected in the graduated cylinder was recorded. The test was performed with both sides of the material ( $n = 6$  for each surface). The hydrostatic PI was calculated by dividing the volume collected by the area of the porosity testing apparatus' orifice and the duration of the test and reported as mL/min/cm<sup>2</sup>.

**B.3.11 Ball-burst Testing:** The ball burst strength measurement has been previously described<sup>423</sup>. Samples from each test group were cut to a size of at least 6 cm x 6 cm and frozen at -80°C until time for testing (not more than 72 h). The specimens were rehydrated in 0.9%

sodium chloride solution for approximately 15 min. Each specimen was mounted into a ball-burst fixture within the grips to prevent slippage. The ball-burst test, a measure of strength in response to multi-axial loading was conducted in compliance with the Standard Test Method for Bursting Strength of Knitted Goods, Constant-Rate-of-Traverse (CRT) Ball-burst Test (ASTM D 3787-89). A uniaxial tensile testing machine (MTS Insight; 2 kN capacity, MTS Systems Corp., Eden Prairie, MN) was equipped with a ball-burst compression cage in which a 25.4-mm (1-inch) polished stainless steel hemisphere rod was pushed against the material at a rate of 25.4 mm/min until failure. A total of 8 specimens were tested within each group.

**B.3.12 Suture Retention Strength:** The suture retention strength (SRS) test was performed according to ANSI/AAMI VP20–1994 Guidelines for Cardiovascular Implants-Vascular Prostheses. The SRS of a material is defined as the force required to pull a suture through the full thickness of the material at a specified bite depth and a specified pull rate. A 2–0 Prolene suture with a SH taper needle was passed through a square piece of test material with a 2-mm bite depth as shown in Figure 3. The specimen was clamped at one end while the suture was tied with a square knot and the loop attached to the Instron machine (Model 3345 Single Column Materials Testing System) and pulled at a constant rate of 10 cm/min. At least two tests were performed at locations that were 1.5 cm apart on the same edge of the square piece of each test material and the maximum load was recorded. At least 12 tests were performed for each group.

**B.3.13 In-vitro Cytocompatibility:** Dermal ECM sheets from each group were cut to 2 cm diameter circles for use in cell growth studies. Human microvascular endothelial cells (HMEC-1; a gift from Francisco J Candal, Center for Disease Control and Prevention, Atlanta,

GA) were cultured in MCDB-131 medium (Sigma, St. Louis, MO) containing 10% fetal bovine serum, 2 mM L-glutamine (Sigma), 100 U/mL penicillin/ 100 µg/mL streptomycin (Sigma), and 1 µg/mL hydrocortisone (Sigma) as previously described<sup>424</sup>. Cells were grown at 37°C and 5% CO<sub>2</sub>, and media was changed every other day. After allowing the cells to propagate to sufficient numbers, test articles were briefly hydrated with sterile saline in sterile 6-well plates prior to cell seeding. Approximately one million cells were plated per test article. Test articles were seeded in quadruplicate. Cells were placed inside of stainless steel cell culture rings (inner diameter 1.3 cm) and allowed to attach to the test articles for 24 hours. Cell culture rings were removed and cell culture media was changed at 24 hours and every other day throughout experiments.

After 7 days of growth, cell culture media was removed and cells on test articles were immediately fixed in 10% Neutral Buffered Formalin for at least 18 hours. Following fixation, test articles were paraffin embedded, sectioned (5 µm), and mounted on glass slides. Slides were stained with hematoxylin and eosin (H&E) and imaged for analysis. Eight representative microscopic images (40x magnification) were captured for each test article. All images were scored by five blinded investigators using a previously described scoring system based upon cellular confluence (0 to 100%), infiltration (surface only to 100% infiltration), and phenotype (0 to 100% normal)<sup>209</sup>.

**B.3.14 Surgical Procedure and Test Article Collection:** All procedures were performed in accordance with the National Institute of Health (NIH) guidelines for care and use of laboratory animals and with approval of the Institutional Animal Care and Use Committee (IACUC) at the University of Pittsburgh. Sprague Dawley rats (female; 250–350 g) were anesthetized with 1.5–3% isoflurane and maintained at a surgical plane of anesthesia. The surgical site was shaved, disinfected with a betadine solution, and an incision was made into the ventrolateral abdominal wall. Bilateral partial thickness abdominal body wall defects were created by excision of a 1.5 cm × 1.5 cm piece of tissue comprising the internal and external oblique muscles but leaving the

transversalis muscle intact as described previously<sup>425</sup> (Figure 1A). Size matched dermal ECM scaffolds were then sutured into the defect site using nonresorbable 4-0 proline sutures at each of the 4 corners of the device. The skin was closed using 3-0 resorbable vicryl sutures.

Animals were sacrificed at 7, 14 or 35 days post implantation, and test articles were excised. Following euthanasia, the skin was gently dissected, reflected, and the entire body wall that includes the test or control article was explanted *en bloc*. The sample was then cut in half and each half immersed in 10% Neutral Buffered Formalin (NBF) for histologic analysis.

**B.3.15 Histologic Analysis of Tissue Explants:** Explanted test articles were paraffin embedded, sectioned (5  $\mu$ m), and mounted on glass slides. Slides were stained with hematoxylin and eosin (H&E) or Masson's Trichrome and imaged microscopically for analysis. Eight representative microscopic images (40x magnification) were captured for each test article across two distinct interfaces: within the center of the scaffold material and at the abdominal wall / ECM interface (Figure 38B). Five blinded investigators scored all of the images using a previously described semi-quantitative scoring system for cellularity, neovascularization, and multinucleate giant cell formation (Figure 38B)<sup>162,328</sup>.

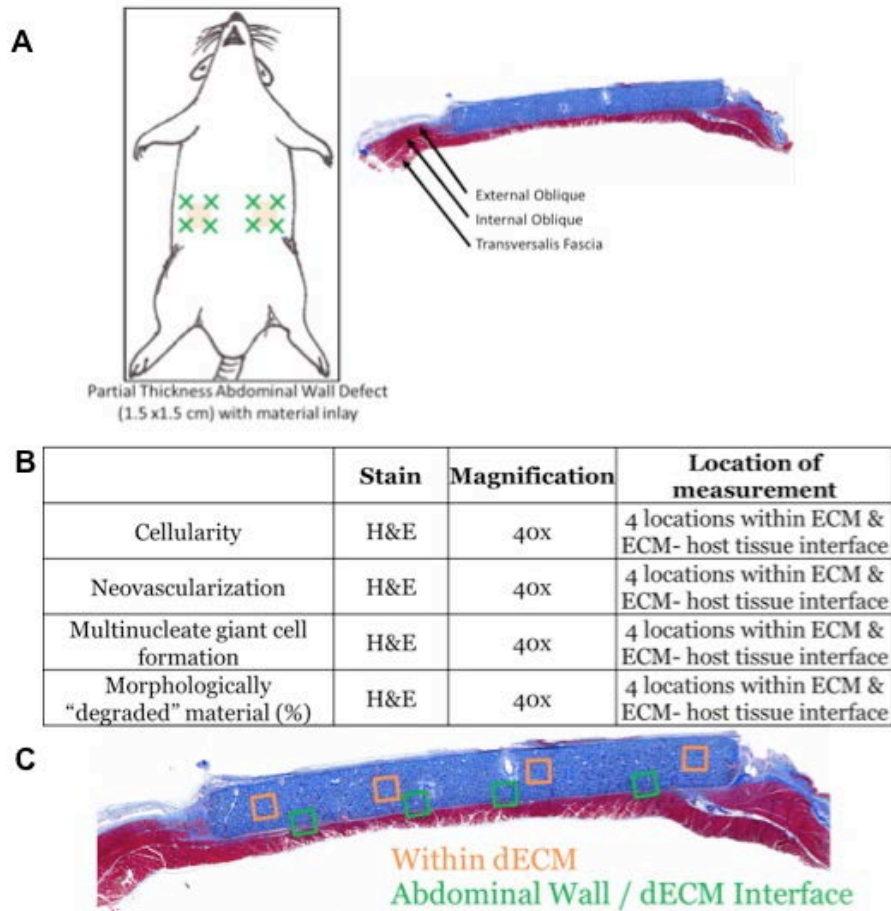


**Figure 38.** Overview of animal model and histologic evaluation schema. (A) Schematic of animal model and histologic cross section. The green “x” represents site of suture placement at corners of each device (yellow squares). The material is explanted en bloc and bisected. The histologic cross section depicts the rat abdominal wall defect, where the external and internal oblique is removed and replaced with a dermal ECM scaffold material. (B) Table describing the scoring system used to evaluate the histologic sections. (C) Schematic of histologic evaluation of explanted materials. Colored boxes represent the approximate location of 20X images used for histologic evaluation for each location.

B.3.16 **Macrophage Immunolabeling:** Immunolabeling of macrophages was performed on tissue sections from day 14 explants. Paraffin embedded sections were deparaffinized with xylene and rehydrated through a graded ethanol series. Heat-mediated antigen retrieval was performed with 0.01 M citrate buffer (pH = 6) at 95–100 °C for 25 min. The tissue sections were subjected to Tris-Buffered Saline Tween-20 (TBST) for 15 min, followed by incubation in blocking

buffer (2% horse serum albumin/1% bovine serum albumin/0.05% Tween-20/0.05% Triton X-100) for 1 h. The primary antibodies, diluted in blocking buffer, were added to the slides for 16 h at 4 °C in a humidified chamber. The slides were then washed three times in PBS prior to the addition of the secondary antibody for 1 h in a humidified chamber at room temperature. DAPI was used as a nuclear counterstain. The primary antibodies used in this study were mouse anti-rat CD68 (1:150, AbD Serotec, Raleigh, NC), goat polyclonal CD206 (Santa Cruz Biotech, Santa Cruz, CA), rabbit anti-rat CD86 (1:150, Abcam, Cambridge, MA) and mouse anti-rat CD68 (1:50, Serotec, Raleigh NC). The secondary antibodies used were Alexa Fluor® donkey anti-mouse 594 (1:200, Invitrogen), Alexa Fluor® donkey anti-goat 488 (1:200, Invitrogen) and donkey anti-rabbit IgG-PerCP-Cy5.5 (1:300, Santa Cruz Biotech, Santa Cruz, CA). CD68 is a pan-macrophage marker. CD86 is an M1 marker. CD206 is an M2 marker. All primary antibodies were confirmed to cross-react with rat epitopes. The sections were imaged at random fields along the interface of the native tissue and ECM scaffold. Quantification of M1/M2 polarization was achieved using a custom image analysis algorithm developed using the cell profiler image analysis package <sup>162</sup>. This algorithm identified and quantified the number of CD68<sup>+</sup>CD86<sup>+</sup> (M1 phenotype) and CD68<sup>+</sup>CD206<sup>+</sup> (M2 phenotype) cells present within the tissue sections. Any cells that co-expressed CD86 and CD206 were not counted. These numbers were then expressed as a ratio of M2/M1.

**B.3.17 Statistical Analysis:** Data sets were analyzed with either a one-way or a two-way analysis of variance (ANOVA) using SigmaStat 12.2 (sigma Aldrich, St. Louis, MO). The Student Newman-Keuls post-hoc test was used to locate the differences between means when the observed F ratio was statistically significant ( $p < 0.05$ ). Data are reported as mean and standard error.

## 12.2.4. Results

B.4.1 **Cellular Content:** No intact nuclei were visible by H&E (Figure 39A) or DAPI staining (Figure 39B) in the decellularized samples. All dermal samples contained less than 100 ng/mg dsDNA following decellularization (Figure 39C). The ETO sterilized samples contained  $30 \pm 10$  ng/mg which was significantly lower ( $p < 0.01$ ) than all other sterilized samples. All DNA remnants were present in fragments less than 200 bp in length (Figure 39D).

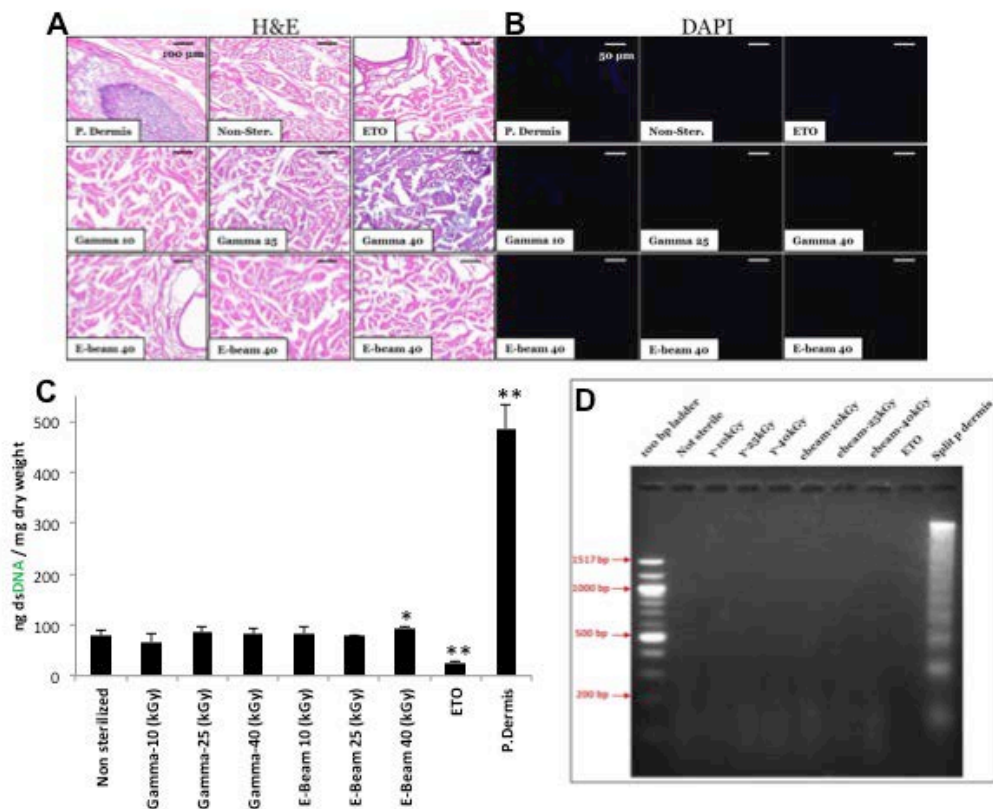


**Figure 39.** Decellularization Quantification. Cellular content of dermis samples was assessed by three previously published criteria: (1) a Quant-iT Pico-Green assay for quantification of double-stranded DNA (A); (2) evaluation of a 2% agarose gel to determine the size of remaining DNA fragments (B); [23] the absence of visible nuclear material on hematoxylin and eosin (H&E) stained (C) and 40,6-diamidino-2-phenylindole (DAPI) stained sections (D).

**B.4.2 Biochemical Properties:** The amount of urea-heparin extractable protein varied across sterilization treatments (data not shown). Extracted protein per gram of dry weight increased with increasing doses of  $\gamma$  and e-beam irradiation. ETO treated dermal ECM had the least ( $p < 0.05$ ) amount of extractable protein. The amount of bFGF in the ECM samples (Figure 40) was similar across groups with the exception of ETO, which had less ( $p < 0.01$ ) extractable bFGF than scaffolds from the other sterilization conditions. The amount of sGAGs in the test samples was equivalent to non-sterilized control values ( $405 \pm 12 \mu\text{g/g}$ ; Data not shown).

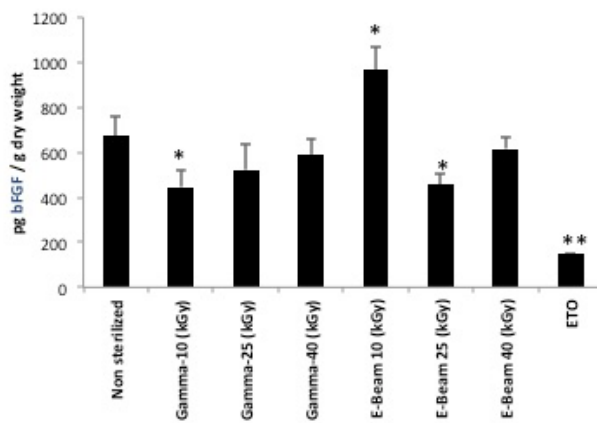


**Figure 40.** Biochemical Composition. Concentration of basic fibroblast growth factor (bFGF) in urea-heparin extracts of samples were determined with the Quantikine Human FGF basic Immunoassay (A). All results were normalized to dry weight tissue. Assays were performed in duplicate on three independent samples for each treatment group.

**B.4.3 Ultrastructural Properties:** Scanning electron micrographs show that the ECM scaffolds subjected to ETO and low dose e-beam and  $\gamma$  irradiation (i.e., 10 kGy) show similar surface topology as control samples (Figure 4). However, alterations to the dermal ECM collagen fiber ultrastructure were observed with increasing doses of  $\gamma$  and e-beam irradiation.

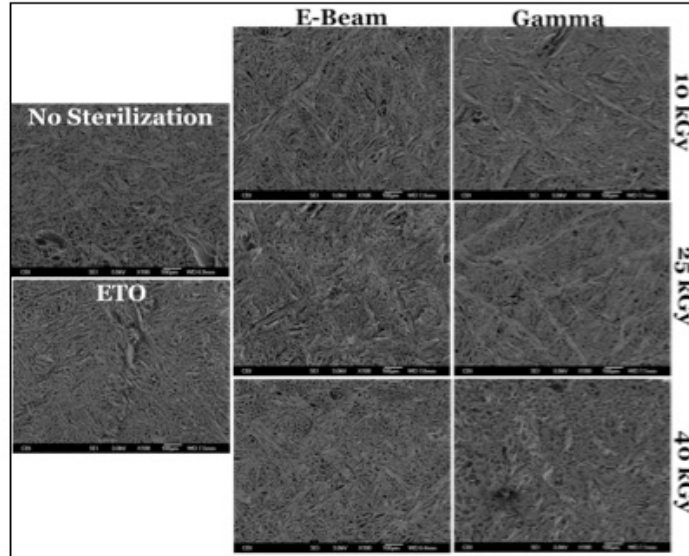


**Figure 41.** Scanning Electron Microscopy. SEM was used to examine the surface topology of each experimental group. SEM images were captured using a JEOL 6335F Field Emission SEM instrument with a backscatter detector.

**B.4.4 Mechanical Properties and Porosity:** The thickness of the scaffold was not affected by type or level of sterilization. Multiaxial strength of the test articles following ETO,  $\gamma$  and e-beam exposure was compared to controls (Figure 42). Burst strength of the ETO-treated sample was similar to that of the control, whereas there was a dose-dependent decrease ( $p < 0.01$ ) in the burst strength of scaffolds exposed to increasing dosages of irradiation (Figure 42A). Suture retention strength was not significantly altered by exposure to ETO and 10 kGy of  $\gamma$  and e-beam irradiation (Figure 42B). However, higher doses of irradiation (i.e., 25 kGy and 40 kGy) resulted in a decreased ( $p < 0.01$ ) suture retention strength compared to the control samples.

Porosity index levels trended towards a lower index level with decreasing doses of  $\gamma$  and e-beam irradiation, when compared to the non-sterilized control (Figure 42C). Gamma and e-beam at 10kGy had the lowest porosity index in their respective groups. The ETO treatment group was found to have the lowest porosity index level compared to control,  $\gamma$  and e-beam.

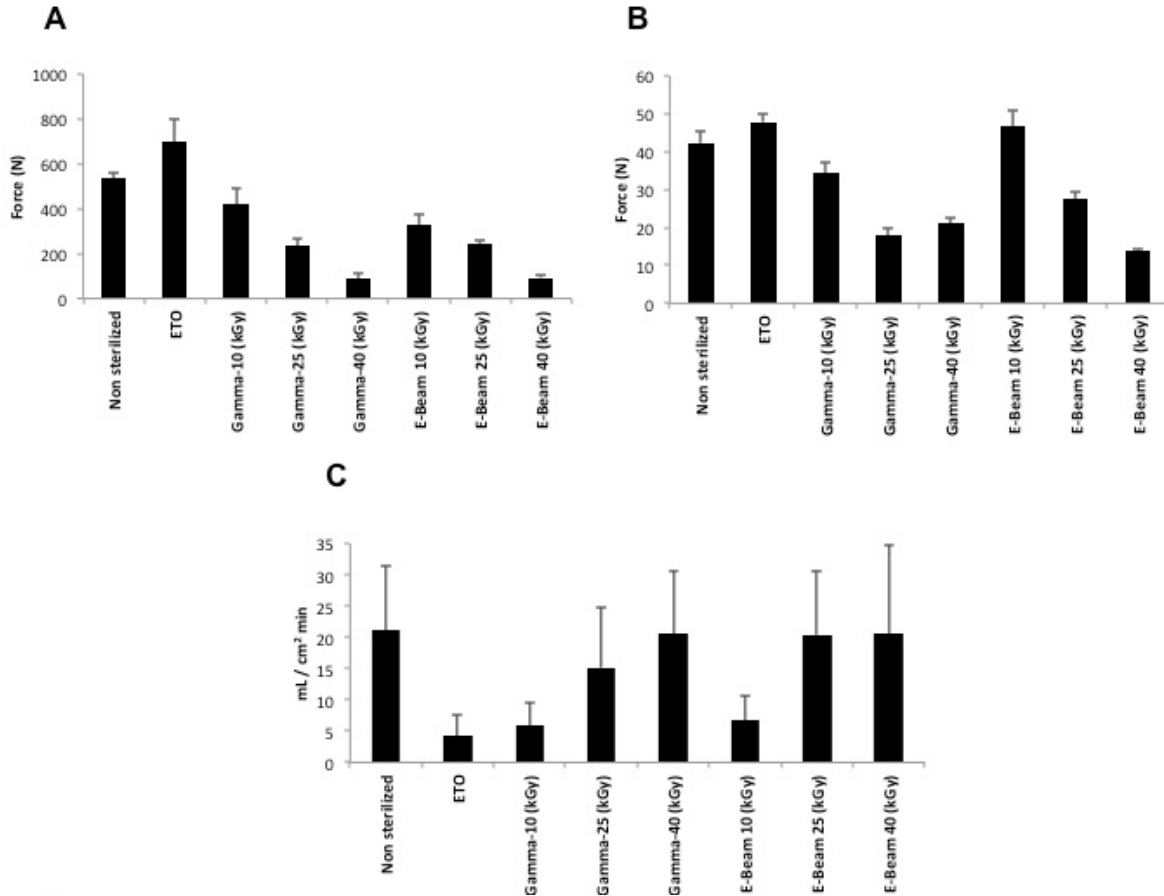


**Figure 42.** Mechanical Properties & Hydrostatic Porosity Index. The ball-burst test conducted in compliance with the Standard Test Method for Bursting Strength of Knitted Goods, Constant-Rate-of-Traverse (CRT) Ball-burst Test (ASTM D 3787-89) (A). The suture retention test was performed according to ANSI/AAMI VP20–1994 Guidelines for Cardiovascular Implants-Vascular Prostheses (B). The hydrostatic PI was calculated by dividing the volume collected by the area of the porosity testing apparatus’ orifice, and the duration of the test (C).

**B.4.5 Cytocompatibility:** All dermal ECM test articles showed equivalent

cytocompatibility scores for HMEC cells at the time point studied. After 7 days in culture, the HMEC cells reached approximately 60% confluence with minimal infiltration and essentially normal cell phenotype (Figure 43).

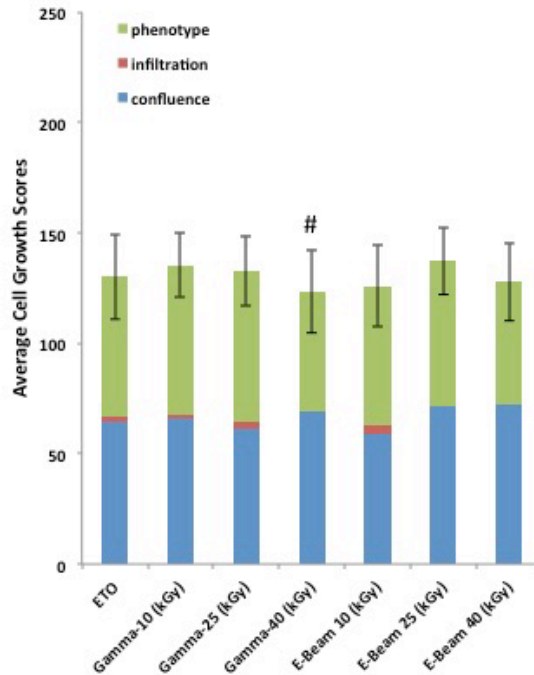


**Figure 43.** Cytocompatibility. HMEC were grown on each test article for 7 days and subsequently scored for cellular confluence, infiltration, and phenotype.

**B.4.6 Host Response:** The host response to dermal ECM scaffolds was evaluated at 7, 14, and 35 days (Figure 44). Gross images of the test article in-situ at time of sacrifice show that the test articles were clearly identifiable at all time points with the exception of those test articles subjected to 40 kGy doses of  $\gamma$  and e-beam which were nearly transparent at 35 d post-op (Figure 44A). These observations were corroborated by representative Masson's Trichome stained histologic sections where less scaffold (indicated by blue color) was present at the higher doses of irradiation compared to the ETO and 10 kGy irradiation samples (Figure 44B). Qualitatively, cell infiltration into all scaffolds increased with time. Little or no cell infiltration was present at 7 days and increasing depth and number of cells was present at 14 and 35 d post operatively, respectively (Figure 44C).

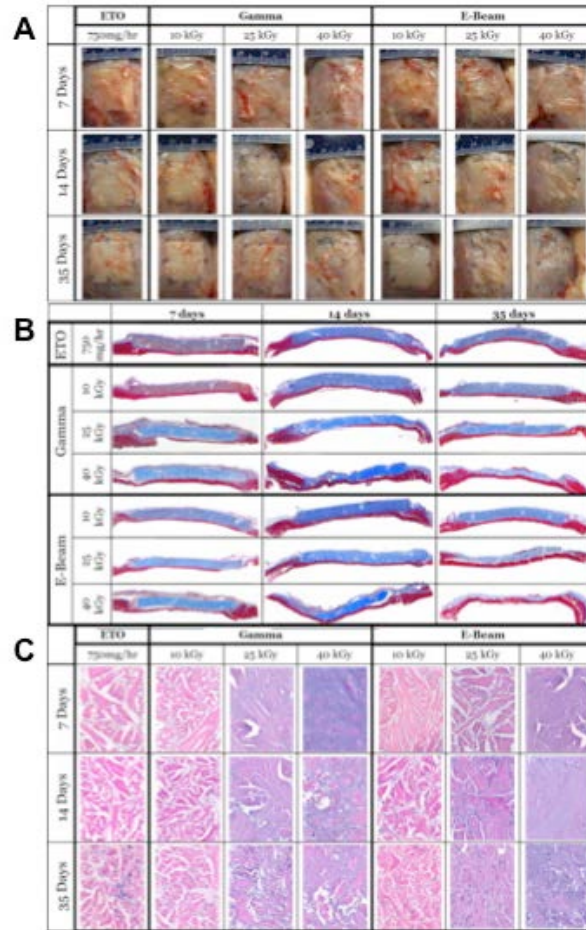


**Figure 44.** In Vivo Remodeling Response. Following euthanasia, the skin was gently dissected, reflected, and photographs were taken of each animal and each test or control article *in situ* (A). The entire body wall that includes the test or control article was explanted *en bloc*. The sample was then cut in half and submitted for histological analysis. Masson's Trichrome stained slides were mosaic imaged to illustrate the entire cross section of each test article at each time point (B). Additional slides were stained with H&E and imaged for histomorphologic analysis. Representative microscopic images (40x) were captured for each test article (C).

Histologic scoring showed the highest level of cellularity in 40 kGy  $\gamma$  sample at 14d and 40 kGy e-beam sample at 35d (Figure 45A). Vascularity in the samples was largely the same in all test articles with the exception of the 35d e-beam 40 kGy samples (Figure 45B). Similarly, the 40 kGy e-beam samples had the most multinucleate giant cells (MNGCs) among test articles, although it should be noted that on average there were still less than 1 MNGC per high-powered

field of view (Figure 45C). Qualitative histologic scoring showed that the 40 kGy e-beam at 35d had the greatest degree of degradation (Figure 45D).

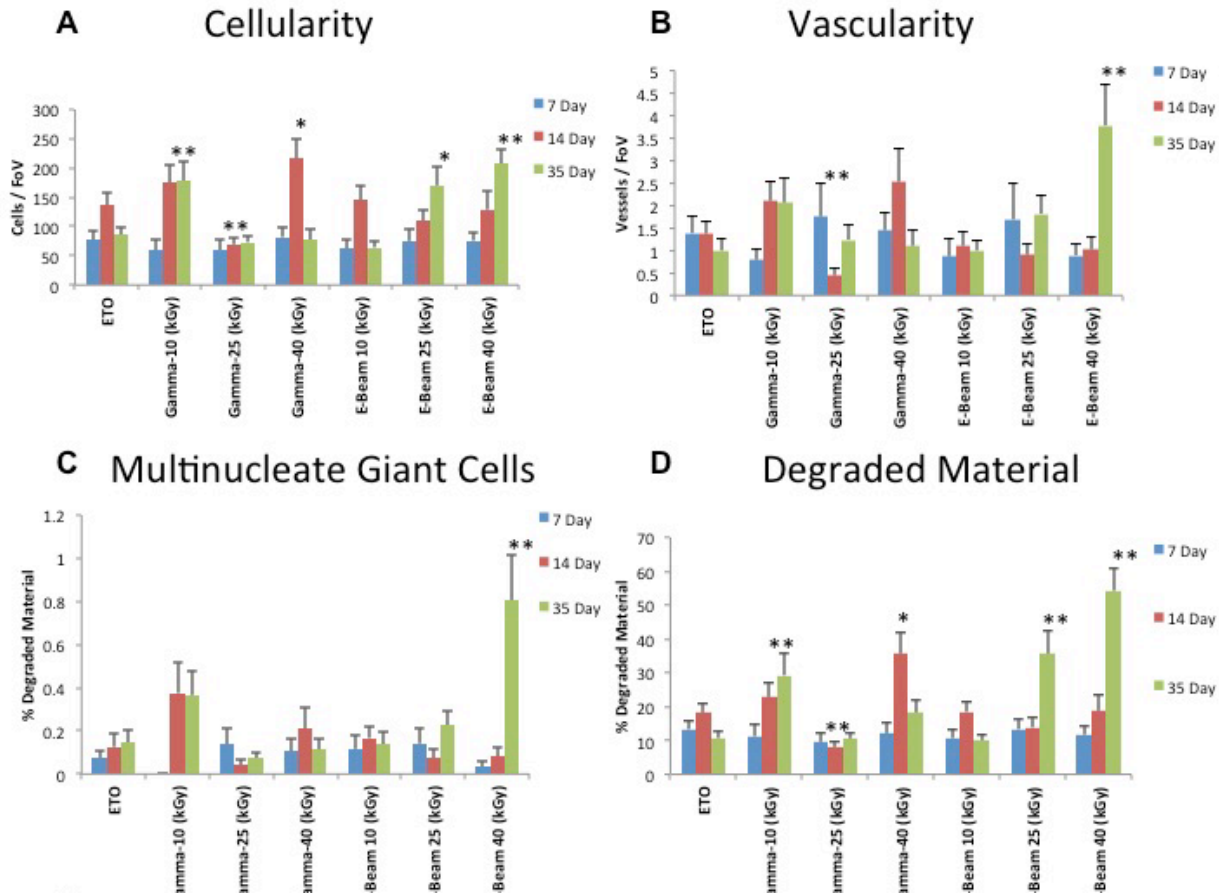


**Figure 45.** Semi-Quantitative Histomorphologic Scoring. Semi-quantitative scoring of each interface of each device was conducted for cellularity (A), neovascularization (B), multinucleate giant cell formation (C), and material degradation (D). Four blinded individuals scored each image independently and the average score was used to compile the results.

Macrophage immunolabeling at 14d post-operative showed a similar M2/M1 ratio among all test articles with a slightly increased ratio in 25kGy  $\gamma$  (Figure 46A). Total number of infiltrating macrophages was similar across groups with the exception of 40kGy  $\gamma$ , which had an increase in macrophage number at 14d post-surgery ( $p < 0.01$ , Figure 46B).

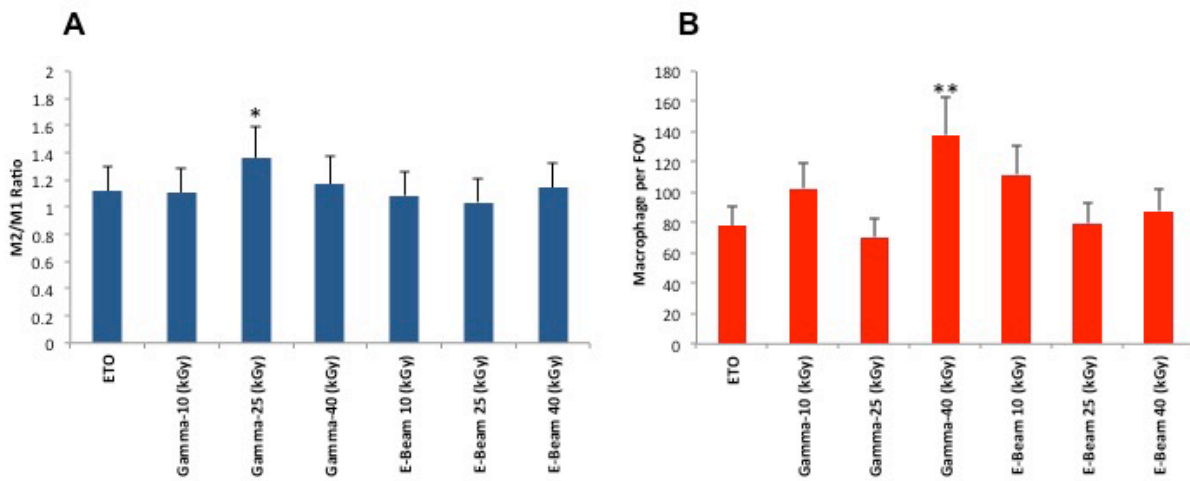


**Figure 46.** Macrophage Phenotype Assessment. Quantification of M1/M2 polarization was achieved using a custom image analysis pipeline developed using the cell profiler image analysis package. This custom pipeline identified and quantified the number of  $CD68^+CD86^+$  (M1 phenotype) and  $CD68^+CD206^+$  (M2 phenotype) cells present within the tissue sections. These numbers were then expressed as a ratio of M2/M1. Any cells that co-express the  $CD86^+$  and  $CD206^+$  markers were counted separately.

## B.5 Discussion

The present study shows that increasing dosage of irradiation results in ultrastructural changes in the collagen fiber architecture, increased total protein extraction, and a dose dependent decrease in mechanical properties compared to untreated controls. ETO-treated porcine dermis

ECM resulted in decreased DNA content, total protein extracted, and bFGF content compared to untreated controls. All ETO,  $\gamma$ , and e-beam treated samples had similar cytocompatibility scores in-vitro. In-vivo results showed an increased rate of degradation of the biologic scaffold materials sterilized by high dose radiation compared to the other groups at both 14 and 35 days post-surgery.

The FDA's classification of biologic scaffold materials as medical devices requires terminal sterilization to assure sterility guidelines are met. Common terminal sterilization methods, such as ETO exposure and irradiation, can achieve effective sterilization but these processes are known to affect the ultrastructure and mechanical properties of the ECM<sup>346</sup>. Material and structural properties, such as burst strength and stiffness, are important parameters for clinical applications such as ventral hernia repair and reconstructive breast surgery<sup>426</sup>. Although ECM scaffolds tend to degrade quickly after implantation due to the host tissue response and the remodeling process, initial material and structural properties are important when the scaffold is intended for load bearing applications<sup>427</sup>. The present study shows that exposure to high levels of e-beam and  $\gamma$  irradiation results in a dose-dependent decrease in the multiaxial strength and suture retention strength of the material.

Previous studies have described effects of terminal sterilization upon the mechanical properties of tissue grafts and different naturally derived biomaterials<sup>161</sup>. However, these studies included materials which differed in preparation methods, hydration states during sterilization, and sterilizing dosage; therefore direct translation of this information to the sterilization method effects on biologic scaffolds is not possible. Since each method of sterilization has distinct effects on ECM constituents (e.g., collagens, proteoglycans, and glycosaminoglycans), a valid comparison of sterilization methods a direct comparison of sterilization requires the same starting material. The present study used the same starting substrate (i.e., decellularized porcine dermis) and

therefore the observed differences in host response and material properties are directly attributable to the method and dose of sterilization.

ETO is a chemical sterilant with an unstable ring structure that alkylates functional groups (amino, carboxyl, hydroxyl, and sulfhydryl) resulting in the inactivation of nucleic acids and proteins<sup>428</sup>. Previous studies have shown little or no change in the mechanical properties of a device following ETO sterilization<sup>161</sup>. The present study showed that ETO exposure resulted in changes to the biochemical composition but, consistent with previous studies, the ultrastructure and mechanical properties were largely unchanged compared to untreated controls. ETO treatment can leave toxic residues that have been implicated as the cause of pro-inflammatory processes and poor outcomes<sup>429</sup>; however, these toxic residues dissipate quickly and it is unlikely that notable amounts remain within a week of ETO exposure. Sterilization with ETO did not adversely affect in-vitro cellular growth or the in-vivo host response in the present study.

The most common technique for sterilization of biologic scaffolds is ionizing radiation, including e-beam and  $\gamma$  irradiation. Radiation exerts sterilization by the production of free radicals that are thought to result in scission of peptide backbones, disruption of hydrogen bonds, and crosslink formation<sup>430</sup>. Previous studies have shown a reduction in mechanical properties of biologic scaffolds following ionizing radiation sterilization<sup>431</sup>. Similarly, radiation has been shown to impair the attachment and growth of cells on biologic scaffolds<sup>432</sup>. Results of the present study showed irradiation results in alterations to the collagen fiber architecture and a dose-dependent decrease in both suture retention strength and maximum tangential stiffness. Radiation did not significantly change in-vitro cytocompatibility but at higher doses of radiation the scaffolds degraded more rapidly in-vivo than those exposed to low dose irradiation or ETO, likely due to increased scission of collagen backbone. The porcine dermal specimens exposed to high dose radiation were also associated with an increased infiltration of macrophages.

There are several key variables associated with the terminal sterilization of an ECM scaffold material. For example, hydration status (lyophilized vs hydrated) and temperature (room temp vs frozen) of the ECM scaffold during sterilization have been suggested to affect the material properties. Although the present study was conducted upon extracellular matrix derived from porcine dermis, it is unknown whether or not the results will be applicable to the preparation of biologic scaffolds from other tissues and organs. Each individual scaffold material, prepared by a specific method, will require similar studies to fully evaluate the effects of terminal sterilization. Studies should be conducted to systematically address these areas in an effort to further improve outcomes.

## **B.6 Conclusion**

The present study shows that 40 kGy of e-beam and  $\gamma$  irradiation causes an adverse effect on the material properties and changes the response to a porcine dermal biologic scaffold both *in vitro* and *in vivo*. However, effective methods of terminal sterilization, such as ETO exposure, can be used with minimal effects upon the structure and function of biologic scaffold materials. These findings emphasize the importance of selecting an appropriate type and dose sterilization for biologic scaffold materials to identify preferred material properties and performance *in vivo*.

## **B.7 Acknowledgements**

The authors would like to thank Deanna Rhoads of the McGowan Histology Center for histologic section preparation, Victoria Bain and Sandy Lui for dermal ECM material preparation,

and Scott A. Johnson for gamma sterilization of the materials. Funding for this study was provided, in part by C.R. Bard, Inc. This material is based upon work supported by the National Science Foundation Graduate Research Fellowship under Grant No. DGE-1247842 (to T.J.K.). Disclaimer: the views expressed in this presentation are those of the authors and do not necessarily reflect the official policy or position of the National Science Foundation, Department of the Army, Department of Defense, nor the U.S. Government.

## BIBLIOGRAPHY

- 1 Adams, J. E., Zobitz, M. E., Reach, J. S., Jr., An, K. N. & Steinmann, S. P. Rotator cuff repair using an acellular dermal matrix graft: an in vivo study in a canine model. *Arthroscopy* **22**, 700-709, doi:10.1016/j.arthro.2006.03.016 (2006).
- 2 Langer, R. & Vacanti, J. P. Tissue engineering. *Science* **260**, 920-926 (1993).
- 3 Williams, D. F. On the nature of biomaterials. *Biomaterials* **30**, 5897-5909, doi:10.1016/j.biomaterials.2009.07.027 (2009).
- 4 Badylak, S., Kokini, K., Tullius, B. & Whitson, B. Strength over time of a resorbable bioscaffold for body wall repair in a dog model. *J Surg Res* **99**, 282-287, doi:10.1006/jsre.2001.6176 (2001).
- 5 Mann, B. K., Gobin, A. S., Tsai, A. T., Schmedlen, R. H. & West, J. L. Smooth muscle cell growth in photopolymerized hydrogels with cell adhesive and proteolytically degradable domains: synthetic ECM analogs for tissue engineering. *Biomaterials* **22**, 3045-3051 (2001).
- 6 Mann, B. K. & West, J. L. Cell adhesion peptides alter smooth muscle cell adhesion, proliferation, migration, and matrix protein synthesis on modified surfaces and in polymer scaffolds. *Journal of Biomedical Materials Research* **60**, 86-93 (2002).
- 7 Liu Tsang, V. *et al.* Fabrication of 3D hepatic tissues by additive photopatterning of cellular hydrogels. *FASEB J* **21**, 790-801, doi:10.1096/fj.06-7117com (2007).
- 8 Schmidt, D. R. & Kao, W. J. Monocyte activation in response to polyethylene glycol hydrogels grafted with RGD and PHSRN separated by interpositional spacers of various lengths. *J Biomed Mater Res A* **83**, 617-625, doi:10.1002/jbm.a.31270 (2007).
- 9 Fittkau, M. H. *et al.* The selective modulation of endothelial cell mobility on RGD peptide containing surfaces by YIGSR peptides. *Biomaterials* **26**, 167-174, doi:10.1016/j.biomaterials.2004.02.012 (2005).
- 10 Hynd, M. R., Frampton, J. P., Dowell-Mesfin, N., Turner, J. N. & Shain, W. Directed cell growth on protein-functionalized hydrogel surfaces. *J Neurosci Methods* **162**, 255-263, doi:10.1016/j.jneumeth.2007.01.024 (2007).

- 11 Weber, L. M. & Anseth, K. S. Hydrogel encapsulation environments functionalized with extracellular matrix interactions increase islet insulin secretion. *Matrix Biol* **27**, 667-673, doi:10.1016/j.matbio.2008.08.001 (2008).
- 12 Weber, L. M., Hayda, K. N., Haskins, K. & Anseth, K. S. The effects of cell-matrix interactions on encapsulated beta-cell function within hydrogels functionalized with matrix-derived adhesive peptides. *Biomaterials* **28**, 3004-3011, doi:10.1016/j.biomaterials.2007.03.005 (2007).
- 13 Mann, B. K., Tsai, A. T., Scott-Burden, T. & West, J. L. Modification of surfaces with cell adhesion peptides alters extracellular matrix deposition. *Biomaterials* **20**, 2281-2286 (1999).
- 14 Saha, K., Irwin, E. F., Kozhukh, J., Schaffer, D. V. & Healy, K. E. Biomimetic interfacial interpenetrating polymer networks control neural stem cell behavior. *J Biomed Mater Res A* **81**, 240-249, doi:10.1002/jbm.a.30986 (2007).
- 15 Liu, S. Q., Ee, P. L., Ke, C. Y., Hedrick, J. L. & Yang, Y. Y. Biodegradable poly(ethylene glycol)-peptide hydrogels with well-defined structure and properties for cell delivery. *Biomaterials* **30**, 1453-1461, doi:10.1016/j.biomaterials.2008.11.023 (2009).
- 16 Herten, M. *et al.* Biodegradation of different synthetic hydrogels made of polyethylene glycol hydrogel/RGD-peptide modifications: an immunohistochemical study in rats. *Clin Oral Implants Res* **20**, 116-125, doi:10.1111/j.1600-0501.2008.01622.x (2009).
- 17 Salinas, C. N. & Anseth, K. S. The enhancement of chondrogenic differentiation of human mesenchymal stem cells by enzymatically regulated RGD functionalities. *Biomaterials* **29**, 2370-2377, doi:10.1016/j.biomaterials.2008.01.035 (2008).
- 18 DeForest, C. A., Polizzotti, B. D. & Anseth, K. S. Sequential click reactions for synthesizing and patterning three-dimensional cell microenvironments. *Nat Mater* **8**, 659-664, doi:10.1038/nmat2473 (2009).
- 19 Zhu, J., Tang, C., Kottke-Marchant, K. & Marchant, R. E. Design and synthesis of biomimetic hydrogel scaffolds with controlled organization of cyclic RGD peptides. *Bioconjug Chem* **20**, 333-339, doi:10.1021/bc800441v (2009).
- 20 Lutolf, M. P. *et al.* Repair of bone defects using synthetic mimetics of collagenous extracellular matrices. *Nat Biotechnol* **21**, 513-518, doi:10.1038/nbt818 (2003).
- 21 Mann, B. K., Schmedlen, R. H. & West, J. L. Tethered-TGF-beta increases extracellular matrix production of vascular smooth muscle cells. *Biomaterials* **22**, 439-444 (2001).
- 22 Gobin, A. S. & West, J. L. Val-ala-pro-gly, an elastin-derived non-integrin ligand: smooth muscle cell adhesion and specificity. *J Biomed Mater Res A* **67**, 255-259, doi:10.1002/jbm.a.10110 (2003).
- 23 Hersel, U., Dahmen, C. & Kessler, H. RGD modified polymers: biomaterials for stimulated cell adhesion and beyond. *Biomaterials* **24**, 4385-4415 (2003).
- 24 Ruoslahti, E. The RGD story: a personal account. *Matrix Biol* **22**, 459-465 (2003).

- 25 Romano, N. H., Sengupta, D., Chung, C. & Heilshorn, S. C. Protein-engineered biomaterials: nanoscale mimics of the extracellular matrix. *Biochim Biophys Acta* **1810**, 339-349, doi:10.1016/j.bbagen.2010.07.005 (2011).
- 26 Lutolf, M. P. *et al.* Synthetic matrix metalloproteinase-sensitive hydrogels for the conduction of tissue regeneration: engineering cell-invasion characteristics. *Proc Natl Acad Sci U S A* **100**, 5413-5418, doi:10.1073/pnas.0737381100 (2003).
- 27 Lee, S. H., Miller, J. S., Moon, J. J. & West, J. L. Proteolytically degradable hydrogels with a fluorogenic substrate for studies of cellular proteolytic activity and migration. *Biotechnol Prog* **21**, 1736-1741, doi:10.1021/bp0502429 (2005).
- 28 Pratt, A. B., Weber, F. E., Schmoekel, H. G., Muller, R. & Hubbell, J. A. Synthetic extracellular matrices for in situ tissue engineering. *Biotechnol Bioeng* **86**, 27-36, doi:10.1002/bit.10897 (2004).
- 29 Raeber, G. P., Lutolf, M. P. & Hubbell, J. A. Molecularly engineered PEG hydrogels: a novel model system for proteolytically mediated cell migration. *Biophys J* **89**, 1374-1388, doi:10.1529/biophysj.104.050682 (2005).
- 30 Kraehenbuehl, T. P. *et al.* Three-dimensional extracellular matrix-directed cardioprogenitor differentiation: systematic modulation of a synthetic cell-responsive PEG-hydrogel. *Biomaterials* **29**, 2757-2766, doi:10.1016/j.biomaterials.2008.03.016 (2008).
- 31 Raeber, G. P., Lutolf, M. P. & Hubbell, J. A. Mechanisms of 3-D migration and matrix remodeling of fibroblasts within artificial ECMs. *Acta Biomater* **3**, 615-629, doi:10.1016/j.actbio.2007.03.013 (2007).
- 32 Patel, P. N., Gobin, A. S., West, J. L. & Patrick, C. W., Jr. Poly(ethylene glycol) hydrogel system supports preadipocyte viability, adhesion, and proliferation. *Tissue Eng* **11**, 1498-1505, doi:10.1089/ten.2005.11.1498 (2005).
- 33 Lee, S. H., Moon, J. J., Miller, J. S. & West, J. L. Poly(ethylene glycol) hydrogels conjugated with a collagenase-sensitive fluorogenic substrate to visualize collagenase activity during three-dimensional cell migration. *Biomaterials* **28**, 3163-3170, doi:10.1016/j.biomaterials.2007.03.004 (2007).
- 34 Gobin, A. S. & West, J. L. Effects of epidermal growth factor on fibroblast migration through biomimetic hydrogels. *Biotechnol Prog* **19**, 1781-1785, doi:10.1021/bp0341390 (2003).
- 35 Aimetti, A. A., Tibbitt, M. W. & Anseth, K. S. Human neutrophil elastase responsive delivery from poly(ethylene glycol) hydrogels. *Biomacromolecules* **10**, 1484-1489, doi:10.1021/bm9000926 (2009).
- 36 Midha, R., Munro, C. A., Dalton, P. D., Tator, C. H. & Shoichet, M. S. Growth factor enhancement of peripheral nerve regeneration through a novel synthetic hydrogel tube. *J Neurosurg* **99**, 555-565, doi:10.3171/jns.2003.99.3.0555 (2003).
- 37 Lee, A. C. *et al.* Controlled release of nerve growth factor enhances sciatic nerve regeneration. *Exp Neurol* **184**, 295-303 (2003).

- 38 DeLong, S. A., Moon, J. J. & West, J. L. Covalently immobilized gradients of bFGF on hydrogel scaffolds for directed cell migration. *Biomaterials* **26**, 3227-3234, doi:10.1016/j.biomaterials.2004.09.021 (2005).
- 39 He, X., Ma, J. & Jabbari, E. Effect of grafting RGD and BMP-2 protein-derived peptides to a hydrogel substrate on osteogenic differentiation of marrow stromal cells. *Langmuir* **24**, 12508-12516, doi:10.1021/la802447v (2008).
- 40 Schmoekel, H. G. *et al.* Bone repair with a form of BMP-2 engineered for incorporation into fibrin cell ingrowth matrices. *Biotechnol Bioeng* **89**, 253-262, doi:10.1002/bit.20168 (2005).
- 41 Silva, E. A., Kim, E. S., Kong, H. J. & Mooney, D. J. Material-based deployment enhances efficacy of endothelial progenitor cells. *Proc Natl Acad Sci U S A* **105**, 14347-14352, doi:10.1073/pnas.0803873105 (2008).
- 42 den Braber, E. T., de Ruijter, J. E., Ginsel, L. A., von Recum, A. F. & Jansen, J. A. Orientation of ECM protein deposition, fibroblast cytoskeleton, and attachment complex components on silicone microgrooved surfaces. *Journal of Biomedical Materials Research* **40**, 291-300 (1998).
- 43 Yim, E. K. *et al.* Nanopattern-induced changes in morphology and motility of smooth muscle cells. *Biomaterials* **26**, 5405-5413, doi:10.1016/j.biomaterials.2005.01.058 (2005).
- 44 Dalby, M. J. *et al.* Nanotopographical stimulation of mechanotransduction and changes in interphase centromere positioning. *J Cell Biochem* **100**, 326-338, doi:10.1002/jcb.21058 (2007).
- 45 Gaubert, H. E. & Frey, W. Highly parallel fabrication of nanopatterned surfaces with nanoscale orthogonal biofunctionalization imprint lithography. *Nanotechnology* **18**, 135101, doi:10.1088/0957-4484/18/13/135101 (2007).
- 46 Champion, J. A. & Mitragotri, S. Role of target geometry in phagocytosis. *Proc Natl Acad Sci U S A* **103**, 4930-4934, doi:10.1073/pnas.0600997103 (2006).
- 47 Champion, J. A., Katare, Y. K. & Mitragotri, S. Making polymeric micro- and nanoparticles of complex shapes. *Proc Natl Acad Sci U S A* **104**, 11901-11904, doi:10.1073/pnas.0705326104 (2007).
- 48 Rolland, J. P. *et al.* Direct fabrication and harvesting of monodisperse, shape-specific nanobiomaterials. *J Am Chem Soc* **127**, 10096-10100, doi:10.1021/ja051977c (2005).
- 49 Euliss, L. E., DuPont, J. A., Gratton, S. & DeSimone, J. Imparting size, shape, and composition control of materials for nanomedicine. *Chem Soc Rev* **35**, 1095-1104, doi:10.1039/b600913c (2006).
- 50 Geng, Y. *et al.* Shape effects of filaments versus spherical particles in flow and drug delivery. *Nat Nanotechnol* **2**, 249-255, doi:10.1038/nnano.2007.70 (2007).

- 51 Barradas, A. M. *et al.* Surface modifications by gas plasma control osteogenic differentiation of MC3T3-E1 cells. *Acta Biomater* **8**, 2969-2977, doi:10.1016/j.actbio.2012.04.021 (2012).
- 52 Chen, C. S., Mrksich, M., Huang, S., Whitesides, G. M. & Ingber, D. E. Geometric control of cell life and death. *Science* **276**, 1425-1428 (1997).
- 53 McBeath, R., Pirone, D. M., Nelson, C. M., Bhadriraju, K. & Chen, C. S. Cell shape, cytoskeletal tension, and RhoA regulate stem cell lineage commitment. *Dev Cell* **6**, 483-495 (2004).
- 54 Rehfeldt, F., Engler, A. J., Eckhardt, A., Ahmed, F. & Discher, D. E. Cell responses to the mechanochemical microenvironment--implications for regenerative medicine and drug delivery. *Adv Drug Deliv Rev* **59**, 1329-1339, doi:10.1016/j.addr.2007.08.007 (2007).
- 55 Engler, A. J., Sen, S., Sweeney, H. L. & Discher, D. E. Matrix elasticity directs stem cell lineage specification. *Cell* **126**, 677-689, doi:10.1016/j.cell.2006.06.044 (2006).
- 56 Beningo, K. A. & Wang, Y. L. Fc-receptor-mediated phagocytosis is regulated by mechanical properties of the target. *J Cell Sci* **115**, 849-856 (2002).
- 57 van den Dries, K. *et al.* Geometry sensing by dendritic cells dictates spatial organization and PGE(2)-induced dissolution of podosomes. *Cell Mol Life Sci* **69**, 1889-1901, doi:10.1007/s00018-011-0908-y (2012).
- 58 Mitragotri, S. & Lahann, J. Physical approaches to biomaterial design. *Nat Mater* **8**, 15-23, doi:10.1038/nmat2344 (2009).
- 59 Nelson, C. M. & Bissell, M. J. Of extracellular matrix, scaffolds, and signaling: tissue architecture regulates development, homeostasis, and cancer. *Annu Rev Cell Dev Biol* **22**, 287-309, doi:10.1146/annurev.cellbio.22.010305.104315 (2006).
- 60 Bissell, M. J. & Aggeler, J. Dynamic reciprocity: how do extracellular matrix and hormones direct gene expression? *Progress in clinical and biological research* **249**, 251-262 (1987).
- 61 van der Rest, M. & Garrone, R. Collagen family of proteins. *FASEB journal : official publication of the Federation of American Societies for Experimental Biology* **5**, 2814-2823 (1991).
- 62 Schwarzbauer, J. E. Fibronectin: from gene to protein. *Current opinion in cell biology* **3**, 786-791 (1991).
- 63 Ponce, M. L. *et al.* Identification of endothelial cell binding sites on the laminin gamma 1 chain. *Circulation research* **84**, 688-694 (1999).
- 64 Scott, J. E. Extracellular matrix, supramolecular organisation and shape. *J Anat* **187 ( Pt 2)**, 259-269 (1995).

- 65 Voytik-Harbin, S. L., Brightman, A. O., Kraine, M. R., Waisner, B. & Badylak, S. F. Identification of extractable growth factors from small intestinal submucosa. *J Cell Biochem* **67**, 478-491 (1997).
- 66 Agrawal, V. *et al.* Epimorphic regeneration approach to tissue replacement in adult mammals. *Proc Natl Acad Sci U S A* **107**, 3351-3355, doi:10.1073/pnas.0905851106 (2010).
- 67 Reing, J. E. *et al.* Degradation products of extracellular matrix affect cell migration and proliferation. *Tissue Eng Part A* **15**, 605-614, doi:10.1089/ten.tea.2007.0425 (2009).
- 68 Hynes, R. O. & Zhao, Q. The evolution of cell adhesion. *The Journal of cell biology* **150**, F89-96 (2000).
- 69 Hutter, H. *et al.* Conservation and novelty in the evolution of cell adhesion and extracellular matrix genes. *Science* **287**, 989-994 (2000).
- 70 Kramer, J. M. in *C. elegans II* (eds D. L. Riddle, T. Blumenthal, B. J. Meyer, & J. R. Priess) (1997).
- 71 Burgeson, R. E. & Christiano, A. M. The dermal-epidermal junction. *Current opinion in cell biology* **9**, 651-658 (1997).
- 72 Constantinou, C. D. & Jimenez, S. A. Structure of cDNAs encoding the triple-helical domain of murine alpha 2 (VI) collagen chain and comparison to human and chick homologues. Use of polymerase chain reaction and partially degenerate oligonucleotide for generation of novel cDNA clones. *Matrix* **11**, 1-9 (1991).
- 73 Exposito, J. Y., D'Alessio, M., Solursh, M. & Ramirez, F. Sea urchin collagen evolutionarily homologous to vertebrate pro-alpha 2(I) collagen. *The Journal of biological chemistry* **267**, 15559-15562 (1992).
- 74 Okumura, M. *et al.* Comparison of CD45 extracellular domain sequences from divergent vertebrate species suggests the conservation of three fibronectin type III domains. *J Immunol* **157**, 1569-1575 (1996).
- 75 Iozzo, R. V. Perlecan: a gem of a proteoglycan. *Matrix Biol* **14**, 203-208 (1994).
- 76 Liu, C., Dib-Hajj, S. D. & Waxman, S. G. Fibroblast growth factor homologous factor 1B binds to the C terminus of the tetrodotoxin-resistant sodium channel rNav1.9a (NaN). *J Biol Chem* **276**, 18925-18933, doi:10.1074/jbc.M101606200 (2001).
- 77 Badylak, S. F., Taylor, D. & Uygun, K. Whole-organ tissue engineering: decellularization and recellularization of three-dimensional matrix scaffolds. *Annu Rev Biomed Eng* **13**, 27-53, doi:10.1146/annurev-bioeng-071910-124743 (2011).
- 78 Courtman, D. W. *et al.* Development of a pericardial acellular matrix biomaterial: biochemical and mechanical effects of cell extraction. *Journal of Biomedical Materials Research* **28**, 655-666, doi:10.1002/jbm.820280602 (1994).
- 79 Schmidt, C. E. & Baier, J. M. Acellular vascular tissues: natural biomaterials for tissue repair and tissue engineering. *Biomaterials* **21**, 2215-2231 (2000).

- 80 Dahl, S. L., Koh, J., Prabhakar, V. & Niklason, L. E. Decellularized native and engineered arterial scaffolds for transplantation. *Cell Transplant* **12**, 659-666 (2003).
- 81 Conklin, B. S., Richter, E. R., Kreutziger, K. L., Zhong, D. S. & Chen, C. Development and evaluation of a novel decellularized vascular xenograft. *Med Eng Phys* **24**, 173-183 (2002).
- 82 Badylak, S., Liang, A., Record, R., Tullius, R. & Hodde, J. Endothelial cell adherence to small intestinal submucosa: an acellular bioscaffold. *Biomaterials* **20**, 2257-2263 (1999).
- 83 Badylak, S. F., Lantz, G. C., Coffey, A. & Geddes, L. A. Small intestinal submucosa as a large diameter vascular graft in the dog. *J Surg Res* **47**, 74-80 (1989).
- 84 Remlinger, N. T. *et al.* Hydrated xenogeneic decellularized tracheal matrix as a scaffold for tracheal reconstruction. *Biomaterials* **31**, 3520-3526, doi:10.1016/j.biomaterials.2010.01.067 (2010).
- 85 Gilbert, T. W., Gilbert, S., Madden, M., Reynolds, S. D. & Badylak, S. F. Morphologic assessment of extracellular matrix scaffolds for patch tracheoplasty in a canine model. *Ann Thorac Surg* **86**, 967-974; discussion 967-974, doi:10.1016/j.athoracsur.2008.04.071 (2008).
- 86 French, K. M. *et al.* A naturally derived cardiac extracellular matrix enhances cardiac progenitor cell behavior in vitro. *Acta Biomater* **8**, 4357-4364, doi:10.1016/j.actbio.2012.07.033 (2012).
- 87 Wainwright, J. M. *et al.* Right ventricular outflow tract repair with a cardiac biologic scaffold. *Cells Tissues Organs* **195**, 159-170, doi:10.1159/000331400 (2012).
- 88 Robinson, K. A. *et al.* Extracellular matrix scaffold for cardiac repair. *Circulation* **112**, 1135-1143, doi:10.1161/CIRCULATIONAHA.104.525436 (2005).
- 89 Seif-Naraghi, S. B. *et al.* Safety and efficacy of an injectable extracellular matrix hydrogel for treating myocardial infarction. *Sci Transl Med* **5**, 173ra125, doi:10.1126/scitranslmed.3005503 (2013).
- 90 Valentin, J. E., Turner, N. J., Gilbert, T. W. & Badylak, S. F. Functional skeletal muscle formation with a biologic scaffold. *Biomaterials* **31**, 7475-7484, doi:10.1016/j.biomaterials.2010.06.039 (2010).
- 91 Mase, V. J., Jr. *et al.* Clinical application of an acellular biologic scaffold for surgical repair of a large, traumatic quadriceps femoris muscle defect. *Orthopedics* **33**, 511, doi:10.3928/01477447-20100526-24 (2010).
- 92 Badylak, S. F. *et al.* Esophageal preservation in five male patients after endoscopic inner-layer circumferential resection in the setting of superficial cancer: a regenerative medicine approach with a biologic scaffold. *Tissue Eng Part A* **17**, 1643-1650, doi:10.1089/ten.TEA.2010.0739 (2011).
- 93 Badylak, S. F. *et al.* Esophageal reconstruction with ECM and muscle tissue in a dog model. *Journal of Surgical Research* **128**, 87-97, doi:10.1016/j.jss.2005.03.002 (2005).

- 94 Nieponice, A., Gilbert, T. W. & Badylak, S. F. Reinforcement of esophageal anastomoses with an extracellular matrix scaffold in a canine model. *Ann Thorac Surg* **82**, 2050-2058, doi:10.1016/j.athoracsur.2006.06.036 (2006).
- 95 Nieponice, A. *et al.* An extracellular matrix scaffold for esophageal stricture prevention after circumferential EMR. *Gastrointest Endosc* **69**, 289-296, doi:10.1016/j.gie.2008.04.022 (2009).
- 96 Hoppo, T., Badylak, S. F. & Jobe, B. A. A novel esophageal-preserving approach to treat high-grade dysplasia and superficial adenocarcinoma in the presence of chronic gastroesophageal reflux disease. *World J Surg* **36**, 2390-2393, doi:10.1007/s00268-012-1698-6 (2012).
- 97 Uygun, B. E. *et al.* Organ reengineering through development of a transplantable recellularized liver graft using decellularized liver matrix. *Nat Med* **16**, 814-820, doi:10.1038/nm.2170 (2010).
- 98 Lin, P., Chan, W. C., Badylak, S. F. & Bhatia, S. N. Assessing porcine liver-derived biomatrix for hepatic tissue engineering. *Tissue Eng* **10**, 1046-1053, doi:10.1089/ten.2004.10.1046 (2004).
- 99 Petersen, T. H. *et al.* Tissue-engineered lungs for in vivo implantation. *Science* **329**, 538-541, doi:10.1126/science.1189345 (2010).
- 100 Badylak, S. F., Freytes, D. O. & Gilbert, T. W. Extracellular matrix as a biological scaffold material: Structure and function. *Acta Biomater* **5**, 1-13, doi:10.1016/j.actbio.2008.09.013 (2009).
- 101 Sacks, M. S. & Gloeckner, D. C. Quantification of the fiber architecture and biaxial mechanical behavior of porcine intestinal submucosa. *J Biomed Mater Res* **46**, 1-10 (1999).
- 102 Gilbert, T. W. *et al.* Collagen fiber alignment and biaxial mechanical behavior of porcine urinary bladder derived extracellular matrix. *Biomaterials* **29**, 4775-4782, doi:10.1016/j.biomaterials.2008.08.022 (2008).
- 103 Colwell, A. S., Longaker, M. T. & Lorenz, H. P. Mammalian fetal organ regeneration. *Advances in biochemical engineering/biotechnology* **93**, 83-100 (2005).
- 104 Calve, S., Odelberg, S. J. & Simon, H. G. A transitional extracellular matrix instructs cell behavior during muscle regeneration. *Developmental biology* **344**, 259-271, doi:10.1016/j.ydbio.2010.05.007 (2010).
- 105 Sicari, B. M. *et al.* The effect of source animal age upon the in vivo remodeling characteristics of an extracellular matrix scaffold. *Biomaterials* **33**, 5524-5533, doi:10.1016/j.biomaterials.2012.04.017 (2012).
- 106 Genovese, L. *et al.* Cellular localization, invasion, and turnover are differently influenced by healthy and tumor-derived extracellular matrix. *Tissue Eng Part A* **20**, 2005-2018, doi:10.1089/ten.TEA.2013.0588 (2014).

- 107 Meijer, M. J. *et al.* Increased mucosal matrix metalloproteinase-1, -2, -3 and -9 activity in patients with inflammatory bowel disease and the relation with Crohn's disease phenotype. *Dig Liver Dis* **39**, 733-739, doi:10.1016/j.dld.2007.05.010 (2007).
- 108 Slivka, P. F. *et al.* Fractionation of an ECM hydrogel into structural and soluble components reveals distinctive roles in regulating macrophage behavior. *Biomaterials Science* **2**, 1521, doi:10.1039/c4bm00189c (2014).
- 109 Sellaro, T. L., Ravindra, A. K., Stolz, D. B. & Badylak, S. F. Maintenance of hepatic sinusoidal endothelial cell phenotype in vitro using organ-specific extracellular matrix scaffolds. *Tissue engineering* **13**, 2301-2310, doi:10.1089/ten.2006.0437 (2007).
- 110 Sellaro, T. L. *et al.* Maintenance of human hepatocyte function in vitro by liver-derived extracellular matrix gels. *Tissue Eng Part A* **16**, 1075-1082, doi:10.1089/ten.TEA.2008.0587 (2010).
- 111 Allen, R. A. *et al.* Adrenal extracellular matrix scaffolds support adrenocortical cell proliferation and function in vitro. *Tissue engineering. Part A* **16**, 3363-3374, doi:10.1089/ten.TEA.2010.0005 (2010).
- 112 French, K. M. *et al.* A naturally derived cardiac extracellular matrix enhances cardiac progenitor cell behavior in vitro. *Acta biomaterialia*, doi:10.1016/j.actbio.2012.07.033 (2012).
- 113 Zhang, Y. *et al.* Tissue-specific extracellular matrix coatings for the promotion of cell proliferation and maintenance of cell phenotype. *Biomaterials* **30**, 4021-4028, doi:10.1016/j.biomaterials.2009.04.005 (2009).
- 114 Cortiella, J. *et al.* Influence of acellular natural lung matrix on murine embryonic stem cell differentiation and tissue formation. *Tissue Eng Part A* **16**, 2565-2580, doi:10.1089/ten.tea.2009.0730 (2010).
- 115 Brennan, E. P., Tang, X. H., Stewart-Akers, A. M., Gudas, L. J. & Badylak, S. F. Chemoattractant activity of degradation products of fetal and adult skin extracellular matrix for keratinocyte progenitor cells. *J Tissue Eng Regen Med* **2**, 491-498, doi:10.1002/term.123 (2008).
- 116 Crapo, P. M. *et al.* Biologic scaffolds composed of central nervous system extracellular matrix. *Biomaterials* **33**, 3539-3547, doi:10.1016/j.biomaterials.2012.01.044 (2012).
- 117 Beattie, A. J., Gilbert, T. W., Guyot, J. P., Yates, A. J. & Badylak, S. F. Chemoattraction of progenitor cells by remodeling extracellular matrix scaffolds. *Tissue Eng Part A* **15**, 1119-1125, doi:10.1089/ten.tea.2008.0162 (2009).
- 118 Medberry, C. J. *et al.* Hydrogels derived from central nervous system extracellular matrix. *Biomaterials* **34**, 1033-1040, doi:10.1016/j.biomaterials.2012.10.062 (2013).
- 119 Wolf, M. T., Daly, K. A., Reing, J. E. & Badylak, S. F. Biologic scaffold composed of skeletal muscle extracellular matrix. *Biomaterials* **33**, 2916-2925, doi:10.1016/j.biomaterials.2011.12.055 (2012).

- 120 Badylak, S. F. *et al.* The Use of Xenogeneic Small-Intestinal Submucosa as a Biomaterial for Achilles-Tendon Repair in a Dog-Model. *J Biomed Mater Res* **29**, 977-985 (1995).
- 121 Marcal, H., Ahmed, T., Badylak, S. F., Tottey, S. & Foster, L. J. A comprehensive protein expression profile of extracellular matrix biomaterial derived from porcine urinary bladder. *Regen Med* **7**, 159-166, doi:10.2217/rme.12.6 (2012).
- 122 Fata, J. E., Werb, Z. & Bissell, M. J. Regulation of mammary gland branching morphogenesis by the extracellular matrix and its remodeling enzymes. *Breast Cancer Res* **6**, 1-11, doi:10.1186/bcr634 (2004).
- 123 Huttenlocher, A., Sandborg, R. R. & Horwitz, A. F. Adhesion in cell migration. *Curr Opin Cell Biol* **7**, 697-706 (1995).
- 124 Humphries, M. J. & Newham, P. The structure of cell-adhesion molecules. *Trends Cell Biol* **8**, 78-83 (1998).
- 125 Cohen, M., Joester, D., Geiger, B. & Addadi, L. Spatial and temporal sequence of events in cell adhesion: from molecular recognition to focal adhesion assembly. *Chembiochem* **5**, 1393-1399, doi:10.1002/cbic.200400162 (2004).
- 126 Hoppo, T., Badylak, S. F. & Jobe, B. A. A Novel Esophageal-preserving Approach to Treat High-grade Dysplasia and Superficial Adenocarcinoma in the Presence of Chronic Gastroesophageal Reflux Disease. *World journal of surgery*, doi:10.1007/s00268-012-1698-6 (2012).
- 127 Bible, E. *et al.* Non-invasive imaging of transplanted human neural stem cells and ECM scaffold remodeling in the stroke-damaged rat brain by (19)F- and diffusion-MRI. *Biomaterials* **33**, 2858-2871, doi:10.1016/j.biomaterials.2011.12.033 (2012).
- 128 Merguerian, P. A. *et al.* Acellular bladder matrix allografts in the regeneration of functional bladders: evaluation of large-segment (> 24 cm) substitution in a porcine model. *BJU Int* **85**, 894-898 (2000).
- 129 Sicari, B. M. *et al.* An acellular biologic scaffold promotes skeletal muscle formation in mice and humans with volumetric muscle loss. *Sci Transl Med* **6**, 234ra258, doi:10.1126/scitranslmed.3008085 (2014).
- 130 Sutherland, R. S., Baskin, L. S., Hayward, S. W. & Cunha, G. R. Regeneration of bladder urothelium, smooth muscle, blood vessels and nerves into an acellular tissue matrix. *J Urol* **156**, 571-577 (1996).
- 131 Zantop, T., Gilbert, T. W., Yoder, M. C. & Badylak, S. F. Extracellular matrix scaffolds are repopulated by bone marrow-derived cells in a mouse model of achilles tendon reconstruction. *J Orthop Res* **24**, 1299-1309, doi:10.1002/jor.20071 (2006).
- 132 Brown, B. N. *et al.* Macrophage phenotype as a predictor of constructive remodeling following the implantation of biologically derived surgical mesh materials. *Acta Biomater* **8**, 978-987, doi:10.1016/j.actbio.2011.11.031 (2012).

- 133 Brown, B. N., Valentin, J. E., Stewart-Akers, A. M., McCabe, G. P. & Badylak, S. F. Macrophage phenotype and remodeling outcomes in response to biologic scaffolds with and without a cellular component. *Biomaterials* **30**, 1482-1491, doi:10.1016/j.biomaterials.2008.11.040 (2009).
- 134 Sicari, B. M. *et al.* The promotion of a constructive macrophage phenotype by solubilized extracellular matrix. *Biomaterials* **35**, 8605-8612, doi:10.1016/j.biomaterials.2014.06.060 (2014).
- 135 Hodde, J. P., Badylak, S. F., Brightman, A. O. & Voytik-Harbin, S. L. Glycosaminoglycan content of small intestinal submucosa: a bioscaffold for tissue replacement. *Tissue Eng* **2**, 209-217, doi:10.1089/ten.1996.2.209 (1996).
- 136 Hodde, J. P., Record, R. D., Liang, H. A. & Badylak, S. F. Vascular endothelial growth factor in porcine-derived extracellular matrix. *Endothelium* **8**, 11-24 (2001).
- 137 Record, R. D. *et al.* In vivo degradation of <sup>14</sup>C-labeled small intestinal submucosa (SIS) when used for urinary bladder repair. *Biomaterials* **22**, 2653-2659 (2001).
- 138 Keane, T. J., Londono, R., Turner, N. J. & Badylak, S. F. Consequences of ineffective decellularization of biologic scaffolds on the host response. *Biomaterials* **33**, 1771-1781, doi:10.1016/j.biomaterials.2011.10.054 (2012).
- 139 Barnes, C. A. *et al.* in *Biomaterials* Vol. 32 137-143 (2011).
- 140 Hülsmann, J. *et al.* in *Xenotransplantation* Vol. 19 286-297 (2012).
- 141 Wilshaw, S.-P., Kearney, J. N., Fisher, J. & Ingham, E. in *Tissue Eng*. Vol. 12 2117-2129 (2006).
- 142 Reing, J. E. *et al.* in *Biomaterials* Vol. 31 8626-8633 (2010).
- 143 Choi, Y. C. *et al.* in *Tissue Eng Part C Methods* Vol. 18 866-876 (2012).
- 144 Flynn, L. E. in *Biomaterials* Vol. 31 4715-4724 (2010).
- 145 Baert, Y. *et al.* in *Hum. Reprod.* (2014).
- 146 Kutten, J. C. *et al.* in *Tissue Eng Part A* (2014).
- 147 Miyazaki, K. & Maruyama, T. in *Biomaterials* Vol. 35 8791-8800 (2014).
- 148 Remlinger, N. T. *et al.* in *Biomaterials* Vol. 31 3520-3526 (2010).
- 149 Wang, Q. *et al.* in *J Biomed Mater Res A* Vol. 102 4301-4308 (2014).
- 150 Zang, M., Zhang, Q., Chang, E. I., Mathur, A. B. & Yu, P. in *Plast. Reconstr. Surg.* Vol. 132 549e-559e (2013).
- 151 Gilpin, S. E. *et al.* in *J. Heart Lung Transplant.* Vol. 33 298-308 (2014).
- 152 Goh, S.-K. *et al.* in *Biomaterials* Vol. 34 6760-6772 (2013).

- 153 Mirmalek-Sani, S.-H., Sullivan, D. C., Zimmerman, C., Shupe, T. D. & Petersen, B. E. in *Am. J. Pathol.* Vol. 183 558-565 (2013).
- 154 Price, A. P. *et al.* in *Tissue Eng Part C Methods* (2014).
- 155 Struecker, B. *et al.* in *Tissue Eng Part C Methods* (2014).
- 156 Wang, Y. *et al.* in *Xenotransplantation* (2014).
- 157 Cebotari, S. *et al.* in *Artif Organs* Vol. 34 206-210 (2010).
- 158 Nonaka, P. N. *et al.* in *J Biomed Mater Res A* Vol. 102 413-419 (2014).
- 159 Pulver *et al.* in *Cryo Letters* Vol. 35 400-406 (2014).
- 160 Yang, B. *et al.* Development of a porcine bladder acellular matrix with well-preserved extracellular bioactive factors for tissue engineering. *Tissue Eng Part C Methods* **16**, 1201-1211, doi:10.1089/ten.TEC.2009.0311 (2010).
- 161 Freytes, D. O., Stoner, R. M. & Badylak, S. F. Uniaxial and biaxial properties of terminally sterilized porcine urinary bladder matrix scaffolds. *Journal of biomedical materials research. Part B, Applied biomaterials* **84**, 408-414, doi:10.1002/jbm.b.30885 (2008).
- 162 Keane, T. J. *et al.* Preparation and characterization of a biologic scaffold from esophageal mucosa. *Biomaterials* **34**, 6729-6737, doi:10.1016/j.biomaterials.2013.05.052 (2013).
- 163 Marzaro, M. *et al.* In vitro and in vivo proposal of an artificial esophagus. *J Biomed Mater Res A* **77**, 795-801 (2006).
- 164 Baiguera, S. *et al.* Tissue engineered human tracheas for in vivo implantation. *Biomaterials* **31**, 8931-8938, doi:10.1016/j.biomaterials.2010.08.005 (2010).
- 165 Stern, M. M. *et al.* The influence of extracellular matrix derived from skeletal muscle tissue on the proliferation and differentiation of myogenic progenitor cells ex vivo. *Biomaterials* **30**, 2393-2399, doi:S0142-9612(08)01068-5 [pii]10.1016/j.biomaterials.2008.12.069 (2009).
- 166 Gillies, A. R., Smith, L. R., Lieber, R. L. & Varghese, S. Method for decellularizing skeletal muscle without detergents or proteolytic enzymes. *Tissue Eng Part C Methods* **17**, 383-389, doi:10.1089/ten.TEC.2010.0438 (2011).
- 167 Tudorache, I. *et al.* Tissue engineering of heart valves: biomechanical and morphological properties of decellularized heart valves. *J Heart Valve Dis* **16**, 567-573; discussion 574 (2007).
- 168 Cebotari, S. *et al.* Detergent decellularization of heart valves for tissue engineering: toxicological effects of residual detergents on human endothelial cells. *Artif Organs* **34**, 206-210, doi:AOR796 [pii]10.1111/j.1525-1594.2009.00796.x (2010).

- 169 Karabekmez, F. E., Duymaz, A. & Moran, S. L. Early clinical outcomes with the use of decellularized nerve allograft for repair of sensory defects within the hand. *Hand (N Y)* **4**, 245-249, doi:10.1007/s11552-009-9195-6 (2009).
- 170 Guo, S. Z., Ren, X. J., Wu, B. & Jiang, T. Preparation of the acellular scaffold of the spinal cord and the study of biocompatibility. *Spinal Cord* **48**, 576-581, doi:sc2009170 [pii]10.1038/sc.2009.170 (2010).
- 171 Elder, B. D., Kim, D. H. & Athanasiou, K. A. Developing an articular cartilage decellularization process toward facet joint cartilage replacement. *Neurosurgery* **66**, 722-727; discussion 727, doi:10.1227/01.NEU.0000367616.49291.9F00006123-201004000-00024 [pii] (2010).
- 172 Cheng, N. C., Estes, B. T., Awad, H. A. & Guilak, F. Chondrogenic differentiation of adipose-derived adult stem cells by a porous scaffold derived from native articular cartilage extracellular matrix. *Tissue Eng Part A* **15**, 231-241, doi:10.1089/ten.tea.2008.0253 (2009).
- 173 Reing, J. E. *et al.* The effects of processing methods upon mechanical and biologic properties of porcine dermal extracellular matrix scaffolds. *Biomaterials* **31**, 8626-8633, doi:10.1016/j.biomaterials.2010.07.083 (2010).
- 174 Xu, H. *et al.* Host response to human acellular dermal matrix transplantation in a primate model of abdominal wall repair. *Tissue Eng Part A* **14**, 2009-2019, doi:10.1089/ten.tea.2007.0316 (2008).
- 175 Crapo, P. M., Gilbert, T. W. & Badylak, S. F. An overview of tissue and whole organ decellularization processes. *Biomaterials* **32**, 3233-3243, doi:10.1016/j.biomaterials.2011.01.057 (2011).
- 176 Bhrany, A. D. *et al.* Development of an esophagus acellular matrix tissue scaffold. *Tissue Eng* **12**, 319-330, doi:10.1089/ten.2006.12.319 (2006).
- 177 Ozeki, M. *et al.* Evaluation of decellularized esophagus as a scaffold for cultured esophageal epithelial cells. *J Biomed Mater Res A* **79**, 771-778, doi:10.1002/jbm.a.30885 (2006).
- 178 Totonelli, G. *et al.* Detergent enzymatic treatment for the development of a natural acellular matrix for oesophageal regeneration. *Pediatr Surg Int* **29**, 87-95, doi:10.1007/s00383-012-3194-3 (2013).
- 179 Jungebluth, P. *et al.* Structural and morphologic evaluation of a novel detergent-enzymatic tissue-engineered tracheal tubular matrix. *J Thorac Cardiovasc Surg* **138**, 586-593; discussion 592-583, doi:10.1016/j.jtcvs.2008.09.085 (2009).
- 180 Zang, M., Zhang, Q., Chang, E. I., Mathur, A. B. & Yu, P. Decellularized tracheal matrix scaffold for tissue engineering. *Plast Reconstr Surg* **130**, 532-540, doi:10.1097/PRS.0b013e31825dc084 (2012).
- 181 Haykal, S., Soleas, J. P., Salna, M., Hofer, S. O. & Waddell, T. K. Evaluation of the structural integrity and extracellular matrix components of tracheal allografts following

- cyclical decellularization techniques: comparison of three protocols. *Tissue Eng Part C Methods* **18**, 614-623, doi:10.1089/ten.TEC.2011.0579 (2012).
- 182 Macchiarini, P. *et al.* Clinical transplantation of a tissue-engineered airway. *Lancet* **372**, 2023-2030, doi:S0140-6736(08)61598-6 [pii]10.1016/S0140-6736(08)61598-6 (2008).
- 183 Elliott, M. J. *et al.* Stem-cell-based, tissue engineered tracheal replacement in a child: a 2-year follow-up study. *Lancet* **380**, 994-1000, doi:10.1016/S0140-6736(12)60737-5 (2012).
- 184 Montoya, C. V. & McFetridge, P. S. Preparation of ex vivo-based biomaterials using convective flow decellularization. *Tissue Eng Part C Methods* **15**, 191-200, doi:10.1089/ten.tec.2008.0372 (2009).
- 185 Bolland, F. *et al.* Development and characterisation of a full-thickness acellular porcine bladder matrix for tissue engineering. *Biomaterials* **28**, 1061-1070 (2007).
- 186 Funamoto, S. *et al.* The use of high-hydrostatic pressure treatment to decellularize blood vessels. *Biomaterials* **31**, 3590-3595, doi:S0142-9612(10)00105-5 [pii]10.1016/j.biomaterials.2010.01.073 (2010).
- 187 Sasaki, S. *et al.* In vivo evaluation of a novel scaffold for artificial corneas prepared by using ultrahigh hydrostatic pressure to decellularize porcine corneas. *Mol Vis* **15**, 2022-2028 (2009).
- 188 Hashimoto, Y. *et al.* in *Biomaterials* Vol. 31 3941-3948 (2010).
- 189 Sasaki, S. *et al.* in *Mol. Vis.* Vol. 15 2022-2028 (2009).
- 190 Funamoto, S. *et al.* in *Biomaterials* Vol. 31 3590-3595 (2010).
- 191 Sawada, K., Terada, D., Yamaoka, T., Kitamura, S. & Fujisato, T. Cell removal with supercritical carbon dioxide for acellular artificial tissue. *Journal of Chemical Technology and Biotechnology* **83**, 943-949, doi:Doi 10.1002/Jctb.1899 (2008).
- 192 Tsuchiya, T. *et al.* Influence of pH on extracellular matrix preservation during lung decellularization. *Tissue Eng Part C Methods* **20**, 1028-1036, doi:10.1089/ten.TEC.2013.0492 (2014).
- 193 Prasertsung, I., Kanokpanont, S., Bunaprasert, T., Thanakit, V. & Damrongsakkul, S. Development of acellular dermis from porcine skin using periodic pressurized technique. *J Biomed Mater Res B Appl Biomater* **85**, 210-219, doi:10.1002/jbm.b.30938 (2008).
- 194 Komai, Y. & Ushiki, T. The three-dimensional organization of collagen fibrils in the human cornea and sclera. *Invest Ophthalmol Vis Sci* **32**, 2244-2258 (1991).
- 195 Sheridan, W. S., Duffy, G. P. & Murphy, B. P. Mechanical characterization of a customized decellularized scaffold for vascular tissue engineering. *J Mech Behav Biomed Mater* **8**, 58-70, doi:10.1016/j.jmbbm.2011.12.003 (2012).

- 196 Choi, J. S. *et al.* Bioengineering endothelialized neo-corneas using donor-derived corneal endothelial cells and decellularized corneal stroma. *Biomaterials* **31**, 6738-6745, doi:S0142-9612(10)00638-1 [pii]10.1016/j.biomaterials.2010.05.020 (2010).
- 197 Mendoza-Novelo, B. *et al.* Decellularization of pericardial tissue and its impact on tensile viscoelasticity and glycosaminoglycan content. *Acta Biomater* **7**, 1241-1248, doi:10.1016/j.actbio.2010.11.017 (2011).
- 198 Dong, X. *et al.* RGD-modified acellular bovine pericardium as a bioprosthetic scaffold for tissue engineering. *J Mater Sci Mater Med*, doi:10.1007/s10856-009-3791-4 (2009).
- 199 Dong, X. *et al.* in *J Mater Sci Mater Med* Vol. 20 2327-2336 (2009).
- 200 Nakayama, K. H., Batchelder, C. A., Lee, C. I. & Tarantal, A. F. Decellularized rhesus monkey kidney as a three-dimensional scaffold for renal tissue engineering. *Tissue Eng Part A* **16**, 2207-2216, doi:10.1089/ten.TEA.2009.0602 (2010).
- 201 Cartmell, J. S. & Dunn, M. G. Effect of chemical treatments on tendon cellularity and mechanical properties. *J Biomed Mater Res* **49**, 134-140 (2000).
- 202 Woods, T. & Gratzner, P. F. Effectiveness of three extraction techniques in the development of a decellularized bone-anterior cruciate ligament-bone graft. *Biomaterials* **26**, 7339-7349, doi:S0142-9612(05)00457-6 [pii]10.1016/j.biomaterials.2005.05.066 (2005).
- 203 Deeken, C. R. *et al.* Method of preparing a decellularized porcine tendon using tributyl phosphate. *J Biomed Mater Res B Appl Biomater*, doi:10.1002/jbm.b.31753 (2010).
- 204 Meyer, S. R. *et al.* Comparison of aortic valve allograft decellularization techniques in the rat. *J Biomed Mater Res A* **79**, 254-262, doi:10.1002/jbm.a.30777 (2006).
- 205 Liao, J., Yang, L., Grashow, J. & Sacks, M. S. The relation between collagen fibril kinematics and mechanical properties in the mitral valve anterior leaflet. *J Biomech Eng* **129**, 78-87 (2007).
- 206 Rieder, E. *et al.* Decellularization protocols of porcine heart valves differ importantly in efficiency of cell removal and susceptibility of the matrix to recellularization with human vascular cells. *J Thorac Cardiovasc Surg* **127**, 399-405 (2004).
- 207 Grauss, R. W., Hazekamp, M. G., van Vliet, S., Gittenberger-de Groot, A. C. & DeRuiter, M. C. Decellularization of rat aortic valve allografts reduces leaflet destruction and extracellular matrix remodeling. *J Thorac Cardiovasc Surg* **126**, 2003-2010, doi:10.1016/S0022 (2003).
- 208 Liao, J., Joyce, E. M. & Sacks, M. S. Effects of decellularization on the mechanical and structural properties of the porcine aortic valve leaflet. *Biomaterials* **29**, 1065-1074, doi:10.1016/j.biomaterials.2007.11.007 (2008).
- 209 Faulk, D. M. *et al.* The effect of detergents on the basement membrane complex of a biologic scaffold material. *Acta Biomater* **10**, 183-193, doi:10.1016/j.actbio.2013.09.006 (2014).

- 210 Vavken, P., Joshi, S. & Murray, M. M. in *J Orthop Res* Vol. 27 1612-1618 (2009).
- 211 Vavken, P., Joshi, S. & Murray, M. M. TRITON-X is most effective among three decellularization agents for ACL tissue engineering. *J Orthop Res* **27**, 1612-1618, doi:10.1002/jor.20932 (2009).
- 212 Mendoza-Novelo, B. *et al.* in *Acta Biomater* Vol. 7 1241-1248 (2011).
- 213 Gilbert, T. W., Sellaro, T. L. & Badylak, S. F. Decellularization of tissues and organs. *Biomaterials* **27**, 3675-3683, doi:10.1016/j.biomaterials.2006.02.014 (2006).
- 214 Zhou, J. *et al.* Impact of heart valve decellularization on 3-D ultrastructure, immunogenicity and thrombogenicity. *Biomaterials* **31**, 2549-2554, doi:10.1016/j.biomaterials.2009.11.088 (2010).
- 215 Hudson, T. W., Liu, S. Y. & Schmidt, C. E. Engineering an improved acellular nerve graft via optimized chemical processing. *Tissue Eng* **10**, 1346-1358 (2004).
- 216 Lumpkins, S. B., Pierre, N. & McFetridge, P. S. A mechanical evaluation of three decellularization methods in the design of a xenogeneic scaffold for tissue engineering the temporomandibular joint disc. *Acta Biomater* **4**, 808-816, doi:S1742-7061(08)00027-5 [pii]10.1016/j.actbio.2008.01.016 (2008).
- 217 Ott, H. C. *et al.* Perfusion-decellularized matrix: using nature's platform to engineer a bioartificial heart. *Nat Med*, doi:nm1684 [pii]10.1038/nm1684 (2008).
- 218 O'Neill, J. D. *et al.* Decellularization of human and porcine lung tissues for pulmonary tissue engineering. *Ann Thorac Surg* **96**, 1046-1056, doi:10.1016/j.athoracsur.2013.04.022 (2013).
- 219 Petersen, T. H., Calle, E. A., Colehour, M. B. & Niklason, L. E. Matrix composition and mechanics of decellularized lung scaffolds. *Cells Tissues Organs* **195**, 222-231, doi:10.1159/000324896 (2012).
- 220 Du, L., Wu, X., Pang, K. & Yang, Y. Histological evaluation and biomechanical characterisation of an acellular porcine cornea scaffold. *Br J Ophthalmol*, doi:bjo.2008.142539 [pii]10.1136/bjo.2008.142539 (2010).
- 221 Xu, C. C., Chan, R. W. & Tirunagari, N. A biodegradable, acellular xenogeneic scaffold for regeneration of the vocal fold lamina propria. *Tissue Eng* (2006).
- 222 Srinivasan, M., Sedmak, D. & Jewell, S. Effect of fixatives and tissue processing on the content and integrity of nucleic acids. *Am J Pathol* **161**, 1961-1971, doi:10.1016/S0002-9440(10)64472-0 (2002).
- 223 Flynn, L. E. The use of decellularized adipose tissue to provide an inductive microenvironment for the adipogenic differentiation of human adipose-derived stem cells. *Biomaterials* **31**, 4715-4724, doi:S0142-9612(10)00292-9 [pii]10.1016/j.biomaterials.2010.02.046 (2010).
- 224 Brown, B. N. *et al.* Comparison of three methods for the derivation of a biologic scaffold composed of adipose tissue extracellular matrix. *Tissue Eng Part C Methods* **17**, 411-421, doi:10.1089/ten.TEC.2010.0342 (2011).

- 225 Ponce Marquez, S. *et al.* Decellularization of bovine corneas for tissue engineering applications. *Acta Biomater* **5**, 1839-1847, doi:10.1016/j.actbio.2009.02.011 (2009).
- 226 Levy, R. J. *et al.* Inhibition of cusp and aortic wall calcification in ethanol- and aluminum-treated bioprosthetic heart valves in sheep: background, mechanisms, and synergism. *J Heart Valve Dis* **12**, 209-216; discussion 216 (2003).
- 227 Stenn, K. S., Link, R., Moellmann, G., Madri, J. & Kuklinska, E. Dispase, a neutral protease from *Bacillus polymyxa*, is a powerful fibronectinase and type IV collagenase. *J Invest Dermatol* **93**, 287-290 (1989).
- 228 Gonzalez-Andrades, M. *et al.* Generation of bioengineered corneas with decellularized xenografts and human keratocytes. *Invest Ophthalmol Vis Sci* **52**, 215-222, doi:10.1167/iovs.09-4773 (2011).
- 229 Walter, R. J., Matsuda, T., Reyes, H. M., Walter, J. M. & Hanumadass, M. Characterization of acellular dermal matrices (ADMs) prepared by two different methods. *Burns* **24**, 104-113 (1998).
- 230 Grauss, R. W. *et al.* Histological evaluation of decellularised porcine aortic valves: matrix changes due to different decellularisation methods. *Eur J Cardiothorac Surg* **27**, 566-571 (2005).
- 231 Fitzpatrick, J. C., Clark, P. M. & Capaldi, F. M. Effect of decellularization protocol on the mechanical behavior of porcine descending aorta. *Int J Biomater* **2010**, doi:10.1155/2010/620503 (2010).
- 232 Lynch, A. P. & Ahearne, M. Strategies for developing decellularized corneal scaffolds. *Exp Eye Res* **108**, 42-47, doi:10.1016/j.exer.2012.12.012 (2013).
- 233 Huang, M. *et al.* Using acellular porcine limbal stroma for rabbit limbal stem cell microenvironment reconstruction. *Biomaterials* **32**, 7812-7821, doi:10.1016/j.biomaterials.2011.07.012 (2011).
- 234 Zhang, A. Y. *et al.* Tissue-engineered intrasynovial tendons: optimization of acellularization and seeding. *J Rehabil Res Dev* **46**, 489-498 (2009).
- 235 Ott, H. C. *et al.* Perfusion-decellularized matrix: using nature's platform to engineer a bioartificial heart. *Nat Med* **14**, 213-221, doi:10.1038/nm1684nm1684 [pii] (2008).
- 236 Price, A. P. *et al.* Automated Decellularization of Intact, Human-Sized Lungs for Tissue Engineering. *Tissue engineering. Part C, Methods*, doi:10.1089/ten.TEC.2013.0756 (2014).
- 237 Melo, E. *et al.* in *Tissue Eng Part C Methods* Vol. 20 412-422 (2014).
- 238 Nagao, R. J. *et al.* in *J Mater Chem B Mater Biol Med* Vol. 1 4801-4808 (2013).
- 239 Ott, H. C. *et al.* in *Nat. Med.* Vol. 16 927-933 (2010).
- 240 Petersen, T. H. *et al.* in *Science* Vol. 329 538-541 (2010).

- 241 Cortiella, J. *et al.* Influence of acellular natural lung matrix on murine embryonic stem cell differentiation and tissue formation. *Tissue engineering. Part A* **16**, 2565-2580, doi:10.1089/ten.tea.2009.0730 (2010).
- 242 Ott, H. C. *et al.* Regeneration and orthotopic transplantation of a bioartificial lung. *Nature medicine* **16**, 927-933, doi:10.1038/nm.2193 (2010).
- 243 Price, A. P., England, K. A., Matson, A. M., Blazar, B. R. & Panoskaltsis-Mortari, A. Development of a decellularized lung bioreactor system for bioengineering the lung: the matrix reloaded. *Tissue Eng Part A* **16**, 2581-2591, doi:10.1089/ten.TEA.2009.0659 (2010).
- 244 Nichols, J. E. *et al.* Production and assessment of decellularized pig and human lung scaffolds. *Tissue engineering. Part A* **19**, 2045-2062, doi:10.1089/ten.TEA.2012.0250 (2013).
- 245 Uygun, B. E. *et al.* Organ reengineering through development of a transplantable recellularized liver graft using decellularized liver matrix. *Nature medicine* **16**, 814-820, doi:10.1038/nm.2170 (2010).
- 246 Soto-Gutierrez, A. *et al.* A whole-organ regenerative medicine approach for liver replacement. *Tissue engineering. Part C, Methods* **17**, 677-686, doi:10.1089/ten.TEC.2010.0698 (2011).
- 247 Jiang, W.-C. *et al.* Cryo-chemical decellularization of the whole liver for mesenchymal stem cells-based functional hepatic tissue engineering. *Biomaterials* **35**, 3607-3617, doi:10.1016/j.biomaterials.2014.01.024 (2014).
- 248 Shupe, T., Williams, M., Brown, A., Willenberg, B. & Petersen, B. E. Method for the decellularization of intact rat liver. *Organogenesis* **6**, 134-136 (2010).
- 249 Barakat, O. *et al.* Use of decellularized porcine liver for engineering humanized liver organ. *The Journal of surgical research* **173**, e11-25, doi:10.1016/j.jss.2011.09.033 (2012).
- 250 De Kock, J. *et al.* Simple and quick method for whole-liver decellularization: a novel in vitro three-dimensional bioengineering tool? *Archives of toxicology* **85**, 607-612, doi:10.1007/s00204-011-0706-1 (2011).
- 251 Kajbafzadeh, A.-M., Javan-Farazmand, N., Monajemzadeh, M. & Baghayee, A. Determining the optimal decellularization and sterilization protocol for preparing a tissue scaffold of a human-sized liver tissue. *Tissue engineering. Part C, Methods* **19**, 642-651, doi:10.1089/ten.TEC.2012.0334 (2013).
- 252 Sabetkish, S. *et al.* Whole-organ tissue engineering: Decellularization and recellularization of three-dimensional matrix liver scaffolds. *Journal of biomedical materials research. Part A*, doi:10.1002/jbm.a.35291 (2014).

- 253 Struecker, B. *et al.* Improved rat liver decellularization by arterial perfusion under oscillating pressure conditions. *Journal of tissue engineering and regenerative medicine*, doi:10.1002/term.1948 (2014).
- 254 Shupe, T., Williams, M., Brown, A., Willenberg, B. & Petersen, B. E. Method for the decellularization of intact rat liver. *Organogenesis* **6**, 134-136 (2010).
- 255 Soto-Gutierrez, A. *et al.* A whole-organ regenerative medicine approach for liver replacement. *Tissue Eng Part C Methods* **17**, 677-686, doi:10.1089/ten.tec.2010.0698 (2011).
- 256 Ross, E. A. *et al.* Embryonic stem cells proliferate and differentiate when seeded into kidney scaffolds. *J Am Soc Nephrol* **20**, 2338-2347, doi:10.1681/ASN.2008111196 (2009).
- 257 Song, J. J. *et al.* Regeneration and experimental orthotopic transplantation of a bioengineered kidney. *Nat Med* **19**, 646-651, doi:10.1038/nm.3154 (2013).
- 258 Guyette, J. P. *et al.* Perfusion decellularization of whole organs. *Nat Protoc* **9**, 1451-1468, doi:10.1038/nprot.2014.097 (2014).
- 259 Santoso, E. G. *et al.* in *PLoS ONE* Vol. 9 e103201 (2014).
- 260 Gratzer, P. F., Harrison, R. D. & Woods, T. Matrix alteration and not residual sodium dodecyl sulfate cytotoxicity affects the cellular repopulation of a decellularized matrix. *Tissue Eng* **12**, 2975-2983, doi:10.1089/ten.2006.12.2975 (2006).
- 261 Daly, K. A. *et al.* The host response to endotoxin-contaminated dermal matrix. *Tissue Eng Part A* **18**, 1293-1303, doi:10.1089/ten.TEA.2011.0597 (2012).
- 262 Zhang, Q. *et al.* Circulating mitochondrial DAMPs cause inflammatory responses to injury. *Nature* **464**, 104-107, doi:10.1038/nature08780 (2010).
- 263 Yoganarasimha, S. *et al.* Peracetic acid: a practical agent for sterilizing heat-labile polymeric tissue-engineering scaffolds. *Tissue engineering. Part C, Methods* **20**, 714-723, doi:10.1089/ten.TEC.2013.0624 (2014).
- 264 Turner, N. J. *et al.* Xenogeneic extracellular matrix as an inductive scaffold for regeneration of a functioning musculotendinous junction. *Tissue Eng Part A* **16**, 3309-3317, doi:10.1089/ten.TEA.2010.0169 (2010).
- 265 Quarti, A., Nardone, S., Colaneri, M., Santoro, G. & Pozzi, M. Preliminary experience in the use of an extracellular matrix to repair congenital heart diseases. *Interactive cardiovascular and thoracic surgery* **13**, 569-572, doi:10.1510/icvts.2011.280016 (2011).
- 266 Badylak, S. F. *et al.* The use of extracellular matrix as an inductive scaffold for the partial replacement of functional myocardium. *Cell transplantation* **15 Suppl 1**, S29-40 (2006).
- 267 Boruch, A. V., Nieponice, A., Qureshi, I. R., Gilbert, T. W. & Badylak, S. F. Constructive remodeling of biologic scaffolds is dependent on early exposure to physiologic bladder

- filling in a canine partial cystectomy model. *J Surg Res* **161**, 217-225, doi:10.1016/j.jss.2009.02.014 (2010).
- 268 Reddy, P. P. *et al.* Regeneration of functional bladder substitutes using large segment acellular matrix allografts in a porcine model. *The Journal of urology* **164**, 936-941 (2000).
- 269 Cook, J. L., Fox, D. B., Kuroki, K., Jayo, M. & De Deyne, P. G. In vitro and in vivo comparison of five biomaterials used for orthopedic soft tissue augmentation. *American journal of veterinary research* **69**, 148-156, doi:10.2460/ajvr.69.1.148 (2008).
- 270 Valentin, J. E., Badylak, J. S., McCabe, G. P. & Badylak, S. F. Extracellular matrix bioscaffolds for orthopaedic applications. A comparative histologic study. *The Journal of bone and joint surgery. American volume* **88**, 2673-2686, doi:10.2106/JBJS.E.01008 (2006).
- 271 Walton, J. R., Bowman, N. K., Khatib, Y., Linklater, J. & Murrell, G. A. Restore orthobiologic implant: not recommended for augmentation of rotator cuff repairs. *The Journal of bone and joint surgery. American volume* **89**, 786-791, doi:10.2106/JBJS.F.00315 (2007).
- 272 Zalavras, C. G. *et al.* Reconstruction of large rotator cuff tendon defects with porcine small intestinal submucosa in an animal model. *Journal of shoulder and elbow surgery / American Shoulder and Elbow Surgeons ... [et al.]* **15**, 224-231, doi:10.1016/j.jse.2005.06.007 (2006).
- 273 Soler, J. A., Gidwani, S. & Curtis, M. J. Early complications from the use of porcine dermal collagen implants (Permacol) as bridging constructs in the repair of massive rotator cuff tears. A report of 4 cases. *Acta orthopaedica Belgica* **73**, 432-436 (2007).
- 274 Freytes, D. O., Tullius, R. S., Valentin, J. E., Stewart-Akers, A. M. & Badylak, S. F. Hydrated versus lyophilized forms of porcine extracellular matrix derived from the urinary bladder. *Journal of biomedical materials research. Part A* **87**, 862-872, doi:10.1002/jbm.a.31821 (2008).
- 275 Galili, U., Clark, M. R., Shohet, S. B., Buehler, J. & Macher, B. A. Evolutionary relationship between the natural anti-Gal antibody and the Gal alpha 1----3Gal epitope in primates. *Proceedings of the National Academy of Sciences of the United States of America* **84**, 1369-1373 (1987).
- 276 Stone, K. R., Abdel-Motal, U. M., Walgenbach, A. W., Turek, T. J. & Galili, U. Replacement of human anterior cruciate ligaments with pig ligaments: a model for anti-non-gal antibody response in long-term xenotransplantation. *Transplantation* **83**, 211-219, doi:10.1097/01.tp.0000250598.29377.13 (2007).
- 277 Daly, K. A. *et al.* Effect of the alphaGal epitope on the response to small intestinal submucosa extracellular matrix in a nonhuman primate model. *Tissue engineering. Part A* **15**, 3877-3888, doi:10.1089/ten.TEA.2009.0089 (2009).
- 278 Konakci, K. Z. *et al.* Alpha-Gal on bioprostheses: xenograft immune response in cardiac surgery. *Eur J Clin Invest* **35**, 17-23, doi:10.1111/j.1365-2362.2005.01441.x (2005).

- 279 Zheng, M. H. *et al.* Porcine small intestine submucosa (SIS) is not an acellular collagenous matrix and contains porcine DNA: possible implications in human implantation. *Journal of biomedical materials research. Part B, Applied biomaterials* **73**, 61-67, doi:10.1002/jbm.b.30170 (2005).
- 280 Valentin, J. E., Stewart-Akers, A. M., Gilbert, T. W. & Badylak, S. F. Macrophage participation in the degradation and remodeling of extracellular matrix scaffolds. *Tissue Eng Part A* **15**, 1687-1694, doi:10.1089/ten.tea.2008.0419 (2009).
- 281 Ingulli, E. Mechanism of cellular rejection in transplantation. *Pediatr Nephrol* **25**, 61-74, doi:10.1007/s00467-008-1020-x (2010).
- 282 Guo, S. & DiPietro, L. A. Factors affecting wound healing. *Journal of dental research* **89**, 219-229, doi:10.1177/0022034509359125 (2010).
- 283 Badylak, S. F. & Gilbert, T. W. Immune response to biologic scaffold materials. *Seminars in immunology* **20**, 109-116, doi:10.1016/j.smim.2007.11.003 (2008).
- 284 Allman, A. J., McPherson, T. B., Merrill, L. C., Badylak, S. F. & Metzger, D. W. The Th2-restricted immune response to xenogeneic small intestinal submucosa does not influence systemic protective immunity to viral and bacterial pathogens. *Tissue engineering* **8**, 53-62, doi:10.1089/107632702753503054 (2002).
- 285 Allman, A. J. *et al.* Xenogeneic extracellular matrix grafts elicit a TH2-restricted immune response. *Transplantation* **71**, 1631-1640 (2001).
- 286 Ansaloni, L. *et al.* Immune response to small intestinal submucosa (surgisis) implant in humans: preliminary observations. *Journal of investigative surgery : the official journal of the Academy of Surgical Research* **20**, 237-241, doi:10.1080/08941930701481296 (2007).
- 287 Badylak, S. F. The extracellular matrix as a biologic scaffold material. *Biomaterials* **28**, 3587-3593, doi:10.1016/j.biomaterials.2007.04.043 (2007).
- 288 Mirza, R., DiPietro, L. A. & Koh, T. J. Selective and specific macrophage ablation is detrimental to wound healing in mice. *The American journal of pathology* **175**, 2454-2462, doi:10.2353/ajpath.2009.090248 (2009).
- 289 Arnold, L. *et al.* Inflammatory monocytes recruited after skeletal muscle injury switch into antiinflammatory macrophages to support myogenesis. *The Journal of experimental medicine* **204**, 1057-1069, doi:10.1084/jem.20070075 (2007).
- 290 Godwin, J. W., Pinto, A. R. & Rosenthal, N. A. Macrophages are required for adult salamander limb regeneration. *Proceedings of the National Academy of Sciences of the United States of America*, doi:10.1073/pnas.1300290110 (2013).
- 291 Mills, C. D., Kincaid, K., Alt, J. M., Heilman, M. J. & Hill, A. M. M-1/M-2 macrophages and the Th1/Th2 paradigm. *J Immunol* **164**, 6166-6173 (2000).

- 292 Mantovani, A., Sica, A. & Locati, M. Macrophage polarization comes of age. *Immunity* **23**, 344-346, doi:10.1016/j.immuni.2005.10.001 (2005).
- 293 Mantovani, A. *et al.* The chemokine system in diverse forms of macrophage activation and polarization. *Trends Immunol* **25**, 677-686, doi:10.1016/j.it.2004.09.015 (2004).
- 294 Martinez, F. O., Gordon, S., Locati, M. & Mantovani, A. Transcriptional profiling of the human monocyte-to-macrophage differentiation and polarization: new molecules and patterns of gene expression. *J Immunol* **177**, 7303-7311 (2006).
- 295 Porcheray, F. *et al.* Macrophage activation switching: an asset for the resolution of inflammation. *Clin Exp Immunol* **142**, 481-489, doi:10.1111/j.1365-2249.2005.02934.x (2005).
- 296 Daly, K. A. *et al.* Damage associated molecular patterns within xenogeneic biologic scaffolds and their effects on host remodeling. *Biomaterials* **33**, 91-101, doi:10.1016/j.biomaterials.2011.09.040 (2012).
- 297 Jenkins, E. D., Yip, M., Melman, L., Frisella, M. M. & Matthews, B. D. Informed consent: cultural and religious issues associated with the use of allogeneic and xenogeneic mesh products. *Journal of the American College of Surgeons* **210**, 402-410, doi:10.1016/j.jamcollsurg.2009.12.001 (2010).
- 298 Smith, P. D. *et al.* Intestinal macrophages and response to microbial encroachment. *Mucosal Immunol* **4**, 31-42, doi:10.1038/mi.2010.66 (2011).
- 299 Pierce, R. H., Vail, M. E., Ralph, L., Campbell, J. S. & Fausto, N. Bcl-2 expression inhibits liver carcinogenesis and delays the development of proliferating foci. *Am J Pathol* **160**, 1555-1560, doi:10.1016/S0002-9440(10)61101-7 (2002).
- 300 Jiang, G. L. *et al.* The prevention of colitis by E Prostanoid receptor 4 agonist through enhancement of epithelium survival and regeneration. *J Pharmacol Exp Ther* **320**, 22-28, doi:10.1124/jpet.106.111146 (2007).
- 301 Grobe, A. C. *et al.* A study of the junction between glutaraldehyde-treated allogeneic aorta and host aorta. *The Journal of heart valve disease* **9**, 570-575 (2000).
- 302 Hodde, J., Janis, A. & Hiles, M. Effects of sterilization on an extracellular matrix scaffold: part II. Bioactivity and matrix interaction. *Journal of materials science. Materials in medicine* **18**, 545-550, doi:10.1007/s10856-007-2301-9 (2007).
- 303 Hodde, J. *et al.* Effects of sterilization on an extracellular matrix scaffold: part I. Composition and matrix architecture. *Journal of materials science. Materials in medicine* **18**, 537-543, doi:10.1007/s10856-007-2300-x (2007).
- 304 Hafeez, Y. M. *et al.* Effect of freeze-drying and gamma irradiation on biomechanical properties of bovine pericardium. *Cell and tissue banking* **6**, 85-89, doi:10.1007/s10561-004-1888-z (2005).
- 305 Badylak, S. F., Valentin, J. E., Ravindra, A. K., McCabe, G. P. & Stewart-Akers, A. M. Macrophage phenotype as a determinant of biologic scaffold remodeling. *Tissue Eng Part A* **14**, 1835-1842, doi:10.1089/ten.tea.2007.0264 (2008).

- 306 Crisan, M. *et al.* Purification and long-term culture of multipotent progenitor cells affiliated with the walls of human blood vessels: myoendothelial cells and pericytes. *Methods in cell biology* **86**, 295-309, doi:10.1016/S0091-679X(08)00013-7 (2008).
- 307 Crisan, M. *et al.* A perivascular origin for mesenchymal stem cells in multiple human organs. *Cell Stem Cell* **3**, 301-313, doi:10.1016/j.stem.2008.07.003 (2008).
- 308 Tottey, S. *et al.* Extracellular matrix degradation products and low-oxygen conditions enhance the regenerative potential of perivascular stem cells. *Tissue Eng Part A* **17**, 37-44, doi:10.1089/ten.TEA.2010.0188 (2011).
- 309 Kamentsky, L. *et al.* Improved structure, function and compatibility for CellProfiler: modular high-throughput image analysis software. *Bioinformatics* **27**, 1179-1180, doi:10.1093/Bioinformatics/Btr095 (2011).
- 310 Lamprecht, M. R., Sabatini, D. M. & Carpenter, A. E. CellProfiler: free, versatile software for automated biological image analysis. *BioTechniques* **42**, 71-75 (2007).
- 311 Billiar, K. L. & Sacks, M. S. Biaxial mechanical properties of the natural and glutaraldehyde treated aortic valve cusp--Part I: Experimental results. *J Biomech Eng* **122**, 23-30 (2000).
- 312 Freytes, D. O., Tullius, R. S. & Badylak, S. F. Effect of storage upon material properties of lyophilized porcine extracellular matrix derived from the urinary bladder. *Journal of biomedical materials research. Part B, Applied biomaterials* **78**, 327-333, doi:10.1002/jbm.b.30491 (2006).
- 313 Totonelli, G. *et al.* Esophageal tissue engineering: a new approach for esophageal replacement. *World journal of gastroenterology : WJG* **18**, 6900-6907, doi:10.3748/wjg.v18.i47.6900 (2012).
- 314 Koch, H. *et al.* Xenogenic esophagus scaffolds fixed with several agents: comparative in vivo study of rejection and inflammation. *Journal of biomedicine & biotechnology* **2012**, 948320, doi:10.1155/2012/948320 (2012).
- 315 Kasimir, M. T. *et al.* Comparison of different decellularization procedures of porcine heart valves. *The International journal of artificial organs* **26**, 421-427 (2003).
- 316 Du, L., Wu, X., Pang, K. & Yang, Y. Histological evaluation and biomechanical characterisation of an acellular porcine cornea scaffold. *The British journal of ophthalmology* **95**, 410-414, doi:10.1136/bjo.2008.142539 (2011).
- 317 Nyland, J., Larsen, N., Burden, R., Chang, H. & Caborn, D. N. Biomechanical and tissue handling property comparison of decellularized and cryopreserved tibialis anterior tendons following extreme incubation and rehydration. *Knee surgery, sports traumatology, arthroscopy : official journal of the ESSKA* **17**, 83-91, doi:10.1007/s00167-008-0610-2 (2009).
- 318 Ortega, N. & Werb, Z. New functional roles for non-collagenous domains of basement membrane collagens. *Journal of cell science* **115**, 4201-4214 (2002).

- 319 Sundaramoorthy, M., Meiyappan, M., Todd, P. & Hudson, B. G. Crystal structure of NC1 domains. Structural basis for type IV collagen assembly in basement membranes. *The Journal of biological chemistry* **277**, 31142-31153, doi:10.1074/jbc.M201740200 (2002).
- 320 Brown, B., Lindberg, K., Reing, J., Stolz, D. B. & Badylak, S. F. The basement membrane component of biologic scaffolds derived from extracellular matrix. *Tissue engineering* **12**, 519-526, doi:10.1089/ten.2006.12.519 (2006).
- 321 Brown, B. N. & Badylak, S. F. Expanded applications, shifting paradigms and an improved understanding of host-biomaterial interactions. *Acta Biomater* **9**, 4948-4955, doi:10.1016/j.actbio.2012.10.025 (2013).
- 322 Gordon, S. & Taylor, P. R. Monocyte and macrophage heterogeneity. *Nat Rev Immunol* **5**, 953-964, doi:10.1038/nri1733 (2005).
- 323 Loftus, E. V., Jr. Clinical epidemiology of inflammatory bowel disease: Incidence, prevalence, and environmental influences. *Gastroenterology* **126**, 1504-1517 (2004).
- 324 Byrne, T. A., Persinger, R. L., Young, L. S., Ziegler, T. R. & Wilmore, D. W. A new treatment for patients with short-bowel syndrome. Growth hormone, glutamine, and a modified diet. *Annals of surgery* **222**, 243-254; discussion 254-245 (1995).
- 325 Bitar, K. N. & Raghavan, S. Intestinal tissue engineering: current concepts and future vision of regenerative medicine in the gut. *Neurogastroenterology and motility : the official journal of the European Gastrointestinal Motility Society* **24**, 7-19, doi:10.1111/j.1365-2982.2011.01843.x (2012).
- 326 Shin, H., Jo, S. & Mikos, A. G. Biomimetic materials for tissue engineering. *Biomaterials* **24**, 4353-4364 (2003).
- 327 Anderson, J. M., Rodriguez, A. & Chang, D. T. Foreign body reaction to biomaterials. *Semin Immunol* **20**, 86-100, doi:10.1016/j.smim.2007.11.004 (2008).
- 328 Brown, B. N., Valentin, J. E., Stewart-Akers, A. M., McCabe, G. P. & Badylak, S. F. in *Biomaterials* Vol. 30 1482-1491 (2009).
- 329 Hodde, J. P., Record, R. D., Tullius, R. S. & Badylak, S. F. Retention of endothelial cell adherence to porcine-derived extracellular matrix after disinfection and sterilization. *Tissue engineering* **8**, 225-234, doi:10.1089/107632702753724996 (2002).
- 330 Badylak, S., Kokini, K., Tullius, B., Simmons-Byrd, A. & Morff, R. Morphologic study of small intestinal submucosa as a body wall repair device. *J Surg Res* **103**, 190-202, doi:10.1006/jsre.2001.6349S0022480401963498 [pii] (2002).
- 331 Chen, M. K. & Badylak, S. F. Small bowel tissue engineering using small intestinal submucosa as a scaffold. *The Journal of surgical research* **99**, 352-358, doi:10.1006/jsre.2001.6199 (2001).
- 332 Cobb, M. A., Badylak, S. F., Janas, W., Simmons-Byrd, A. & Boop, F. A. Porcine small intestinal submucosa as a dural substitute. *Surgical neurology* **51**, 99-104 (1999).

- 333 Badylak, S. F., Kropp, B., McPherson, T., Liang, H. & Snyder, P. W. Small intestinal submucosa: a rapidly resorbed bioscaffold for augmentation cystoplasty in a dog model. *Tissue engineering* **4**, 379-387 (1998).
- 334 Badylak, S. F., Record, R., Lindberg, K., Hodde, J. & Park, K. Small intestinal submucosa: a substrate for in vitro cell growth. *Journal of biomaterials science. Polymer edition* **9**, 863-878 (1998).
- 335 Prevel, C. D. *et al.* Small intestinal submucosa: utilization as a wound dressing in full-thickness rodent wounds. *Annals of plastic surgery* **35**, 381-388 (1995).
- 336 Prevel, C. D. *et al.* Small intestinal submucosa: utilization for repair of rodent abdominal wall defects. *Annals of plastic surgery* **35**, 374-380 (1995).
- 337 Freytes, D. O., Martin, J., Velankar, S. S., Lee, A. S. & Badylak, S. F. Preparation and rheological characterization of a gel form of the porcine urinary bladder matrix. *Biomaterials* **29**, 1630-1637, doi:10.1016/j.biomaterials.2007.12.014 (2008).
- 338 Wolf, M. T. *et al.* Polypropylene surgical mesh coated with extracellular matrix mitigates the host foreign body response. *J Biomed Mater Res A*, doi:10.1002/jbm.a.34671 (2013).
- 339 Freytes, D. O., Tullius, R. S. & Badylak, S. F. Effect of storage upon material properties of lyophilized porcine extracellular matrix derived from the urinary bladder. *Journal of Biomedical Materials Research Part B-Applied Biomaterials* **78B**, 327-333, doi:10.1002/Jbm.B.30491 (2006).
- 340 Wolf, M. T. *et al.* A hydrogel derived from decellularized dermal extracellular matrix. *Biomaterials* **33**, 7028-7038, doi:10.1016/j.biomaterials.2012.06.051 (2012).
- 341 Watters, D. A., Smith, A. N., Eastwood, M. A., Anderson, K. C. & Elton, R. A. Mechanical properties of the rat colon: the effect of age, sex and different conditions of storage. *Quarterly journal of experimental physiology* **70**, 151-162 (1985).
- 342 Wang, W. *et al.* Dynamic changes and functions of macrophages and M1/M2 subpopulations during ulcerative colitis-associated carcinogenesis in an AOM/DSS mouse model. *Molecular medicine reports* **11**, 2397-2406, doi:10.3892/mmr.2014.3018 (2015).
- 343 Cosin-Roger, J. *et al.* M2 macrophages activate WNT signaling pathway in epithelial cells: relevance in ulcerative colitis. *PloS one* **8**, e78128, doi:10.1371/journal.pone.0078128 (2013).
- 344 Keane, T. J., Swinehart, I. & Badylak, S. F. Methods of Tissue Decellularization Used for Preparation of Biologic Scaffolds and In-vivo Relevance. *Methods*, doi:10.1016/j.ymeth.2015.03.005 (2015).
- 345 Vorotnikova, E. *et al.* Extracellular matrix-derived products modulate endothelial and progenitor cell migration and proliferation in vitro and stimulate regenerative healing in vivo. *Matrix biology : journal of the International Society for Matrix Biology* **29**, 690-700, doi:10.1016/j.matbio.2010.08.007 (2010).

- 346 Freytes, D. O., Stoner, R. M. & Badylak, S. F. in *J. Biomed. Mater. Res. Part B Appl. Biomater.* Vol. 84 408-414 (2008).
- 347 DeWard, A. D., Cramer, J. & Lagasse, E. Cellular heterogeneity in the mouse esophagus implicates the presence of a nonquiescent epithelial stem cell population. *Cell Rep* **9**, 701-711, doi:10.1016/j.celrep.2014.09.027 (2014).
- 348 Doupe, D. P. *et al.* A single progenitor population switches behavior to maintain and repair esophageal epithelium. *Science* **337**, 1091-1093, doi:10.1126/science.1218835 (2012).
- 349 Johnston, B., Kim, C. H., Soler, D., Emoto, M. & Butcher, E. C. Differential chemokine responses and homing patterns of murine TCR alpha beta NKT cell subsets. *J Immunol* **171**, 2960-2969 (2003).
- 350 Keane, T. J. & Badylak, S. F. The host response to allogeneic and xenogeneic biological scaffold materials. *J Tissue Eng Regen Med*, doi:10.1002/term.1874 (2014).
- 351 Kaplan, G. G. The global burden of IBD: from 2015 to 2025. *Nat Rev Gastroenterol Hepatol* **12**, 720-727, doi:10.1038/nrgastro.2015.150 (2015).
- 352 Danese, S. & Fiocchi, C. Ulcerative colitis. *N Engl J Med* **365**, 1713-1725, doi:10.1056/NEJMra1102942 (2011).
- 353 Molodecky, N. A. *et al.* Increasing incidence and prevalence of the inflammatory bowel diseases with time, based on systematic review. *Gastroenterology* **142**, 46-54 e42; quiz e30, doi:10.1053/j.gastro.2011.10.001 (2012).
- 354 de Souza, H. S. & Fiocchi, C. Immunopathogenesis of IBD: current state of the art. *Nat Rev Gastroenterol Hepatol* **13**, 13-27, doi:10.1038/nrgastro.2015.186 (2016).
- 355 Chen, M. K. & Badylak, S. F. Small bowel tissue engineering using small intestinal submucosa as a scaffold. *Journal of Surgical Research* **99**, 352-358, doi:10.1006/Jsre.2001.6199 (2001).
- 356 Gilbert, T. W., Stewart-Akers, A. M. & Badylak, S. F. A quantitative method for evaluating the degradation of biologic scaffold materials. *Biomaterials* **28**, 147-150, doi:10.1016/j.biomaterials.2006.08.022 (2007).
- 357 Kammer, H. W. Adhesion between Polymers - Review. *Acta Polymerica* **34**, 112-118, doi:10.1002/Actp.1983.010340210 (1983).
- 358 Dieleman, L. A., Ridwan, B. U., Tennyson, G. S., Beagley, K. W. & Elson, C. O. Dextran Sodium-Sulfate (Dss)-Induced Colitis Occurs in Severe Combined Immunodeficient (Scid) Mice. *Gastroenterology* **104**, A692-A692 (1993).
- 359 Valatas, V., Vakas, M. & Kolios, G. The value of experimental models of colitis in predicting efficacy of biological therapies for inflammatory bowel diseases. *Am J Physiol Gastrointest Liver Physiol* **305**, G763-785, doi:10.1152/ajpgi.00004.2013 (2013).

- 360 Hermiston, M. L. & Gordon, J. I. Inflammatory bowel disease and adenomas in mice expressing a dominant negative N-cadherin. *Science* **270**, 1203-1207 (1995).
- 361 Meng, F., Modo, M. & Badylak, S. F. Biologic scaffold for CNS repair. *Regen Med* **9**, 367-383, doi:10.2217/rme.14.9 (2014).
- 362 Agrawal, V. *et al.* An isolated cryptic peptide influences osteogenesis and bone remodeling in an adult mammalian model of digit amputation. *Tissue Eng Part A* **17**, 3033-3044, doi:10.1089/ten.TEA.2011.0257 (2011).
- 363 Fishman, J. M. *et al.* Immunomodulatory effect of a decellularized skeletal muscle scaffold in a discordant xenotransplantation model. *Proc Natl Acad Sci U S A* **110**, 14360-14365, doi:10.1073/pnas.1213228110 (2013).
- 364 Khamsi, R. A gut feeling about immunity. *Nat Med* **21**, 674-676, doi:10.1038/nm.3906 (2015).
- 365 Mantovani, A. & Marchesi, F. IL-10 and macrophages orchestrate gut homeostasis. *Immunity* **40**, 637-639, doi:10.1016/j.immuni.2014.04.015 (2014).
- 366 Marchesi, J. R. *et al.* The gut microbiota and host health: a new clinical frontier. *Gut* **65**, 330-339, doi:10.1136/gutjnl-2015-309990 (2016).
- 367 Kayama, H. & Takeda, K. Functions of innate immune cells and commensal bacteria in gut homeostasis. *J Biochem* **159**, 141-149, doi:10.1093/jb/mvv119 (2016).
- 368 Magro, F. *et al.* Is it possible to change phenotype progression in Crohn's disease in the era of immunomodulators? Predictive factors of phenotype progression. *Am J Gastroenterol* **109**, 1026-1036, doi:10.1038/ajg.2014.97 (2014).
- 369 Neurath, M. F. & Travis, S. P. Mucosal healing in inflammatory bowel diseases: a systematic review. *Gut* **61**, 1619-1635, doi:10.1136/gutjnl-2012-302830 (2012).
- 370 Sadtler, K. *et al.* Developing a pro-regenerative biomaterial scaffold microenvironment requires T helper 2 cells. *Science* **352**, 366-370, doi:10.1126/science.aad9272 (2016).
- 371 Chazaud, B. Macrophages: supportive cells for tissue repair and regeneration. *Immunobiology* **219**, 172-178, doi:10.1016/j.imbio.2013.09.001 (2014).
- 372 Novak, M. L. & Koh, T. J. Phenotypic transitions of macrophages orchestrate tissue repair. *Am J Pathol* **183**, 1352-1363, doi:10.1016/j.ajpath.2013.06.034 (2013).
- 373 Weidenbusch, M. & Anders, H. J. Tissue microenvironments define and get reinforced by macrophage phenotypes in homeostasis or during inflammation, repair and fibrosis. *J Innate Immun* **4**, 463-477, doi:10.1159/000336717 (2012).
- 374 Papadakis, K. A. & Targan, S. R. Role of cytokines in the pathogenesis of inflammatory bowel disease. *Annu Rev Med* **51**, 289-298, doi:10.1146/annurev.med.51.1.289 (2000).
- 375 Akhyari, P., Kamiya, H., Haverich, A., Karck, M. & Lichtenberg, A. Myocardial tissue engineering: the extracellular matrix. *Eur J Cardiothorac Surg* **34**, 229-241, doi:10.1016/j.ejcts.2008.03.062 (2008).

- 376 Kochupura, P. V. *et al.* Tissue-engineered myocardial patch derived from extracellular matrix provides regional mechanical function. *Circulation* **112**, 1144-149, doi:10.1161/CIRCULATIONAHA.104.524355 (2005).
- 377 Badylak, S. F. *et al.* The use of extracellular matrix as an inductive scaffold for the partial replacement of functional myocardium. *Cell Transplant* **15 Suppl 1**, S29-40 (2006).
- 378 Nieponice, A., Gilbert, T. W. & Badylak, S. F. Reinforcement of esophageal anastomoses with an extracellular matrix scaffold in a canine model. *Ann Thorac Surg* **82**, 2050-2058, doi:10.1016/j.athoracsur.2006.06.036 (2006).
- 379 Nieponice, A. *et al.* An extracellular matrix scaffold for esophageal stricture prevention after circumferential EMR. *Gastrointest Endosc* **69**, 289-296, doi:10.1016/j.gie.2008.04.022 (2009).
- 380 Brigido, S. A., Boc, S. F. & Lopez, R. C. Effective management of major lower extremity wounds using an acellular regenerative tissue matrix: A pilot study. *Orthopedics* **27**, S145-S149 (2004).
- 381 Aurora, A., McCarron, J., Iannotti, J. P. & Derwin, K. Commercially available extracellular matrix materials for rotator cuff repairs: state of the art and future trends. *J Shoulder Elbow Surg* **16**, S171-178, doi:10.1016/j.jse.2007.03.008 (2007).
- 382 De Deyne, P. G. & Kladakis, S. M. Bioscaffolds in tissue engineering: a rationale for use in the reconstruction of musculoskeletal soft tissues. *Clin Podiatr Med Surg* **22**, 521-532, v, doi:10.1016/j.cpm.2005.07.006 (2005).
- 383 Dejardin, L. M., Arnoczky, S. P., Ewers, B. J., Haut, R. C. & Clarke, R. B. Tissue-engineered rotator cuff tendon using porcine small intestine submucosa - Histologic and mechanical evaluation in dogs. *Am J Sport Med* **29**, 175-184 (2001).
- 384 Snyder, S. J., Arnoczky, S. P., Bond, J. L. & Dopirak, R. Histologic evaluation of a biopsy specimen obtained 3 months after rotator cuff augmentation with GraftJacket Matrix. *Arthroscopy* **25**, 329-333, doi:10.1016/j.arthro.2008.05.023 (2009).
- 385 Turner, N. J. & Badylak, S. F. Regeneration of skeletal muscle. *Cell Tissue Res*, doi:10.1007/s00441-011-1185-7 (2011).
- 386 Badylak, S. F., Freytes, D. O. & Gilbert, T. W. Extracellular matrix as a biological scaffold material: Structure and function. *Acta Biomater* **5**, 1-13, doi:10.1016/j.actbio.2008.09.013 (2009).
- 387 Ayyildiz, A. *et al.* Use of porcine small intestinal submucosa in bladder augmentation in rabbit: long-term histological outcome. *Anz J Surg* **78**, 82-86, doi:10.1111/j.1445-2197.2007.04361.x (2008).
- 388 Zalavras, C. G. *et al.* Reconstruction of large rotator cuff tendon defects with porcine small intestinal submucosa in an animal model. *J Shoulder Elbow Surg* **15**, 224-231, doi:10.1016/j.jse.2005.06.007 (2006).

- 389 Adams, J. E., Zobitz, M. E., Reach, J. S., An, K. N. & Steinmann, S. P. Rotator cuff repair using an acellular dermal matrix graft: An in vivo study in a canine model. *Arthroscopy-the Journal of Arthroscopic and Related Surgery* **22**, 700-709, doi:DOI 10.1016/j.arthro.2006.03.016 (2006).
- 390 Badylak, S. F. *et al.* Esophageal preservation in five male patients after endoscopic inner-layer circumferential resection in the setting of superficial cancer: a regenerative medicine approach with a biologic scaffold. *Tissue Eng Part A* **17**, 1643-1650, doi:10.1089/ten.TEA.2010.0739 (2011).
- 391 Metcalf, M., Savoie, F. & Kellum, B. Surgical technique for xenograft (SIS) augmentation of rotator-cuff repairs. *Operative Techniques in Orthopaedics* **12**, 204-208, doi:10.1053/otor.2002.36298 (2002).
- 392 Zheng, M. H. *et al.* Porcine small intestine submucosa (SIS) is not an acellular collagenous matrix and contains porcine DNA: possible implications in human implantation. *J Biomed Mater Res B Appl Biomater* **73**, 61-67, doi:10.1002/jbm.b.30170 (2005).
- 393 Doede, T., Bondartschuk, M., Joerck, C., Schulze, E. & Goernig, M. Unsuccessful alloplastic esophageal replacement with porcine small intestinal submucosa. *Artif Organs* **33**, 328-333, doi:10.1111/j.1525-1594.2009.00727.x (2009).
- 394 Walton, J. R., Bowman, N. K., Khatib, Y., Linklater, J. & Murrell, G. A. C. Restore orthobiologic implant: Not recommended for augmentation of rotator cuff repairs. *Journal of Bone and Joint Surgery-American Volume* **89A**, 786-791, doi: 10.2106/Jbjs.F.00315 (2007).
- 395 Soler, J. A., Gidwani, S. & Curtis, M. J. Early complications from the use of porcine dermal collagen implants (Permacol (TM)) as bridging constructs in the repair of massive rotator cuff tears - A report of 4 cases. *Acta Orthop Belg* **73**, 432-436 (2007).
- 396 Hodde, J. P., Badylak, S. F. & Shelbourne, K. D. The effect of range of motion on remodeling of small intestinal submucosa (SIS) when used as an Achilles tendon repair material in the rabbit. *Tissue Eng* **3**, 27-37 (1997).
- 397 Boruch, A. V., Nieponice, A., Qureshi, I. R., Gilbert, T. W. & Badylak, S. F. Constructive remodeling of biologic scaffolds is dependent on early exposure to physiologic bladder filling in a canine partial cystectomy model. *J Surg Res* **161**, 217-225, doi:10.1016/j.jss.2009.02.014 (2010).
- 398 Gilbert, T. W., Freund, J. M. & Badylak, S. F. Quantification of DNA in biologic scaffold materials. *J Surg Res* **152**, 135-139, doi:10.1016/j.jss.2008.02.013 (2009).
- 399 Mantovani, A. *et al.* The chemokine system in diverse forms of macrophage activation and polarization. *Trends Immunol* **25**, 677-686, doi:10.1016/j.it.2004.09.015 (2004).
- 400 Martinez, F. O., Sica, A., Mantovani, A. & Locati, M. Macrophage activation and polarization. *Front Biosci* **13**, 453-461 (2008).

- 401 Mantovani, A., Sozzani, S., Locati, M., Allavena, P. & Sica, A. Macrophage polarization: tumor-associated macrophages as a paradigm for polarized M2 mononuclear phagocytes. *Trends Immunol* **23**, 549-555 (2002).
- 402 Wong, S. C. *et al.* Macrophage polarization to a unique phenotype driven by B cells. *Eur J Immunol* **40**, 2296-2307, doi:10.1002/eji.200940288 (2010).
- 403 Clark, R. A. Biology of dermal wound repair. *Dermatol Clin* **11**, 647-666 (1993).
- 404 Gurtner, G. C., Werner, S., Barrandon, Y. & Longaker, M. T. Wound repair and regeneration. *Nature* **453**, 314-321, doi:nature07039 [pii]10.1038/nature07039 (2008).
- 405 Jimenez, P. A. & Jimenez, S. E. Tissue and cellular approaches to wound repair. *Am J Surg* **187**, 56S-64S, doi:10.1016/S0002-9610(03)00305-2S0002961003003052 [pii] (2004).
- 406 Badylak, S. F., Valentin, J. E., Ravindra, A. K., McCabe, G. P. & Stewart-Akers, A. M. Macrophage phenotype as a determinant of biologic scaffold remodeling. *Tissue Eng Part A* **14**, 1835-1842, doi:10.1089/ten.tea.2007.0264 (2008).
- 407 Valentin, J. E., Stewart-Akers, A. M., Gilbert, T. W. & Badylak, S. F. Macrophage participation in the degradation and remodeling of extracellular matrix scaffolds. *Tissue Eng Part A* **15**, 1687-1694, doi:10.1089/ten.tea.2008.0419 (2009).
- 408 Badylak, S. F. *et al.* Biologic scaffolds for constructive tissue remodeling. *Biomaterials* **32**, 316-319 (2011).
- 409 Badylak, S. F., Lantz, G. C., Coffey, A. & Geddes, L. A. Small intestinal submucosa as a large diameter vascular graft in the dog. *J Surg Res* **47**, 74-80 (1989).
- 410 Brown, B., Lindberg, K., Reing, J., Stolz, D. B. & Badylak, S. F. The basement membrane component of biologic scaffolds derived from extracellular matrix. *Tissue Eng* **12**, 519-526, doi:10.1089/ten.2006.12.519 (2006).
- 411 Lamprecht, M. R., Sabatini, D. M. & Carpenter, A. E. CellProfiler(TM): free, versatile software for automated biological image analysis. *Biotechniques* **42**, 71-75, doi:Doi 10.2144/000112257 (2007).
- 412 Derwin, K. A., Baker, A. R., Spragg, R. K., Leigh, D. R. & Iannotti, J. P. Commercial extracellular matrix scaffolds for rotator cuff tendon repair. Biomechanical, biochemical, and cellular properties. *J Bone Joint Surg Am* **88**, 2665-2672, doi:10.2106/JBJS.E.01307 (2006).
- 413 Sandor, M. *et al.* Host response to implanted porcine-derived biologic materials in a primate model of abdominal wall repair. *Tissue Eng Part A* **14**, 2021-2031, doi:10.1089/ten.tea.2007.0317 (2008).
- 414 Rieder, E. *et al.* Tissue engineering of heart valves: decellularized porcine and human valve scaffolds differ importantly in residual potential to attract monocytic cells. *Circulation* **111**, 2792-2797, doi:10.1161/CIRCULATIONAHA.104.473629 (2005).

- 415 Ariganello, M. B., Labow, R. S. & Lee, J. M. In vitro response of monocyte-derived macrophages to a decellularized pericardial biomaterial. *J Biomed Mater Res A* **93**, 280-288, doi:10.1002/jbm.a.32554 (2010).
- 416 Valentin, J. E., Badylak, J. S., McCabe, G. P. & Badylak, S. F. Extracellular matrix bioscaffolds for orthopaedic applications. A comparative histologic study. *J Bone Joint Surg Am* **88**, 2673-2686, doi:10.2106/JBJS.E.01008 (2006).
- 417 Rhodes, A., Wort, S. J., Thomas, H., Collinson, P. & Bennett, E. D. Plasma DNA concentration as a predictor of mortality and sepsis in critically ill patients. *Crit Care* **10**, - , doi:Artn R60Doi 10.1186/Cc4894 (2006).
- 418 Gill, R. *et al.* Systemic inflammation and liver injury following hemorrhagic shock and peripheral tissue trauma involve functional TLR9 signaling on bone marrow-derived cells and parenchymal cells. *Shock* **35**, 164-170, doi:10.1097/SHK.0b013e3181eddcb (2011).
- 419 Butt, A. N. & Swaminathan, R. Overview of circulating nucleic acids in plasma/serum. *Ann N Y Acad Sci* **1137**, 236-242, doi:10.1196/annals.1448.002 (2008).
- 420 Hashizume, R. *et al.* Morphological and mechanical characteristics of the reconstructed rat abdominal wall following use of a wet electrospun biodegradable polyurethane elastomer scaffold. *Biomaterials* **31**, 3253-3265, doi:10.1016/j.biomaterials.2010.01.051 (2010).
- 421 Butler, C. E. & Prieto, V. G. Reduction of Adhesions with Composite AlloDerm/Polypropylene Mesh Implants for Abdominal Wall Reconstruction. *Plastic and Reconstructive Surgery* **114**, 464-473, doi:10.1097/01.prs.0000132670.81794.7e (2004).
- 422 Thoren, K. & Aspenberg, P. Ethylene oxide sterilization impairs allograft incorporation in a conduction chamber. *Clinical orthopaedics and related research*, 259-264 (1995).
- 423 Freytes, D. O. *et al.* Analytically derived material properties of multilaminated extracellular matrix devices using the ball-burst test. *Biomaterials* **26**, 5518-5531, doi:10.1016/j.biomaterials.2005.01.070 (2005).
- 424 Ades, E. W. *et al.* HMEC-1: establishment of an immortalized human microvascular endothelial cell line. *J Invest Dermatol* **99**, 683-690 (1992).
- 425 Sicari, B., Turner, N. & Badylak, S. F. An in vivo model system for evaluation of the host response to biomaterials. *Methods Mol Biol* **1037**, 3-25, doi:10.1007/978-1-62703-505-7\_1 (2013).
- 426 Sahoo, S., DeLozier, K. R., Erdemir, A. & Derwin, K. A. Clinically relevant mechanical testing of hernia graft constructs. *J Mech Behav Biomed Mater* **41**, 177-188, doi:10.1016/j.jmbbm.2014.10.011 (2015).
- 427 Gilbert, T. W., Stewart-Akers, A. M., Simmons-Byrd, A. & Badylak, S. F. Degradation and remodeling of small intestinal submucosa in canine Achilles tendon repair. *J Bone Joint Surg Am* **89**, 621-630, doi:10.2106/JBJS.E.00742 (2007).

- 428 Dellarco, V. L., Generoso, W. M., Sega, G. A., Fowle, J. R., 3rd & Jacobson-Kram, D. Review of the mutagenicity of ethylene oxide. *Environmental and molecular mutagenesis* **16**, 85-103 (1990).
- 429 Jackson, D. W., Windler, G. E. & Simon, T. M. Intraarticular reaction associated with the use of freeze-dried, ethylene oxide-sterilized bone-patella tendon-bone allografts in the reconstruction of the anterior cruciate ligament. *The American journal of sports medicine* **18**, 1-10; discussion 10-11 (1990).
- 430 Gaughran, E. R. L. G., A. J | Johnson and Johnson (Company) Sterilization by ionizing radiation. (1978).
- 431 You, F., Li, Y., Zuo, Y. & Li, J. The influence of gamma-ray irradiation on the mechanical and thermal behaviors of nHA/PA66 composite scaffolds. *TheScientificWorldJournal* **2013**, 162384, doi:10.1155/2013/162384 (2013).
- 432 Gouk, S. S., Lim, T. M., Teoh, S. H. & Sun, W. Q. Alterations of human acellular tissue matrix by gamma irradiation: histology, biomechanical property, stability, in vitro cell repopulation, and remodeling. *Journal of biomedical materials research. Part B, Applied biomaterials* **84**, 205-217, doi:10.1002/jbm.b.30862 (2008).